Università degli Studi di Urbino "Carlo Bo"
Dipartimento di Scienze di Base e Fondamenti - DiSBeF

Corso di Dottorato di Ricerca in
scienze della terra, scienza della complessitá
ciclo XXVIII

Titolo della Tesi

Adaptive models of learning in complex physical and social systems

Settore scientifico disciplinare: MAT/07 Fisica Matematica

Relatori:
Chiar.mo Prof. Gian Italo Bischi
Chiar.mo Prof. Gianluca M. Guidi

Dottorando:
Dott. Lorenzo Cerboni Baiardi

Anno Accademico 2014/2015

To my family

Abstract

This thesis is developed in the framework of the PhD school in complexity science at the University of Urbino. As a consequence of the interdisciplinary nature of such PhD program, the present work deals with different research areas: it includes economic modeling and physical system control design through reinforcement learning techniques.

In the first Chapter a nonlinear discrete-time dynamic system proposed in economic literature, as a market share attraction model, is studied. A rich scenario of local and global bifurcations is obtained even with just two competing firms and the effects of heterogeneities between them are investigated.

In the second Chapter the view point on economic modeling is enlarged to critically discuss about assumptions of synchronization of economic agent allowing the description in terms of a representative one stressing the role of heterogeneities even when these are very small.

In the subsequent two Chapters the analysis of two evolutionary games in which players in the population choose between two different strategies according to a profit-driven evolutionary selection rule is carried out. The resulting discrete dynamical systems, represented by two and three-dimensional nonlinear maps respectively, are characterized by the presence of invariant manifolds on which the dynamics are governed by the restrictions of evolution equations and represent synchronized populations of players that adopt the same strategies.

Finally, in the last Chapter an adaptive nonlinear feedback controller is designed based on reinforcement learning techniques, implemented through a neural network and applied to a coupled two-pendulum system in order to improve stability and performance of classical PID linear controller. This kind of approach improves performances in particular when the available model of the real plant is wrong, a circumstance that reduces benefits of optimal control design and provides superior limits for feedback values avoiding problems of reliability of real feedback actuators.

Table of contents

Chapter 1

Introduction

This thesis is developed in the framework of the PhD school in complexity science at the University of Urbino. As a consequence of the interdisciplinary nature of such PhD program, the present work concerns different research areas: it includes economic modeling and physical system control design. Further, this work is inspired by, and based on, a quite large and interdisciplinary bibliography. Part of the work presented here has been published on international journals and contributes to different stream of literature.

1.1 Dynamic games: behavior and learning

In this section we illustrate some basic assumptions and methods of classical game theory restricted to static games in strategic form and the role of rationality of the individuals in taking most profitable decisions, *playing the Nash equilibrium*.

Classical game theory considers multiple decision makers, also known as players or agents, that interact among each other through actions, or *strategies*, which they choose to maximize (or increase) their utility (or payoff), according to a given ranking of preferences, in their environment. In a static game, in particular, a single decision is made by each player who has no knowledge about the decision made by the others before making its own decision. The outcome of the game is then the set of strategies that all players adopt simultaneously.

A game in strategic form has three elements: the set of *players*, $i \in \mathcal{N} := \{1, 2, ...n\}$, the *pure-strategy space* S_i for each player i and *payoff functions* u_i that give players i's von Neumann-Morgenstern utility $u_i(\boldsymbol{\sigma})$ for each profile of strategies $\boldsymbol{\sigma} = (\sigma_1, \sigma_2, ..., \sigma_n)$, that is for each outcome of the game (for details on the von Neumann-Morgenstern utilities see [78]). For the sake of completeness it can be noted that, in general, the

strategy σ_i of player i is a *mixed strategy*, that is a weighted sum of pure strategies of S_i where weights are the probability (i.e. a *lottery*) associated to these pure strategies. Here, however, we deal with the case in which players adopt only pure strategy, that is $\sigma_i \in S_i$, for $i \in \mathcal{N}$. The interpretations of the solution concept of a game is straightforward extended to mixed strategy profiles.

Each player's objective is to maximize his own payoff function and tries to do this from selecting his best response, that is the strategy that returns to him the highest payoff given the strategy of others. A Nash equilibrium is, by definition, a profile of strategies so that each player's strategy is the best response to the other players' strategies. To express formally the previous statement let $\boldsymbol{\sigma}_{-i}$ denote the strategy profile for all players but i and $(\boldsymbol{\sigma}_{-i}, \sigma_i')$ denote the strategy profile given by $(\sigma_1, ..., \sigma_{i-1}, \sigma_i', \sigma_{i+1}, ..., \sigma_n)$. So the strategy profile $\boldsymbol{\sigma}^* = (\sigma_1^*, \sigma_2^*, ..., \sigma_n^*)$ is a Nash equilibrium if, for every player, it results $\pi_i(\boldsymbol{\sigma}^*) \geqslant \pi_i(\boldsymbol{\sigma}_{-i}^*, \sigma_i)$. By this, it is meant that, for player i, choosing $\sigma_i^* = (\boldsymbol{\sigma}^*)_i$ is at least as good as choosing any other strategy σ_i given that the strategies of the others $\boldsymbol{\sigma}_{-i}^*$ remain the same.

Classical game theory is a framework to model decisions where players are endowed with sufficient information and rationality to make the best choice assuming the ability of forecasting the behaviors of others. The solution concept of Nash equilibrium as the outcome of a game can be (roughly) motivated by assuming that players are rational and informed, meaning by this that they are endowed with sufficient computational abilities and have perfect knowledge of the payoffs' structures of all the players. By this they are able to forecast the strategy of others and then to choose the strategy that maximizes their own payoff. In other words, the players of classical game theory are capable to compute their own best strategy solving an optimization problem having correct expectations, namely *rational expectations*, on others' strategies. In a deterministic framework this leads to *perfect foresight* in the sense that they are able to build the economic model and therefore they correctly anticipate the future states of the economy. For a more exhaustive overview of game theory see e.g. [39], [15], [128] or any other standard text of game theory.

Rational expectations seem to be too strong an assumption, a kind of limiting case in which players are perfectly rational and informed, if compared with real economic systems where agents have a limited ability to compute. Indeed the assumptions of classical game theory allow the players to solve the game and play the Nash equilibrium in a single decision. However, if the same assumptions are weakened, then the rational process that leads each agent to forecast others' strategy and to choose the better

action is not efficient enough to compute the best response for all the players, and then to play the Nash equilibrium, in a one shot game.

So economic models should take into account human limited ability to make forecastings. This leads players to replace one shot optimal decision with repeated myopic or adaptive decisions, that is to carry out a dynamic process that may or may not converge to a Nash Equilibrium, provided it is an equilibrium point of the dynamical system as well.

It is then introduced the weaker assumption of *bounded rationality* according to which agents compute expected future variables of the economy by some behavioral method: they could behave adaptively or adopting heuristics or learning by doing as well as through trial and error explorations. Sometimes no one optimizes at all and just follows rough rules of thumb. Deterministic repeated games usually take the form of discrete time dynamical systems that read generically as:

$$\sigma_{i,t+1} = \Phi_i(\boldsymbol{\sigma}^{(e)}_{i,t+1}, \boldsymbol{\sigma}_t, \boldsymbol{\sigma}_{t-1}, ..., t) \tag{1.1a}$$

$$\boldsymbol{\sigma}^{(e)}_{i,t+1} = \Psi_i\left(\boldsymbol{\sigma}_t, \boldsymbol{\sigma}_{t-1}, ..., t\right) \tag{1.1b}$$

for all $i \in \{1, ..., n\}$ and where t is a discrete temporal parameter. The equations (1.1) account for the behavioral rules that real economic agents elaborate to make forecastings and to update their own strategy. The equations of motion (1.1) are in general nonlinear and, because of this, a single model of an economic scenario may be characterized by very different scenarios highlighting different dynamic properties of the system: depending on the local stability property of the fixed points, convergence may occur as well as cyclic or chaotic dynamics may arise. To study the convergence towards Nash equilibrium, the behavioral rule of the i-th agent described by the function Φ_i has to be consistent with the underlying game. One can think of modeling the behaviors of the players in order to make the Nash equilibrium of the real and unknown economic model fixed points of dynamic equation (1.1a). When this occurs and assuming naïve expectations, that is assuming that the equation (1.1b) reduces to $\boldsymbol{\sigma}^{(e)}_{i,t+1} = \boldsymbol{\sigma}_{i,t}$, then at the Nash equilibrium the players have correct expectations.[1] This scenario is like those presented in the following economic applications.

It can also be noted that when multiple Nash equilibriums are present the step by step dynamic process may act as a selection device since their stability determine

[1] More generally this holds true for adaptive expectations of the form $x^{(e)}_{t+1} = x^{(e)}_t + \alpha\left(x_t - x^{(e)}_t\right) = (1-\alpha)\, x^{(e)}_t + \alpha x_t$, where $\alpha \in [0,1]$ is a speed of adjustment, that are commonly used in economic modeling (see [52]). Naïve expectations are adaptive expectations in the case in which $\alpha = 1$.

which one prevails in the long run or with which probability each of them is reached. In this context information about path dependence on historical accidents are obtained from the study of basin of attractions. Indeed, in situations of multistability, the initial conditions have a crucial importance. However, sometimes such repeated adaptive processes never converge, and continue to move around an equilibrium point following some periodic or chaotic time patterns. Or they may even irreversibly depart from it and even diverge. In such cases some global analysis may be required to understand the kind of time evolutions that characterize the long run behavior of the repeated game.

It can be noted that very rarely the situations of the strategic interactions are reproduced unchanged in the real-world. However one of the most important reason that induces the study of repeated games is the spontaneous emergence of cooperation in a non cooperative context (that is in the absence of institutions that guarantee the compliance of agreements eventually signed by the parties). An example is provided by cartels among economic agents in an oligopolistic market that emerge and persist spontaneously. The emerging of collective and organized dynamics is related to the remarkable result that regards whether a repeated boundedly rational (or trial-and-error) decision leads to an adaptive (or myopic) process that converges, in the long run, to the same 'optimal' equilibrium chosen in one shot by rational and informed players of classical theory with high computational abilities. In fact, such boundedly rational players, whose behavior is much more similar to real imperfect people, play the game repeatedly over time until they reach a situation where there is no further room for improvement. Convergence emerges spontaneously as as a sort of some collective coordination mechanism (i.e. the "Adam Smith invisible hand") that leads them to the optimal outcome of the game. From this point of view, a fixed point argument provides the *evolutionary explanation* of the asymptotic outcome of the Nash equilibrium.

Conversely, when a Nash equilibrium is an asymptotic outcome of some learning process that takes place during the evolution of the economy, than its local stability can be interpreted as the evolutive learning explanation of the perfect foresight solution[2]. In other words agents are able to learn it endogenously and convergence of the learning scheme to a perfect foresight solution reinforces it as interpretation of the real world. Divergence means that the rational expectation solution is not really relevant because it cannot be endogenously learned by boundedly rational agents according to the learning

[2] Of course, also in this case, this requires that the Nash equilibrium must be an equilibrium for the model with learning.

rule adopted. Furthermore, when multiple Nash equilibriums are present, only the ones which are stable under learning are important since they can be learned by the agents.

1.2 Some words about learning

What we have to learn to do, we learn by doing.
Aristotele, Nocomacheam Ethics, Book II.

It is widely acknowledged, from ancient times, that *learning is the product of experience* (see [11]). Indeed an intelligent agent chooses the action to execute on the environment in which he lives, or in which interacts strategically with others, in order to change it and to receive some utility. This is possible if the agent owns some knowledge about the environment which, moreover, can be acquired through the observation of data concerning the environments' evolution. Besides acquiring information, the agent should be able to use it efficiently: "*In the language of the learning theory, an animal can gain selective advantage not from its performance on the training data but only from its performance at generalization. Generalizing, and not "over-fitting" the training data, is precisely the problem of isolating the features of the data that have predictive value*". This sentence, taken from [127], highlights the importance of the prediction phenomenon of generalization in learning. It is the skills, acquired through learning, to generalize the knowledge gained from the observation of a finite number of events or data to deal with new scenarios of which it hasn't had any direct experience.

In the context of game theory, different learning methodologies can be designed to model boundedly rational learners that interact in a strategic environment. Indeed, the learning in games replies to the need of making the behavioral rules and the heuristics of players consistent with the underlying game. More precisely, the inclusion of a learning process explains the way in which the available information is used to play in a non cooperative context and to forecast others' strategies. Behavioral rules are learned and built from experience during the play and not assigned a priori. In other words the players acquire, through the learning process, the rationality needed to make the best use of their experience.

The common knowledge argument of the classical game theory suggests that, to compute the Nash equilibrium, an algorithm of a certain degree of computational complexity has to be implemented by the rational and informed players. When players are boundedly rational learners, a similar ability is demanded to them after a training process and the result of the learning will depends on the informational complexity

contained in the observed data, the cognitive abilities of the players and whether they have experienced a suitable number training data.

Reinforcement learning methods are widely applied to economic modeling as well as in control theory, machine learning and robotics, which are situations characterized by a high level of complexity. However in the present thesis reinforcement learning techniques are not used to endow players with learning skills to compete in games through strategic interactions, but they are used to develop a nonlinear controller which will be applied to regulate a physical plant.

From the paper [47] a sketch of description of reinforcement learning methods can be found: "*The theory of reinforcement learning provides a normative account, deeply rooted in psychological and neuroscientific perspectives on animal behavior, of how agents may optimize their control of an environment. To use reinforcement learning successfully in situations approaching real-world complexity, however, agents are confronted with a difficult task: they must derive efficient representations of the environment from high-dimensional sensory inputs, and use these to generalize past experience to new situations. Remarkably, humans and other animals seem to solve this problem through a harmonious combination of temporal difference reinforcement learning algorithm and hierarchical sensory processing systems [...].*"

In its general outlines, reinforcement learning methodology consists in assigning a value to the strategies on the basis of the expected effects they will produce. Such values are adjusted adaptively as learning proceeds through trial and error actions. More precisely, when the environment is unknown, the exploration activity prevails, random actions are performed and their effects are observed. As the number of transitions between successive states of the environment increases, the ability to forecast the future effect of actions increases as well, and exploitation of the acquired knowledge will prevail over the exploration of the environment. Furthermore, in order to model the generalization capability of the intelligent agent, a parametrized function approximator is used to represents the agent's preferences on the possible states of the environment and, because of its interpolating nature, it is capable of suggesting what actions to take also in states of the environment that are not been previously experienced.

1.3 Thesis' structure

The plan of the thesis is as follows. In Chapter 2 we will consider a nonlinear discrete-time dynamic model proposed by Farris et al. in the paper "When five is a crowd in the market share attraction model: the dynamic stability of competition",

Journal of Research and Management (2005), [105], where a market share attraction model with two firms that decide marketing efforts over time, according to best reply strategies with naïve expectations, is presented. The model also considers an adaptive adjustment towards best reply, a form of inertia or anchoring attitude, and the effects of heterogeneities among firms are investigated. A rich scenario of local and global bifurcations is obtained even with just two competing firms, and a comparison is proposed with apparently similar duopoly models based on repeated best reply dynamics with naïve expectations and adaptive adjustment. The contents of this Chapter is an adaptation of the paper "A dynamic marketing model with best reply and inertia" by Gian Italo Bischi and Lorenzo Cerboni Baiardi in the journal *Chaos, Solitons and Fractals*, (2015), see [60].

In Chapter 3 the view point on economic modeling is enlarged to critically discuss about assumptions of synchronization of economic agent allowing the description in terms of a representative one stressing the role of heterogeneities even when these are very small. In particular some nonlinear discrete-time dynamic model (proposed in the literature to represent marketing competition are considered and used to critically discuss the statement, often made in economic literature, that identical agents behave identically and quasi-identical ones behave in a similar way. Through examples and some general mathematical statements, it will be shown that the one-dimensional model of a representative agent, whose dynamics summarize the common behavior of identical interacting agents, may be misleading. In order to discuss these topics some simple methods for the study of local stability and bifurcations are employed, as well as numerical examples where some results taken from the literature on chaos synchronization are applied to two-dimensional marketing models that exhibit riddling, blowout and other global phenomena related to the existence of measure-theoretic attractors. The contents of this Chapter is an adaptation of the paper "Fallacies of composition in nonlinear marketing models" by Gian Italo Bischi and Lorenzo Cerboni Baiardi in the journal *Communication in nonlinear science and numerical simulation*, (2015), [61].

In particular Chapter 4 deals with a discrete time version of the model proposed by Lamantia and Radi (2015) [89], to describe a fishery where a population regulated by a logistic growth function is exploited by a pool of agents that can choose, at each time period, between two different harvesting strategies according to a profit-driven evolutionary selection rule. The resulting discrete dynamical system, represented by a two-dimensional nonlinear map, is characterized by the presence of invariant lines on which the dynamics are governed by one-dimensional restrictions that represent

pure, i.e. adopted by all players, strategies. However, interesting dynamics related to interior attractors, where players playing both strategies coexist, are evidenced by analytical as well as numerical methods that reveal local and global bifurcations. The contents of this Chapter is an adaptation of the paper "On a discrete-time model with replicator dynamics in renewable resource exploitation" by Gian Italo Bischi, Lorenzo Cerboni Baiardi and Davide Radi in *Chaos, Solitons and fractals*, (2015), see [59].

In Chapter 5 a 3-D evolutionary model of oligopoly competition in which economic agents can select between different behavioral rules to make decisions on productions, is considered. We state the model as a general class of evolutionary oligopoly games and then we consider an example with two specific rules, namely Local Monopolistic Approximation and Gradient dynamics. We provide several results on the global dynamic properties of the model, showing that in some cases the attractor of the system may belong to an invariant plane where only one behavioral rule is adopted (homomorphic state). The attractors on the invariant planes can be either strong attractors or weak attractors. However, we also explain why the system can be in a state of *Evolutionary Stable Heterogeneity*, where it is more profitable for the agents to employ both heuristics in the long term (polymorphic state). The contents of this Chapter is an adaptation of the paper "Evolutionary competition between boundedly rational behavioral rules in oligopoly games" by Lorenzo Cerboni Baiardi, Fabio Lamantia and Davide Radi in *Chaos, Solitons and fractals*, (2015), see [87].

Finally, in Chapter 6 an adaptive nonlinear feedback controller is designed based on reinforcement learning techniques implemented through a neural network applied to a coupled two-pendulum system in order to improve stability and performance of classical PID linear feedback. The reinforcement learning controller learns how to act on the system being trained on estimations of dynamical states time series of the physical system searching among feedback actions which maximize the expected future discounted rewards. The training process leads the reinforcement learning controller to build the state-action value function which approximates the solution of the optimality Bellman equation of the system and which provides the actions' selection mechanism in order to drive the system towards its reference signal. This kind of controller improves performances in particular when the available model of the real plant is wrong, a circumstance that reduces benefits of optimal control design, and provides superior limits for feedbacks when so are the actions.

Chapter 2

Case study: a dynamic marketing model with best reply and inertia

2.1 Introduction

An important stream in the literature on dynamic models in marketing is based on *market share attraction models*, where several firms selling the same good (or more generally homogeneous goods) are competing in a market with a given sales potential, and each firm has to decide its marketing effort in order to maximize (or at least increase) its market share (see e.g. [40], [70], [91], [68], [105]). Here is considered the discrete-time dynamic model proposed by Farris et al. [105] where, at each time step t, in order to decide their marketing effort at time $t+1$, the firms solve an optimization problem to maximize their expected profits. However, their information set is limited as they do not know the effort decisions of their competitors and their are assumed to adopt naïve expectations about competitors' choices, i.e. they guess that marketing efforts will be the same as in the current period. The resulting model, denoted as Best Response with naïve expectations, is well known in the literature since the pioneering work of Cournot (1838) on mathematical modeling of oligopolies (see [37] or any standard textbook on oligopoly modeling). As suggested in [105], as well as by several other authors, see e.g. [107], [69], the awareness of the systematic error in the assumption of naïve expectations, as well as the difficulties to change the marketing policy, may induce the firms to adopt a compromise (a convex combination) between the computed best response and the previously adopted efforts, a form of inertia or anchoring attitude. This leads to the adaptive adjustment model considered in what follows. The analysis of this model given in [105] is mainly focused on the case of n homogeneous firms, i.e. characterized by identical parameters, in order to study the

relation between market stability and the number of firms, by taking the number n as a bifurcation parameter in a one-dimensional model that summarizes the common behavior of the identical firms. Here a complementary approach is followed, in the sense that just two firms competing in the same market are considered in order to stress the effects of heterogeneities, i.e. how the differences between the parameters, that characterize the dynamic behavior of the two firms, influence the equilibrium points, their stability and bifurcations, as well as the global dynamic scenarios of the model.

A rich spectrum of dynamic behaviors arising from the two-dimensional discrete-time model exhibits under different parameters' constellations is worth to be studied, in particular in regions of parameters' space where heterogeneity between the two firms may play an important role. Analytical results can be easily proved for the model obtained under assumptions of some (not all) identical parameters. Moreover, even if numerical explorations are necessary in order to investigate the global properties of the model with arbitrary parameters' values, some general statements can still be given and may stimulate further studies concerning both the economic and the mathematical properties of the model.

The plan of the present Chapter is as follows. In Section 2.2 the economic model is described and it is written in the form of two-dimensional map with a simple mathematical structure. In Section 2.3 existence and stability of equilibrium points is proved for the case with identical efforts' effectiveness and different inertia of firms, and some numerical simulations are given to confirm and extend the analytical results. In Section 2.4 a complete analytical study of the existence of equilibrium points is given for arbitrary values of the parameters, and some numerical simulations are provided in order to characterize the role of marketing efforts on the dynamic properties of the model. Section 2.5 concludes.

2.2 The model

Let consider n firms that sell homogeneous goods in a market with sales potential B (in terms of overall customers' market expenditures, also denoted as *market contribution* MC by some authors, see e.g. [105]), and let $A_i(t)$, $i = 1, ..., n$, denote the attraction of customers to firm i at time period t, where $t \in \mathbb{N}$ denotes an event-driven discrete time variable. The key assumption in marketing literature is that the market share for

firm i at time t is given by

$$s_i(t) = \frac{A_i(t)}{\sum_{j=1}^{n} A_j(t)} \tag{2.1}$$

If x_i denotes marketing spending of firm i, following [91], see also [105], we assume that attraction is given by

$$A_i = a_i x_i^{\beta_i}$$

where the positive constants a_i denote the relative effectiveness of effort expended by the firm i and the parameter β_i denote the elasticity of the attraction of firm (or brand) i with regard to the marketing effort, as $\frac{dA_i}{dx_i}\frac{x_i}{A_i} = \beta_i$. On the basis of these assumptions, the one-period net profit of firm i is given by

$$\Pi_i(t) = Bs_i(t) - x_i(t) = B\frac{a_i x_i^{\beta_i}(t)}{a_i x_i^{\beta_i}(t) + \sum_{j\neq i} a_j x_j^{\beta_j}(t)} - x_i(t) \tag{2.2}$$

In [105] the case of unit elasticities $\beta_i = 1$, $i = 1, ..., n$, is considered and at each time t agents are assumed to decide next period spending $x_i(t+1)$ by solving the optimization problem

$$\max_{x_i} \Pi_i^{(e)}(t+1) = \max_{x_i} \left(B\frac{a_i x_i}{a_i x_i + \sum_{j\neq i} a_j x_j^{(e)}(t+1)} - x_i \right)$$

where $\Pi_i^{(e)}(t+1)$ is the expected profit at time $t+1$ and $x_j^{(e)}(t+1)$ represent the expectation of firm i about firm j spending at time $t+1$ on the basis of the information set of firm i at time t. From the first order conditions $\frac{\partial \Pi_i(t+1)}{\partial x_i} = 0$, one gets

$$x_i(t+1) = \sqrt{B\frac{\sum_{j\neq i} a_j x_j^{(e)}(t+1)}{a_i}} - \sum_{j\neq i} a_j x_j^{(e)}(t+1)$$

Assuming naïve expectations

$$x_j^{(e)}(t+1) = x_j(t)$$

the following dynamic model is obtained

$$x_i(t+1) = R_i\left(\sum_{j\neq i} a_j x_j(t)\right) = \sqrt{B\frac{\sum_{j\neq i} a_j x_j(t)}{a_i}} - \sum_{j\neq i} a_j x_j(t) \tag{2.3}$$

usually denoted as "Best Response" with naïve expectations. Notice that the parameter B is just a scale parameter, that has no influence on the dynamic properties of the model. So, without loss of generality we shall consider $B = 1$ in the following.

In [105] also a different adjustment process is proposed, known as *adaptive adjustment towards best reply*, see also [107], [85], [69], given by

$$x_i(t+1) = (1-\lambda_i)x_i(t) + \lambda_i R_i\left(\sum_{j\neq i} a_j x_j(t)\right) \qquad i = 1, ..., n \tag{2.4}$$

where the constants $\lambda_i \in [0,1]$ represent the attitude of firm i to adopt the best reply, whereas $(1-\lambda_i)$ is the anchoring attitude to maintain the previous spending decision, i.e. a measure of firms' inertia to modify their marketing efforts. The model (2.4) is a generalization of (2.3) because it reduces to it for $\lambda_i = 1$, $i = 1, ..., n$, whereas it tends to complete inertia of firm i, i.e. $x_i(t+1) = x_i(t)$, as $\lambda_i \to 0$. It is straightforward to see that for $\lambda_i \neq 0$, $i = 1, ...n$, the model with inertia (2.4) has the same equilibrium points as the model (2.3). These equilibrium points, being located at the intersections between the two best response functions (2.3), are Nash equilibria. However the presence of inertia influences their stability properties.

In the following is considered the case of two firms, $n = 2$, with the dynamic variables rescaled as

$$x = a_1 a_2 x_1 \ , \quad y = a_1 a_2 x_2 \tag{2.5}$$

so that the dynamic model which will be study assumes the form of the map $T : (x, y) \to (x', y')$ with

$$T : \begin{cases} x' = (1-\lambda_1)x + a_2\lambda_1\left(\sqrt{y} - y\right) \\ y' = (1-\lambda_2)y + a_1\lambda_2\left(\sqrt{x} - x\right) \end{cases} \tag{2.6}$$

where $'$ denotes the unit-time advancement operator, that is, if the right-hand side variables are productions of period t then the left-hand ones represent productions of period $(t+1)$. The same notation will be used in the rest of this thesis. The map (2.6) is defined for nonnegative values of x and y. Starting from a given initial condition $(x_0, y_0) \in \mathbb{R}^2_+$, where $\mathbb{R}^2_+ = \{(x, y) \in \mathbb{R}^2 | x \geq 0 \text{ and } y \geq 0\}$ denotes the set of nonnegative state variables, the iteration of (2.6) generates an infinite sequence of states, or a *trajectory*

$$\left\{(x_t, y_t) = T^t(x_0, y_0), t = 1, 2, ...\right\} \tag{2.7}$$

provided that (x_0, y_0), as well as all its images $T^t(x_0, y_0)$ of any rank t, belong to $\mathbb{R}^2_+$. If $a_i \leq 4$, $i = 1, 2$, then the square $S = [0,1] \times [0,1]$ is a trapping region, i.e. trajectories starting inside S remain in it for each $t \geq 0$. However, feasible (i.e. non-interrupted) trajectories can be even obtained for $a_i > 4$ provided that $\lambda_j a_i \leq 4$, $i = 1, 2$, $j = 1, 2$,

$j \neq i$, but this depends on the initial condition, i.e. in this case trajectories starting inside S may be interrupted because of negative values of a dynamic variable. In the following we shall denote unfeasible region the set of points that generate interrupted trajectories and the considered initial conditions will be taken outside such region.

A similar dynamic model has been proposed as a Cournot duopoly model with isoelastic demand and linear cost functions in [107] (see Appendix A for details where is showed that the duopoly model reduces to the present model for $a_1 a_2 = 1$), see also [3] and [1] for a deeper local and global dynamic analysis of such duopoly model. However, despite such apparently similar form of the maps, the dynamic properties of the marketing model (2.6) reveal to be significantly different with respect to duopoly Cournot model with inertia in [107] since it has only one nontrivial equilibrium point that may lose stability via a Neimark-Sacker bifurcation, whereas the former, as it will be showed in the following, may have more than one equilibrium, and different kinds of bifurcations can be observed, such as pitchfork, flip or saddle node bifurcations.

For $\lambda_i \neq 0$ the fixed points of the map (2.6), obtained by imposing the conditions $x' = x$ and $y' = y$, are the real and non-negative solutions of the algebraic system

$$\begin{cases} x &= a_2 \left(\sqrt{y} - y\right) \\ y &= a_1 \left(\sqrt{x} - x\right) \end{cases} \tag{2.8}$$

It is straightforward to see that $E_0 = (0, 0)$ is always a fixed point and a further real positive solution of (2.8) always exists, say $E_1 = (x_1, y_1)$ with $x_1 \in (0, 1)$ and $y_1 \in (0, 1)$. Furthermore, as is proved in the following, a couple of real positive solutions, say $E_2 = (x_2, y_2)$ and $E_3 = (x_3, y_3)$ may exist according to the parameters' values a_1 and a_2.

It is noted that, from (2.2) with the new variables (2.5) and unit elasticities $\beta_i = 1$, the profits assume the form

$$\Pi_1(x, y) = \frac{a_1 x}{a_1 x + a_2 y} - \frac{x}{a_1 a_2}; \quad \Pi_2(x, y) = \frac{a_2 y}{a_1 x + a_2 y} - \frac{y}{a_1 a_2} \tag{2.9}$$

and after some trivial algebra the inequality $\Pi_1 > \Pi_2$ becomes

$$G(x, y) = a_1 x^2 + (a_2 - a_1)\, xy - a_2 y^2 - a_1^2 a_2 x + a_1 a_2^2 y < 0 \tag{2.10}$$

hence the isoprofit curve $G(x, y) = 0$ is an hyperbola with symmetry center

$$(x_c, y_c) = \left(\frac{a_1 a_2^2 \,(3a_1 - a_2)}{(a_1 + a_2)^2}, \frac{a_1^2 a_2 \,(3a_2 - a_1)}{(a_1 + a_2)^2} \right)$$

and asymptotes of slopes a_2 and $-a_1$ respectively. As we shall see, the asymmetric dynamics of the dynamical system (2.6) may converge to different attractors. According to the region in which such attractors are included one or the other firm may gain higher profits. When several different attractors coexist this crucially depends on initial conditions, so a study of the global structure of the basins of attraction gives information about the firm that prevail in the market, in the sense of gaining higher profits.

Before starting to analyze the local and global dynamic properties of the map (2.6) it is worth to notice that it is a *noninvertible map*, because if we compute (x, y) in terms of a given (x', y') by solving the system (2.6) we can get up to four real solutions. i.e. a point can have several rank-1 preimages. Geometrically, the action of a noninvertible map can be expressed by saying that it "folds and pleats" the phase space, because distinct points are mapped into the same point. This is equivalently stated by saying that several inverses are defined that "unfold" the phase space. For a noninvertible map, the phase space can be subdivided into regions Z_k, $k \geq 0$, whose points have k distinct rank-1 preimages (see e.g. [33]). Generally, for a continuous map, as the point $\mathbf{x}'$ varies in $\mathbb{R}^2$, pairs of preimages appear or disappear as it crosses the boundaries separating different regions. Such boundaries, denoted as LC (from the French "Ligne Critique") are defined as sets of points with two merging preimages, located on LC_{-1} (following the notations of [77], [33]). For a differentiable noninvertible map of the plane, the set LC_{-1} is the set where the Jacobian determinant vanishes:

$$LC_{-1} = \left\{(x, y) \in \mathbb{R}^2 | \det \mathbf{J} = 0\right\} \tag{2.11}$$

(see again [77], [33]) where, in our case,

$$\boldsymbol{J}(x, y) = \begin{pmatrix} 1 - \lambda_1 & \lambda_1 a_2 \left(\dfrac{1}{2\sqrt{y}} - 1\right) \\ \lambda_2 a_1 \left(\dfrac{1}{2\sqrt{x}} - 1\right) & 1 - \lambda_2 \end{pmatrix} \tag{2.12}$$

So, we get the following equation for LC_{-1}

$$\left(\frac{1}{2\sqrt{x}} - 1\right)\left(\frac{1}{2\sqrt{y}} - 1\right) = \frac{(1 - \lambda_1)(1 - \lambda_2)}{a_1 a_2 \lambda_1 \lambda_2} \tag{2.13}$$

formed by the union of two disjoint branches, say $LC_{-1} = LC_{-1}^{(a)} \cup LC_{-1}^{(b)}$. Also $LC = T(LC_{-1})$ is the union of two branches: $LC^{(a)} = T(LC_{-1}^{(a)})$ and $LC^{(b)} = T(LC_{-1}^{(b)})$. The branch $LC^{(a)}$ separates the regions Z_0, whose points have no preimages, from the

region Z_2, whose points have two distinct rank-1 preimages. The other branch, $LC^{(b)}$, separates the region Z_2 from Z_4, whose points have four distinct preimages. For further details on noninvertible maps and their anallysis with critic lines see Appendix B.

2.3 The case $a_1 = a_2$

In this section is considered the case of identical effort effectiveness

$$a_1 = a_2 = a \tag{2.14}$$

so that the firms can only differ with respect to their inertia, expressed by the parameters λ_1 and λ_2. Under this assumption the system (2.8) can be analytically solved, and besides E_0 the following fixed points are obtained

$$E_1 = \left(\frac{a^2}{(1+a)^2}, \frac{a^2}{(1+a)^2} \right)$$

located on the diagonal $\Delta = \{(x, y) \in \mathbb{R}^2 | x = y\}$ and, for $a \geq 3$, two further fixed points in symmetric positions with respect to Δ are given by

$$E_2 = \frac{a^2}{2(a-1)^2(a+1)} \left(a - 1 + \sqrt{(a+1)(a-3)},\ a - 1 - \sqrt{(a+1)(a-3)} \right)$$
$$E_3 = \frac{a^2}{2(a-1)^2(a+1)} \left(a - 1 - \sqrt{(a+1)(a-3)},\ a - 1 + \sqrt{(a+1)(a-3)} \right)$$

The local stability of the fixed points is described by the following statement.

Proposition 1. *The fixed point $E_1 \in \Delta$ is locally asymptotically stable for $a < a_p = 3$. At $a = a_p$ a pitchfork bifurcation occurs at which the two fixed points E_2 and E_3 are created and are stable nodes just after the bifurcation. The fixed point $E_1 \in \Delta$ also undergoes a flip bifurcation at $a = a_f \geq 3$, being*

$$a_f = 1 + 2\sqrt{1 + 2\frac{2 - \lambda_1 - \lambda_2}{\lambda_1 \lambda_2}} \tag{2.15}$$

at which a cycle of period 2 is created along Δ*. For* $a > a_h$*, with*

$$a_h = 1 + \sqrt[3]{2\left(\frac{1}{\lambda_1}+\frac{1}{\lambda_2}\right) + 2\sqrt{\left(\frac{1}{\lambda_1}+\frac{1}{\lambda_2}\right)^2 - \frac{16}{27}}} + \\ + \sqrt[3]{2\left(\frac{1}{\lambda_1}+\frac{1}{\lambda_2}\right) - 2\sqrt{\left(\frac{1}{\lambda_1}+\frac{1}{\lambda_2}\right)^2 - \frac{16}{27}}} \tag{2.16}$$

the two fixed points E_2 *and* E_3 *lose stability via a Neimark-Sacker bifurcation.*

Proof. The Jacobian matrix (2.12), with $a_1 = a_2 = a$, computed at the fixed point E_1 becomes

$$\boldsymbol{J}(E_1) = \begin{pmatrix} 1-\lambda_1 & \lambda_1\dfrac{1-a}{2} \\ \lambda_2\dfrac{1-a}{2} & 1-\lambda_2 \end{pmatrix}$$

From its characteristic equation

$$P(z) = z^2 - \mathrm{tr}\boldsymbol{J}\cdot z + \det\boldsymbol{J} = 0$$

where $\mathrm{tr}\boldsymbol{J} = 2-\lambda_1-\lambda_2$ and $\det\boldsymbol{J} = (1-\lambda_1)(1-\lambda_2) - \lambda_1\lambda_2(1-a)^2/4$ are the trace and the determinant of $\boldsymbol{J}(E_1)$ respectively, a sufficient condition for the stability is expressed by the following system of inequalities (known as Schur or Jury's conditions, see e.g. [53], [45], [2])

$$P(1) = 1 - \mathrm{tr}\boldsymbol{J} + \det\boldsymbol{J} > 0\ , \quad P(-1) = 1 + \mathrm{tr}\boldsymbol{J} + \det\boldsymbol{J} > 0\ , \quad 1 - \det\boldsymbol{J} > 0 \tag{2.17}$$

which are equivalent to state that the two eigenvalues are located inside the unit circle of the complex plane. In the present case

$$P(1) = \lambda_1\lambda_2\left(1 - \frac{(1-a)^2}{4}\right) > 0 \text{ for } a < 3$$

$$P(-1) > 0 \ \text{ for } a < a_f$$

$$1 - \det\boldsymbol{J} = \lambda_1 + \lambda_2 - \lambda_1\lambda_2 + \lambda_1\lambda_2\frac{(1-a)^2}{4} > 0\ \forall a,\ \lambda_i \in [0,1]$$

where

$$a_f = 1 + 2\sqrt{1 + 2\frac{2-\lambda_1-\lambda_2}{\lambda_1\lambda_2}}$$

For $a > 3$, the Jacobian matrix (2.12) computed at the two symmetric fixed points $E_2 = (x_2, y_2)$ and $E_3 = (y_2, x_2)$ is the same, and has has complex conjugate eigenvalues

$$z_{1,2} = \frac{1}{2}(2 - \lambda_1 - \lambda_2) \pm \sqrt{(\lambda_1 - \lambda_2)^2 + \lambda_1\lambda_2(-a^3 + 3a^2 + a + 1)}$$

hence they are on the unit circle for $a = a_h$ at which $\det(J(E_2)) = z_1 z_2 = |z_1|^2 = 1$, and exit the unit circle, i.e. $z_1 z_2 = |z_1|^2 > 1$, for $a > a_h$. This completes the proof. ■

Notice that $a_f = a_p = 3$ if and only if $\lambda_1 = \lambda_2 = 1$, i.e. the two firms exhibit no inertia. In this case at $a = 3$ a degenerate bifurcation of codimension 2 occurs at which the fixed point $E_1 \in \Delta$ is transformed from stable node into unstable node and, simultaneously a pair of stable fixed points are created in symmetric positions with respect to the diagonal Δ and a stable cycle of period 2 is created along the invariant diagonal Δ, as well. So, after this bifurcation, three coexisting attractors are present, each with its own basin of attraction (see figure 2.1a, obtained with parameters $\lambda_1 = \lambda_2 = 1$ and $a = 3.03 > a_p$). The particular "rectangular shaped" structure of the basins is a consequence of the fact that for $\lambda_1 = \lambda_2 = 1$ the map (2.6) assumes the form $(x', y') = T(x, y) = (f(y), g(x))$, hence it maps horizontal lines into vertical lines and vice-versa. The properties of attractors and basins of these maps, characterized by the fact that $T^2(x, y) = (f(g(x)), g(f(y)))$ is uncoupled, are studied in [65].

Instead, if $\lambda_1 = \lambda_2 = \lambda < 1$, i.e. the firms are homogeneous with the same degree of inertia, the structure of attractors and basins is still symmetric with respect to the invariant diagonal Δ, but with a more smooth shape. Moreover, from (2.15) it follows that $a_f > a_p = 3$: in this case as the parameter a crosses the bifurcation value a_p, the fixed point E_1 is transformed from a stable node into a saddle point, with local stable set along the invariant diagonal Δ, which becomes a boundary that separates the basin of the two newly born stable nodes E_2 and E_3 (see the situation represented in figure 2.1b, obtained with $\lambda = 0.9$ and $a = 3.3$, i.e. $3 = a_p < a < a_f = 3.\overline{4}$). If the parameter a is further increased across the bifurcation value a_f, at which the flip bifurcation occurs, the saddle point E_1 gives rise to a saddle cycle of period 2 with periodic points along Δ. As a is further increased this saddle cycle gains transverse stability via a subcritical flip bifurcation and this leads to the dynamic scenario represented in figure 2.1c, obtained with $\lambda = 0.9$ and $a = 3.7$. So, at this stage there are again three coexisting attractors, one along Δ (a cycle of period 2) and two steady states in symmetric positions with respect to Δ, each with its own basin of attraction, represented by different gray shades in figure 2.1. Notice that the basins are non connected sets, a phenomenon that can only be observed with noninvertible maps.

With the same parameters λ_i, $i = 1, 2$, the Neimark-Sacker bifurcation occurs at $a_h \simeq 3.71$, according to (2.16) of Proposition 2.3, and the two fixed points E_2 and E_3 become unstable focuses, and they are surrounded by stable closed invariant curves along which quasi-periodic motion occurs. This numerically proves that the Neimark-Sacker bifurcation is supercritical (see figure 2.1d).

It is worth to notice that, from (2.16), it results $a_h \geq 3.645$, as $\left(\frac{1}{\lambda_1} + \frac{1}{\lambda_2}\right) \geq 2$ and being a_h increasing with $\left(\frac{1}{\lambda_1} + \frac{1}{\lambda_2}\right)$.

Up to now we have only been concerned with the time evolution of marketing efforts $x_1(t)$ and $x_2(t)$ of the two firms, related to the rescaled dynamic variables $x(t)$ and $y(t)$ by (2.5). It is now important to consider the time evolution of profits as well. If $a_1 = a_2 = a$ then the condition (2.10), equivalent to $\Pi_1 > \Pi_2$, becomes

$$(x - y)\left(x + y - a^2\right) < 0, \tag{2.19}$$

i.e. the hyperbola $G(x, y) = 0$ degenerates into the pair of orthogonal lines $y = x$ and $y = -x + a^2$, crossing at $(x_c, y_c) = \left(\frac{a^2}{2}, \frac{a^2}{2}\right)$, that divide the phase space into four sectors such that $\Pi_1 > \Pi_2$ in the two sectors above both lines and below both lines, and $\Pi_1 < \Pi_2$ in the other two sectors. At the equilibrium E_1, being $x = y$, the two firms have the same profits, whereas for $a > 3$ at the two equilibrium points E_2 and E_3 the inequalities $\Pi_1 > \Pi_2$ and $\Pi_1 < \Pi_2$ hold respectively. In fact, at E_2 and E_3 we have $x + y = \frac{a^2}{a^2-1} < a^2$, so it is easy to realize that at the equilibrium E_2, characterized by $x > y$ (i.e. firm 1 spends more in marketing efforts) we have $\Pi_1 > \Pi_2$, i.e. firm 1 makes more profits, and vice-versa in the equilibrium E_3. Similar situations are obtained in the case of more complex attractors, located around these equilibria when they are unstable, in the sense that $\Pi_1 > \Pi_2$ when the dynamics occur along attractors located in the region with $x > y$ (i.e. below the diagonal Δ) and vice-versa for attractors in the region $x < y$ (above the diagonal Δ). In fact, for $a > 3$ the line $x + y = a^2$ is outside the region where the asymptotic dynamics of the model take place, so that only the first factor in (2.19) determines the difference between the two profits. Instead, in the case of attractors that include both regions with $x > y$ and $x < y$, time periods with $\Pi_1 > \Pi_2$ alternate with time periods with $\Pi_1 < \Pi_2$.

This occurs, for example, in the case of homogeneous firms when the coexisting chaotic attractors created around the unstable equilibrium points E_2 and E_3 merge and form a unique large chaotic attractor, as shown in fig. 2. In the left panel (figure 2.2a) when the asymptotic motion occurs along the attractor surrounding the equilibrium E_2 then firm 1 makes more profits, and vice-versa for the trajectories converging to

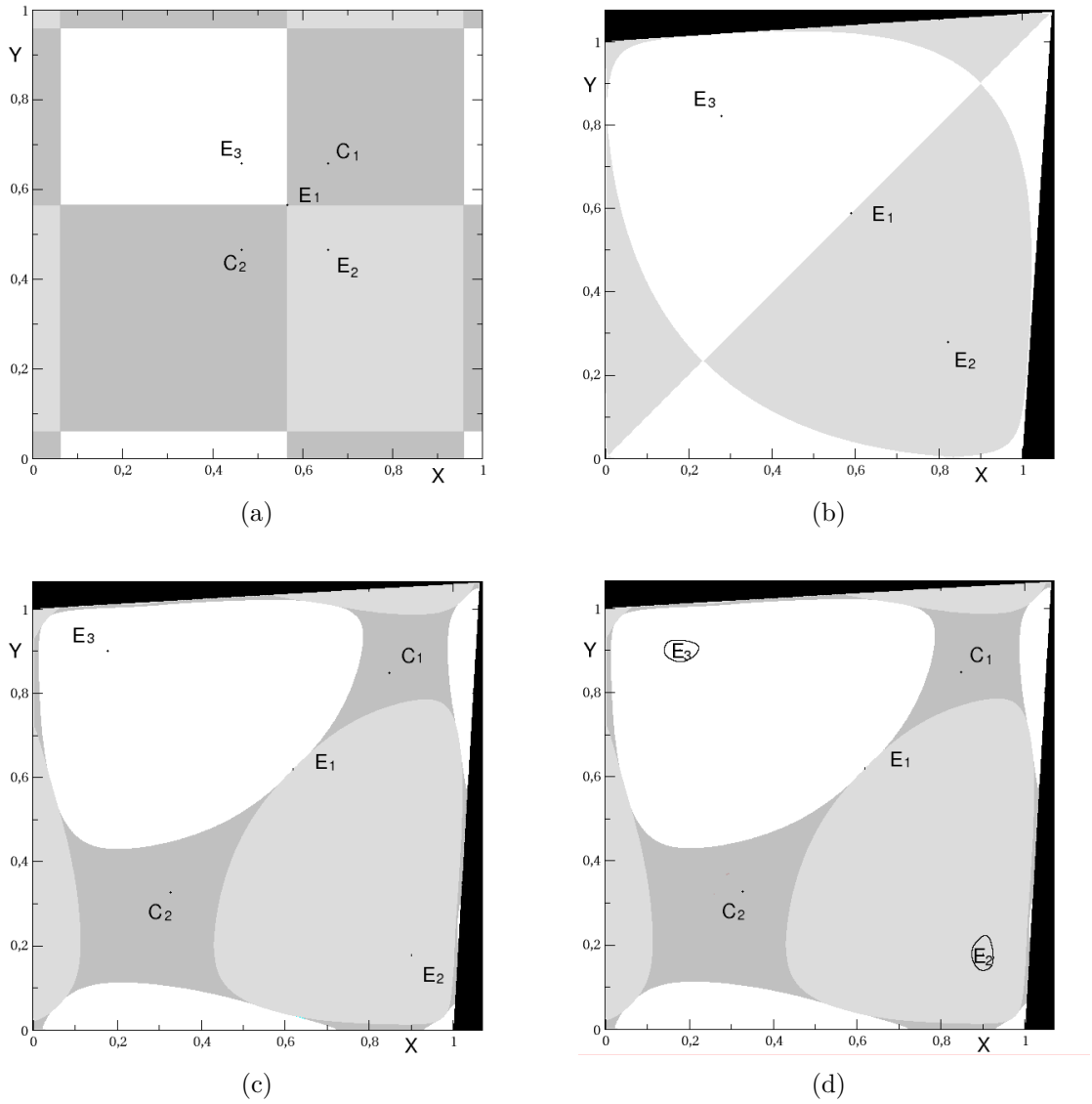

Fig. 2.1 Panel (a): $\lambda_1 = \lambda_2 = 1$ and $a = 3.03 > a_p$, just after the codimension 2 bifurcation at which simultaneous flip and pitchfork bifurcations occur. Panel (b): $\lambda_1 = \lambda_2 = 0.9$ and $a = 3.3$, just after the pitchfork bifurcation: $3 = a_p < a < a_f = 3.\overline{4}$. Panel (c): $\lambda_1 = \lambda_2 = 0.9$ and $a = 3.7$, just after the subcritcal flip bifurcation of the cycle of period 2 along the diagonal. Panel (d): $\lambda_1 = \lambda_2 = 0.9$ and $a = 3.72$, just after the Neimark-Sacker bifurcation of equilibrium points E_2, E_3, being $a_h = 3.71$. The different gray shades represent basins of attraction, wherease the black region represents the initial conditions that generate unfeasible trajectories, i.e. involving negative values of the dynamic variables.

the upper attractor around E_3. After the contact between the two attractors along the diagonal Δ, occurring for increasing values of a, the motion along the unique large

attractor is characterized by alternating time periods with higher profit for one firm or the other one.

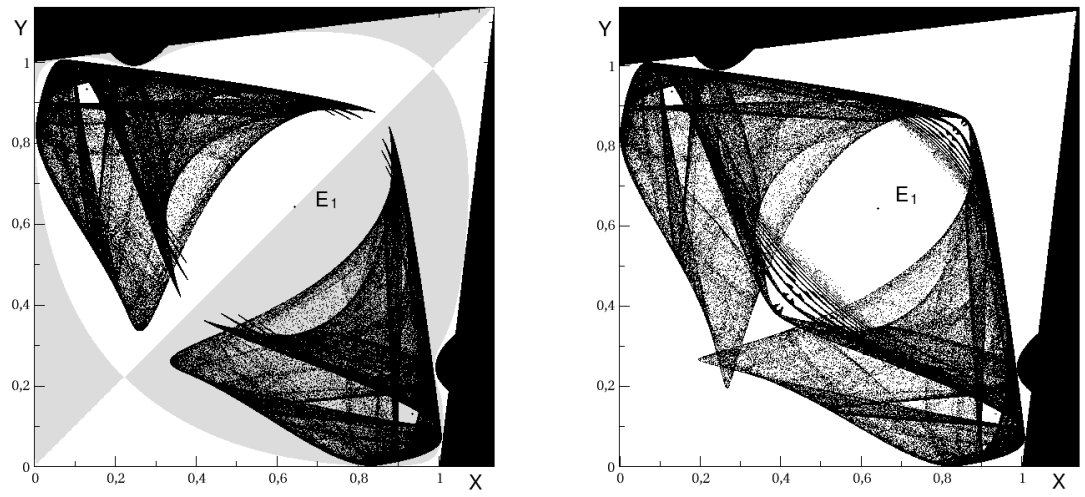

(a) (b)

Fig. 2.2 Panel (a): for $\lambda_1 = \lambda_2 = 0.8$ and $a = 4.05$ two chaotic attractors coexist each with its own basin of attraction. Panel (b): for $\lambda_1 = \lambda_2 = 0.8$ and $a = 4.0565$ a unique symmetric chaotic attractor exists.

However, as stated in the Introduction, in this Chapter we are mainly interested to study the cases of heterogeneous firms. We start by discussing the effects of different inertia, i.e. $\lambda_1 \neq \lambda_2$. As stated at the beginning of this Chapter, the focus will now be turn on the study of heterogeneous firms. Different inertia, i.e. $\lambda_1 \neq \lambda_2$, as source of heterogeneity is investigated first. In this case the diagonal is no longer invariant, i.e. $x = y$ in (2.6) does not imply $x' = y'$. This has a remarkable effect on the shape of the basins, as shown in figure 2.3a, obtained with $\lambda_1 = 0.5$ and $\lambda_2 = 0.7$ (i.e. firm 1 has more inertia in revising efforts than firm 2) and $a = 4$, i.e. just after the Neimark-Sacker bifurcation of E_2 and E_3. In this case the stable set of the saddle point E_1, which constitutes the boundary that separates the two basins of attraction, is folded so that the basin of the attractor below the diagonal, where firm 1 makes more profits, is smaller. Notice that firm 1 is the one with more inertia. In the situation shown in figure 2.3b, obtained again for $a = 4$ but with $\lambda_1 = 0.7$ and $\lambda_2 = 1$ (firm 2 exhibit no inertia, i.e. it moves directly to the computed best reply marketing effort) the two attractors become chaotic, and the basin of attraction of the one surrounding E_2 (characterized by higher profits of firm 1) shrinks further. As it can be seen in figure 2.3b, the chaotic attractor around E_2 is quite close to the basin boundary. Indeed,

if λ_1 is slightly increased, then such a contact occurs, leading to the disappearance of the chaotic attractor around E_2, a global (or contact) bifurcation known as "final bifurcation" (see [33]) or "boundary crisis" (see [32]). After this contact bifurcation the generic trajectory goes to the chaotic attractor around E_3 (see figure 2.3c, obtained with $\lambda_1 = 0.75$, $\lambda_2 = 1$ and $a = 4$). The former chaotic attractor around E_2 is transformed into a chaotic repellor, formed by the dense and unstable set of periodic points that constituted the skeleton of the just disappeared attractor: such chaotic repellor is often denoted as the "ghost" of the attractor, and its presence gives rise to long chaotic transients along the former chaotic attractor before the generic trajectory reaches the other attracting set (now globally attracting).

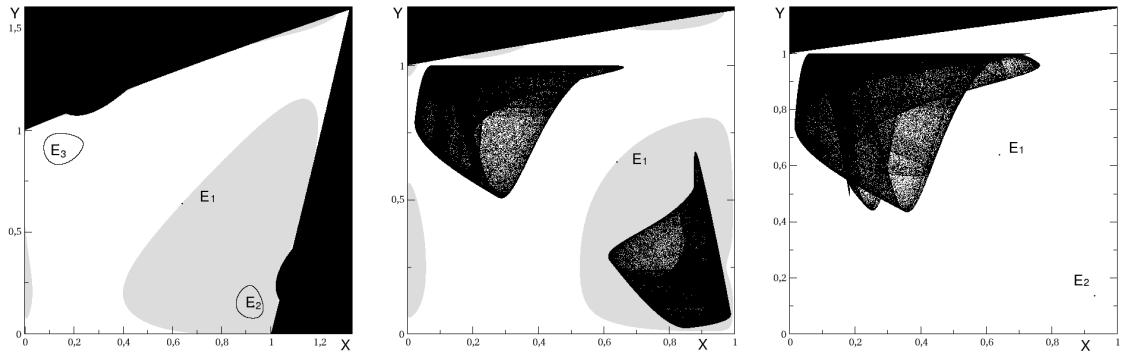

(a) (b) (c)

Fig. 2.3 Panel (a): $\lambda_1 = 0.5$, $\lambda_2 = 0.7$ and $a = 4$. Panel (b): $\lambda_1 = 0.7$, $\lambda_2 = 1$ and $a = 4$. Panel (c): $\lambda_1 = 0.75$, $\lambda_2 = 1$ and $a = 4$. The white and the light gray in (a) and (b) represent the basins of the two coexisting attractors, whereas in (c) the generic trajectory starting from an initial condition in the white region enters the unique (chaotic) global attractor.

In the dynamic scenarios shown in figures 2.3a,b, as well as those in figure 2.1, the feature of non connected basins of attraction is quite evident, a property specific to noninvertible maps which is very important in applications, as it has a strong influence on path dependence. This property is now well known, after the books [77] and [33], as well as many papers and books dealing with applications, see e.g. [109], [68], [66], where the transition between connected and non connected basins is explained in terms of the unfolding action of critical curves. Here is given just a short qualitative explanation, based on the fact that in the context of noninvertible maps it is useful to define the *immediate basin* $\mathcal{B}_0(A)$, of an attracting set A, as the widest connected

component of the basin which contains A. Then the total basin can be expressed as

$$\mathcal{B}(A) = \bigcup_{n=0}^{\infty} T^{-n}(\mathcal{B}_0(A))$$

where $T^{-n}(x)$ represents the set of all the rank-n preimages of x, i.e. the set of points which are mapped in x after n iterations of the map T. The backward iteration of a noninvertible map *repeatedly unfolds* the phase space, and this implies that the basins may be non-connected, i.e. formed by several disjoint portions. As recalled at the end of Section 2.2, each branch of critical curve $LC = T(LC_{-1})$ separates regions of the phase plane characterized by different numbers of preimages. So, if a portion of a basin, after a contact with a critical curve, enters the region Z_k characterized by a higher number of preimages, then the extra preimages created after the contact may form a nonconnected portion of the basin.

On the basis of these arguments, in figure 2.4 is showed how the creation of a nonconnected portion of a basin for the map (2.6) can be explained in terms of a contact between the immediate basin and a branch of critical curve $LC = T(LC_{-1})$, where LC_{-1} is given by (2.13). In figure 2.4a, obtained for $\lambda_1 = 0.4$ and $\lambda_2 = 0.6$, with $a = 3.2$, the two equilibria E_2 and E_3 are stable focuses, with the stable set of E_1 that separates the two basins, represented by light gray and white respectively. When λ_1 is increased from 0.4 to 0.5 the boundary of the light gray basin of E_2 has a contact with LC and a portion of it enters the region Z_4. This gives rise to the creation of a new non connected portion of the same basin, formed by the union of the two further preimages merging along LC_{-1}, of the portion of the basin that entered the region Z_4 after the contact.

To sum up, by tuning the different values of the inertia parameters λ_1 and λ_2, with a fixed common value of marketing effectiveness a, both the kind of attractors and the structure of the basins can be strongly influenced.

2.4 The general case

In this Section is considered the further source of heterogeneity results from relaxing the assumption (2.14) of identical effort effectiveness, i.e. $a_1 \neq a_2$, so that the two firms can differ both for their effort effectiveness and for their inertia. Unfortunately the simple analytical expression of the fixed points obtained in the previous section is lost, however the following general result concerning their existence can be given.

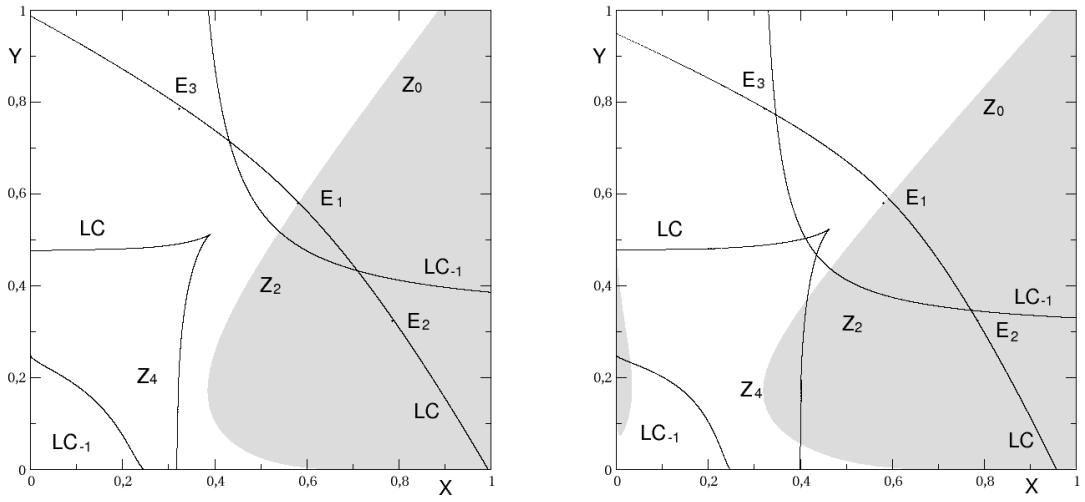

Fig. 2.4 Panel (a): $\lambda_1 = 0.4$, $\lambda_2 = 0.6$, $a = 3.2$. Panel (b): $\lambda_1 = 0.5$ with the other parameters at the same value as in (a).

Proposition 2. *Besides $E_0 = (0,0)$ a non vanishing fixed point always exists in the region $S = (0,1) \times (0,1)$. If $a_1 a_2 \neq 1$ then two further distinct fixed points exist in the region S if the following inequality holds*

$$D(a_1, a_2) = \frac{a_1^2 a_2^4}{108\,(1 - a_1 a_2)^6} \left[27 + a_1 a_2\,(4a_1 + 4a_2 - 18) - a_1^2 a_2^2\right] < 0 \tag{2.20}$$

and if $D(a_1, a_2) = 0$ these two further fixed points are merging, i.e. there are two real coincident solutions of (2.8). In the particular case $a_1 a_2 = 1$ the unique fixed point $E = \left(\frac{1}{(a_1+1)^2}, \frac{1}{(a_2+1)^2}\right)$ is get.

Proof. The algebraic system (2.8), whose solutions are the fixed points of the map (2.6), can be rewritten as

$$\begin{cases} \zeta - \dfrac{1 - a_1 a_2}{a_2}\eta^2 - a_1 \eta = 0 \\ \eta \left[\dfrac{(1 - a_1 a_2)^2}{a_1 a_2}\eta^3 + 2\,(1 - a_1 a_2)\,\eta^2 + a_2\,(a_1 + 1)\,\eta - a_2\right] = 0 \end{cases} \tag{2.21}$$

where $\eta = \sqrt{x}$ and $\zeta = \sqrt{y}$. The roots of the third degree polynomial inside square brackets can be found by Cardano's formula. In fact it can be written as

$$\xi^3 + p\xi + q = 0$$

with $\xi = \eta + \dfrac{2a_1a_2}{3\left(1-a_1a_2\right)}$ and coefficients

$$p = a_1a_2^2\frac{3-a_1}{3\left(1-a_1a_2\right)^2}\ ,\quad q = \frac{a_1a_2}{27\left(1-a_1a_2\right)^3}\left(-27a_2+9a_1a_2^2-2a_1^2a_2^2\right)$$

and the condition for the existance of three real solutions is given by $D = q^2/4+p^3/27 < 0$ (see e.g. [115]), that is readily transformed in the form (2.20). In particular, if $a_2 = 1/a_1$ then the system (2.21)

$$\begin{cases} \zeta - a_1\eta &= 0 \\ \dfrac{\eta}{a_1}\left[\left(a_1+1\right)\eta - 1\right] &= 0 \end{cases}$$

from which the unique non vanishing solution is $\eta = (a_1+1)^{-1}$, $\zeta = a_1(a_1+1)^{-1} = (a_2+1)^{-1}$, and, consequently, $x = \eta^2 = (a_1+1)^{-2}$, $y = \zeta^2 = (a_2+1)^{-2}$.

Finally, the fact that the real solutions (x, y) of (2.8) are inside the region S follows easily from direct inspection of (2.8). In fact, if $y < 0$ then from the second equation x cannot assume a real value, and analogously if $x < 0$ then y cannot be real; if $y > 1$, then from the first equation $x < 0$, which is a contradiction according to the argument given above. ■

The graph of $D(a_1, a_2) = 0$ in the parameters' plane (a_1, a_2), shown in figure 2.5, is symmetric with respect to the diagonal $a_1 = a_2$ as $D(a_1, a_2) = D(a_2, a_1)$, and is formed by two smooth branches joining at the cusp point located in $a_1 = a_2 = 3$. If the two parameters are below the line $a_1 + a_2 = 6$ then only one equilibrium can exist.

Notice that the particular case $a_1a_2 = 1$ corresponds to the duopoly model with isoelastic demand proposed in [107] (see the Appendix A). This model is obtained only in a subset of zero measure in the parameters' plane (a_1, a_2), represented by the dotted curve in figure 2.5, which is entirely included inside the region R_1 where only one equilibrium exists.

If the values of the parameters a_1 and a_2 are allowed to change in the portion of the parameters' plane with $a_1 + a_2 > 6$ a saddle-node bifurcation occurs when a smooth branch of the curve $D = 0$ is crossed, i.e. two equilibrium points are created as the branch is crossed towards the region R_3 bounded by the two branches. Whenever the parameters (a_1, a_2) are located along a branch of $D = 0$ two merging equilibria exist, that split inside the region characterized by $D(a_1, a_2) < 0$ (denoted by R_3 in figure 2.5) giving rise to a stable node and a saddle point, whose stable set represents the boundary of the basin of the stable node. Instead, at the cusp point three merging equilibria are obtained, and if the parameters (a_1, a_2) enter region R_3 across the cusp

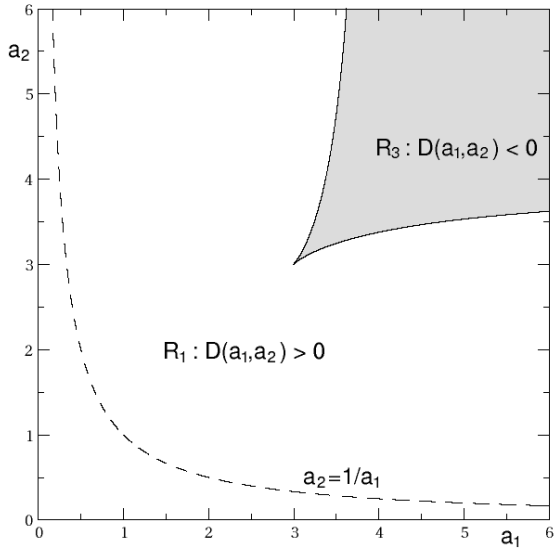

Fig. 2.5 In the parameters' plane (a_1, a_2) the region R_1 (white), where one non trivial equilibrium point exists, and the region R_3 (light gray), where three non trivial equilibrium points exist, are shown. R_1 and R_3 are bounded by the curve $D(a_2, a_2) = 0$. The dotted line is the curve $a_2 = a_1^{-1}$.

point $(3, 3)$ then a pitchfork bifurcation occurs according to Proposition 1. Three bifurcation diagrams are shown in figure 2.6, obtained when the parameters (a_1, a_2) are varied along the paths shown in the small pictures reported inside. As it can be seen in panels (a) and (b) the saddle-node bifurcations, at which pairs of equilibrium points are created or destroyed, give rise to typical hysteresis effects. Instead, the bifurcation path shown in panel (c), across the cusp point, gives rise to the typical pitchfork bifurcation already discussed in the previous Section.

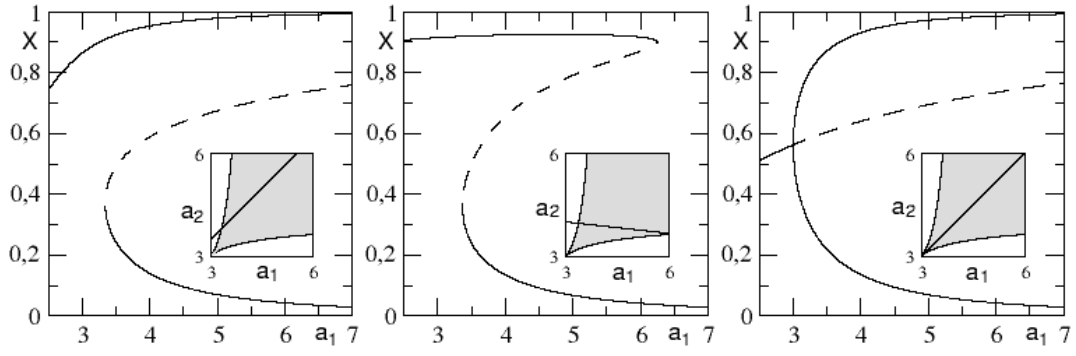

Fig. 2.6 Three bifurcation diagrams when the parameters (a_1, a_2) are varied along the paths shown in the small pictures reported inside.

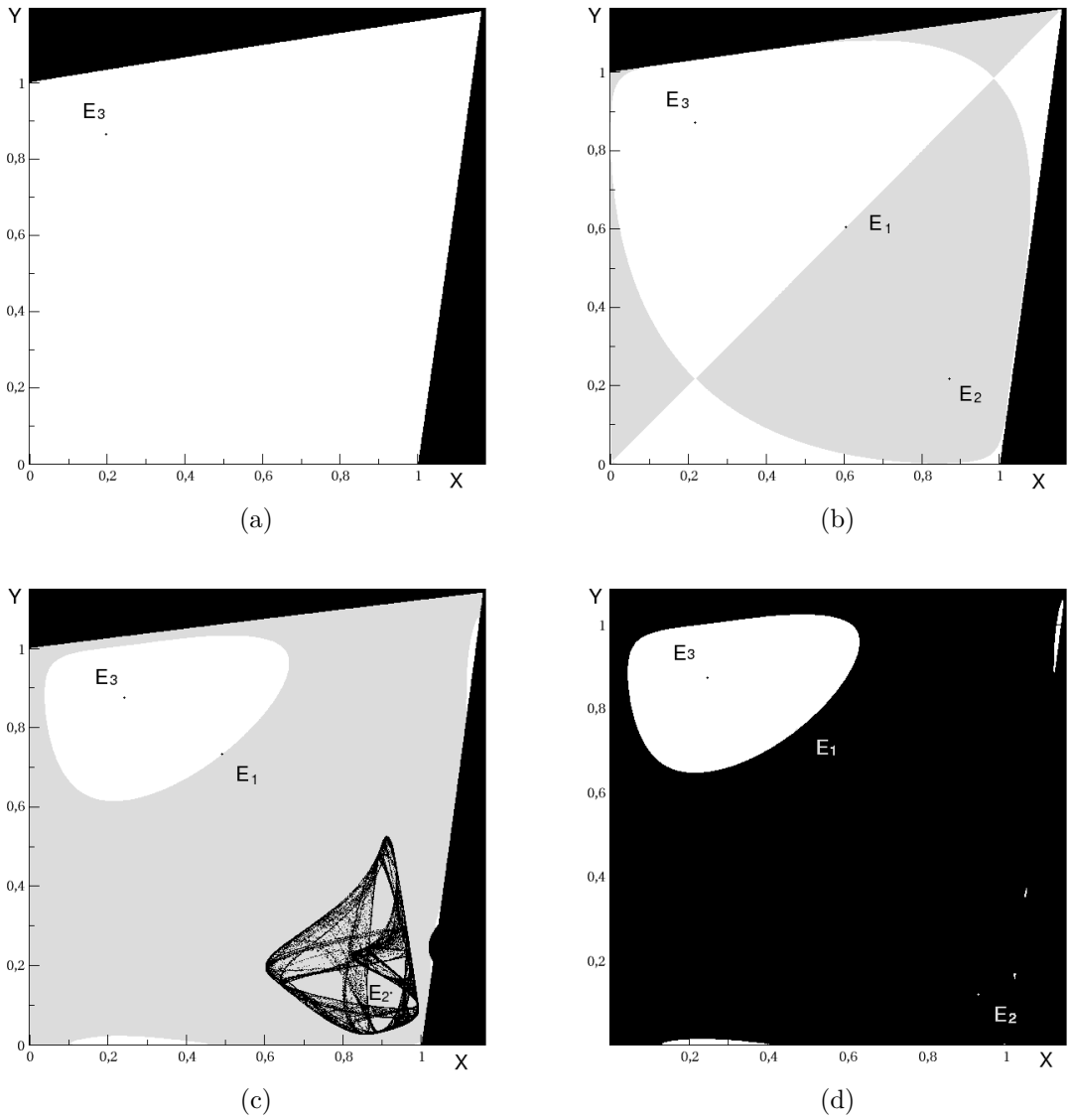

Fig. 2.7 $\lambda_1 = \lambda_2 = 0.8$, $a_1 = 3.5$. In panel (a) $a_2 = 3$; in (b) $a_2 = 3.5$, in (c) $a_2 = 4$; in (d) $a_2 = 4.1$. The white region is the basins of the upper attractor, the light gray region is the basin of the lower attractor, whereas the black region represents the set of points that generate unfeasible trajectories (i.e. entering the negative orthants).

Some numerical explorations are performed in order to discuss the role of the parameters a_1 and a_2 on the dynamic scenarios of the model. Let first consider a sequence of numerical simulations obtained with identical inertia parameters $\lambda_1 = \lambda_2 = 0.8$, starting from a simple dynamic situation, obtained for $a_1 = 3.5$ and $a_2 = 3$, characterized by a unique globally stable equilibrium, denoted by $E_3 = (0.196, 0.864)$ in figure 2.7a. As a_2 is increased a couple of further equilibrium points, say E_1 and

E_2, is created through a saddle-node bifurcation, the stable set of the saddle E_1 being the boundary that separates the basin of the two attracting equilibria E_2 and E_3. The symmetric case with $a_1 = a_2 = 3.5$ is shown in figure 2.7b. As the parameter a_2 is further increased, the equilibrium point E_2 loses its stability via a supercritical Neimark-Sacker bifurcation at which a stable closed invariant curve is created, which is transformed into a chaotic attractor as a_2 increases more and more, see figure 2.7c obtained with $a_2 = 4$. If a_2 is further increased then the chaotic attractor enlarges until it has a contact with the boundary that separates its basin with the set of unfeasible trajectories, i.e. the set of points that generate trajectories involving negative values, existing outside the phase space $S = [0, 1] \times [0, 1]$. At this contact a final bifurcation (or boundary crisis) occurs and, as already described in the previous Section, after this contact the generic trajectory starting outside the basin of E_3, is an interrupted path leading to negative values (one firm stops marketing efforts, i.e. it exits the market) as shown in figure 2.7d. To sum up, two contrasting effects are obtained by increasing the effort effectiveness a_2 of firm 2: it first leads to the creation of a second attractor and then it leads to its destruction.

A similar effect is obtained when different levels of inertia are considered, like in the sequence of numerical simulations shown in figure 2.8 obtained with $\lambda_1 = 0.9$ and $\lambda_2 = 0.7$. In this case the initial dynamic scenario, obtained for $a_1 = 4$ and $a_2 = 3$, is given by the presence of a unique equilibrium, say $E_3 = (0.12, 0.91)$, which is an unstable focus surrounded by a stable periodic cycle of period 5 (five periodic points located along an invariant closed curve) which is a global attractor, i.e. it attracts the generic initial condition in the square $S = [0, 1] \times [0, 1]$. As a_2 increases, a saddle-node bifurcation occurs at which the two equilibrium points E_1 (saddle) and E_2 (stable node) are created, as shown in figure 2.8b obtained with $a_2 = 3.4$. Just after the saddle-node bifurcation the basin of E_2 is very small, being it bounded, as usual, by the stable set of E_1. However this basin, or the basin of the attractor around the originary fixed point, enlarges more and more when a_2 is further increased, as shown in figure 2.8c obtained for $a_2 = 3.8$. This is a remarkable global phenomenon, that cannot be revealed through a linear approximations around the attracting sets, and can generally be detected by computer-aided analysis. Also in this case, like in the sequence of numerical simulations analyzed in figure 2.7, as a_2 is further increased the attractor around the equilibrium E_2 becomes chaotic, and its size increases until its has a contact with the basin of unfeasible trajectories at which it disappears, i.e. it is transformed into a chaotic repellor that influences the chaotic transient before the trajectories are interrupted.

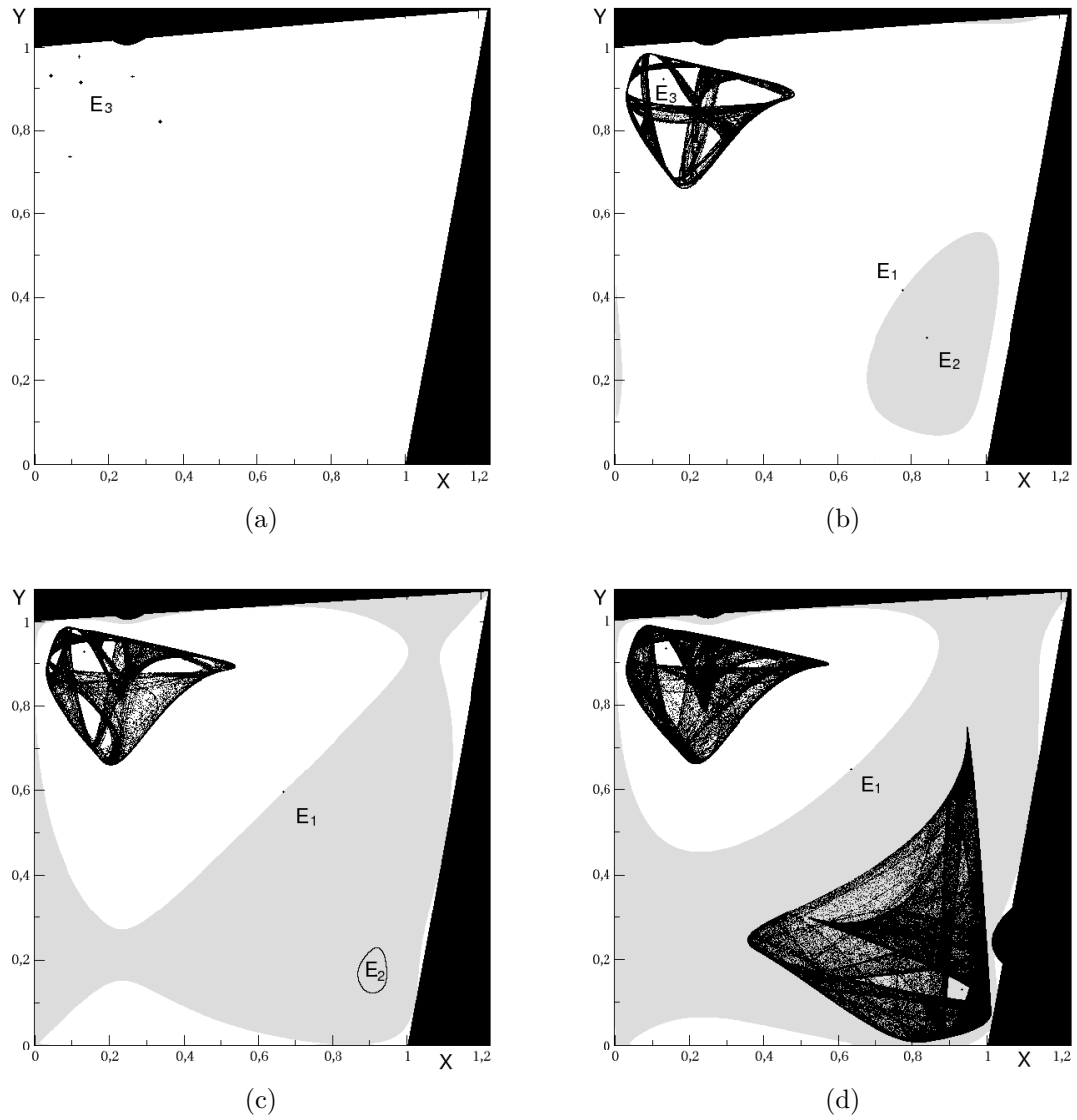

Fig. 2.8 $\lambda_1 = 0.9$, $\lambda_2 = 0.7$, $a_1 = 4$. In panel (a) $a_2 = 3$; in (b) $a_2 = 3.4$; in (c) $a_2 = 3.8$; in (d) $a_2 = 4.05$. The white region is the basins of the upper attractor, the light gray region is the basin of the lower attractor, whereas the black region represents the set of points that generate unfeasible trajectories (i.e. entering the negative orthants

2.5 Conclusions

To conclude it can be stated that the role of heterogeneities on the existence, stability and structure of the basins of attraction have been stressed through analytical results and numerical analysis. An analytic study of the existence and stability properties of equilibrium points has been given, showing how local and global bifurcations are

influenced by differences in the parameters measuring inertia (or prudence) of firms, as well as differences in the relative effectiveness of effort. In particular, it has been shown that increasing inertia often leads, as expected, to more stability of the steady states. However the basin of attraction of the attractor where the profit of the firm with increasing inertia is higher shrinks, up to causing the disappearance of the attractor through final bifurcations (or boundary crisis). Similar phenomena occurs when the parameters that represent marketing efforts effectiveness are increased. These parameters give rise to hysteresis phenomena due to the occurrence of saddle node bifurcations at which couples of steady states are created or destroyed. Moreover, a gradual increase of one of these effort efficiency parameters first cause the creation of a coexisting attractors, and then its disappearance, when it becomes too large, due to a contact bifurcation with the set of points that generate unfeasible trajectories.

The global bifurcations leading to the creation of non connected basins of attraction are discussed, and their meaning in terms of strong path dependence is stressed. The role of heterogeneities has been stressed both in stability properties and in the structure of the basins, as well as the relations between symmetry properties and bifurcation scenarios. A global study of the basins' structure is crucial to forecast which firm will prevale in the market in the sense of gaining higher profits. In fact, the dynamic complexities shown in our analysis include coexistence of attractors of different kinds (steady states, periodic cycles, quasi-periodic and chaotic motions) on which firms have different profits in the long run, with topologically complicated structures of the basins, due to noninvertibility of the discrete dynamical system. This gave us the possibility to stress how the discrete dynamical system considered is quite interesting even from the mathematical point of view. Moreover, the comparison with the (apparently) very similar model proposed in [107] as a discrete-time model of a duopoly game with isoelastic demand function, allowed us to stress that the latter is a quite particular subclass of the marketing model considered here, and consequently the dynamic scenarios analyzed in the marketing model are much richer than the ones observed in the literature for that duopoly game.

Chapter 3

Critique study: fallacies of composition in nonlinear marketing models

3.1 Introduction

"*The conventional assumption made in macroeconomic theory is that there are many identical agents, whose behavior is summarized by that of the representative agent*". This sentence, taken from [124], expresses a quite evident property provided that the economic agents are truly identical, i.e. characterized by the same features and identical starting conditions. Indeed, the concept of representative agent is widely used (even abused) in economic modeling (see e.g. [49], [82], [124], [93]). Moreover, a stream of literature exists where the common time evolution of n identical agents is reduced to a one-dimensional dynamic model that summarizes the common aggregate behavior of the n agents, and their numerosity n is taken as a bifurcation parameter, so that the relation between stability and the number of agents is studied (see e.g. [119] and [69] in oligopoly theory, [105] in marketing modeling). This is a classical issue in ecological modeling as well, where the trade-off between the number of species and ecosystem stability is often considered (see e.g. [97]). Analogously, in economics the relation between market stability and the number of firms producing homogeneous goods is often considered.

However, it's quite evident that the assumption of agents with absolutely identical features and identical starting conditions is not generic, one may say a zero probability event, as in real systems one can at most say that agents are practically identical,

or almost identical or quite similar and so on. Of course, economists are aware of this difficulty, and in fact statements like the following are very common (we quote again [124]) "*although simple examples can be constructed wherein the preferences of the aggregate might misrepresent those of diverse agents, it has not been established that this is a significant problem in the analysis of macroeconomic shocks. (...) Unless the agents have very different characteristics, it seems reasonable to expect that each individual will respond to aggregate macroeconomic shocks hitting the general economy in more or less the same qualitative way (though not necessarily identically), in which case the aggregate should behave in a qualitative similar way as well*". In other words, unless the agents have very different characteristics, it seems reasonable to expect that each individual will behave in more or less the same qualitative way (though not necessarily identically) so that the behavior of the aggregate system is still sufficiently well summarized by the behavior of the representative agent. However, this point has been recently criticized by some authors ([82], [117], [10], [58]).

A more formal statement of the problem is the following. If the time evolution of an economic system with several interacting agents is represented by an n-dimensional dynamical system, when the agents are identical, i.e. they are characterized by identical parameters, then the dynamical system becomes symmetric in the sense that it remains the same by interchanging the agents. This symmetry property implies that an invariant one-dimensional subspace exists, corresponding to the obvious statement that identical agents, starting from identical initial conditions, behave identically for each time, i.e. if n identical agents start from identical initial conditions, say $x_1(0) = x_2(0) = ... = x_n(0)$, then their dynamic behavior will be characterized by $x_1(t) = x_2(t) = ... = x_n(t)$ for each $t \geq 0$. Such synchronized dynamics are governed by a one-dimensional dynamical system, given by the restriction of the n-dimensional system to the invariant subspace on which the synchronized dynamics occur, which can be seen as the model of a representative agent, whose dynamic behavior summarizes the common behavior of the identical agents (see e.g. [58], [95]).

The main goal of the work presented in this Chapter is to show, through some examples and some general mathematical statements, that the one-dimensional restriction may be quite misleading. In order to support this claim two kinds of arguments are used. First are showed some examples, taken from the literature, where, due to algebraic simplifications or mathematical cancellations along the invariant submanifold, the dynamic properties of the one-dimensional system may be completely different from those of the complete model. In those cases it can happens that highly nonlinear models with very complicated dynamic behaviors may dramatically collapse into a trivial linear

dynamic model when identical agents are considered. Further, models based on similar kinds of dynamic interactions, which exhibit similar dynamic behaviors, give rise to quite different kinds of dynamic qualitative behaviors when the assumption of identical agents is imposed and the corresponding restrictions are considered.

The second argument consists in investigating the question of the effects of small heterogeneities, i.e. small deviations from the condition of identical agents, on the basis of a stream of literature on symmetric dynamical systems (see [30] and references therein). Indeed, even in the case of identical agents, if their time paths start from slightly different initial conditions they may not synchronize in the long run, so that their asymptotic behaviors become very different from the one expected according to the model of representative agent. Moreover, a slight modification of the parameters with respect to the symmetric situation, may lead to a qualitatively different dynamic evolution (see e.g. [110], [12], [114], [132]). In other words, the destruction of the invariant submanifold, on which synchronized dynamics takes place, implies that the attractors that characterize the long-run behavior of the one-dimensional model of the representative agent are substituted by new attractors that may be very different from those existing when symmetry is present.

Even if the examples here considered are taken from the literature on dynamic marketing models, the results obtained can be applied to a broad class of multi-agent dynamic models in economics and social sciences with interacting agents, as well as in ecological models of interacting species sharing the same (or similar) ecological niche, or more generally in physical and engineering systems where identical or almost identical coupled nonlinear oscillators are represented.

The plan of the present Chapter is as follows.

In Section 3.2 are considered three different kinds of adaptive adjustment models, proposed in the literature to represent market share attraction of firms which compete in the market and it is showed that even if the models with heterogeneous interacting firms exhibit similar properties, in the symmetric case of identical firms starting from identical initial conditions, whose dynamics are governed by the restrictions to invariant subspace where synchronized dynamics occur, the dynamic properties are quite different and in some cases even misleading.

In Section 3.3.2 we focus on two of the dynamic marketing models examined in section 3.2, the one proposed in [105] and studied in Chapter 2 and one proposed in [68] (see also [63], [95]) with two interacting firms, and is analyzed what happens in the case of identical firms starting from slightly different initial conditions as well as in the case of slight differences in one parameter.

Section 3.4 concludes.

Some details on the study of local stability and bifurcations of the steady states of models considered in the Chapter are given in the Appendix C, whereas in the Appendix D a short overview of some recent results about chaos synchronization and related phenomena is reported.

3.2 Some examples of representative firm dynamics in marketing models

In this Section are considered three different n-dimensional dynamic marketing models belonging to the class of market share attraction models. Let consider n firms that sell homogeneous goods in a market with sales potential B, from the standard assumptions in marketing modeling the one-period net profit of the i-th firm results to be given by

$$\Pi_i(t) = Bs_i(t) - x_i(t) = B\frac{a_i x_i^{\beta_i}(t)}{a_i x_i^{\beta_i}(t) + \sum_{j\neq i} a_j x_j^{\beta_j}(t)} - x_i(t) \tag{3.1}$$

where $i = 1, ..., n$. Here is reminded that s_i is the market share for firm i, x_i denotes the marketing spending of firm i, the positive constants a_i denote the relative effectiveness of effort expended by the firm i and the parameters β_i denote the elasticity of the attraction of firm i with regard to its marketing effort. For further details see Section 2.2 of Chapter 2 and the cited bibliography.

The models considered in the following differ only in the adaptive methods used by firms to decide next period efforts, being these methods based on the same profit function (3.1). The models are then similar since derive from similar adaptive adjustment processes and exhibit similar dynamic behaviors (at least in the two-dimensional case). Despite these facts it is showed that they are characterized by completely different behaviors when their one-dimensional restriction governing the synchronized dynamics is considered.

3.2.1 The model with best reply

As it is pointed out in Section 2.2 of Chapter 2, following Farris et al. [105], the dynamics of n agents resulting by considering the case of unit elasticities $\beta_i = 1$, $i = 1, ..., n$ and assuming that agents at each time t decide next period spending $x_i(t+1)$ by solving the optimization problem $\max_{x_i} \Pi_i(t+1)$, where Π_i is given by (3.1), is get from the first order conditions $\partial\Pi_i(t+1)/\partial x_i = 0$ which leads to the

following recurrence

$$x_i(t+1) = \sqrt{B\frac{\sum_{j\neq i} a_j x_j^{(e)}(t+1)}{a_i}} - \sum_{j\neq i} a_j x_j^{(e)}(t+1)$$

where is reminded that $x_j^{(e)}(t+1)$ represent the expectation of firm i about firm j spending at time $t+1$ on the basis of the information set of firm i at time t. Assuming naive expectations $x_j^{(e)}(t+1) = x_j(t)$ Farris et al. [105] get the "Best Reply with naive expectations" dynamic model

$$x_i(t+1) = R_i\left(\sum_{j\neq i} a_j x_j(t)\right) = \sqrt{B\frac{\sum_{j\neq i} a_j x_j(t)}{a_i}} - \sum_{j\neq i} a_j x_j(t) \tag{3.2}$$

In particular they consider the symmetric case of identical players

$$a_i = a \text{ and } x_i(0) = x(0) \text{ for each } i \tag{3.3}$$

which implies that $x_i(t) = x(t)$ for each $t \geq 0$. In this case $\sum_{j\neq i} a_j x_j(t) = (n-1)\, ax(t)$ and the common dynamic behavior of the identical firms is governed by the one-dimensional difference equation

$$x(t+1) = f(x(t)) = \sqrt{B(n-1)x(t)} - (n-1)ax(t)\ . \tag{3.4}$$

Farris et al. [105] numerically show that (3.4) exhibits a bifurcation from stable equilibrium to stable periodic oscillations, and then chaotic dynamics, as the number n of firms increases. Indeed, this statement can be analytically proved as follows. The first order derivative

$$f'(x) = \frac{\sqrt{B(n-1)}}{2\sqrt{x}} - (n-1)a$$

computed at the unique positive equilibrium

$$x^* = \frac{B(n-1)}{(1+(n-1)a)^2} \tag{3.5}$$

becomes $f'(x^*) = (1-(n-1)a)/2$, and from the stability condition $-1 < f'(x^*) < 1$, it results

$$(n-1)\, a \leq 3, \text{ i.e. } n < 1 + \frac{3}{a} \tag{3.6}$$

In the case of unit efficiency $a = 1$, it follows that the marketing system loses stability when the number of firms exceeds 4, expressed in [105] by the statement "5 is a crowd", in the sense that 5 firms imply instability.

Farris et al. [105] also propose a different adjustment, known as adaptive adjustment towards best reply, see also [107], [85], [69]

$$x_i(t+1) = (1-\lambda_i)x_i(t) + \lambda_i R_i \left(\sum_{j \neq i} a_j x_j(t) \right) \tag{3.7}$$

where $i = 1, ..., n$ and the constants $\lambda_i \in [0, 1]$ represent the attitude of firm i to adopt the best reply, whereas $(1 - \lambda_i)$ is the anchoring attitude to maintain the previous spending decision, i.e. a measure of inertia. The model (3.7) is a generalization of (3.2) because it reduces to it for $\lambda_i = 1$, $i = 1, ..., n$, whereas it tends to absolute inertia of firm i, i.e. $x_i(t+1) = x_i(t)$, as $\lambda_i \to 0$. Moreover, the model (3.7) has the same equilibria as the best reply model (3.2), and under the assumption

$$a_i = a,\ \lambda_i = \lambda \text{ and } x_i(0) = x(0) \text{ for each } i \tag{3.8}$$

the one-dimensional model of the representative agent

$$x(t+1) = (1-\lambda)x(t) + \lambda \left(\sqrt{B(n-1)x(t)} - (n-1)ax(t) \right)$$

ensures asymptotic stability of the positive equilibrium (3.5) provided that

$$(n-1)\, a < \frac{4-\lambda}{\lambda}, \text{ i.e. } n < 1 + \frac{4-\lambda}{\lambda a}$$

hence the stability condition holds for an arbitrarily large number of firms provided that λ is sufficiently small, i.e. under the assumption of inertia or "prudent behavior" of the identical firms. Of course, the dynamic behavior of the complete n-dimensional marketing model, with heterogeneous firms due to differences in some parameters and/or in the initial conditions, is more rich. As an example is showed a numerical snapshots of dynamic scenarios of the model (3.7) with $n = 2$ in figure 3.1 (see also dynamic scenario presented in Chapter 2). A comprehensive analytical and numerical study on existence and local stability of the equilibrium points of (3.7) with $n = 2$ is given in Sections 2.3 and 2.4 of Chapter 2, whereas, for the sake of completeness, a short analytical one is reported in the Appendix C.

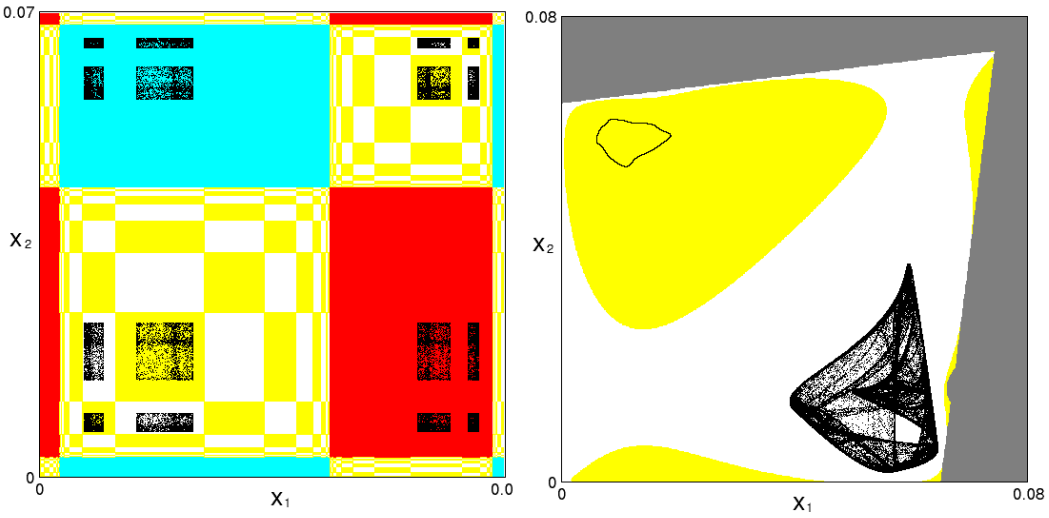

Fig. 3.1 Two dynamic scenarios for the model (3.2) with $n = 2$ identical firms starting with different initial conditions. Left: $a_1 = a_2 = 3.79$, $\lambda_1 = \lambda_2 = 1$. Right: $a_1 = 3.85$, $a_2 = 4$, $\lambda_1 = \lambda_2 = 0.8$. The different grey shades represent the basins of attraction of the coexisting attractors, represented by black dots.

3.2.2 A different kind of adjustment

Following [68] and several other authors, see e.g. [40], [70], [36], is now considered the assumption that the two competitors change their marketing efforts adaptively in response to the profits achieved in the previous period. In particular, the marketing efforts in period $t + 1$ are determined by

$$x_i(t+1) = x_i(t) + \lambda_i x_i(t)\Pi_i(t) = x_i(t) + \lambda_i x_i(t)\left(B\frac{a_i x_i^{\beta_i}(t)}{\sum_{j=i}^{n} a_j x_j^{\beta_j}(t)} - x_i(t)\right) \tag{3.9}$$

where (3.1) has been used. In this model the decision of the firms is driven by profits obtained in the previous period with a type of anchoring and adjustment heuristic widely used in decision theory (see e.g. [116], [14]). The parameters $\lambda_i > 0$ measure the speed of adjustment. Also in this case a wide spectrum of rich dynamic scenarios is obtained, see [68] for an extensive study of the case with $n = 2$. Two exemplary cases are shown in figure 3.2 (see Appendix C for a brief analytical study of equilibrium stability).

It can be said that the global dynamic properties of this model are similar to the ones observed in the profit optimization model of the previous subsection. However, under the assumption of identical firms starting from identical initial conditions the

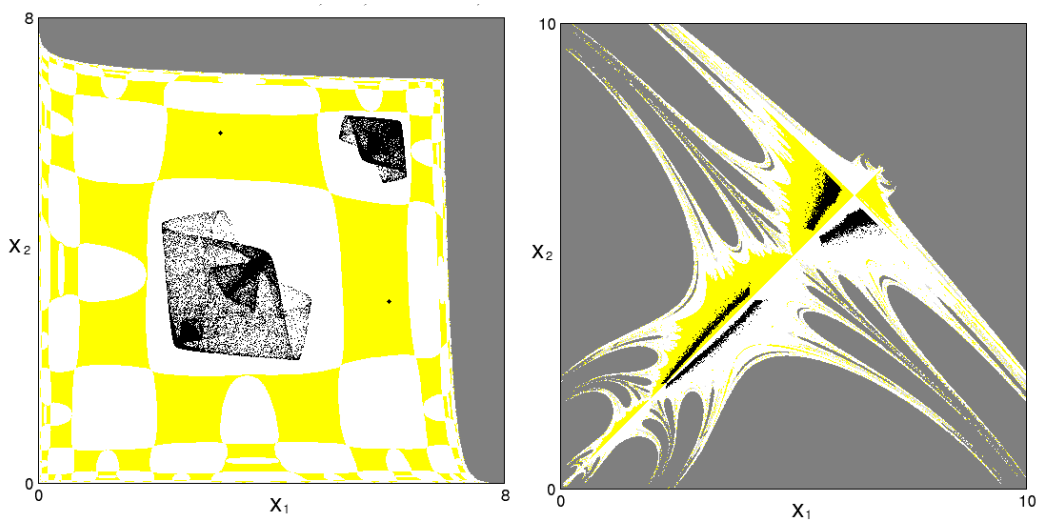

Fig. 3.2 Two dynamic scenarios for the model (3.9) with $n = 2$ identical firms with different initial conditions. The parameter values are $B = 10$, $\lambda_1 = \lambda_2 = 0.514961$, $a_1 = a_2 = 1$. Left: $\beta_1 = \beta_2 = 0.05$, a two-cyclic chaotic attractor coexists with a stable cycle of period 2. Right: $\beta_1 = \beta_2 = 1.136$ two chaotic attractors coexist in symmetric positions. The different grey shades represent the basins of attraction of the coexisting attractors, represented by black dots, and the dark grey region represents the set of initial conditions that generate diverging trajectories.

one-dimensional restriction of (3.9) to the invariant diagonal is

$$x(t+1) = x(t)\left(1 + \frac{\lambda B}{n} - \lambda x(t)\right) \tag{3.10}$$

a quadratic map conjugate to the logistic map $z(t+1) = \mu z(t)\,(1 - z(t))$ with $z = n\lambda/(n + \lambda B)$ and parameter $\mu = 1 + \lambda B/n$. Hence in this case the unique positive equilibrium $x^* = B/n$ is stable for

$$1 + \frac{\lambda B}{n} \leq 3, \text{ i.e. } n \geq \frac{\lambda B}{2} \tag{3.11}$$

a result completely different from the one obtained by Farris et al. [105] and recalled above, being in this case the system stable for a sufficiently large number of firms.

3.2.3 Gradient dynamics

Let now consider here a dynamic adjustment based on profit gradient (or marginal profits) a decision rule often proposed in the economic literature on boundedly rational

agents (see e.g. [83], [130], [125], [51], [27], [48], [113], [57], [67])

$$x_i(t+1) = x_i(t) + \lambda_i x_i(t)\frac{\partial \Pi_i(t)}{\partial x_i} = x_i(t) + \lambda_i \left(B\beta_i \frac{a_i x_i^{\beta_i}(t) \sum_{j\neq i} a_j x_j^{\beta_j}(t)}{\left(\sum_{j=i}^{n} a_j x_j^{\beta_j}(t)\right)^2} - x_i(t) \right) \tag{3.12}$$

where $\lambda_i > 0$, $i = 1, ...n$, is the speed of adjustment which measures how strongly agent i reacts to signals of increasing or decreasing profits by increasing or decreasing marketing efforts respectively. The model (3.12) with $n = 2$ has been studied in [67], where it is shown that a unique positive equilibrium exists that loses stability giving rise to oscillatory behaviors, see e.g. figure 3.3 (and the corresponding analytic study of local stability in the Appendix C).

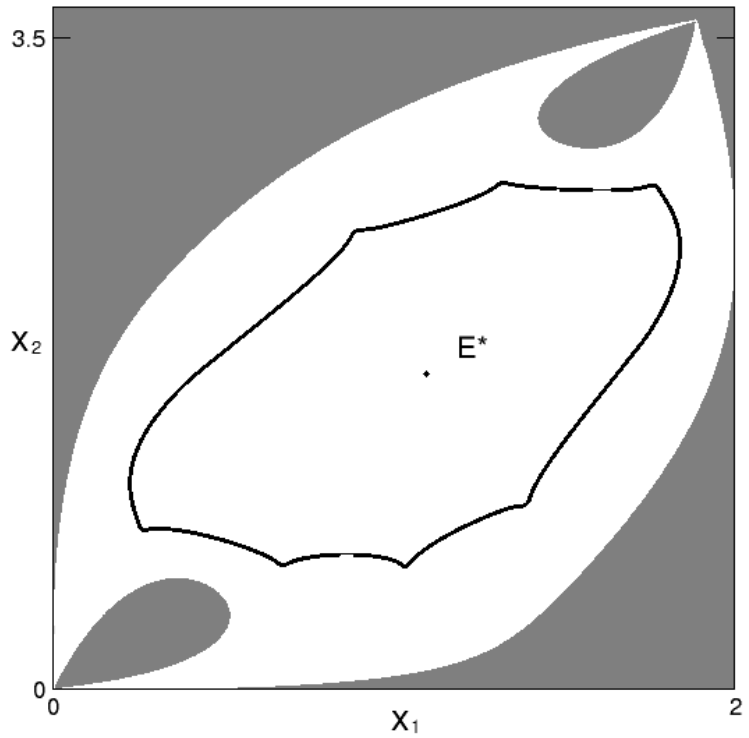

Fig. 3.3 A dynamic scenario for the model (3.12) with $n = 2$ and parameters $B = 20$, $a_1 = 1$, $a_2 = 1.572$ $\beta_1 = 0.7$, $\beta_2 = 0.72$, $\lambda_1 = 2.25$, $\lambda_2 = 1.824$. E^* is the unique Nash equilibrium, unstable for this set of parameters, surrounded by an annular attractor whose basin is represented by the white region, whereas the grey region represents the set of initial conditions that generate diverging trajectories.

Consider again the case of n identical players

$$\lambda_i = \lambda,\ a_i = a,\ \beta_i = \beta \text{ and } x_i(0) = x(0)\ ,\ i = 1, ..., n$$

and compute the one-dimensional restriction that governs the corresponding dynamics of the representative agent

$$x(t+1) = (1-\lambda)x(t) + \frac{B(n-1)}{n^2 a x^{1-\beta}} \tag{3.13}$$

Notice that in the case of unit elasticity $\beta = 1$ (as assumed in [105]) it becomes a linear contractive one-dimensional map, hence always globally asymptotically stable (independently of the number of firms n).

3.3 The problem of synchronization in the case of two firms

In this Section are studied two of the dynamic marketing models presented in the previous section with $n = 2$, and the two firms are assumed to be identical, i.e. characterized by the same parameters and starting from the same initial conditions, or quasi-identical, i.e. with a slight difference between the parameters and/or their initial conditions. A recent stream in the literature on applied mathematics shows that the symmetric models which derive from the assumption of identical coupled units (agents, oscillators etc.) exhibit, in many situations, non-generic dynamical behaviors. First is considered the case of two identical firms that start from different initial effort allocations, with the related question if the trajectories synchronize over time, i.e., if $\|x_1(t) - x_2(t)\| \to 0$ as $t \to +\infty$. In this case, the initial difference between the marketing efforts of the two firms, $\|x_1(0) - x_2(0)\| > 0$, would cancel out within a reasonably short time span, so it can be safely ignored the transient dynamics of the two-dimensional system, and consider the one-dimensional model of the representative firm instead. If synchronization takes very long or does not occur at all, then the concept of the representative firm becomes meaningless. This leads to the following question: under which conditions do the trajectories of identical competitors which start from different initial effort choices synchronize, and how does this depend on the initial conditions themselves, that is on the difference of the initial efforts?

The second topic considered concerns the question if small heterogeneities between the two firms - a small mismatch of some of the parameters - matter for synchronization or not. Answering these questions is not easy, since new dynamic phenomena may appear, especially in the presence of chaotic behavior. In this case *chaotic synchronization* may occur, a phenomenon that has been extensively studied in the recent physical and mathematical literature. In the Appendix D is given a short overview of some

notions and results that can be found in this stream of literature, and the reader is referred to [80], [104], [30], [114], [64], [63] and references therein for a deeper insight.

3.3.1 Synchronization and synchronization failure in two marketing models

Let now first consider model (3.9) with $n = 2$ competitors.

$$T^k : \begin{cases} x_1' &= x_1 + \lambda_1 x_1 \left(B \dfrac{a_1 x_1^{\beta_1}}{a_1 x_1^{\beta_1} + a_2 x_2^{\beta_2}} - x_1 \right) \\ x_2' &= x_2 + \lambda_2 x_2 \left(B \dfrac{a_2 x_2^{\beta_2}}{a_1 x_1^{\beta_1} + a_2 x_2^{\beta_2}} - x_2 \right) \end{cases} \tag{3.14}$$

A general study of this map is given in [68], and its features in the symmetric case, i.e. identical competitors for which

$$\lambda_1 = \lambda_2 := \lambda;\ \beta_1 = \beta_2 := \beta;\ a_1 = a_2$$

are considered in [63], where it is argued that the parameter β measures the degree of competition between the firms. This example is now used to show the effects of small heterogeneities in the initial condition by using the methods described in the previous subsection. The restriction of the resulting symmetric map to the invariant diagonal Δ (see (D.2) in Appendix D) is given by

$$T_\Delta^k(x) = \left(1 + \frac{\lambda B}{2}\right) x - \lambda x^2. \tag{3.15}$$

which can be rewritten as a standard logistic map $z' = \mu z(1 - z)$ throw the linear transformation $x = \dfrac{z}{\lambda}\left(1 + \dfrac{\lambda B}{2}\right)$, where

$$\mu = 1 + \frac{1}{2}\lambda B \tag{3.16}$$

For the symmetric map, the Jacobian matrix, computed at a point of the diagonal Δ results

$$\boldsymbol{J} = \begin{pmatrix} 1 - 2\lambda x + \dfrac{\lambda B(\beta + 2)}{4} & -\dfrac{\lambda B \beta}{4} \\ -\dfrac{\lambda B \beta}{4} & 1 - 2\lambda x + \dfrac{\lambda B(\beta + 2)}{4} \end{pmatrix} \tag{3.17}$$

hence the eigenvalues are given by

$$\nu_{\parallel} = 1 - 2\lambda x + \frac{\lambda B}{2}, \quad \nu_{\perp} = 1 - 2\lambda x + \frac{\lambda B}{2}(1+\beta)$$

It is important to note that the parameter β only appears in the transverse eigenvalue $\nu_{\perp}$, so it is a *normal parameter*, i.e. it has no influence on the dynamics along the invariant submanifold Δ, and only influences the transverse stability: the associated transverse Lyapunov exponent becomes (see the Appendix D)

$$\Lambda_{\perp} = \lim_{N\to\infty} \frac{1}{N} \sum_{n=0}^{N} \ln \left| 1 - 2\lambda x_n + \frac{\lambda B}{2}(1+\beta) \right|$$

This allows to consider fixed values of the parameters λ and B, such that a chaotic attractor $A_s \subset \Delta$ of the map (3.15) exists, with an absolutely continuous invariant measure on it. So, it can be studied the transverse stability of A_s as the degree of competition, measured by the parameter β, varies. Suitable values of the aggregate parameter λB, at which chaotic intervals for the restriction (3.15) exist, are obtained from the well known properties of the logistic map (see e.g. [6], [134]). For example, at the parameter value $\overline{\mu}_1 = 3.5925721841...$ the period-2 cycle of the logistic map undergoes the homoclinic bifurcation, at which two cyclic chaotic intervals are obtained by the merging of four cyclic chaotic intervals. By using $\lambda B = 2(\overline{\mu}_1 - 1)$ we get a two-band chaotic set A_s along the diagonal Δ, and the transverse Lyapunov exponent is shown in Figure 4 as a function of β.

The plot in figure (3.4) shows the comparison between $\Lambda_{\perp}^{\text{nat}}$, the natural transverse Lyapunov exponent, and $\Lambda_{\perp}^{(2)}$, the transverse Lyapunov exponent associated to the period-2 cycle in Δ. For the values of β for which $\Lambda_{\perp}^{\text{nat}} < 0$ and $\Lambda_{\perp}^{(2)} > 0$ it can be asserted that the set A_s is certainly a non topological Milnor attractor, since $\Lambda_{\perp}^{\text{Max}} \geq \Lambda_{\perp}^{(2)} > 0$ (see again the Appendix D). This is the situation shown in figure 3.5, obtained for $\beta = 0.83$, at which $\Lambda_{\perp}^{\text{nat}} \simeq -0.11$ and $\Lambda_{\perp}^{(2)} > 0$. The generic trajectory starting from initial conditions taken in the white region of figure 3.5 leads to synchronization, whereas the points of the gray region generate interrupted trajectories, involving negative values of the state variables.

The Milnor attractor A_s is included inside a minimal invariant absorbing area whose boundary can be easily obtained by arcs of critical curves as explained in [62] (see also Appendix B). This absorbing area, represented in the left panel of figure 3.6, constitutes a trapping region inside which the asynchronous dynamics observed during the transient are contained. Indeed, along the transient, the time evolution of the

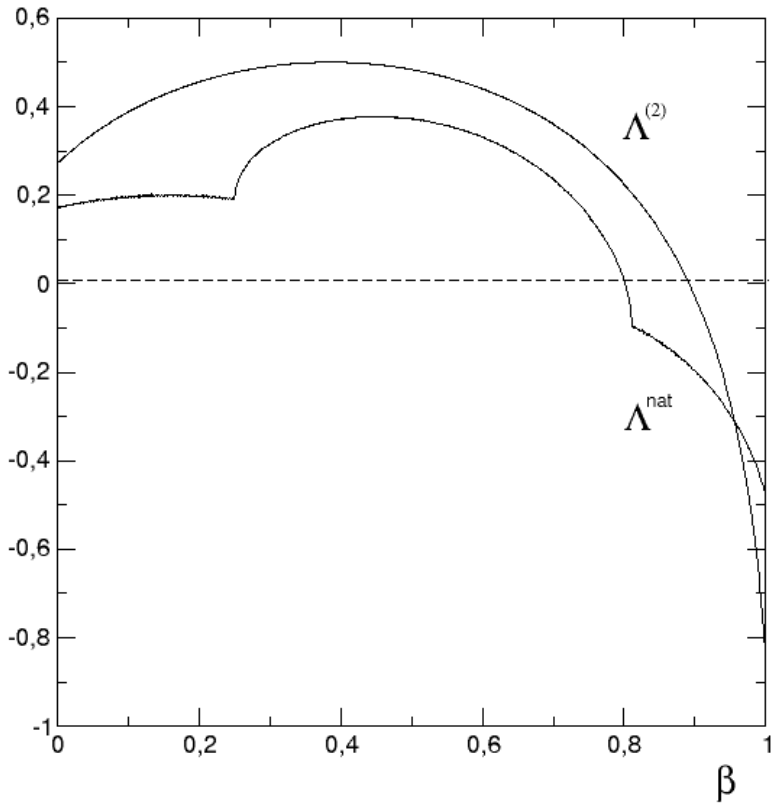

Fig. 3.4 The comparison between the natural transverse Lyapunov exponents $\Lambda_{\perp}^{\mathrm{nat}}$ and the transverse Lyapunov exponent $\Lambda_{\perp}^{(2)}$ associated to the lower cycle of period two included in A_s which gives a lower approximation of the maximum Lyapunov exponent $\Lambda_{\perp}^{\mathrm{nat}}$.

system is characterized by several bursts away from Δ before synchronization occurs. This characteristic dynamical pattern, named on-off intermittency, is highlighted in the right panel of figure 6 where the difference $\|x_1(t) - x_2(t)\|$ is represented versus time.

If the value of β is decreased $\Lambda_{\perp}^{\mathrm{nat}}$ goes positive and A_s becomes a chaotic saddle i.e. a blowout bifurcation occurs. In the present case the so called blowout bifurcation is preceded by the contact between critical lines and the basin of negative numbers: the basin of Δ becomes riddled and, after a transient which can also be very long, almost all trajectories goes towards negative values. For further details about blowout bifurcation and riddled basins see Appendix D. In the left panel of figure 3.7, obtained for $\beta = 0.8$, at which $\Lambda_{\perp}^{\mathrm{nat}} > 0$ the transient is represented. On the right panel of the same figure 3.7 bursts which characterize the transient are represented as $\|x_1(t) - x_2(t)\|$ and exhibit the same time patterns of on-off intermittency.

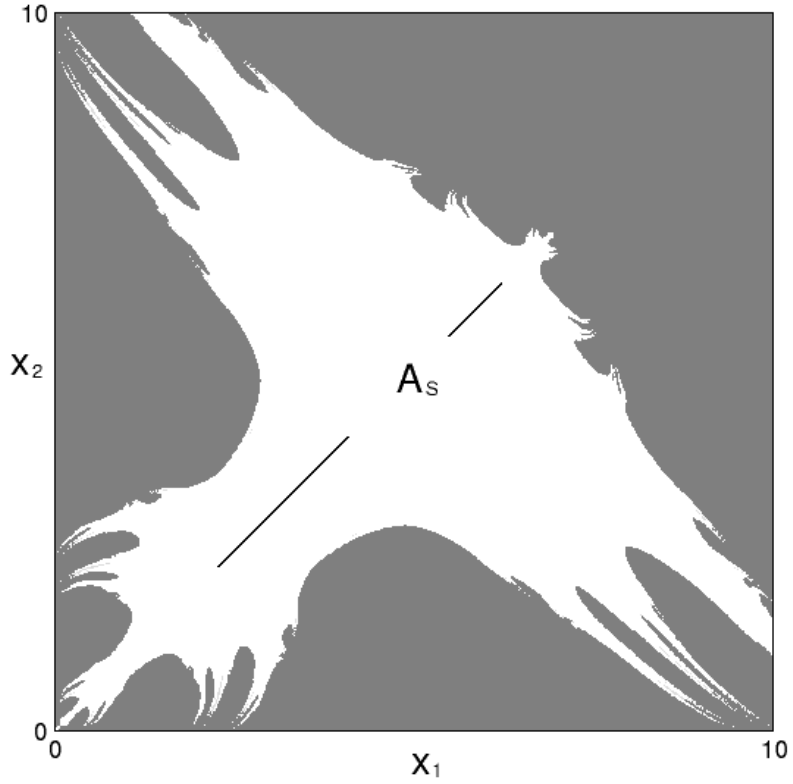

Fig. 3.5 Synchronous dynamic of the system (3.9) for $n = 2$ in the long run. The attractor A_s is included in the minimal absorbing area. The parameter set is: $\beta = 0.83$, $B = 10$ and $\mu = \bar{\mu}_1$; if follows that the transversal Lyapunov exponent value is $\Lambda_{\perp}^{\text{nat}} \simeq -0.11$. We notice that $\Lambda_{\perp}^{\text{nat}} > 0$ so A_s is a non topological Milnor attractor.

To sum up, when $\Lambda_{\perp}^{\text{nat}} > 0$ a small heterogeneity in the initial efforts of identical firms imply that the trajectory obtained never synchronizes, so that the one-dimensional dynamics of the representative agent cannot be used to represent the dynamic evolution of the marketing system.

Another dynamic situation is shown in figure 3.8, obtained with parameters $\beta = 0.84$, $B = 10$ and λ such that $\mu = \bar{\mu}_1$, where it can be observed the presence of a new attractor C_4 far from the diagonal Δ. The presence of this attractor, whose basin reaches the invariant diagonal Δ where chaotic dynamics occur, gives rise to the dynamic scenario of global riddling.

In fact C_4 can be reached by a trajectory that starting from an arbitrarily small neighborhood of the transversely unstable 2-cycle embedded in A_s, namely along a small tongue of the basin of C_4 located around the transverse unstable manifold issuing from the two periodic points. As in A_s there is pure chaos, the preimages of the points of the 2-cycle are densely distributed along A_s, and the same occurs for the tongues of

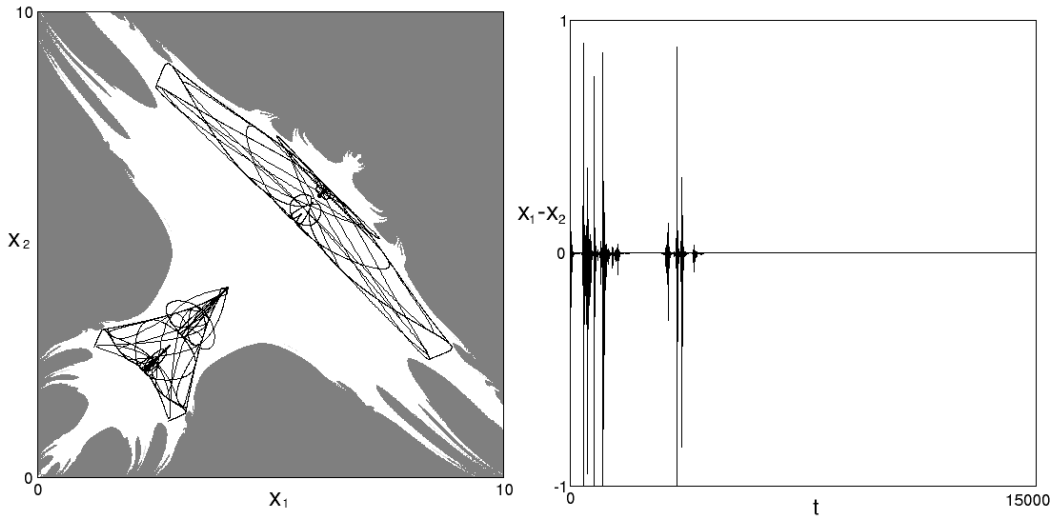

Fig. 3.6 Left: critical lines that bounds the minimal absorbing area which contains the trajectories after synchronization are represented. Right: transient part of the trajectory for which, before synchronization, the phenomenon of on-off intermittency is observed. The parameters are $\mu = \bar{\mu}_1$, $\beta = 0.83$.

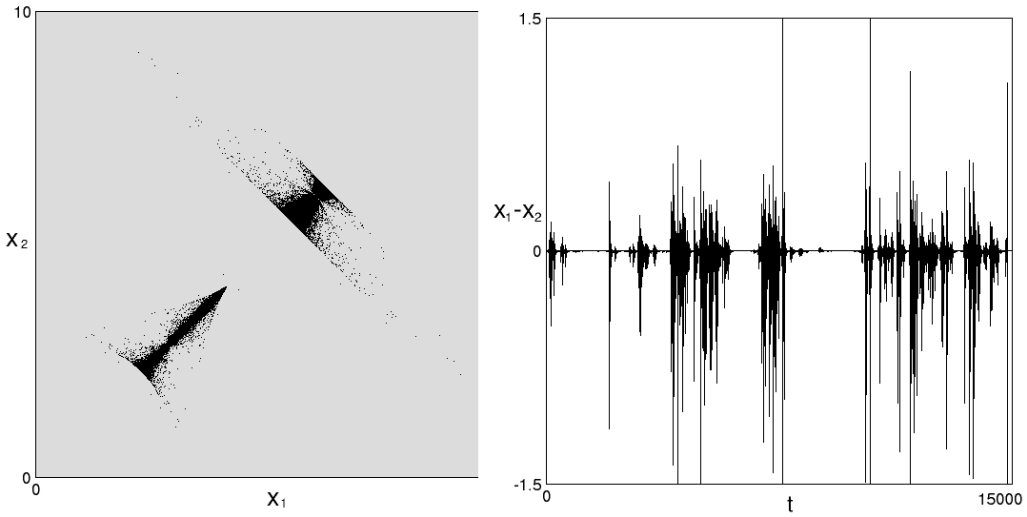

Fig. 3.7 Plot of the transient of a trajectory with $\Lambda_{\perp}^{\text{nat}} > 0$. In the first part of the trajectory on-off intermittency occurs but in the long run the dynamics goes to infinity. In this case we have a contact between critical lines and the basin of infinity before blowout bifurcation, so the basin of A_s becomes riddled and only a set of zero Lebesgue measure leads to synchronization. The parameter set is: $\beta_1 = \beta_2 = 0.8$ for which $\Lambda_{\perp}^{\text{nat}} = 7 \times 10^{-3}$.

the basin of the attractor C_4 located far from Δ. This implies that many trajectories that are locally repelled away from Δ reach C_4, whose basin is consequently densely

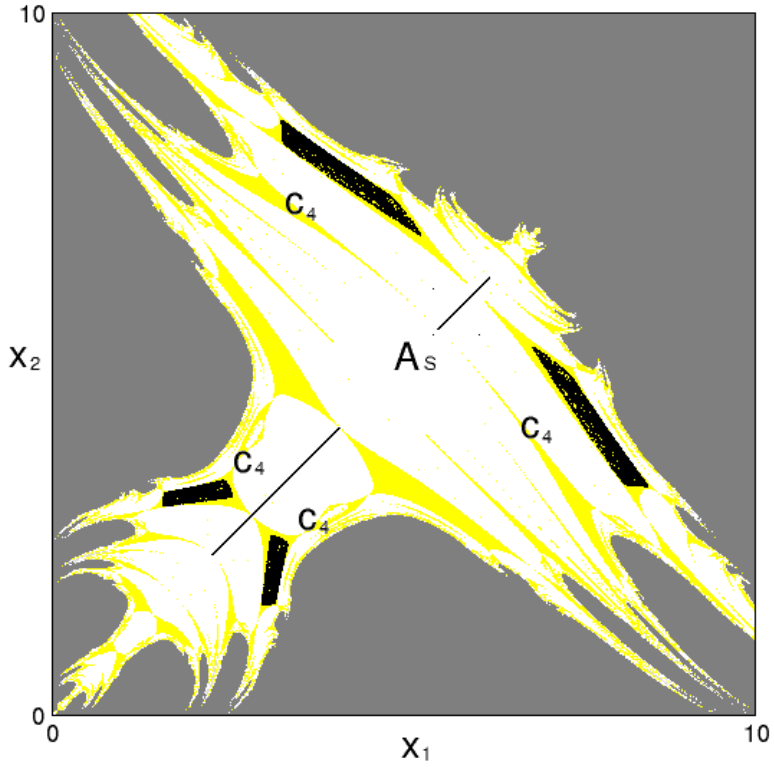

Fig. 3.8 For the parameter set $\beta = 0.84$, $B = 10$ and $\mu = \bar{\mu}_1$ we observe the comparison of a new attractor C_4 outside Δ coexisting with the non topological Milnor attractor A_s.

distributed inside the realm of attraction of A_s, thus giving the typical structure of a riddled basin (see [80]). The two basins of $A_s \subset \Delta$ and C_4 are shown in the figure 3.8, however the graphical resolution does not give sufficiently clear idea of such a complexity.

In figure 3.9 two trajectories starting from initial conditions very close each other taken in a neighborhood of a periodic point of the transversely unstable 2-cycle embedded into A_s, i.e.

$$x_1^c = x_2^c = \frac{\mu + 1 \pm \sqrt{\mu^2 - 2\mu - 3.}}{2\lambda}$$

are represented, one folded back towards the diagonal Δ and the other one reaching the attractor C_4 outside it.

So, even in this case, two almost identical initial efforts of identical firms give rise to very different long run evolutions, one synchronizing in the long run and the other one

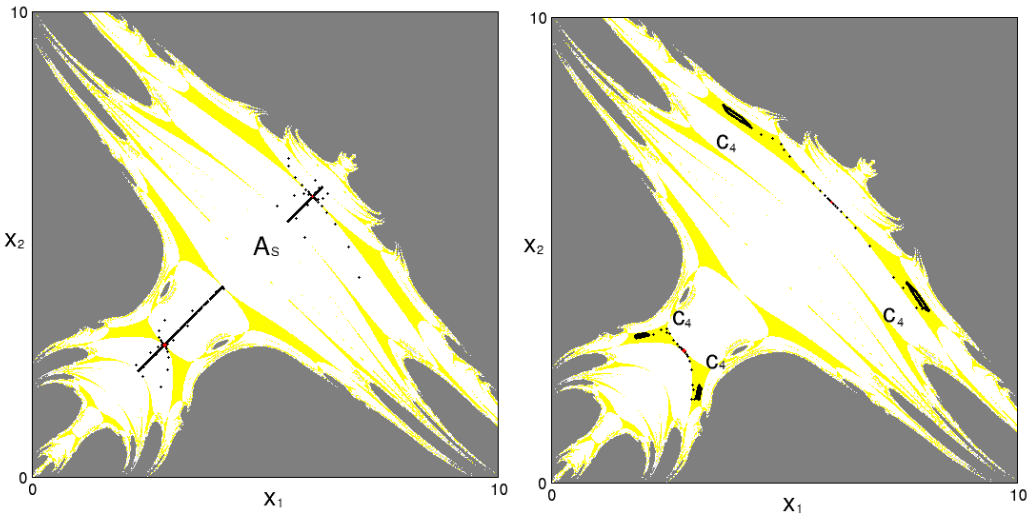

Fig. 3.9 Different trajectories for almost identical initial conditions taken close to unstable two-cycle along the direction of the unstable manifold (left) and along a slightly different direction (right). Left: $x_1(0) = x_1^{c,1} + 10^{-3} \times \cos(3\pi/4)$, $x_2(0) = x_1^{c,1} + 10^{-3} \times \sin(3\pi/4)$. Right: $x_1(0) = x_1^{c,1} + 10^{-3} \times \cos(3\pi/4 + \epsilon)$, $x_2(0) = x_1^{c,1} + 10^{-3} \times \sin(3\pi/4 + \epsilon)$ where $\epsilon = 2.7 \times 10^{-4}$. The parameter set is: $\beta = 0.85$, $B = 10$ and $\mu = \bar{\mu}_1$.

converging to a cyclic attractor far from the submanifold where synchronized dynamics occur.

Let now consider the model with best reply and inertia (3.7) with 2 firms and $B = 1$:

$$T^f = \begin{cases} x_1' &= (1-\lambda_1)x_1 + \lambda_1 \left(\sqrt{\dfrac{a_2 x_2}{a_1}} - a_2 x_2 \right) \\ x_2' &= (1-\lambda_2)x_2 + \lambda_2 \left(\sqrt{\dfrac{a_1 x_1}{a_2}} - a_1 x_1 \right) \end{cases} \tag{3.18}$$

The symmetric counterpart of recurrence (3.18) is provided by the conditions on coefficients $\lambda_i = \lambda$ and $a_i = a$, $i, j = 1, 2$, and the restriction of the resulting symmetric map to the invariant diagonal Δ is given by

$$T_\Delta^f = (1-\lambda)x + \lambda(\sqrt{x} - ax) \tag{3.19}$$

From the Jacobian matrix relative to the symmetric case, see (C.2) in Appendix B, the normal and transversal Lyapunov exponent are obtained and are respectively given by

$$\Lambda_{\parallel} = \lim_{n\to\infty} \frac{1}{n} \sum_{k=0}^{n} \ln \left| 1 - \lambda + \lambda \left(\frac{1}{2} \sqrt{\frac{1}{x_k}} - a \right) \right| \tag{3.20a}$$

$$\Lambda_{\perp} = \lim_{n\to\infty} \frac{1}{n} \sum_{k=0}^{n} \ln \left| 1 - \lambda - \lambda \left(\frac{1}{2} \sqrt{\frac{1}{x_k}} - a \right) \right| \tag{3.20b}$$

Both $\Lambda_{\parallel}$ and $\Lambda_{\perp}$ depend on a and λ, so there are no *normal parameters*. It is noted that for $\lambda = 1$ (no inertia) it results $\Lambda_{\perp} = \Lambda_{\parallel}$ and they are showed in figure 3.10 as the parameter a varies.

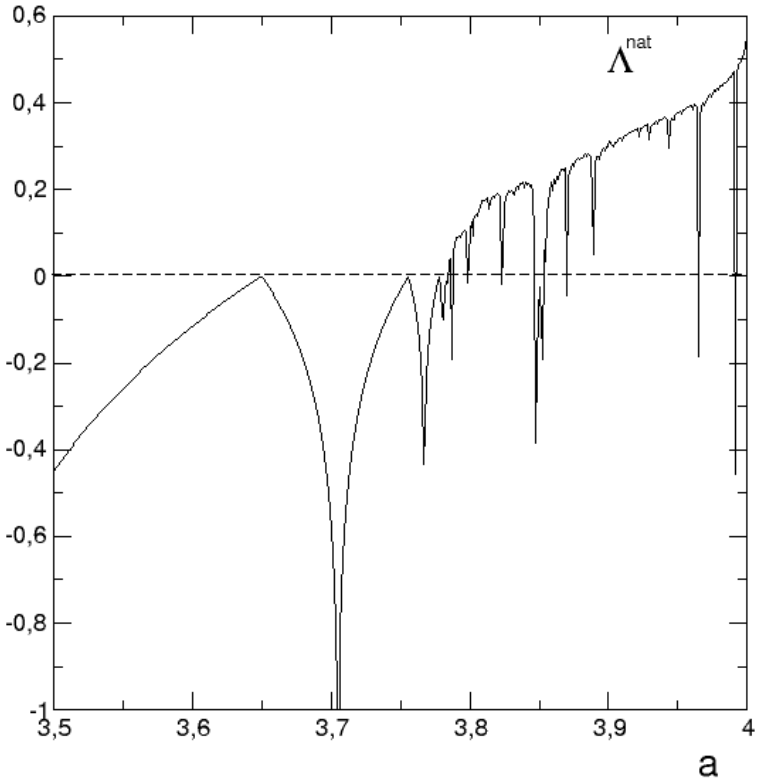

Fig. 3.10 Plot of $\Lambda_{\parallel} = \Lambda_{\perp}$ versus a in the case $\lambda = 1$.

In this case every stable cycle of period n, C^n, is a topological attractor characterized both by negative Lyapunov exponents. Pure chaos exists in a set of positive Lebesgue measure in the parameter space (see [79], or [Thunberg] for a survey) and, since $\Lambda_{\perp}^{\text{nat}} > 0$, subsets $A_s^k \in \Delta$ in which chaotic dynamics occur are chaotic saddles. As stressed in [105], synchronization can occur for certain parameters' constellations giving negative values of $\Lambda_{\perp}^{\text{nat}}$ (and for certain initial conditions) as showed in figure 3.11.

However, in the same figure 3.11 is observed the existence of other attractors in the two-dimensional phase space out of Δ coexisting with the stable cycles on the diagonal. In other words, even if stable cycles may exist embedded into the diagonal Δ, their basins may be quite intermingled with the basins of other stable cycles located outside Δ.

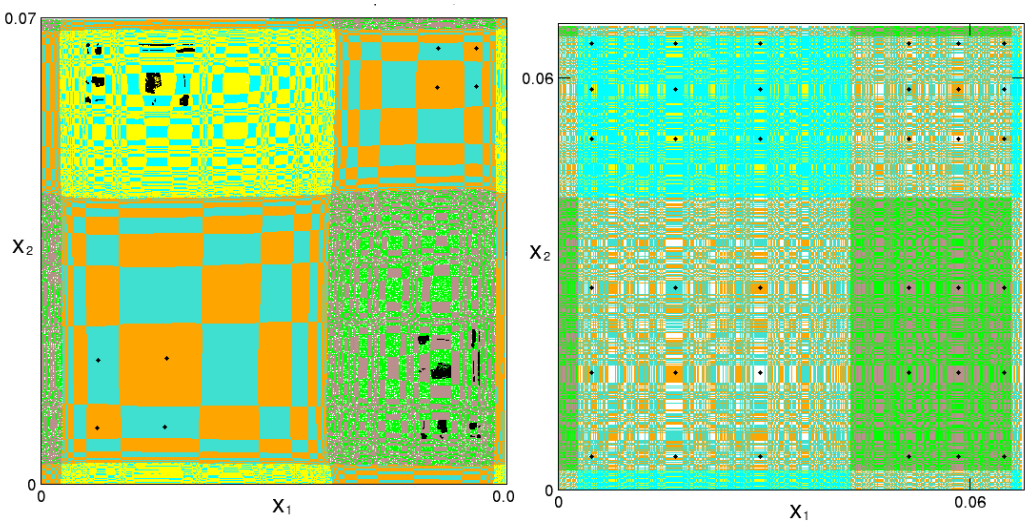

Fig. 3.11 Two different scenarios resulting from the model (3.18) in which a stable periodic cycle with $\Lambda_\perp < 0$ is embedded into Δ. Synchronization occurs for initial conditions in the white basin, while other different initial conditions lead the trajectories towards other attractors out of the synchronization manifold Δ. The parameter values are: $a = 3.79$, $\lambda = 0.99$ (left) and $a = 3.84818$, $\lambda = 1$ (right).

When no stable cycles exist along Δ, than trajectories never synchronize, except the non generic case of identical firms that start with identical initial conditions, i.e. only for a set of initial conditions belonging to Δ which has zero Lebesgue measure in $\mathbb{R}^2$. It is plain that in this case the one-dimensional synchronized dynamics of the representative agent has no economic meaning. In figure 3.12 an example of a typical dynamic scenario of the model (3.18) with $\Lambda_\perp^{\text{nat}} > 0$ is shown.

3.3.2 Quasi-homogeneous firms and symmetry loss

The very restrictive assumption that the firms' structural parameters are the same and the difference between the competitors lies only in their initial effort allocations are now relaxed. Although synchronization does not necessarily occur for all initial effort allocations, it could be determined for which parameters' constellations and initial conditions the two-dimensional model may be substituted by the one-dimensional model of a representative agent as far as long run dynamics is concerned.

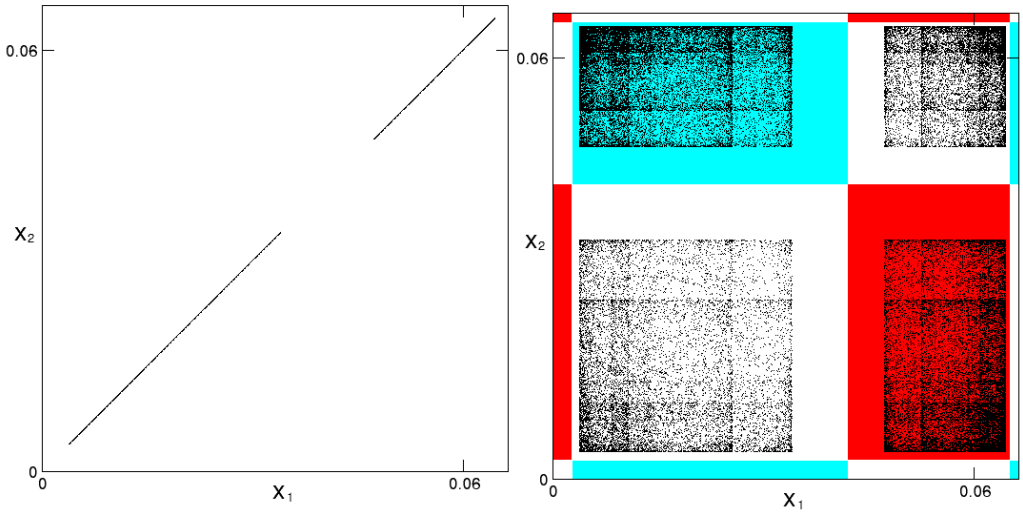

Fig. 3.12 Two different scenarios resulting from the market model (3.18) for different initial conditions. The system is characterized by $\lambda = 1$, $a = 3.878$ for which $\Lambda_{\perp}^{\text{nat}} \simeq 0.27 > 0$. Left: a non generic trajectory obtained with initial conditions on Δ. Right: a chaotic trajectories with initial conditions out of Δ.

For practical purposes, it can now be checked, by using the marketing model (3.9) as a paradigmatic example, what happens as a consequence of *small heterogeneities* due to small parameters' mismatches. It is noted first that a parameters' mismatch causes the destruction of the invariance of Δ, due to the fact that the map is no longer symmetric. This may lead to quite different dynamics since, after the parameters' mismatch, synchronization along Δ can no longer occur and the generic trajectory fills up the minimal absorbing area around the former invariant set A_s (see e.g. [63], [62]). However, if the attractor A_s existing along Δ before the parameters' mismatch is a *topological attractor*, that is $\Lambda_{\perp}^{\text{Max}} < 0$, then the introduction of small heterogeneities does not have such a disruptive effect, and the symmetric model still serves as a good approximation of the behavior of the two firms. Such a situation is shown in the figure 3.13 where identical firms are characterized by a set of parameters such that the one-dimensional chaotic attractor embedded into the diagonal is an asymptotic attractor, i.e. $\Lambda_{\perp}^{\text{Max}} < 0$. It has to be stressed that this is not easy to be proved in general, since the cycles included in a chaotic attractor are infinitely many. However it is claimed that the natural transverse Lyapunov exponent has a strong negative value, as shown in figure 3.4, and the periodic cycles of lower period are transversely stable. This last point constitutes a well known conjecture, based on the fact that if $\Lambda_{\perp}^{\text{nat}} < 0$ and $\Lambda_{\perp}^{\text{Max}} > 0$, then some low period cycles should be transversely unstable, because if

a cycle of high period is transversely unstable, i.e. its transverse Lyapunov exponent is positive, also $\Lambda_{\perp}^{\text{nat}}$ should be positive, see e.g. [133].

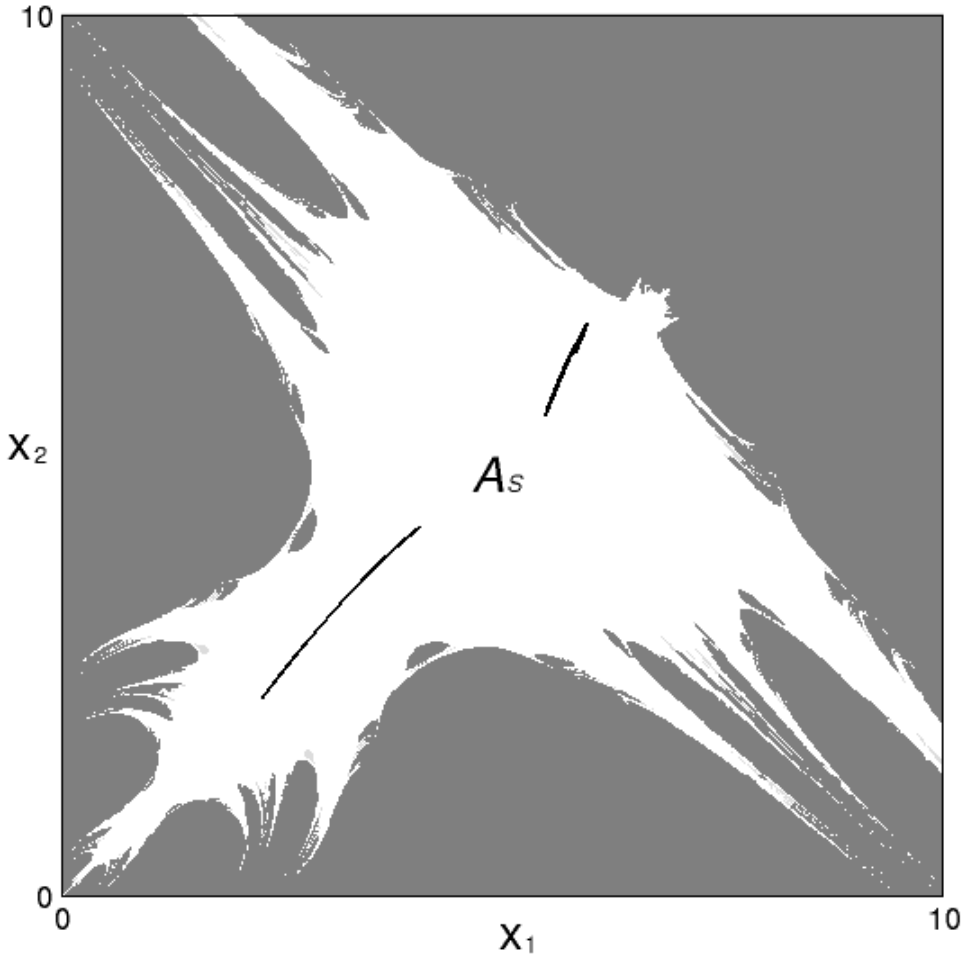

Fig. 3.13 Quasi-synchronization due to a mismach of parameters: $a_1 = 1$, $a_2 = 1.01$. The attractor A_s is, with gratest probablity, a topological one, argued by the fact that, for $\beta = 0.97$ and in the symmetric case, we have $\Lambda_{\perp}^{\text{nat}} \simeq -0.35$ and $\Lambda_{\perp}^{\text{nat}} > \Lambda_{\perp}^{(2)}$.

So, the fact that the chaotic set on which synchronized dynamics occur is an asymptotic attractor for the two-dimensional map implies two things: first, the synchronization of trajectories starting out of it, and in its basin, is very fast; second, if is introduced a small parameter mismatch, the resulting trajectories are "almost synchronized" (see figure 3.13). Instead, if the introduction of a parameters' mismatch occurs starting from a symmetric situation where the chaotic one-dimensional invariant set $A_s \subset \Delta$ is an attractor only in Milnor sense (i.e. not asymptotic) then a quite different effect generally occurs, because after the symmetry breaking endless intermittency filling up the minimal absorbing area around A_s is observed. This is illustrated in figure

3.14, obtained starting from the situation already discussed in the previous subsection and illustrated in figure 3.6 after the introduction of a very small difference between the response parameters of the firms, namely $a_1 = a_2$ and $\beta_1 = 0.83$ while $\beta_2 = \beta_1 - 10^{-5}$. Such a small perturbation leads to quite different dynamics, since synchronization no longer occurs, and the bursts never stop. The generic trajectory fills up the absorbing area, which now appears to be a two-dimensional chaotic area, as shown in figure 3.14. In the left panel is showed the evolution of the system starting from the initial effort allocation $(x_1(0), x_2(0)) = (3.5, 3.5) \in \Delta$, i.e., from homogeneous initial choices, is represented in the phase space (x_1, x_2), whereas in the right panel of the same figure 3.14 the difference of the marketing efforts over time, $(x_1(t) - x_2(t))$, is represented over 5000 periods. It is evident that long time intervals exist in which the two firms show quasi-synchronized behavior, but in-between such intervals asynchronous behavior emerges with an apparently random pattern.

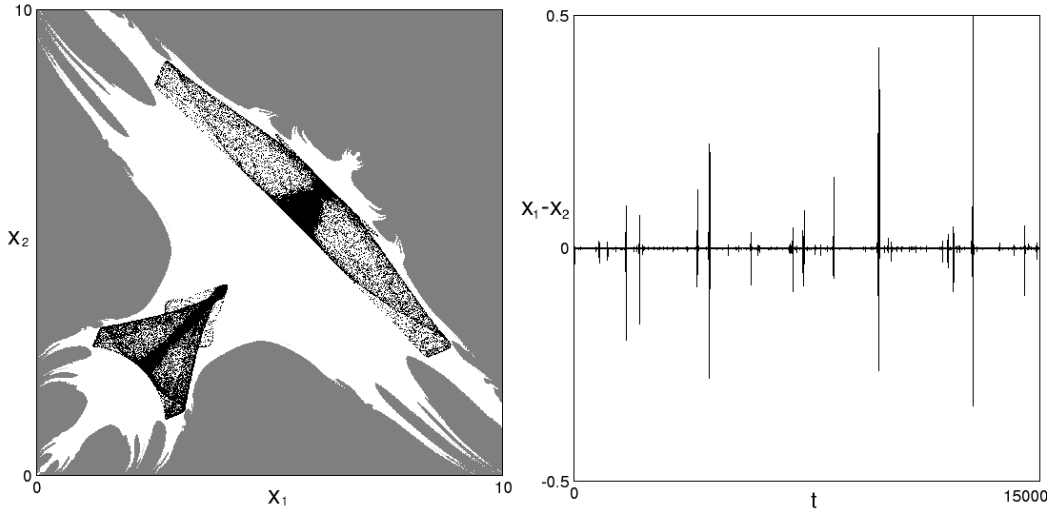

Fig. 3.14 Left: an example of a trajectories which fills up the whole minimal absorbing area due to a mismatch of parameters. Right: the corresponding never ending on-off intermittency. The parameter values are: $\beta_1 = 0.83$, $\beta_2 = \beta_1 - 10^{-5}$, $\mu = \bar{\mu}_1$.

Of course, the study of the effects of small parameters' mismatches may be important in economic dynamic modeling, as stressed in [58] and [95].

3.4 Conclusions

In this Chapter we have critically considered a common practice, in economic literature, that consists in the reduction of a model describing n identical agents to a one-dimensional dynamical system that governs the asymptotic dynamics of a representative

agent that summarizes the common behavior of the n identical firms. Often the same equation is assumed to represent the dynamics of the system even in the presence of "sufficiently small" heterogeneities, and is often used to study the trade-off between stability of the overall system and the number n of firms, that can be seen as a bifurcation parameter of the one-dimensional restriction. This approach can be found in several books and papers, see e.g. [124], [119], [105], [69].

In particular, starting from some market share attraction models commonly used in the literature to describe marketing dynamics with adaptive firms, we have shown how dangerous (sometimes even misleading) this approach may be. First of all, we have shown that similar nonlinear models based on adaptive profit increasing mechanism, that exhibit similar and quite rich dynamic behaviors, may collapse into qualitatively different one-dimensional models (and sometimes even leading to opposite stability statements) when identical agents are considered. Moreover, by using some advanced tools from the recent literature on symmetric dynamic models, we have shown under which conditions the one-dimensional restriction is robust with respect to the introduction of small asymmetries in the initial conditions and/or in the parameters of the model. The theoretical as well as the numerical results suggest that the study of the transverse Lyapunov exponents gives important suggestions about both questions. In fact, negative values of the transverse Lyapunov exponent guarantees synchronization in the long run (sometimes after a long transient characterized by on-off intermittency) so that the one-dimensional reduction of the system remains meaningful even if the identical firms start from (slightly) different initial conditions. However the question of coexistence of attracting sets, with the related phenomenon of riddled basins, should be carefully considered as well. Analogously, when small parameters' mismatches are introduced, if all the transverse Lyapunov exponents are negative then only small changes in the shape of the attractor are observed, so that the long run dynamics of quasi-identical agents are still well approximated by the one-dimensional model. Instead, in the presence of some positive transverse Lyapunov exponents (even if the natural transverse Lyapunov exponent is negative, so that the one-dimensional invariant set along the diagonal is an attractor only in Milnor sense) a quite different asymptotic dynamics may arise, along an attractor whose shape and extension depend on the global properties of the dynamical system.

These results suggest that even if the restriction of the complete dynamical system to the diagonal (where synchronized dynamics occur) may be meaningful in some cases, in general this is not the case (see also [95] on this point).

In order to address this general idea in the simplest case, the given examples and numerical simulations are referred to marketing models with just two firms, represented by two-dimensional dynamical systems. Similar arguments may be applied to higher dimensional models, that represent systems with more than two firms, where conditions for complete synchronization (i.e. all firms synchronize) or partial synchronization (i.e. only a subset of firms synchronize) may be given. This will be a natural continuation of the research stream whose early modest steps are moved by this work.

From an economic point of view, the obtained results make us aware how an assumptions made in (or almost throughout) the economic literature should be critically considered. In fact, if the assumption of aggregate dynamics where all identical agents are summarized by the behavior of a representative agent is made for analytical tractability, we should be aware that such aggregation represents a very special case. The reason is that for dynamic models the symmetric case is often non-generic.

Chapter 4

Case study: on a discrete-time model with replicator dynamics in renewable resource exploitation

4.1 Introduction

In this Chapter is presented a discrete time version of the model proposed in [89] to describe a fishery where two different harvesting strategies can be employed, one denoted as standard and the other one more ecological (less intensive, hence more environmentally friendly). At any time period, the fish population is assumed to reproduce according to a discrete-time logistic growth function (see e.g. [28], second Chapter, and [55]), and the agents that exploit the fishery are assumed to update their harvesting strategy according to a profit-driven adaptive mechanism based on the evolutionary selection rule known as replicator dynamics (see e.g. [118] and [73]).

For what concerns this Chapter it is now pointed out that, even if dynamic models in ecology have been traditionally formulated in continuous time, discrete-time population models have received a great amount of attention not only for the complex and intriguing dynamics that they can produce even in the simplest systems, but also because biological motivations have been proposed to explain their usefulness in ecologic modeling. In fact, several authors stress that discrete-time population models should be used whenever reproduction happens at given breeding seasons, as several animal species successfully mate only during certain times of the year, thus giving non-overlapping generations (see e.g. [54] and [98]). So, more and more discrete-time population models have been proposed in the literature (see e.g. [55], [23] and [38]).

Moreover, as already stressed in [89], in the model here considered decisions about the kind of harvesting strategy to be adopted typically occur in discrete time, as such decisions imply the adoption of different fishing technologies, and/or different numbers of workers with different kinds of equipment, hence they cannot be revised at any time. Sometimes the possibility of switching from a harvesting strategy to another one is allowed only at given time periods by laws that regulate harvesting activities (see [21], [20] and [24]).

On the basis of these motivations, a discrete-time model, represented by a two-dimensional nonlinear map, is studied by using analytical, geometric and numerical methods. The structure of the map is quite interesting from the point of view of its mathematical properties, and is typical (hence representative) for a large class of repeated evolutionary games where a population of n players can choose, at any time, between two strategies. In fact, one dynamic variable, denoted as $r(t) \in [0, 1]$, represents the fraction of players adopting a given strategy at time period $t \in \mathbb{N}$ (of course the complementary fraction $1 - r(t)$ adopts the other strategy at the same time period). As typically occurs in these kind of evolutionary games, the two lines $r = 0$ and $r = 1$, where all players adopt the same strategy, are invariant lines, along which the dynamics characterized by unique kind of players (pure strategy case) are governed by a one-dimensional restriction of the map. In our case, the dynamics along such invariant boundary lines are given by the iteration of a quadratic map, topologically conjugate to the standard logistic map. However, interior attractors, where players carrying out both strategies coexist, can be obtained, and some bifurcations involving interior and boundary invariant sets can be studied. Indeed, very rich dynamic scenarios can be highlighted, both analytically and numerically, and regions of the phase space of the model can be detected in which quasi-periodic motions prevail (i.e. where the linear approximation of the map has complex eigenvalues) and other regions where real eigenvalues give rise to monotonic motions or improper oscillations. In both cases, however, transitions to chaotic behaviors can be observed. Moreover, the existence of non topological Milnor attractors embedded in the invariant lines is proved and numerically shown.

The plan of the present Chapter is as follows. In Section 4.2 the discrete-time model is introduced and the dynamics along the invariant lines where one-dimensional dynamics occurs when all agents adopt the same strategy is discussed. Section 4.3 contains analytical results on the existence of equilibrium points and their local stability properties as well as local bifurcations. In Section 4.4 some statements on

global behavior and some numerical simulations of the model and, also, some brief final considerations are given.

4.2 The model

Following the general setup of the model proposed by [89], let $x(t)$ denote the available quantity at time t of a renewable resource and consider a population of n agents that can exploit the resource by two different technologies: a standard (intensive) one characterized by technology coefficient $q_1 > 0$, and a more environmentally-friendly (let's say ecological) technology characterized by $q_0 \in (0, q_1)$. Let $r(t) \in [0, 1]$ be the fraction of agents that adopt the standard technology during time period t and consequently the complementary fraction of agents $(1 - r(t))$ adopts the ecological technology, so that $r = 0$ means that all the agents adopt the ecological technology q_0, and $r = 1$ means that all the agents adopt the standard technology q_1. If h_i denotes the harvesting of resource by using technology i, $i = 0, 1$, following again [89] is here assumed that the cost functions are given by

$$C_i(h_i) = c_i + \gamma \frac{h_i^2}{q_i x};\ i = 0, 1 \tag{4.1}$$

where $c_i \leq 0$ represents fixed costs and $\gamma > 0$ is a cost coefficient. Finally, denoting by $a_0 > 0$ the constant price at which consumers buy the resource harvested by ecological technology and by $a_1 \in (0, a_0)$ the price at which they buy the standard one, the generic profits associated to the i-th behavioral rule reads as

$$\pi_i(x) = a_i h_i(x) - c_i - \gamma \frac{h_i^2(x)}{q_i x};\ i = 0, 1 \tag{4.2}$$

As showed in [89], the optimal harvesting, computed as Nash equilibrium, of the representative player that uses technology i is get from the first order condition $\partial \pi / \partial h_i = 0$ and is given by

$$h_i(x) = \frac{a_i q_i}{2\gamma} x;\ i = 0, 1 \tag{4.3}$$

In the following $a_0 > a_1$ will be assumed, i.e. the loss in efficiency of the more ecological harvesting strategy is counterbalanced by a higher price that consumers wish to pay for the more environmentally-friendly product.

As pointed out in the Introduction 4.1 a discrete-time model is considered here: the resource is assumed to be obtained from a population with non-overlapping generations growing according to the following discrete-time logistic equation

$$x(t+1) = x(t) + \alpha x(t)\left(1 - \frac{x(t)}{k}\right) - Nr(t)h_1(t) - N(1-r(t))h_0(t) \tag{4.4}$$

where the parameter $\alpha > 0$ is the natural growth rate of the resource, $k > 0$ represents the carrying capacity, that is the equilibrium level of the resource in the absence of harvesting. The fraction $r(t)$ is assumed to evolve according to the discrete time exponential replicator dynamics driven by the profits (see e.g. [35] and [73]) that is according to the following discrete time recurrence

$$r(t+1) = \frac{r(t)e^{\beta\pi_1(t)}}{r(t)e^{\beta\pi_1(t)} + (1-r(t))e^{\beta\pi_0(t)}} = \frac{r(t)}{r(t) + (1-r(t))e^{\beta(\Delta\pi(t))}} \tag{4.5}$$

where $\beta \in [0, +\infty)$ is the so called intensity of choice parameter and measures the reactiveness of agents to adopt the more profitable strategy and $\Delta\pi(t)$ is the difference between the two profits which, according to relations (4.3) and (4.2), results to be given by

$$\Delta\pi(t) = \pi_0(t) - \pi_1(t) = \frac{a_0^2 q_0 - a_1^2 q_1}{4\gamma} x(t) - \xi \tag{4.6}$$

with $\xi = c_0 - c_1$. The parameter $\xi \in \mathbb{R}$ represents the difference between fixed costs associated with the two technologies, and may be considered as a government parameter as it includes taxes imposed in order to obtain the prevalence of one technology over the other. In the following is considered the restriction $\xi \leq 0$, coming from the consideration that fixed costs for the more intensive harvesting method are higher, due to more sophisticated technology and higher taxes, or equivalently to government subsidies for agents adopting the more ecological fishing methods. The resulting dynamic model is the two-dimensional iterated map $T : (x, y) \to (x', y')$ explicitly given by

$$T : \begin{cases} x' &= \left(1 + \alpha - \dfrac{N a_0 q_0}{2\gamma}\right) x - \dfrac{\alpha}{k} x^2 + \dfrac{N}{2\gamma}\left(a_0 q_0 - a_1 q_1\right) xr \\ \\ r' &= r\left[r + (1-r)e^{\beta\left(\frac{a_0^2 q_0 - a_1^2 q_1}{4\gamma} x - \xi\right)}\right]^{-1} \end{cases} \tag{4.7}$$

The dynamic variable (x, r) represents a feasible state of the system if $x \geq 0$ and $0 \leq r \leq 1$.

Let now consider the one-dimensional dynamics along the invariant lines. It is first noted that the lines of pure strategies $r = 0$ and $r = 1$ where all agents adopt the same harvesting rule, as well as the line of resource extinction $x = 0$, are invariant sets. In particular the dynamics along the invariant line $x = 0$ is governed by the one-dimensional restriction

$$x = 0: \quad r' = g(r) = \frac{r}{r + (1 - r)\, e^{-\xi}} \tag{4.8}$$

which is a convex function in the interval $r \in [0, 1]$ with fixed points in $r = 0$ (stable) and $r = 1$ (unstable). The dynamics along the invariant line $r = 0$, where all the agents adopt the ecological strategy, are governed by the one-dimensional restriction

$$r = 0: \quad x' = f_0(x) = \left(1 + \alpha - \frac{Na_0q_0}{2\gamma}\right) x - \frac{\alpha}{k}x^2 \tag{4.9}$$

topologically conjugate to the standard logistic map $z' = \mu z\,(1 - z)$ by the transformation $z = \dfrac{2\gamma\alpha}{k\,[2\gamma(1 + \alpha) - Na_0q_0]}x$ and parameter $\mu = 1 + \alpha - \frac{Na_0q_0}{2\gamma}$. Its two fixed points are given by $x_0^0 = 0$ (extinction equilibrium) and

$$x_0^* = \frac{k\,(2\alpha\gamma - Na_0q_0)}{2\alpha\gamma} \tag{4.10}$$

that represents the viable equilibrium under ecological harvesting. Notice that x_0^* is stable for the dynamics along the line $r = 0$ provided that

$$\alpha - 2 < \frac{Na_0q_0}{2\gamma} < \alpha \tag{4.11}$$

where the condition $Na_0q_0/(2\gamma) = \alpha$ represents the transcritical bifurcation along the line $r = 0$ at which the viable equilibrium x_0^* merges with the extinction equilibrium x_0^0, whereas the condition $Na_0q_0/(2\gamma) = \alpha - 2$ represents a period doubling bifurcation, at which a stable cycle becomes the unique attractor along the line $r = 0$. As it is well known, this bifurcation opens the period-doubling cascade, leading to chaotic motion along the line $r = 0$, as the aggregate parameter $Na_0q_0/(2\gamma)$ is further decreased.

The dynamics along the invariant line $r = 1$, where all agents adopt the standard (more intensive) fishing strategy, is governed by the map

$$r = 1: \quad x' = f_1(x) = \left(1 + \alpha - \frac{Na_1q_1}{2\gamma}\right) x - \frac{\alpha}{k}x^2 \tag{4.12}$$

conjugate to the logistic map $z' = \mu z\,(1-z)$ by the transformation $z = \dfrac{2\gamma\alpha}{k\,[2\gamma(1+\alpha) - Na_1q_1]}x$ and parameter $\mu = 1 + \alpha - \frac{Na_1q_1}{2\gamma}$. Here, the viable equilibrium is

$$x_1^* = \frac{k\,(2\alpha\gamma - Na_1q_1)}{2\alpha\gamma} \tag{4.13}$$

Notice $x_0^* > x_1^*$ if $a_0q_0 < a_1q_1$, a parameters' restriction assumed in the following in order to characterize the technology q_0 as more ecological. Calculus shows that the stability of the equilibrium x_1^* along the line $r = 1$ is assured by the conditions

$$\alpha - 2 < \frac{Na_1q_1}{2\gamma} < \alpha \tag{4.14}$$

Analogous statements about the transcritical and period doubling bifurcations already made for x_0^*, hold for x_1^*.

The existence of these invariant lines that bound the two-dimensional phase space of the dynamical system (4.7) is important in order to characterize its global dynamical properties. Moreover, the knowledge of the kind of dynamic motion occurring along the two lines where a single pure strategy exists, tells what will happen in the long run when one of the two strategies becomes dominant in terms of profits so that it will prevail due to evolutionary pressure. The latter problem may be equivalently stated by asking when the one-dimensional attractors of the restrictions along the invariant lines $r = 0$ and $r = 1$ given by (4.9) and (4.12) respectively, are also attractors of the two-dimensional dynamical system. This depends on the transverse stability as well as on the existence of attractors interior to the phase space, i.e. characterized by $r \in (0, 1)$. These are the questions examined, analytically and numerically, in the next Sections. Here, for the sake of clarity, it is worth specifying that the j-cycle ($\mathrm{j} \geq 1$) laying on an invariant line has one of its eigenvectors that is along the invariant line itself, while the other eigenvector has generally another direction. This last eigenvector is commonly named transverse eigenvector, which is tangent to the so-called transverse invariant manifold.

4.3 Existence and stability of equilibrium points

The equilibrium points of the model (4.7) are solutions of the system

$$\begin{cases} x\left[\alpha - \dfrac{Na_0q_0}{2\gamma} - \dfrac{\alpha}{k}x + \dfrac{N}{2\gamma}\left(a_0q_0 - a_1q_1\right)r\right] = 0 \\ \\ r(1-r)\left[e^{\beta\left(\frac{a_0^2q_0 - a_1^2q_1}{4\gamma}x - \xi\right)} - 1\right] = 0 \end{cases} \tag{4.15}$$

The extinction fixed points $E_0^0 = (0,0)$ and $E_1^0 = (0,1)$ always exist. Moreover, if $\xi = 0$ then any point of the whole segment $(0,r)$, with $r \in [0,1]$, is a fixed point. Other boundary equilibrium points are $E_0^* = (x_0^*, 0)$ with x_0^* given by (4.10) and $E_1^* = (x_1^*, 1)$ with x_1^* given by (4.13). Furthermore, an interior equilibrium may exist, characterized by the co-existence of both harvesting strategies, given by $E^* = (x^*, r^*)$ with

$$x^* = \frac{4\gamma\xi}{a_0^2q_0 - a_1^2q_1}; \quad r^* = \frac{2\alpha\gamma(k - x^*) - Nka_0q_0}{Nk\left(a_1q_1 - a_0q_0\right)} \tag{4.16}$$

provided that $x^* > 0$ and $r^* \in (0,1)$.

Let notice that if $\xi < 0$, i.e. $c_0 < c_1$ as argued above, then $x^* > 0$ provided that $a_0^2q_0 < a_1^2q_1$, which is a more stringent condition than $a_0q_0 < a_1q_1$ being $a_0 > a_1$. It will be assumed that this condition is satisfied in the following[1]. It is worth noticing that the condition $r^* \in (0,1)$ can be easily expressed in term of the carrying capacity k, as $r^* = 0$ for $k = k_0$ with

$$k_0 = \frac{2\alpha\gamma x^*}{2\alpha\gamma - Na_0q_0} = \frac{8\alpha\gamma^2\xi}{\left(2\alpha\gamma - Na_0q_0\right)\left(a_0^2q_0 - a_1^2q_1\right)} \tag{4.17}$$

and $r^* = 1$ for $k = k_1$ with

$$k_1 = \frac{2\alpha\gamma x^*}{2\alpha\gamma - Na_1q_1} = \frac{8\alpha\gamma^2\xi}{\left(2\alpha\gamma - Na_1q_1\right)\left(a_0^2q_0 - a_1^2q_1\right)} \tag{4.18}$$

with $k_0 < k_1$ being $a_0q_0 < a_1q_1$, so that $r^* \in (0,1)$ for $k_0 < k < k_1$.

These existence conditions are the same as the ones given in [89] for the model in continuous time, whereas the stability conditions now are different. In order to study

[1]For sake of completeness, we stress that if $\xi > 0$, i.e. $c_0 > c_1$, then $x^* > 0$ provided that $a_0^2q_0 > a_1^2q_1$, that together with the condition $a_0q_0 < a_1q_1$ implies $\frac{a_1^2q_1}{a_0} < a_0q_0 < a_1q_1$, which is a nonempty set being $a_0 > a_1$.

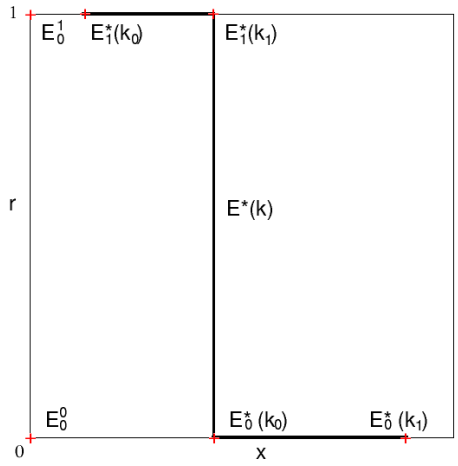

Fig. 4.1 Fixed points $E^*(k)$, $E_0^*(k)$ and $E_1^*(k)$ are shown as $k \in [k_0, k_1]$. The point E^* merges with E_0^* in $r = 0$ for $k = k_0$ and merges with E_1^* in $r = 1$ for $k = k_1$. Other fixed points do not depend on k.

the local stability of the equilibrium points we consider the Jacobian matrix

$$\boldsymbol{J}(x,r) = \begin{bmatrix} 1+\alpha-\dfrac{Na_0}{2\gamma}-\dfrac{2\alpha}{k}x-\dfrac{N}{2\gamma}\left(a_1q_1-a_0q_0\right)r & -\dfrac{N\left(a_1q_1-a_0q_0\right)x}{2\gamma} \\ \dfrac{\beta r(1-r)\left(a_1^2q_1-a_0^2q_0\right)e^{\beta\Delta\pi}}{4\gamma\left(r+(1-r)e^{\beta\Delta\pi}\right)^2} & \dfrac{e^{\beta\Delta\pi}}{\left(r+(1-r)e^{\beta\Delta\pi}\right)^2} \end{bmatrix} \tag{4.19}$$

In E_0^0 it results that

$$\boldsymbol{J}(0,0) = \begin{bmatrix} 1+\alpha-\frac{Na_0q_0}{2\gamma} & 0 \\ 0 & e^{\beta\xi} \end{bmatrix} \tag{4.20}$$

so E_0^0 is stable along the vertical direction (r direction) and stable along the horizontal one (x direction) provided that $Na_0q_0/(2\gamma) - 2 < \alpha < Na_0q_0/(2\gamma)$. At E_1^0 we have

$$\boldsymbol{J}(0,1) = \begin{bmatrix} 1+\alpha-\dfrac{Na_1q_1}{2\gamma} & 0 \\ 0 & e^{-\beta\xi} \end{bmatrix} \tag{4.21}$$

so E_1^0 is unstable along the vertical direction and stable along the horizontal one provided that $Na_1q_1/(2\gamma) - 2 < \alpha < Na_1q_1/(2\gamma)$.

In E_0^* it results

$$\boldsymbol{J}(x_0^*,0)=\begin{bmatrix} 1-\alpha+\dfrac{Na_0q_0}{2\gamma} & -\dfrac{N\left(a_1q_1-a_0q_0\right)\left(2\alpha\gamma-Na_0q_0\right)}{2\alpha\gamma^2} \\ 0 & e^{\beta\left(\frac{k\left(a_1^2q_1-a_0^2q_0\right)\left(2\alpha\gamma-Na_0q_0\right)}{8\alpha\gamma^2}+\xi\right)} \end{bmatrix} \tag{4.22}$$

so E_0^* is stable along the eigendirection transverse to $r=0$ if $k<k_0$, with k_0 given by (4.17), and stable along the horizontal direction if $Na_0q_0/(2\gamma)<\alpha<Na_0q_0/(2\gamma)+2$.

In E_1^* it results

$$\boldsymbol{J}(x_1^*,1)=\begin{bmatrix} 1-\alpha+\dfrac{Na_1q_1}{2\gamma} & -\dfrac{N\left(a_1q_1-a_0q_0\right)\left(2\alpha\gamma-Na_1q_1\right)}{2\alpha\gamma^2} \\ 0 & e^{-\beta\left(\frac{k\left(a_1^2q_1-a_0^2q_0\right)\left(2\alpha\gamma-Na_1q_1\right)}{8\alpha\gamma^2}+\xi\right)} \end{bmatrix} \tag{4.23}$$

so E_1^* is stable along the eigen-direction transverse to $r=1$ if $k>k_1$ with k_1 given by (4.18), and stable along the horizontal direction if $Na_1q_1/(2\gamma)<\alpha<Na_1q_1/(2\gamma)+2$.

Notice that all the stability conditions along the horizontal invariant lines $r=0$ and $r=1$, on which the boundary fixed points are located, correspond to those already examined for the logistic restrictions (4.9) and (4.12).

Finally, in E^* it results

$$\boldsymbol{J}(x^*,r^*)=\begin{bmatrix} 1-\frac{\alpha x^*}{k} & -\frac{N(a_1q_1-a_0q_0)x^*}{2\gamma} \\ \frac{\beta}{4\gamma}r^*(1-r^*)\left(a_1^2q_1-a_0^2q_0\right) & 1 \end{bmatrix} \tag{4.24}$$

Hence, given that trace and determinant of the matrix (4.24) are respectively

$$\mathrm{tr}\boldsymbol{J}=2-\frac{\alpha x^*}{k}=2-\frac{4\alpha\gamma\xi}{k\left(a_0^2q_0-a_1^2q_1\right)} \tag{4.25}$$

$$\det\boldsymbol{J}=1-\frac{\alpha x^*}{k}+\frac{N\beta}{8\gamma^2}\left(a_1q_1-a_0q_0\right)\left(a_1^2q_1-a_0^2q_0\right)x^*r^*\left(1-r^*\right) \tag{4.26}$$

and, as stated in previous Chapters, a sufficient condition for the local asymptotic stability of E^* is that the eigenvalues of (4.24) are located inside the unit circle of the complex plane. A necessary and sufficient condition for this is given by the system of inequalities (the Schur or Jury's conditions, see e.g. [46]) involving the characteristic

polynomial of the Jacobian matrix $\boldsymbol{J}$ given in (2.17) of Chapter 2. In the present case it results that $P(1) = -\frac{4N\beta\xi}{8\gamma}\left(a_1q_1 - a_0q_0\right)r^*\left(1-r^*\right) > 0$ which vanishes (and then changes sign) when r^* crosses the value $r^* = 0$ from above and when r^* crosses the value $r^* = 1$ from below. These two conditions correspond to transcritical bifurcations when the interior equilibrium $E^* = (x^*, r^*)$ merges with the boundary points E_0^* and E_1^* respectively. In fact, the condition $r^*(x^*) = 0$ implies $x^* = x_0^*$ and $r^*(x^*) = 1$ implies $x^* = x_1^*$. The two bifurcation conditions can easily be expressed in terms of the carrying capacity k as $k = k_0$ and $k = k_1$ respectively, see also figure 4.1, where the equilibrium points are represented for k in the range $[k_0, k_1]$. Notice that a change of sign of $P(1)$ also occurs when ξ changes from negative to positive, and this is a transcritical bifurcation as well, but of codimension two as it occurs when the fixed point E^* crosses at $\xi = 0$ the segment of fixed points along the axis $x = 0$.

Before analyzing the other two stability conditions, consider the condition $(\mathrm{tr}\boldsymbol{J})^2 - 4\mathrm{det}\boldsymbol{J} > 0$ which ensures that the eigenvalues are real. Calculus shows that the previous inequality becomes

$$2\alpha^2\gamma^2x^* + 16k\alpha\gamma^2 > k^2N\beta\left(a_1q_1 - a_0q_0\right)\left(a_1^2q_1 - a_0^2q_0\right)r^*\left(1-r^*\right) \tag{4.27}$$

from which it is evident that it is surely satisfied (hence eigenvalues are reals) when r^* is very close to 0 or 1, whereas it is surely not satisfied (hence eigenvalues are complex conjugate) for intermediate values of r^* and sufficiently high values of the parameter β. Notice also that both x^* and r^* do not depend on the parameter β.

Indeed, if the other parameters are fixed so that $x^* > 0$ and r^* has intermediate values, i.e. it is not too close to the invariant lines of pure strategies, then a Neimark-Sacker bifurcation occurs for increasing values of β. In fact, the third stability condition $1 - \mathrm{det}\boldsymbol{J} > 0$, where a change of sign of the left hand side indicates the occurrence of a Neimark-Sacker bifurcation of E^*, becomes

$$N\beta\left(a_1q_1 - a_0q_0\right)\left(a_1^2q_1 - a_0^2q_0\right)r^*\left(1-r^*\right) < \frac{8\alpha\gamma^2}{k} \tag{4.28}$$

This stability condition can be equivalently written as $\beta < \beta_{NS}$, with

$$\beta_{NS} = \frac{8\alpha\gamma^2}{Nk\left(a_1q_1 - a_0q_0\right)\left(a_1^2q_1 - a_0^2q_0\right)r^*\left(1-r^*\right)} \tag{4.29}$$

and r^* given by (4.16), and a Neimark-Sacker bifurcation occurs when β increases across β_{NS}.

Finally, the stability condition $P(-1) > 0$ becomes

$$32k\gamma^2 + Nk\beta\left(a_1q_1 - a_0q_0\right)\left(a_1^2q_1 - a_0^2q_0\right)x^*r^*\left(1 - r^*\right) > 16\alpha\gamma^2x^* \tag{4.30}$$

that can be equivalently written as $\beta > \beta_F$ with

$$\beta_F = 2\beta_{NS} - \frac{8\gamma}{N\xi\left(a_0q_0 - a_1q_1\right)r^*\left(1 - r^*\right)} \tag{4.31}$$

These results can be summarized by the following statement:

Proposition 1 *The map* (4.7)*, with* $\xi \in (-\infty, +\infty)$ *and positive values of all other parameters, always has the boundary fixed points* $E_0^0 = (0,0)$ *and* $E_1^0 = (0,1)$*, and if* $\xi = 0$ *any point of the whole segment* $(0,r)$*, with* $r \in [0,1]$*, is a fixed point. Moreover, the following holds:*

i.) If $2\alpha\gamma > Na_iq_i$*,* $i = 0,1$*, then two more boundary fixed points exist, namely* $E_0^* = (x_0^*, 0)$ *with* x_0^* *given by (4.10) and* $E_1^* = (x_1^*, 1)$ *with* x_1^* *given by (4.13).*

ii.) If $\xi < 0$*,* $a_0^2q_0 < a_1^2q_1$ *and* $k_0 < k < k_1$ *where* k_0 *and* k_1 *are given by (4.17) and (4.18) respectively, then an interior equilibrium* $E^* = (x^*, r^*)$ *exists with components given by (4.16).*

iii.) If E_0^* *exists (i.e.* $2\alpha\gamma > Na_0q_0$*) then for* $\xi < 0$ E_0^0 *is a saddle point with stable set along the invariant line* $x = 0$ *and unstable set along the invariant line* $r = 0$*.*

iv.) If E_1^* *exists (i.e.* $2\alpha\gamma > Na_1q_1$*) then for* $\xi < 0$ E_1^0 *is an unstable node.*

v.) E_0^* *is a stable node if* $k < k_0$ *and* $\frac{Na_0q_0}{2\gamma} < \alpha < \frac{Na_0q_0}{2\gamma} + 2$*. At* $k = k_0$ *it undergoes a transcritical bifurcation at which it merges with* E^**, at* $\alpha < \frac{Na_0q_0}{2\gamma} + 2$ *it undergoes a flip bifurcation along the invariant line* $r = 0$*.*

vi.) E_1^* *is a stable node if* $k > k_1$ *and* $\frac{Na_1q_1}{2\gamma} < \alpha < \frac{Na_1q_1}{2\gamma} + 2$*. At* $k = k_1$ *it undergoes a transcritical bifurcation at which it merges with* E^**, at* $\alpha < \frac{Na_1q_1}{2\gamma} + 2$ *it undergoes a flip bifurcation along the invariant line* $r = 1$*.*

vii.) The interior fixed point E^* *is stable if* $k_0 < k < k_1$ *and* $\beta_F < \beta < \beta_{NS}$*, where* β_{NS} *and* β_F *are given by (4.29) and (4.31) respectively, hence the range of stability is nonempty provided that* $\alpha\gamma\xi > -k\left(a_1^2q_1 - a_0^2q_0\right)$

It is worth highlighting that condition $\beta_F < \beta_{NS}$ is equivalent to $k < \frac{\alpha x^*}{4}$ that, being $k > k_0$, is verified for $1 + \alpha - \frac{Na_0q_0}{2\gamma} < 5$, that is true when the restriction (4.9) to $r = 0$ has bounded dynamics, i.e. when $1 + \alpha - \frac{Na_0q_0}{2\gamma} \leq 4$. The stability range of the interior equilibrium E^*, as the parameter β varies, is shown by the bifurcation diagrams in Figure 4.2, where the supercritical flip and Neimark-Sacker bifurcations, through which the equilibrium loses its stability for decreasing and increasing values of β respectively, can be clearly seen.

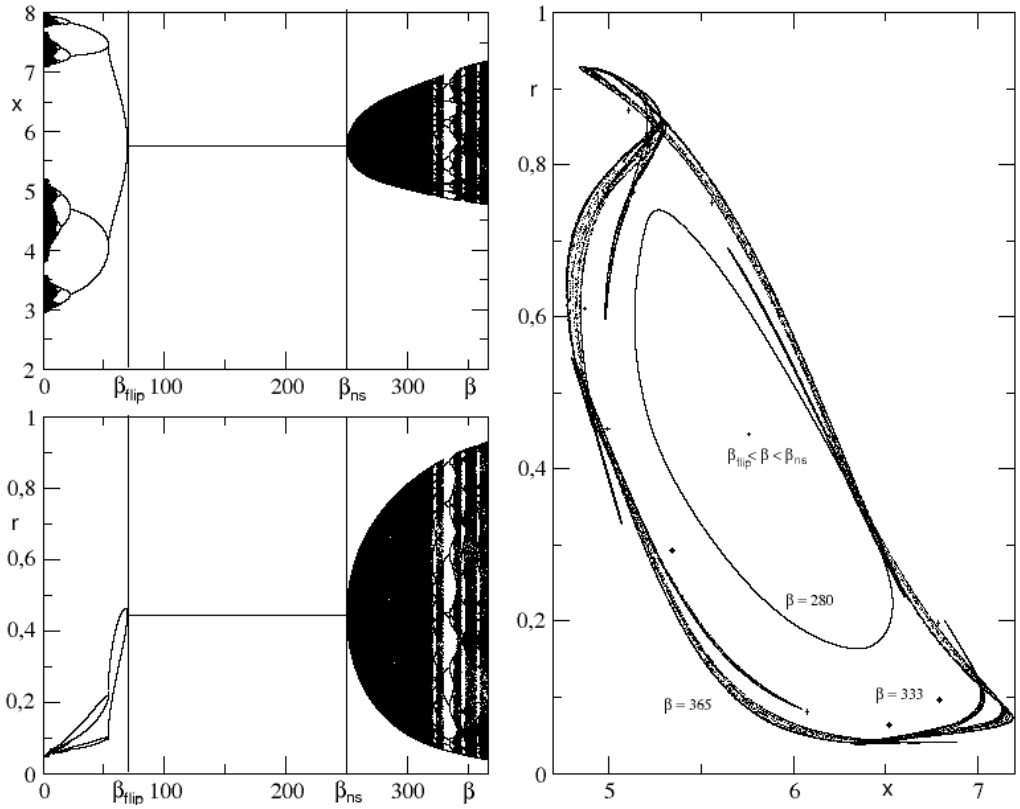

Fig. 4.2 Left column: Bifurcation diagrams for $\beta \in [0, 350]$ showing the asymptotic dynamics of the two state variables x and r. Parameters: $\alpha = 2.7$, $\gamma = 1$, $N = 15$, $a_0 = 1.05487$, $a_1 = 0.5$, $q_0 = 0.01$, $q_1 = 0.2$, $k = 6.7$ and $\xi = -0.056$. Right column: Attractors on the (x, r) phase space for different values of β. The other parameters are as in the left column.

4.4 Global dynamics

Here are presented further analytical results and numerical explorations of some global dynamic scenarios of the discrete dynamical system (4.7) under the constraints on the parameters imposed by the economic and ecologic meaning of the model. The numerical

simulations will confirm the analytical results on local stability and bifurcations given in the Section 4.3 and some snapshots about global dynamic behaviors are given.

First consider the bifurcation diagrams in Figure 4.2. They show the long run dynamics of the model varying the intensity of choice parameter β, that represents the evolutionary propensity to switch to the more profitable technology. In evolutionary models a common occurrence is that an increase of the value of β leads to instability and complex dynamics, see e.g. [73]. However, this is not necessarily true in the case of the evolutionary model studied herein. Indeed, starting from values of the parameter β colse to zero, as it is increased, is observed a transition from oscillatory dynamics (periodic or chaotic) towards non oscillatory dynamics through a cascade of period-halving bifurcations leading to the stability of the fixed point E^*. Moreover, there is a range of the values of β, namely $\beta \in (\beta_F, \beta_{NS})$ as stated in Proposition 1, such that the fixed point E^* is stable. Furthermore, for $\beta > \beta_{NS}$, the equilibrium point E^* becomes unstable again through a supercritical Neimark-Sacker bifurcation, at which a stable invariant closed curve is created around E^* itself, whose amplitude increases as β increases, see figure 4.2 right panel. So, this example underlines the unusual result that low values of intensity of choice, as well as high values, lead to instability of the fixed point E^* with the creation of periodic or quasi-periodic or even chaotic attractors, whereas intermediate levels of the intensity of choice are required for the local asymptotic stability of E^*.

Other interesting results regard the evolutionary dominance of one of the two harvesting strategies. On the basis of the analytical results of Section 4.3 is known that, as long as E^* exists, then the two fixed points E_0^* and E_1^* are transversally unstable. At first sight, this may suggest that an evolutionary dominant strategy, that is an attractor along the invariant lines $r = 0$ or $r = 1$, exits if and only if the interior fixed point E^* is unfeasible and at the same time an attractor with $r \in (0, 1)$ exits if and only if the interior fixed point E^* is feasible. Instead, interior attractors (cyclic or chaotic) may exist even for $k > k_1$, i.e. after the transcritical bifurcation at which the equilibrium E^* merges with E_1^* and becomes unfeasible. Moreover, convergence towards the invariant line $r = 0$ may occur even when the equilibrium E^* is feasible, i.e. $k_0 < k < k_1$. These two occurrences are summerized respectively by the following two Propositions.

Proposition 2 *Consider map* (4.7). *Let* $\xi < 0$ *and the other parameters are positive and such that* E_1^* *exists and it is unstable along the manifold* $r = 1$, *and a period-2 cycle, say* $\mathcal{C}_1^2 = \{(x_1^{*_1}, 1), (x_1^{*_2}, 1)\}$, *exists on the invariant set* $r = 1$, *as the result of*

the period-doubling bifurcation of E_1^*. If the following condition holds

$$\xi - \frac{k\left(a_0^2 q_0 - a_1^2 q_1\right)}{2\alpha\gamma} < \frac{k\left(a_0^2 q_0 - a_1^2 q_1\right)\left(2\gamma\alpha - N a_1 q_1\right)}{8\alpha\gamma^2} - \xi < 0 \tag{4.32}$$

then the fixed point E_1^* has stable transverse invariant manifold and period-2 cycle $\mathcal{C}_1^2$ is transversely unstable. The contrary cannot occur.

Proof. See Appendix E. ■

The Proposition 2 hints at an interesting dynamic scenarios, confirmed by the numerical simulations shown in Figure 4.3. In this case, although there are no interior fixed points and the border equilibrium E_1^* is transversely stable, the dynamics of the model can still converge in the long run to a stable inner attractor, a stable period-2 cycle $\mathcal{C}_1^2$ shown in Figure 4.3 (left panel). This evidence indicates that the stability of the transverse invariant manifold of E_1^* does not imply the predominance by evolutionary pressure of the standard (or intensive) technology.

The situation is different (and in some sense reverted) when we consider the invariant line $r = 0$, as stated in the following proposition.

Proposition 3 *Consider map* (4.7)*. Let $\xi < 0$ and the other parameters are positive and such that E_0^* exists and it is unstable along the invariant manifold $r = 0$, and a period-2 cycle, say $\mathcal{C}_0^2 = \{(x_0^{*1}, 0), (x_0^{*2}, 0)\}$, exists on the invariant set $r = 0$, as the result of the period-doubling bifurcation of E_0^*. If the following condition holds*

$$\xi - \frac{k\left(a_0^2 q_0 - a_1^2 q_1\right)}{2\alpha\gamma} < \frac{k\left(a_0^2 q_0 - a_1^2 q_1\right)\left(2\gamma\alpha - N a_0 q_0\right)}{8\alpha\gamma^2} - \xi < 0 \tag{4.33}$$

then the fixed point E_0^* is transversely unstable and period-2 cycle $\mathcal{C}_0^2$ has a stable transverse invariant manifold. The contrary cannot occur.

Proof. See Appendix F. ■

The Proposition 3 provides an interesting result highlighted by the numerical simulations shown in figure 4.3 (right panel), where, although the border equilibrium E_0^* is transversally unstable, the 2-cycle $\mathcal{C}_0^2$ is locally asymptotically stable and coexists with the locally asymptotically stable interior fixed point E^*. Numerical investigations suggest that this dynamic scenario occurs due to a specific sequence of bifurcations. In particular, a 2-cycle in the region with negative r, let us name it $\mathcal{C}^2$, undergoes a transcritical bifurcation, merging with the 2-cycle $\mathcal{C}_0^2$ originated by a period-doubling bifurcation of the fixed point E_0^*, and becomes feasible. After the bifurcation $\mathcal{C}_0^2$

becomes local asymptotically stable while $\mathcal{C}^2$ is a saddle 2-cycle and its one-dimensional stable manifold marks the boundary separating the basins of attraction of E^* and $\mathcal{C}_0^2$. Then, changing the values of the parameters in a suitable way, the 2-cycle $\mathcal{C}^2$ disappears through a subcritical flip bifurcation at which E^* looses stability and becomes a saddle fixed point. These bifurcations occur before the merging of E^* with E_0^*. These results underlines that agents can select the environmentally-friendly technology even when E^* is a feasible fixed point and E_0^* is transversely unstable and point out a quite peculiar property of the considered evolutionary model. In fact, the instability of the inner fixed point of the model may lead to an increase in the propensity of the agent to adopt the environmentally-friendly technology. These scenarios do not occur on the continuous (or hybrid) setting of the model analyzed in [89].

The basins of attraction in figure 4.3 reveals further interesting properties of the dynamics of the model. In particular, from the right panel in figure 4.3, it is possible to observe that the transverse unstable manifold of E_0^* belongs to the basin of attraction of E^*, hence such a basin has a contact with the invariant line $r = 0$ at the point E_0^*. This implies that all the preimages of E_0^* along the invariant line $r = 0$, computed according to the restriction (4.9), represent tongues at which the basin of E^* has a contact with line $r = 0$. In the same figure only some of them are visible, but infinitely many exist and accumulate near E_0^0. The fine structure of these tongues is quite complicated and will be analyzed in future works.

It is worth observing that the mechanisms that lead to the evolutionary-dominant environmentally-friendly technology when the fixed point E^* is feasible, can be even different from the described one and, as shown in the following, can be due to the existence of non topological Milnor attractors on the invariant line $r = 0$. For example, the bifurcation diagrams in Figure 4.4, obtained varying parameter a_0 in the range $[0.5, 1.3]$, show another case such that an attracting invariant set $\mathcal{A}_s$, laying on the axis $r = 0$, exists even when the interior equilibrium point E^* is feasible. The measure-theoretic arguments about the transverse attractiveness of the invariant set $\mathcal{A}_s$, already mentioned in Section 3.3 of Chapter 3 and in Appendix D and here recalled, can be used to provide an explanation of this dynamic phenomenon. In particular take into account the transverse Lyapunov exponent (see e.g. [13], [31]) given by

$$\Lambda_\perp = \lim_{N\to\infty} \frac{1}{N} \sum_{n=0}^{N} \ln |\nu_\perp(x_n)| \tag{4.34}$$

where $\{x_n = f_0^n(x_0), n \geqslant 0\}$ is a trajectory embedded in $\mathcal{A}_s$ and $\nu_\perp(x_n)$ is the transverse eigenvalue computed in x_n. Precisely, when $\mathcal{A}_s$ is a k-cycle $\mathcal{C}_0^k$, its transverse attrac-

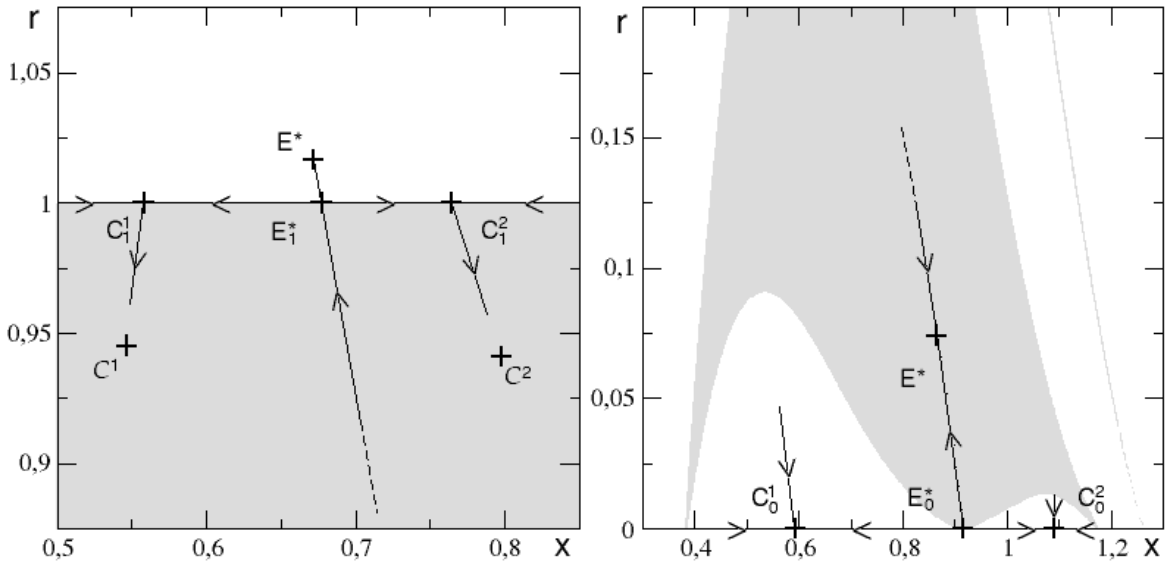

Fig. 4.3 Left panel: The gray region is the basin of attraction of the inner period-2 cycle $\mathcal{C}_1^2$ while the fixed point E_1^* is transversely attractive. The point E^* is unfeasible, i.e. it lies in the region $r > 1$. Parameters' values: $\alpha = 3.1$, $k = 1$, $N = 8$, $q_1 = 1$, $q_0 = 0.01$, $\gamma = 4$, $a_0 = 1.1$, $a_1 = 1$, $\beta = 10$, $\xi = -0.0415$. Right panel: The gray region is the basin of attraction of the transversely stable fixed point E^* and the white region is the basin of attraction of the period-2 cycle $\mathcal{C}_0^2$. Parameters' values: $\alpha = 2.6$, $k = 1$, $N = 8$, $q_1 = 1$, $q_0 = 0.1$, $\gamma = 2$, $a_0 = 1.1$, $a_1 = 1$, $\beta = 80.615$, $\xi = -0.095$.

tiveness is measured by the product of the transverse eigenvalues $\nu_\perp^k = \prod_{i=1}^k \nu_\perp(x_i)$ and, if $\Lambda_\perp(\mathcal{C}^k) = k^{-1} \ln |\nu_\perp^k| < 0$, then $\mathcal{A}_s$ is a topological attractor. Whilst, when the attractor $\mathcal{A}_s$ is chaotic and so includes infinitely many cycles densely distributed within it, each one characterized by its own transversal Lyapunov exponent, transverse attractiveness of $\mathcal{A}_s$ can be measured by the spectrum of the Lyapunov exponents. This is defined, see e.g. [31], as

$$\Lambda_\perp^{\min} \leqslant \cdots \leqslant \Lambda_\perp^{\text{nat}} \leqslant \cdots \leqslant \Lambda_\perp^{\max} \tag{4.35}$$

where $\Lambda_\perp^{\min}$ and $\Lambda_\perp^{\max}$ are the Lyapunov exponents of the most attractive and the most repelling cycles in $\mathcal{A}_s$ respectively. Moreover the *natural Lyapunov exponent* $\Lambda_\perp^{\text{nat}}$ is computed along a generic aperiodic trajectory embedded in $\mathcal{A}_s$, and it measures transversal attractiveness on *average*. In other words, $\Lambda_\perp^{\text{nat}}$ carries contributions to attractiveness from all the trajectories in $\mathcal{A}_s$, giving the mean local behavior in its neighborhood (see e.g. [103]). If $\mathcal{A}_s$ contains at least one transversely repelling cycle with a dense set of preimages embedded in $\mathcal{A}_s$, that is $\Lambda_\perp^{\max} > 0$, than there is no

neighborhood of $\mathcal{A}_s$ containing only points whose ω-limit set belongs to $\mathcal{A}_s$. According to the theorem stated in [5] the latter inequality implies that the one-dimensional invariant chaotic set cannot be a Lyapunov attractor in the two-dimensional space because of the transversely unstable set of the period-2 cycle as well as its preimages. If the inequality $\Lambda_\perp^{\text{nat}} < 0$ holds also, thus the set $\mathcal{A}_s$ attracts a positive measure set of points which converges to it. It follows that this is an attractor in Milnor sense (see [101]). A large number of results about global attractiveness of invariant manifold of lower dimension than the total phase space can be found in the literature, see e.g. [5], [13], [31].

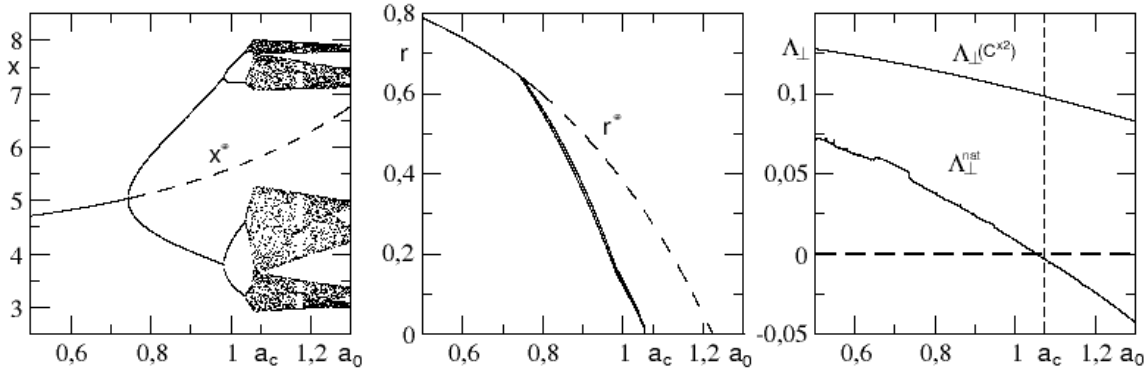

Fig. 4.4 Bifurcation diagram of x vs a_0 (left panel) and r vs a_0 (center panel) varying $a_0 \in (a_1, a_1\sqrt{q_1/q_0})$. Dashed lines represent paths of both x^* and r^*. It can be noted that the asymptotic dynamics is enclosed along the invariant axis $r = 0$ even for $r^*(a_0) > 0$. This is due to the transverse attractiveness of some subsets of the invariant axes $r = 0$ while both the fixed point E_0^* and the period-2 cycle $\mathcal{C}_0^2$ are transversally repelling. For $\mu = 1 + \alpha - Na_0q_0/2\gamma \approx 3.5925721841$ such that $a_0 = a_c = 1.07428$, the attractor $\mathcal{A}_s$ of the logistic map on $r = 0$ is characterized by pure chaos. Since $\Lambda_\perp^{\text{nat}}(\bar{\mu}) \approx -0.0034703 < 0$ while $\Lambda_\perp(\mathcal{C}_0^2) > 0$, it results that $\mathcal{A}_s$ is a non topological Milnor attractor. Parameters' values are as in figure 4.2 except $N = 20$ and $\beta = 5$.

In the right panel of figure 4.4, there are presented both the transverse Lyapunov exponent characterizing transverse attractiveness of $\mathcal{A}_s$ and the transverse Lyapunov exponent of to the period-2 cycle $\mathcal{C}_0^2$. For suitable values of the aggregate parameter $\mu = 1 + \alpha - \dfrac{N}{2\gamma}a_0q_0$, at which the 2-cycle of the logistic map undergoes the homoclinic bifurcation due to which 2-cyclic chaotic intervals are obtained by the merging of 4-cyclic chaotic intervals, pure chaos exists in $\mathcal{A}_s$ (see e.g [96]). For example, for $\alpha = 2.7$, $N = 20$, $\gamma = 1$, $q_0 = 0.01$ and $a_0 = a_c = 1.07428$, we detect the presence of a Milnor attractor when $\mu = \bar{\mu} \approx 3.5925721841$, value at which $\Lambda_\perp^{\text{nat}}(\bar{\mu}) < 0$ while $\Lambda_\perp^{\max} \geqslant \Lambda_\perp(\mathcal{C}_0^2) > 0$. Note that the parameter β is a called normal parameter, that is it

affects only the transverse stability of $\mathcal{A}_s$ and does not have influence on the dynamics inside the invariant set $\mathcal{A}_s$. Setting $\mu = 1 + \alpha - Na_0q_0/(2\gamma) = \bar{\mu}$ and varying β, the spectrum of Lyapunov exponents varies, i.e. the topological property of the invariant set $\mathcal{A}_s$ are changing turning to be a chaotic saddle, a non topological Milnor attractor and a topological Lyapunov stable set. To sum up it can be stated that $\mathcal{A}_s$ can attract a set of positive Lebesgue measures even when it contains repelling cycles together with dense sets of their preimages.

In the last part of the Section, it is pointed out that numerical simulations of the model show dynamic scenarios which are difficult to infer analytically. For example, in figure 4.5 is observed a chaotic attractor in the region $r \in (0, 1)$ where both harvesting strategies coexist, although there is a prevalence of the environmentally-friendly one. The time series $r(t)$ shows an apparently stochastic behavior which typically characterizes the evolutionary dynamics driven by a replicator equation.

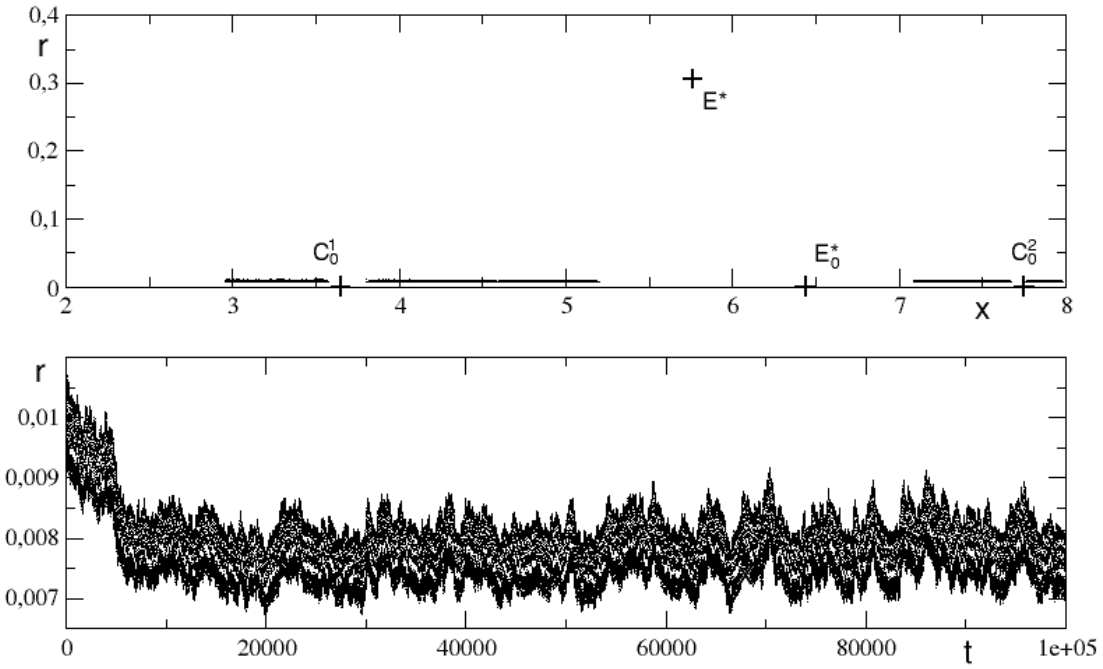

Fig. 4.5 Upper panel: a trajectory in the phase space. Lower panel: a time series of $r(t)$. Parameters' values are as in Figure 4.2 but $N = 20$ and $\beta = 5$.

To conclude, the entire class of evolutionary games that this model could represent reveals some interesting and economically insightful dynamics that are not observable in other and more simple evolutionary games, see e.g. [73]. In particular, Neimark-Sacker bifurcations and cascade of period-doubling bifurcations can lead to quite complicated, even chaotic, dynamics. Moreover, a deeper analytical and numerical analysis reveals

the existence of Milnor attractors. For this reason the presence of the Milnor attractors and the related study of riddled basins for this class of evolutionary games, represent an interesting aspect that deserve further investigation.

Chapter 5

Case study: evolutionary competition between boundedly rational behavioral rules in oligopoly games

5.1 Introduction

It is well known that the solution concept adopted in oligopoly theory is the Cournot-Nash equilibrium. In particular, the Cournot equilibrium, proposed by Cournot in 1838, is the first example of Nash equilibrium, which is a concept elaborated by Nash in 1950 for general n-person games. When all agents are in such an equilibrium, no unilateral deviation by a single agent is profitable and therefore no one has an incentive to deviate from that state.

However, the possibility for the economic agents to reach the Nash equilibrium is not an obvious achievement when the assumptions of perfect rationality and complete information of the classical game theory are not assumed any more.

Indeed, in real-world situations firms are complex organizations that elaborate particular "behavioral rules" to face the market competition in uncertainty conditions and to make their decisions regarding quantities to produce, prices, R&D activities, business strategies, advertisement, etc. If "better" rules are currently available, it seems reasonable that the firm's management would update the previous adopted rules in order to improve the overall "performance" of the firm.

In the economic literature, several studies have been proposed to fill the gap between the theory of oligopoly and a more realistic description of competition. As an example, in the paper "Endogenous fluctuations under evolutionary pressure in Cournot competition", E. Droste et al. (see [43]) present an interesting example with a Cournot duopoly where ex-ante identical firms can employ different behavioral rules to set the quantities to produce. The economic structure of the underlying game is particularly simple, with homogeneous goods, linear demand and quadratic production costs. The fitness of each behavioral rule at each time period is assessed by considering average payoffs obtained by pairs of firms that are randomly matched to play the game. An evolutionary mechanism based on average profits regulates the distribution of the various rules over time. Further, in the same paper ([43]), Droste et al. concentrate on the comparison between a cheap "Best Reply" rule and a costly "Nash" rule and shows that endogenous fluctuations and complicated dynamics may arise, mainly due to the dominance of Best Reply behavior in a neighborhood of the Nash equilibrium because of information costs. Also, in the paper "On the stability of the Cournot equilibrium: An evolutionary approach" by Hommes at al., see [76], is presented a similar setup with linear demand and linear production costs but with random matching of n firms at a time. On the basis of past performance, these firms decide to switch between costly rational and cheap boundedly-rational expectation rules on aggregate output of their rivals. In this framework, Hommes at al. finds that the classic Theocharis' result [120] on the instability of the Nash equilibrium with more than three firms is also confirmed qualitatively in an evolutionary setting.

A Cournot oligopoly game populated by firms that adopt rules based on limited knowledge of the demand function is of interest from an economic prospective, as demand function may often be difficult to be estimated, as pointed out in early contributions on learning of the demand function, see, e.g. [81] and [29], as well as in recent contributions, see, e.g., [26] and [123]. In particular, it can be cited here the contribution from the paper "Learning cycles in Bertrand competition with differentiated commodities and competing learning rules" by M. Anufriev at al. (see [9]) where an oligopoly game with heuristics (analogous to the one here considered) under Bertrand competition with nonlinear demand has been proposed. In that paper, some firms use Least Square Learning, wrongly assuming that demand is linear and does not depend on competitors' prices (analogously to LMA firms), and other firms use Gradient learning (in prices). Nevertheless, in both contributions the possibility to converge to a stable equilibrium depends on the parameters configuration and the presence of heterogeneous learning mechanisms may lead to non stationary dynamics.

In the present Chapter is first presented a general framework for dealing with evolutionary oligopoly models with different behavioral rules and show some general properties of such setting whatever the switching mechanism among the rules is designed.

Afterwards, it is examined a particular example with two specific behavioral rules proposed in the oligopoly literature to model agents with boundedly rational expectations in forecasting next-period outputs. One rule is the so-called Local Monopolistic Approximation (LMA), which was first proposed in [26] to model a dynamic oligopoly where demand is not known by firms but estimated at each time period through market experiments, see also [123]. In particular, in [26] is showed that the dynamics generated through LMA behavior converges to a Nash equilibrium also in cases where the classic Best Reply dynamics fail to converge to it. The second rule is the Gradient (G) dynamics, which was first proposed in [25], to model the behavior of boundedly rational duopolists who decide their production in order to improve their profits over time. In particular, in [25] is established under which conditions this adjustment preserves the convergence to the Nash equilibrium of the game and the possible asymptotic dynamics of the system.

In the evolutionary game here considered firms adopt less cognitively demanding heuristics than in the most related contributions, such as [43], [76] and [22], where at least one behavioral rule employs global knowledge of the demand function. Indeed the specific behavioral rules here considered do not require "global" information about the demand function, but only of "some" information on it is needed. Further, these rules can not be ranked according to the amount of information required or to their 'degree' of rationality. Different rules are just different ways to decide production plans over time. So, different information costs, which may be associated to each behavioral rule (see e.g. [43] or [76]), could be interpreted as a bias for selecting one particular strategy over the other.

In particular, a simple economic setup is assumed, with homogeneous goods and linear production costs. The selling price is obtained through isoelastic demand, widely used in these kinds of models. Moreover, the endogenous switching mechanism among behavioral rules will be the replicator dynamics (see e.g. [118] and [73]), already introduced in Chapter 4, that is a profit-driven adaptive mechanism based on the evolutionary selection rule.

In the dynamic scenarios that arises from the settings depicted above, it results that if the Nash equilibrium of the game is stable under any behavioral rule, then the asymptotic behavior of the model is very simple since the cheapest behavioral rule

will prevail and all agents will end up producing the Nash equilibrium quantity. In this case, the standard results of oligopoly theory are retrieved by the evolutionary model. However, intriguing questions from an economic as well as mathematical point of view arise when the Nash equilibrium is unstable at least under one behavioral rule. Then questions about the most likely short-run and asymptotic production of the industry as well as about the long term distribution of behaviors when firms fail to converge to the Nash equilibrium becomes relevant. Further, it will be important to pay attention to what condition determines the spread through the whole population of a mutation (that is when a behavioral rule adopted by an infinitesimal fraction of agents will be adopted by a finite fraction of the whole population). Moreover, the particular example of evolutionary selection of behavioral rules analyzed herein (G and LMA rules) extends the stream of investigation started in [22] to the case of behavioral rules for which there is no clear hierarchy between them in terms of degree of required information.

Before addressing the complete evolutionary model cases in which fixed fractions of agents employing the behavioral rules are considered. In particular two benchmark cases are particularly important, that is the model with all LMA-players and with all G-players. These system' configurations are described by triangular maps, for which there can be obtained analytically results on the global dynamics, such as measuring the basin of attraction of the Nash equilibrium. It can be anticipated that when all firms adopt the LMA rule, the Nash equilibrium becomes unstable when the number of firms is sufficiently high and a further stable attractor, other than the Nash equilibrium, may exist. On the contrary, when all firms adopt the G rule the feasible oligopolies are characterized by the stability of the Nash equilibrium.

The global analysis of the dynamics reveals that the main differences between [22] and the work presented in this Chapter are due to the differences between the G rule and the Best Reply rule. It will be confirmed that the Best Reply rule has stability properties that are analogous to those of the LMA rule, i.e. instability of the Nash equilibrium occurs if the number of firms is sufficiently high, and in particular is showed that when the G rule is more expensive than the LMA rule, it is never evolutionary dominant while [22] found that when the Best Reply rule is more expensive than the LMA rule, then it can become evolutionary dominant. Moreover, even if it is the cheapest rule, it dominates only when the Nash equilibrium is stable.

The analysis on invariant planes, where only one strategy is played by firms, is particularly important for understanding the complete evolutionary model, since these two planes are invariant for the model under replicator dynamics. Thus, an attractor

on these planes could also be an attractor for the complete model with evolutionary switching of rules. When this happens, the population is in a *monomorphic* state, as all agents employ the same heuristic. Here it is meaningful to study whether this indeed happens once evolutionary pressure is introduced. In fact, if in the population only one behavioral rule is available, it is obvious that all agents must use that rule. However, to to study whether the introduction of an alternative rule (a *mutation*) spreads over the population or not will be focused under which conditions an attractor on an invariant plane is also an attractor for the evolutionary model. This consists in an analysis of the *transverse* stability of the attractors on invariant planes.

Further, attractors outside these invariant planes can exist and are generated through particular codimension-two bifurcations. From an economic point of view the existence of internal attractors, provides evidence that it might be profitable for agents to behave differently than similarly. So behavioral heterogeneity endogenously arise through competition and persists in the long-run evolution. This phenomenon will be referred as *evolutionary stable heterogeneity*: evolutionary pressure selects the best behaviors and it turns out that the presence of both behavioral rules may guarantee, in the long run, an improvement of aggregate welfare to producers, measured by producer surplus. In other words, in some cases it might be more profitable for the firms to be heterogeneous, and employ different heuristics, than to be homogeneous. As a consequence, *polymorphisms* in the population emerges in the adoption of behavioral rules.

The plain of this Chapter is as follows. In Section 5.2 are provided some general properties of the evolutionary oligopoly model. In Section 5.3 it is outlined the competition between the Local Monopolistic Approximation rule and the Gradient rule and are provided useful results on global dynamics through the study of the non-evolutionary version of the model and the transverse stability of attractors located on invariant planes. Finally, it is describe the emergence of inner attractors, where agents' behavioral heterogeneity arises endogenously through evolutionary pressure.

5.2 The general model

Consider an oligopoly market with n ex-ante identical firms that produce homogeneous goods. It is assumed here that the set of strategies is a nonempty compact and convex set of $\mathbb{R}^n$ and each firm's profit is concave in its own strategy.[1] These assumptions

[1] In particular, the case with isoelastic demand and linear costs, which is developed in the next Section, satisfies these assumptions.

guarantee that at least a Nash equilibrium exists, see [111]. The inverse demand function, which specifies the selling price $p(Q)$ as a function of produced quantities Q, is unknown by the agents. For this reason, firms conceive different behavioral rules for setting their next period productions. The present analysis is limited to the case in which two different behavioral rules are available noting, however, that the generalization to more different behavioral rules is straightforward.

Denoting by $x_i^{(k)}$ the production at time t by the k-th firm adopting the i-th rule, then its the next-period production $x_i^{(k)}(t+1)$ is given by the rule it has adopted, which is a function of the expected next-period productions by other firms and of the expected next-period distributions of each rule. For the sake of generality it is noted that behavioral rules may also incorporate older information through a "memory" term (see [22] for details). This last contribution is neglected in the present treatment. For the sake of simplicity firms are assumed identical among them and to bear the same production cost C employing the same technology. Because of agents are identical, is assumed that the ones that adopt the same behavioral rule set the same quantities, that is $x_i^k = x_i$, resulting that such agents are described in term of a representative agent. Moreover, it is assumed that firms have naïve expectations on next-period productions, that is these base their decisions believing the economic scenario will not change in the future. The quantities dynamics are then given by the followings lows of motion:

$$x_i(t+1) = H_i\left(x_1(t), x_2(t), r(t)\right); \quad i = 1, 2 \tag{5.1}$$

where $r(t) \in [0, 1]$ is the distribution frequency among the firms of one behavioral rule at time t and, obviously, the complementary frequency $1 - r(t)$ is the distribution of the other rule at the same time.

The profit obtained by employing behavioral rule i, which entails the fixed "information cost" $K_i \geq 0$, results to be given by

$$\pi_i = (p - C)\, x_i - K_i; \quad i = 1, 2 \tag{5.2}$$

Firms can switch from period to period to the more profitable behavioral rule modifying their the next-period distribution. The evolutionary mechanism here considered is the *exponential replicator* model, which was firstly proposed by [35] (see also [73] and [74] and [86] for an application in oligopoly theory), according to which the frequency r evolve over time as

$$r' = \frac{re^{\beta\pi_1}}{re^{\beta\pi_1} + (1-r)\, e^{\beta\pi_2}} = \frac{r}{r + (1-r)\, e^{\beta(\pi_2 - \pi_1)}} \tag{5.3}$$

where "'" denotes the time advancement operator and the explicit dependence on time are omitted for convenience. In recurrence (5.3) the parameter $\beta \geq 0$ is the *intensity of choice*, which measures how sensitive the players are at selecting profit-increasing behavioral rules. The minimum value $\beta = 0$ corresponds to the case of stationary distribution, being $r(t+1) = r = r$. The other extreme case, $\beta = \infty$, corresponds to a situation where all firms immediately switch to the behavioral rule showing a (even negligible) better performance, i.e. $r \to 1$ if $\pi_1 > \pi_2$ and $r \to 0$ if $\pi_1 < \pi_2$. It can be further noted that, because of the strictly monotone transformation $\pi_i \to e^{\pi_i}$, the exponential replicator guarantees that the fractions obtained through (5.3) are always contained in the interval $[0, 1]$ even when $\pi_i < 0$. It is worth pointing out that the adoption of replicator dynamics, in whatever form, implies a random matching, see, e.g., [106]. Then, r must be interpreted as the probability to meet a G-player, or, better, it is the probability that a firm adopt the G-rule. Because of the firms are representative agents the probability r will indicates also the fraction of firms that are G-players. In the following, the output at time t of a representative G and LMA-firm are denoted, respectively, by x and y.

The dynamics of the quantities (5.1) together with the evolutionary dynamics in (5.3) define a 3D map T in the phase space $(x, y, r) \in A \subseteq \mathbb{R}^2_+ \times [0, 1]$, where $\mathbb{R}_+ = [0, +\infty)$. Nevertheless, because of the presence of the exponential replicator, the planes $r = 0$ and $r = 1$ where only one pure strategy is employed (H_2 or H_1 respectively) are invariant planes, that is if $r = 0, 1$ than at any subsequent time $t' > t$ it is $r(t') = 0, 1$ respectively. It means that absent behaviors remain absent and can not rise up and spread in the population. Conversely, a mutation in agents' behavior may spread over the population or may be reabsorbed depending on the transverse stability of attractors of the two-dimensional restrictions of T on invariant planes. In general, an attractor on such a plane may be *transversely stable*, so that it attracts trajectories starting outside the restriction, i.e. from $r(0) \in (0, 1)$ being also an attractor of the three-dimensional map T. *Otherwise, the attractor on the restriction is transversely unstable, so that it might not be reached by trajectories coming from inside the phase space.

By assumption, at least one Nash equilibrium of the game always exist and, since agents are homogeneous, at least one symmetric Nash equilibrium must exists too, which is then characterized by the same production by all agents, i.e. $x_1^* = x_2^* = x^*$.[2] The present analysis is now restricted to cases in which the behavioral rules are consistent

[2]This class of behavioral rules includes as a particular case the so called *unbiased rules*, see, e.g., [43], which are characterized by having the symmetric Nash equilibrium x^* as their unique equilibrium quantity.

with the corresponding evolutionary game played by the agents in the hypothesis that they know the real demand function. This means that behavioral rules are required to be *stationary* at any symmetric Nash equilibrium of the underlying game. So, if the industry is at a Nash equilibrium, each behavioral rule prescribes to stay at that equilibrium regardless of the dynamics of r. This stationary property is expressed as

$$x^* = H_i\left(x^*, x^*\right); \quad i = 1, 2 \tag{5.4}$$

From equation (5.4), together with the specific functional form of the switching mechanism given by the exponential replicator (5.3), it follows that if productions are at a symmetric Nash equilibrium level x^* then the points $E_0 = (x^*, x^*, 0)$, $E_1 = (x^*, x^*, 1)$ and $E = (x^*, x^*, r^*)$, which is present if the condition $\pi_1 = \pi_2$ is satisfied for some r^*, are equilibria of the 3D map T. Regardless of the specific behavioral rules considered, the following stability properties characterize the asymptotic behavior of the evolutionary map T in the hypothesis that the Nash equilibrium is stable for any fixed value of r. It is here noted that, any employed heuristics used to forecast next-period variables, does not affect the stability analysis of the Nash equilibrium since, in this case, firms have correct expectations.

Proposition 4 *Consider the dynamical system T defined by* (5.1) *and* (5.3) *with $\beta > 0$ and where profit functions are given by* (5.2)*. If the symmetric Nash equilibrium (x^*, x^*) is a locally asymptotically stable fixed point of the two-dimensional map* (5.1) *for any fixed value of the frequency $r \in [0, 1]$ then the set $\mathcal{S} = \{(x^*, x^*, r) \mid r \in [0, 1]\}$ is T-invariant, that is $T(\mathcal{S}) \subseteq \mathcal{S}$, and*

- *if $K_1 = K_2$, then each point $E^* \in \mathcal{S}$ is a stable equilibrium.*
- *if $K_1 \neq K_2$, the two extreme points of $\mathcal{S}$ are equilibria, namely $E_0^* = (x^*, x^*, 0)$ and $E_1^* = (x^*, x^*, 1)$. If $K_1 < K_2$ [$K_1 > K_2$] the equilibrium E_1^* [E_0^*] is locally asymptotically stable, whereas E_0^* [E_1^*] is unstable.*

Proof. Assume that firms of either type produce the Nash equilibrium quantity x^*. Then, for any $r \in [0, 1]$, the difference in their profits is get from (5.2) and is given by the information costs, $\pi_1 - \pi_2 = K_2 - K_1$. Therefore, if fixed information costs are equal, i.e. $K_1 = K_2$, the replicator equation in (5.3) reduces to $r(t + 1) = r$ so that any point $E \in \mathcal{S}$ is a fixed point for map T. Instead, if $K_1 \neq K_2$, then at any point $E \in \mathcal{S}$ it results that $\pi_2 \neq \pi_1$ and the stationary condition can be satisfied only at the boundary points $E_0^* = (x^*, x^*, 0)$, and $E_1^* = (x^*, x^*, 1)$, where all agents employing the same behavioral rule.

Stability analysis of equilibria can be studied through the Jacobian matrix $\mathbf{J}_T(E)|_{E\in\mathcal{S}}$ of the map T computed along the invariant set $\mathcal{S}$ where fixed points are located. It results from (5.4) that its entries $\mathbf{J}_{13}$ and $\mathbf{J}_{23}$ are equal to zero, and its characteristic equation becomes

$$P(z) = \left(\frac{e^{\beta(\pi_1+\pi_2)}}{\left((r-1)\,e^{\beta\pi_2} - re^{\beta\pi_1}\right)^2} - z \right) P_2(z)$$

where $P_2(z)$ is the characteristic equation of the two-dimensional model (5.1), whose roots are in modulus less than one by the hypothesis of stability of the Nash equilibrium. Thus in the case $K_1 = K_2$, for which it results $\pi_1 = \pi_2$ along $\mathcal{S}$, the third eigenvalue of $\mathbf{J}_T(E)|_{E\in\mathcal{S}}$ is $z_3 = 1$ and any point $E \in \mathcal{S}$ is a stable equilibrium.

If $K_1 < K_2$ at $r = 0$ and at $r = 1$ the eigenvalues related to the transversal direction with respect to invariant planes, that is the direction identified by the vector $(0, 0, 1)$, are the entries $\mathbf{J}_{33}$ of the Jacobian matrix of the 3D map T which are respectively given by

$$\mathbf{J}_{33}(r=0) = e^{\beta(K_2-K_1)} \in (1, +\infty) \tag{5.5a}$$

$$\mathbf{J}_{33}(r=1) = e^{\beta(K_1-K_2)} \in (0, 1) \tag{5.5b}$$

Analogous calculations can be made in the case $K_2 < K_1$. ■

The conditions under which the symmetric Nash equilibrium is stable can be violated and some attractors can be created through bifurcations, as stated in the following corollary:

Corollary 5 *Consider the dynamical system T defined by* (5.1) *and* (5.3) *with $\beta > 0$ and where profit functions are given by* (5.2)*. When the conditions for local asymptotic stability of the Nash equilibrium (x^*, x^*) are broken in* (5.1) *with $r = r^*$, the following cases occur:*

i) If $K_1 = K_2$, an attractor can appear in $\mathbb{R}_+ \times \mathbb{R}_+ \times [0, 1]$ (or in $\mathbb{R}_+ \times \mathbb{R}_+ \times (0, 1)$ if $r^* \neq 0, 1$) through a bifurcation of codimension 1, 2 or 3.

ii) If $K_1 \neq K_2$, $r^* = 1$ and $K_1 < K_2$ [$r^* = 0$ and $K_1 > K_2$], then equilibrium E_1 [E_0] undergoes a bifurcation and an attractor appears in the invariant subspace $r = 1$ [$r = 0$], whereas E_0 [E_1] remains unstable.

Proof. The first part of the corollary follows observing that two of the roots of the characteristic polynomial associated to the Jacobian matrix of dynamical system T

(defined by (5.1) and (5.3) with $\beta > 0$) computed at the fixed point $E = (x^*, x^*, r^*)$, coincide with the two roots of the characteristic polynomial of the Jacobian matrix of system (5.1) computed at the fixed point (x^*, x^*) with $r = r^*$.

The second part of the corollary follows by noting that the dynamics on the invariant plane $r = 1$ (or $r = 0$) of the dynamical system T is equal to the one of system (5.1) with $r = 1$ (or $r = 0$). ■

On the other hand, if the Nash equilibrium is unstable for the quantity adjustments (5.1) and more complex attractors exist, then the asymptotic behavior of the model becomes more complicated but also more interesting both from a mathematical as well as economic point of view.

5.3 An example with specific behavioral rules

In this Section, we develop the model described above in its general form considering as specific behavioral rules the Local Monopolistic Approximations (LMA) and the Gradient dynamics (G), proposed, respectively, in [26] and [25].

Let us consider an oligopoly with $n \geq 2$ firms that produce homogeneous goods with linear cost given by

$$C_i = cq_i + K_i \tag{5.6}$$

where q_i is the quantity produced by firm that adopt the i-th rule, $i = 12$, and $c > 0$ denotes the marginal cost, the same for all firms, and $K_i \geq 0$ is the information cost associated to the i-th behavioral rule. The true demand function, unknown by firms, is a function of the overall quantity Q in the market and it is assumed to be isoelastic with constant elasticity equal to one[3]:

$$p(Q) = f(Q) = \frac{1}{Q} \tag{5.7}$$

The dynamics can take place only in the case of positive aggregate production, that is if $Q > 0$, whereas the case $Q = 0$ is referred as the *infeasibility of the oligopoly*.[4]

[3]This particular demand function is widely employed in the literature, see, e.g., [108], [16], [122], [4], [90] and [88]. In particular, isoelastic demand is obtained when a representative consumer maximizes a log-linear (or Cobb-Douglas) utility function, see [90] for details.

[4]Note that, for $Q = 0$, the demand function is not defined and therefore the oligopoly is infeasible. An alternative would be to impose that the demand function is equal to a finite amount for $Q = 0$. In this case, $Q = 0$ represents a stable fixed point for the game and the set of trajectories that are now infeasible would converge to such a fixed point. Nevertheless, the economic interpretation of the results would not change as in either cases $Q = 0$ represents the *infeasibility* (or unprofitability) of the oligopoly.

At a given time t, the fraction of players that adopt the *Gradient* behavioral rule, let them be called *G-players*, is denoted by $r \in [0, 1]$, and the complementary fraction of players that adopt the *Local Monopolistic Approximation* rule, let them be called *LMA-players*, is $1 - r$. From the interpretation of r as the probability that a firm adopt the G-rule than r will indicates also the fraction of G-players. In the following, the output at time t of a representative G and LMA-firm are denoted, respectively, by x and y.

Now each representative agent split the total production Q in two contributions, its own current production, x or y, and the current aggregate production Q_{-1} of the rest of the industry, which is defined as

$$Q_{-1} = (N-1)\{rx + (1-r)y\} \tag{5.8}$$

$$Q = x + Q_{-1} \tag{5.9}$$

$$Q = y + Q_{-1} \tag{5.10}$$

$$Q = \frac{N}{N-1} Q_{-1} \tag{5.11}$$

According to the setup here adopted, modeling both G and LMA heuristics requires to know the realized level of production. Indeed, G-firms observe their profits, which are here expressed as a function of the total level of production of the industry. At the same time, LMA-firms observe the current price, which is again expressed as a function of the realized level of production of the industry. However, this modeling setup does not provide the exact level of production of the industry but only its expected value. Thus, for modeling purposes we considered the last one as a proxy for the first one. See also [43] and [22] for the same assumption. This modeling choice implies that G-firms estimate the derivative of their own profits computed at the expected level of production (instead of estimating the derivative of their own realized profits) and LMA-firms approximate the inverse demand function in a neighborhood of the expected level of production (instead of approximating the inverse demand function in a neighborhood of the realized production). However, the expected level of production should be an acceptable proxy for the realized one, at least for a sufficiently high number of players. It is also worth pointing out that in the classical approach of decision theory (see [76] for a similar setup) firms select the Best Reply dynamics maximizing expected profits instead of profits of expected productions. That approach, however, would require to assume (contrary to what we do here) that firms have global knowledge of the demand function. See also [126] for a brief discussion about the issue of discreteness of the space of firms in oligopoly models.

At time t, the representative G-firm sets its next-period production in the direction that maximizes its expected profits. In particular it is assumed to know the derivative of its profit with respect to its own production at the present industry output level and sets quantities in the direction (increment or reduction) such that its expected profit increases avoiding solving an optimization problem. More precisely, from (5.2), its current profits can be expressed as:

$$\pi_G(x, Q_{-1}) = \left(\frac{1}{x + Q_{-1}} - c\right) x - K_G \tag{5.12}$$

where $K_G \geq 0$ is the fixed 'information' cost associated to the G-rule and Q_{-1} is the current production for the rest of the industry. Than the behavior adopted by a G-firm consists on setting its next-period quantity in the follow way:

$$\begin{aligned} x' &= \max\left\{0, x + \lambda x \frac{\partial \pi_G}{\partial x}\right\} = \\ &= \max\left\{0, x + \lambda x \left(\frac{Q_{-1}}{(x + Q_{-1})^2} - c\right)\right\} \\ &= \max\left\{0, x + \lambda x \left(\frac{(N-1)(rx + (1-r)y)}{(x(Nr + 1 - r) + y(N-1)(1-r))^2} - c\right)\right\} \end{aligned} \tag{5.13}$$

where $\lambda \geq 0$ is a speed of adjustment (see [16] for details) equal for all G-players and the definition (5.8) is used in the latter equality.

Similarly, at time t, the representative LMA-firm sets its production in order to maximize its expected profit, expressed in terms of expected price, being able to locally estimate the partial derivative of (5.7) with respect to its own production at the present industry output level and solving a quadratic optimization problem, which involves a linear equation when costs are linear (as in the present case) or quadratic. From (5.2) it results

$$y' = \underset{y_M \geq 0}{\arg\max} \left\{(\widetilde{p}^e - c) y_M - K_L\right\} \tag{5.14}$$

where $K_L \geq 0$ is a fixed information cost for LMA-players and $\widetilde{p}^e$ is exactly the expected next-period price. Further, LMA-firms assess the estimation of future price believing it will varies only due to its own current production (see [26] for details):

$$\begin{aligned} \widetilde{p}^e(y') &= p + \frac{dp}{dy}(y' - y) \\ &= p - \frac{1}{Q^2}(y' - y) \end{aligned} \tag{5.15}$$

Equation (5.15) assert that LMA-players adopt a linear estimation for future price, where the slope of demand is correctly assessed and the increments in quantities disregard the production by the other competitors (from which the name Local Monopolistic Approximation). This is equivalent to say that an LMA-firm assumes that all other firms will produce at time $t+1$ the same quantity produced at time t (as assumed in the well-known Best Reply adjustment, see [16]). Than the behavior adopted by a LMA-firm consists on setting its next-period quantity in the follow way:

$$y' = \max\left\{0, (1-\alpha)y + \alpha\left(\frac{y}{2} + \frac{c-p}{2}\left(\frac{dp}{dy}\right)^{-1}\right)\right\} \tag{5.16}$$

$$= \max\left\{0, (1-\alpha)y + \frac{\alpha}{2}\left(y + \frac{N}{N-1}Q_{-1}\left(1 - c\frac{N}{N-1}Q_{-1}\right)\right)\right\} \tag{5.17}$$

where $\alpha \in (0,1]$ is a speed of adjustment (see [16] for details) equal for all LMA-players. Recurrence (5.16) is computed assuming naïve expectations on the future scenario of the economy, that is $Q^e_{-1}(t+1) = Q_{-1}$, LMA assuming naïve expectations on the future scenario, while the letter equality (5.17) is obtained using the definition (5.8) and the approximation $Q = NQ_{-1}/(N-1)$.

By coupling the dynamics of quantities by G- and LMA-firms, respectively (5.13) and (5.17), with an exponential replicator used as the evolutionary mechanism of switching between the two behaviors, the following 3D map T is obtained:

$$T: \begin{cases} x(t+1) = \max\left\{0, x + \lambda x\left(\dfrac{Q_{-1}}{(x+Q_{-1})^2} - c\right)\right\} \\ y(t+1) = \max\left\{0, (1-\alpha)y + \dfrac{\alpha}{2}\left(y + \dfrac{N}{N-1}Q_{-1}\left(1 - c\dfrac{N}{N-1}Q_{-1}\right)\right)\right\} \\ r(t+1) = \dfrac{re^{\beta\pi_G}}{re^{\beta\pi_G} + (1-r)\,e^{\beta\pi_{LMA}}} \end{cases} \tag{5.18}$$

where Q_{-1} is given in (5.8) and the profits are given by:

$$\pi_G = px - (cx + K_G) = \left(\frac{N-1}{NQ_{-1}} - c\right)x - K_G \tag{5.19}$$

$$\pi_{LMA} = py - (cy + K_L) = \left(\frac{N-1}{NQ_{-1}} - c\right)y - K_L \tag{5.20}$$

The max operator in (5.18) imposes non-negativity of productions whenever a behavioral rule returns a negative quantity, so that the firm simply decides not to

produce for the next time period. Differently, the region where map T is not defined refers to cases of *infeasibility of the oligopoly*, which occurs, as previously recalled, if the demand function (5.7) is not defined, that is for $Q = 0$. So the definition's domain of T, let it be designed by A such that $T : A \to A$, is excluded from including the axes $\{(0, 0, r)\}$, for $r \in [0, 1]$, $\{(0, y, 1)\}$, for $y \geqslant 0$, and $\{(x, 0, 0)\}$, for $x \geqslant 0$, in which it results $Q = 0$ together with the set of their preimages (see [18] for details):

$$A = \left(\mathbb{R}^2_+ \setminus \left(\cup_{n=0}^{+\infty} T^{-n}(0, 0, r) \cup_{n=0}^{+\infty} T^{-n}(0, y, 1) \cup_{n=0}^{+\infty} T^{n}(x, 0, 0)\right)\right) \times [0, 1]$$

5.3.1 The benchmark case $\beta = 0$

The study of the model (5.18) in the case $\beta = 0$ is here provided. This is equivalent to assume that the fraction of G-players (and consequently of LMA-players) is exogenously fixed, i.e. $r' = r$, since benchmark case provides interesting insights on the complete model (5.18). With $\beta = 0$, (5.18) reduces to a two dimensional map $T_2 : A_2 \longrightarrow A_2$ where $A_2 = \mathbb{R}^2_+ \setminus \cup_{n=0}^{+\infty} T_2^{-n}(0, 0)$:[5]

$$T_2 : \begin{cases} x(t+1) = \max\left\{0, x + \lambda x\left(\dfrac{Q_{-1}}{[x + Q_{-1}]^2} - c\right)\right\} \\ y(t+1) = \max\left\{0, (1-\alpha)\, y + \dfrac{\alpha}{2}\left(y + \dfrac{N}{N-1} Q_{-1}\left(1 - c\dfrac{N}{N-1} Q_{-1}\right)\right)\right\} \end{cases} \tag{5.21}$$

where Q_{-1} is given in (5.8).

The unique and symmetric Cournot-Nash equilibrium $E^* = (x^*, x^*)$ is also a fixed point of (5.21) and it is characterized by the same quantity for both kinds of agents:

$$x^* = \frac{N-1}{cN^2} \tag{5.22}$$

The following proposition summarize the stability properties of (5.22).[6]

Proposition 6 *Consider the dynamical system T_2 in* (5.21) *and its non-trivial equilibrium E^* in* (5.22)*. Then*

1. *if $r = 0$ (all LMA-players) the fixed point E^* is a stable node provided that $2 \leq N < 1 + 4/\alpha$ and $\lambda < N/c$:*

[5] It is worth noting that for the case $r = 1$ it is $T_2 : A_2 \longrightarrow A_2$ where $A_2 = \mathbb{R}^2_+ \setminus \cup_{n=0}^{+\infty} T_2^{-n}(0, y)$, while for the case $r = 0$ it is $T_2 : A_2 \longrightarrow A_2$ where $A_2 = \mathbb{R}^2_+ \setminus \cup_{n=0}^{+\infty} T_2^{-n}(x, 0)$.

[6] The first numbered point of Proposition 8 has already been proved in [22].

i) E^* *loses stability through a period doubling bifurcation at* $\lambda = N/c$ *provided that* $2 \leq N < 1 + 4/\alpha$*. The 2-cycle that appears belongs to the subspace* $y = y^*$*;*

ii) E^* *loses stability through a period doubling bifurcation at* $N = \max\{2, 1 + 4/\alpha\}$ *provided that* $\lambda < N/c$*.*

2. *if* $r = 1$ *(all G-players), then* E^* *is a stable node for all* $N \geq 0$ *provided that* $\lambda < 2/c$*; for* $\lambda > \frac{2}{c}$ *the map is eventually defined only on* E^**: any other initial condition will lead the map to the focal point* $(0, 0)$*;*

3. *if* $0 < r < 1$ *(mixed population state) and*

$$2 \leq N < N_b = \frac{5 - 2r}{1 - r} \tag{5.23}$$

then E^* *is a stable node provided that the following condition holds:*

$$\lambda < \lambda^*(\alpha) = \frac{2N(\alpha(1 - 2r - N(1 - r)) + 4)}{c(r(\alpha + 4)(N - 2) - 2\alpha(N - 1) + 8)} \tag{5.24}$$

4. *if* $0 < r < 1$ *(mixed population state) and* $N > N_b$*, then* E^* *is a stable node provided that condition* (5.24) *holds with the following additional condition:*

$$\alpha < \alpha^* = \frac{4}{N(1 - r) + 2r - 1} \tag{5.25}$$

5. *For* $\lambda^*(\alpha) > 0$ *and* $\alpha < \alpha^*$*,* E^* *loses stability at* $\lambda = \lambda^*(\alpha)$ *through a period-doubling bifurcation.*

6. *For* $r \neq 1$*, the map* T_2 *has the additional equilibrium* $E_{x=0} = \left(0, \frac{N-1-Nr}{cN^2(1-r)^2}\right)$*. If* $E_{x=0}$ *is asymptotically stable, then it must be that* $\alpha < \frac{4}{N(1-r)-1}$*.*

Proof. Consider the Jacobian matrix of (5.21) computed at equilibrium (5.22), which is given by

$$J(E^*) = \begin{pmatrix} \frac{N - c\lambda(2 + (N-2)r)}{N} & -\frac{c(N-2)(1-r)\lambda}{N} \\ -\frac{(N-2)r\alpha}{2} & \frac{1}{2}((1 - N(1 - r) - 2r)\alpha + 2) \end{pmatrix} \tag{5.26}$$

For $r = 0$ and $r = 1$, the result follows immediately because $J(E^*)$ becomes a triangular matrix. For the stability of the equilibrium E^* when $0 < r < 1$, it is required that the

following system of inequalities (known as Schur or Jury's conditions, see e.g. [52], [46], [99]) are satisfied:

$$\begin{cases} 1 + trJ\left(E^*\right) + \det J\left(E^*\right) > 0 \\ 1 - trJ\left(E^*\right) + \det J\left(E^*\right) > 0 \\ 1 - \det J\left(E^*\right) > 0 \end{cases} \tag{5.27}$$

where $trJ\left(E^*\right)$ and $\det J\left(E^*\right)$ are, respectively, the trace and the determinant of (5.26). By straightforward calculations, it is possible to verify the following statements. Condition $1-\det J\left(E^*\right)=0$ is never satisfied if the other conditions in (5.27) hold, thus ruling out that E^* can lose stability through a Neimark-Sacker bifurcation. If condition (5.25) holds, then it is $1 - trJ\left(E_*\right) + \det J\left(E^*\right) > 0$. Assuming condition (5.25) and imposing $1 - \det J\left(E^*\right) > 0$, we can solve for $1 + trJ\left(E^*\right) + \det J\left(E^*\right) = 0$, thus obtaining the bifurcation value $\lambda = \lambda^*\left(\alpha\right)$ in (5.24). These conditions are necessary for a flip bifurcation of the two-dimensional map (5.21) to occur. The sufficient conditions can be verified by standard calculations.[7] Moreover, it is worth noting that $\lambda^*\left(\alpha^*\right) = 0$, and that $\lambda^*\left(\alpha\right) > 0$ for $\alpha < \alpha^*$ and $\lambda^*\left(\alpha\right) < 0$ for $\alpha > \alpha^*$, at least in a neighborhood of α^*. This confirms that equilibrium E^* loses stability only at $\lambda = \lambda^*\left(\alpha\right)$. In fact, condition (5.25) ensures that in (5.24) it is $\lambda^*\left(\alpha\right) > 0$. Observe that in (5.25) it is $\alpha^* > 0$. When the number of players is such that $2 \leq N < N_b = \frac{5-2r}{1-r}$, then the denominator in the right-hand side of (5.25) is smaller than 4, so that condition (5.25) is always satisfied, being $\alpha \leq 1$. In other words, if the number of players is smaller than N_b, then condition (5.24) alone guarantees that the Nash equilibrium E^* is a stable node, being $\lambda^*\left(\alpha\right) > 0$ for all $\alpha \in (0, 1]$.

With respect to equilibrium $E_{x=0}$, by employing the component $x+\lambda x\left(\frac{Q_{-1}}{[x+Q_{-1}]^2} - c\right)$ of the first equation in (5.21), the Jacobian matrix assumes the following triangular form

$$J\left(E_{x=0}\right) = \begin{pmatrix} 1 + \frac{c(N(r-2)+1)\lambda}{(N-1)(N(r-1)+1)} & 0 \\ -\frac{(N(r-1)+2)r\alpha}{2(r-1)} & 1 + \frac{1}{2}\left(\left(N\left(r-1\right)+1\right)\alpha\right) \end{pmatrix} \tag{5.28}$$

whose eigenvalues are the entries along the diagonal. It is easy to show that it is impossible for both eigenvalues to be inside the unitary circle. However, when the constraint $x = 0$ is active because of the Max in (5.21), then the entry in the first row and first column of $J\left(E_{x=0}\right)$ becomes zero, because the map is constant. In this case, one eigenvalue is always $z_1 = 0$ and the other eigenvalue is $z_2 = \frac{1}{2}\left(\left(N\left(r-1\right)+1\right)\alpha + 2\right)$. Condition $z_2 \in (-1, 1)$ reduces to $\alpha < \frac{4}{N(1-r)-1}$, which is a necessary condition for the stability of $E_{x=0}$. QED ■

[7] We provide evidence of the 2-cycle by numerical simulations showing its existence.

The stability analysis of the two-dimensional model (5.21) underlines two important differences of the behavioral rules: under the Gradient rule the convergence towards the Nash equilibrium E^* is always ensured by a sufficiently low speed of adjustment, regardless of the number of firms n. On the contrary, the LMA rule guarantees convergence to E^* provided a sufficiently low speed of adjustment α given a certain number n of players. Moreover, when LMA- and G-firms interact at a fixed proportion (at a constant r), then the presence of a positive fraction of LMA-players destabilizes the Nash equilibrium if, for given values of α and λ, the number of players is sufficiently high.

Remark 7 *Proposition 8 states that for $r = 0$ the Nash equilibrium E^* is stable if both the following conditions are satisfied: $2 \leq N < 1 + 4/\alpha$ and $\lambda < N/c$. However, from an economic point of view, the first condition alone is sufficient to ensure that all players select the Nash quantity $y^* = N - 1)/cN^2$. In fact, at $\lambda = N/c$ equilibrium E^* loses stability through a flip bifurcation so that an asymptotically stable 2-cycle appears. However, as stated in Proposition 8, this 2-cycle belongs to the subspace $y = y^*$, i.e. it is of the type $\{(x_1, y^*), (x_2, y^*)\}$. Therefore, although the quantity produced by G-firms changes over time, all players still produce y^*, since no G-firms are present, being $r = 0$.*

These analytical results unveil quite reach dynamic scenarios, which are further investigated in the following by numerical analysis. In particular, it is provided a detailed investigation of all the possible scenarios of the 2D model here considered, with the aim to provide a better understanding of the 3D dynamical system.

Let it starts by taking the speed of adjustment α of LMA-players as a bifurcation parameter. In particular, it is investigated how the long-run dynamics of the model change as α varies in $(0, 1]$ under two different dynamic scenarios. In the first one, depicted in Figure 5.1, it is considered a situation such that for $r = 1$ (with G-firms only) equilibrium E^* is stable, so that in the long run the level of production converges to the Nash equilibrium. According to Proposition 8, this occurs when $\lambda < 2/c$. In this case, it is observed that as the fraction r of G-firms increases, the values of α at which the Nash equilibrium E^* loses stability increases as well. Moreover, it is observed that for $r = 0$ the oligopoly becomes infeasible as α increases, see Figure 5.1(a). This is due to the fact that the oligopoly competition leads firms to stop the production and the demand function (5.7) is not defined when total production is zero. In the second scenario, when $\lambda > 2/c$, whose simulations are not reported for the sake of brevity, the equilibrium E^* is unstable for $r = 1$ and, the oligopoly becomes infeasible as all the firms eventually decide to stop their production. In addition, as α increases, the

oligopoly becomes infeasible also in the case of a mixed population state, i.e. $r \in (0,1)$, when $\lambda > \lambda^*(\alpha)$.

Let it now performs a similar analysis as λ, the reactivity of G-firms, changes. In Figure 5.2 the limit dynamics of x and y are depicted as λ varies; in these example, the stability condition $\alpha < \alpha^*$ is ensured, i.e. the stability of the Nash equilibrium E^* depends only on λ^*, which in turns depends on r. It is worth noting that if the game is played by LMA-firms only, i.e. $r = 0$, when $\lambda > \lambda^*$ the Nash equilibrium E^* becomes unstable but the oligopoly remains feasible, see Figure 5.2(a). On the contrary, if the game is played by G-firms only, i.e. $r = 1$, the condition $\lambda < \lambda^*$ determines the feasibility of the oligopoly game itself, see Figure 5.2(c). Condition (5.24) for the stability of the Nash equilibrium E^* at $r = 0.5$ is depicted in Figure 5.2(b).

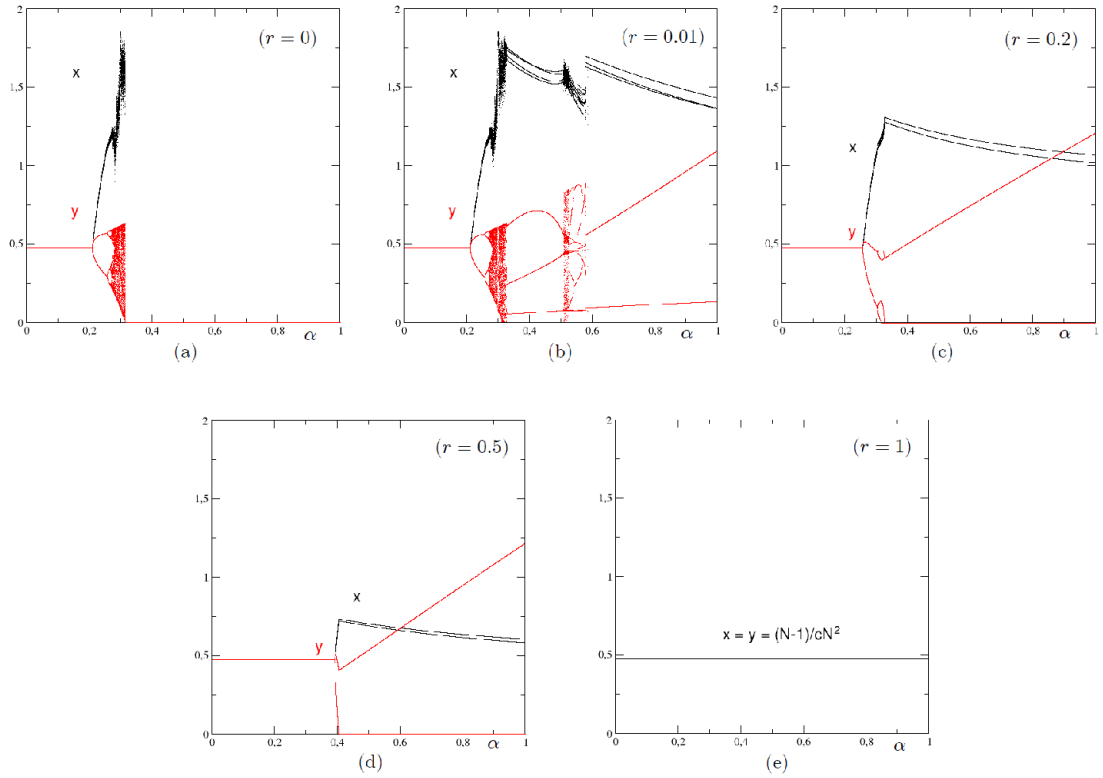

Fig. 5.1 Bifurcation diagrams of x (black) and y (red) for α varying in $(0,1]$. Case $\lambda < \frac{2}{c}$. Panel (a) $r = 0$. Panel (b) $r = 0.01$. Panel (c) $r = 0.2$. Panel (d) $r = 0.5$. Panel (e) $r = 1$. Parameters values: $\lambda = 0.8$, $N = 20$, $c = 0.1$. Black dots in Panel (a) refer to the production level of G-firms the frequency of which is equal to zero ($r = 0$), it follows that such black dots are irrelevant for the description of the oligopoly.

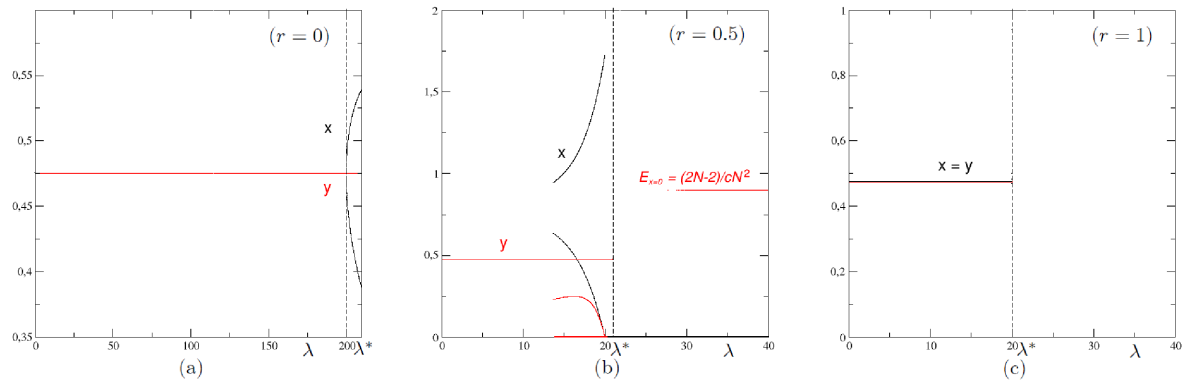

Fig. 5.2 Bifurcation diagrams of x (black) and y (red) for λ varying on $(0, 1]$. Panel (a) $r = 0$. Panel (b) $r = 0.5$. Panel (c) $r = 1$. Parameters values: $\alpha = 0.2$, $N = 20$, $c = 0.1$.

Another aspect worth of investigation is the interaction between the two different behavioral rules as parameter $r \in [0, 1]$ is changed. To this aim, there are presented several simulations in Figure 5.3. In Panel (a), the parameters values are such that the equilibrium E^* is stable both for $r = 0$ and for $r = 1$, i.e. $2 \leq N < 1 + \frac{4}{\alpha}$ and $\lambda < \frac{2}{c}$. We observe that in this case the stability of the Nash equilibrium occurs also for $r \in (0, 1)$. In other words, when the Nash equilibrium is stable with either all LMA-firms or all G-firms, then it is stable for any $r \in (0, 1)$. In Panel (b), the parameters values are such that the Nash equilibrium E^* is unstable with all LMA-firms (i.e. $r = 0$) but it is stable with all G-firms ($r = 1$). In other words, $N > 1 + \frac{4}{\alpha}$ and $\lambda < \frac{2}{c}$. In this case, for small values of r a complex attractor exists, while as the fraction of G-firms in the oligopoly increases, a cascade of halving bifurcations occurs and the Nash equilibrium gains stability already for relatively low values of r. In Panel (c), the parameters values are such that the Nash equilibrium E^* is stable with all LMA-firms and unstable with all G-firms. In particular, parameters are such that $2 \leq N < 1 + \frac{4}{\alpha}$ and $\frac{N}{c} > \lambda > \frac{2}{c}$. In this case, it is observed that the Nash equilibrium is asymptotically stable when the fraction of the LMA-firms in the oligopoly is high (low r), while the oligopoly becomes infeasible, i.e. firms stop production, as the fraction of G-firms increases. In Panel (d), the parameters values are such that the Nash equilibrium is unstable with all LMA-firms as well as with all G-firms. In particular, parameters are such that $N > 1 + \frac{4}{\alpha}$ and $\frac{N}{c} > \lambda > \frac{2}{c}$. In this case, complex dynamics for low fraction of G-firms are observed while the oligopoly becomes infeasible as the fraction r of G-firms increases. In Panel (e), we present the case $2 \leq N < 1 + \frac{4}{\alpha}$ and $\lambda > \frac{N}{c}$. It means

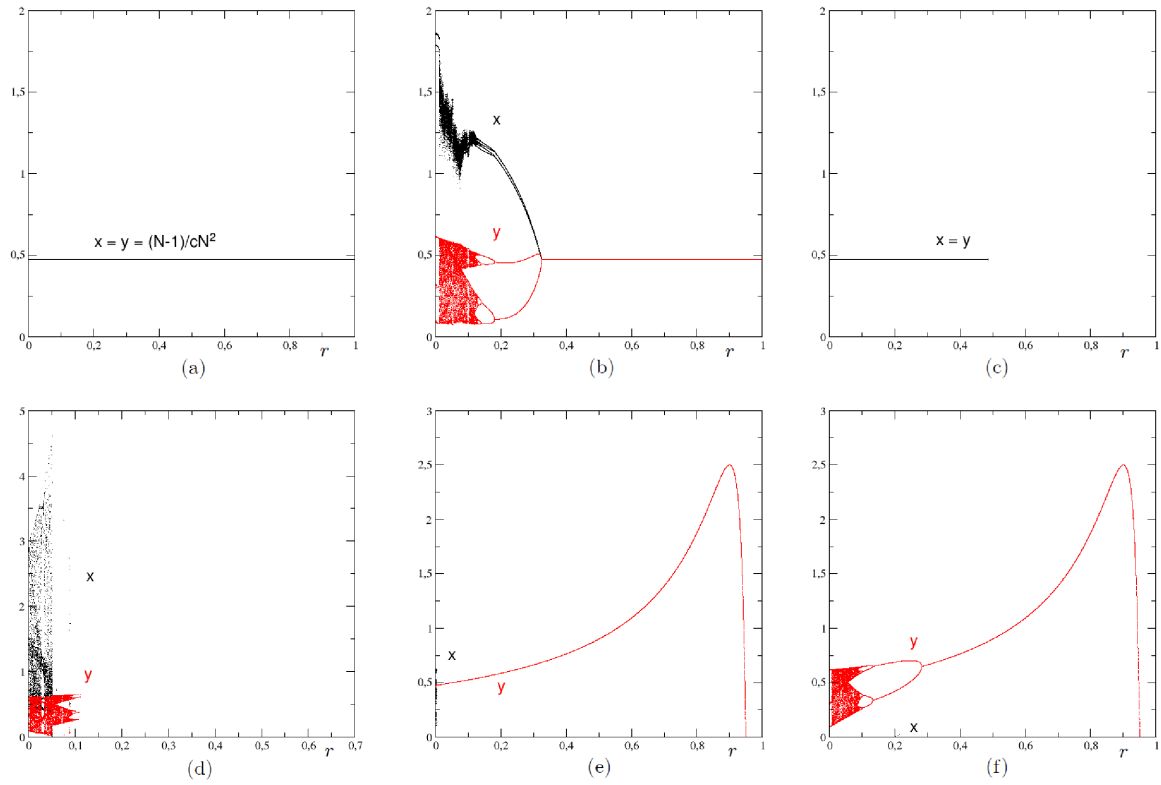

Fig. 5.3 Bifurcation diagrams of x (black) and of y (red) for r varying on $[0, 1]$. Panel (a) $\alpha = 0.5$, $\lambda = 1$. Panel (b) $\alpha = 0.3$, $\lambda = 1$. Panel (c) $\alpha = 0.2$, $\lambda = 21$. Panel (d) $\alpha = 0.3$, $\lambda = 21$. Panel (e) $\alpha = 0.2$, $\lambda = 201$. Panel (f) $\alpha = 0.3$, $\lambda = 201$. Other parameters values: $N = 20$, $c = 0.1$.

that with all LMA-firms the Nash equilibrium is unstable, and the asymptotically stable equilibrium is the equilibrium $E_{x=0}$ defined in Proposition 4. When the fraction of G-firms is increased, this equilibrium loses stability and the oligopoly becomes infeasible. With all G-firms the oligopoly results to be infeasible as well. In Panel (f), it is depicted the case $N > 1 + \frac{4}{\alpha}$ and $\lambda > \frac{N}{c}$, i.e. E^* is unstable for both $r = 1$ and $r = 0$. Paradoxically, in this case, the oligopoly game remains feasible for higher values of r, although two eigenvalues are outside the unit circle, if compared to the case of Panel (d), where equilibrium E^* has only one eigenvalue outside the unit circle for $r = 0$.

The investigation based on bifurcation diagrams reveals that if one starts from a situation where only one of the two heuristics is employed, either G or LMA, and this rule leads the oligopoly to converge to the Nash equilibrium E^*, then the presence of

this 'stable' rule favors the convergence to the Nash equilibrium also when there is a fraction of agents adopting the other available rule.

In addition, the numerical analysis reveals another important aspect of the model, which is related to the lost of asymptotic stability of the Nash equilibrium. In particular, if the oligopoly is populated by LMA-agents only, then the production dynamics are governed by a nonlinear map, with a range of stability of the Nash equilibrium that is lower than with all G-firms; however, when this equilibrium loses stability, the oligopoly remains feasible although fluctuations of the level of production are observed. On the contrary, if the oligopoly is populated by G-firms only, then the level of production depends on a piecewise-linear map. Thus, the Nash equilibrium can be characterized by more stability if one considers the size of its basin of attraction. However, when the Nash equilibrium loses stability, then the only possibility is that of an 'infeasible' oligopoly, with all agents that stop to produce and exit the market.

Global Analysis

In this part, there are provided some considerations on the global dynamics of the map T_2, which are also useful for understanding the behavior of the evolutionary model (5.18). In the following there are analyzed the structure of the basins of attraction of the Nash equilibrium when only one behavioral rule is present, i.e. with $r = 1$ (all G-firms) or $r = 0$ (all LMA-firms) and compare their measure in the two cases. In particular the comparisons are performed when the Nash Equilibrium E^* is asymptotically stable in $r = 0$, that is if $2 \leq N < 1 + \frac{4}{\alpha}$ and $\lambda < \frac{N}{c}$ as stated in Proposition 4, in order to do what? to underline the destabilizing effect of the presence of G-firms in the full evolutionary model?

Proposition 8 *Consider the dynamical system T_2 in* (5.21) *and its non-trivial equilibrium E^* in* (5.22)*. Denote by $\mu(\mathcal{V})$ the measure of a region $\mathcal{V} \subseteq \left\{(x,y) \in \mathbb{R}^2_+\right\}$ and by $\mathcal{B}(V)$ the basin of attraction of an attractor V of T_2. Define the following sets:*

$$\mathcal{B}_1 := \left\{(x,y) \in \mathbb{R}^2_+ | x \geq \frac{\lambda}{c\lambda - 1}\frac{N-1}{N^2}\right\},$$
$$\mathcal{B}_2 := \left\{(x,y) \in \mathbb{R}^2_+ | y \geq \frac{2-\alpha+\alpha N}{\alpha c N^2}\right\}, \text{ and}$$
$$\mathcal{B}_3 := \left\{(x,y) \in \mathbb{R}^2_+ | x^2 + (N-1)^2 y^2 + (N-1)\, xy - \frac{\lambda(N-1)}{\lambda c - 1} y \leq 0\right\}$$

Assume that E^* is asymptotically stable when $r = 0$. Then the following statements hold:

1. *If* $1-\lambda c>0$, *then* $\mu\left(\mathcal{B}\left(E^{*}\right)_{r=0}\right)\leq\mu\left(\mathcal{B}\left(E^{*}\right)_{r=1}\right)$, *where*

$$\mathcal{B}\left(E^{*}\right)_{r=1}:=\mathbb{R}_{+}^{2},\quad\mathcal{B}\left(E^{*}\right)_{r=0}\subseteq\mathbb{R}_{+}^{2}\setminus\cup_{n=0}^{+\infty}T_{2}^{-n}\left(\mathcal{B}_{2}\right)\tag{5.29}$$

2. *If* $0>1-\lambda c>-1$, *and*

$$\frac{\lambda}{c\lambda-1}\frac{N-1}{N^{2}}\geq\frac{2-\alpha+\alpha N}{\alpha cN^{2}}\tag{5.30}$$

then $\mu\left(\mathcal{B}\left(E^{*}\right)_{r=0}\right)\leq\mu\left(\mathcal{B}\left(E^{*}\right)_{r=1}\right)$, *where*

$$\mathcal{B}\left(E^{*}\right)_{r=1}:=\mathbb{R}_{+}^{2}\setminus\mathcal{B}_{1}\quad\textit{and}\quad\mathcal{B}\left(E^{*}\right)_{r=0}\subseteq\mathbb{R}_{+}^{2}\setminus\cup_{n=0}^{+\infty}T_{2}^{-n}\left(\mathcal{B}_{2}\cup\mathcal{B}_{3}\right)\tag{5.31}$$

3. *If* $-1>1-\lambda c$, *then* $\mu\left(\mathcal{B}\left(E^{*}\right)_{r=1}\right)=0\leq\mu\left(\mathcal{B}\left(E^{*}\right)_{r=0}\right)$, *where*

$$\mathcal{B}\left(E^{*}\right)_{r=1}=E^{*}\quad\textit{and}\quad\mathcal{B}\left(E^{*}\right)_{r=0}\subseteq\mathbb{R}_{+}^{2}\setminus\cup_{n=0}^{+\infty}T_{2}^{-n}\left(\mathcal{B}_{2}\cup\mathcal{B}_{3}\right)\tag{5.32}$$

Proof. First of all, recall that, by Proposition 4, conditions $2\leq N<1+\frac{4}{\alpha}$ and $\lambda<\frac{N}{c}$ guarantee that E^{*} is asymptotically stable when $r=0$. Indeed, if $r=1$ (all G-agents), the map (5.21) becomes

$$T_{2,r=1}:\begin{cases}x(t+1)=\max\left\{0,x+\lambda x\left(\dfrac{(N-1)\,x}{x^{2}N^{2}}-c\right)\right\}=\max\left\{0,f_{x}\right\}\\[2ex]y(t+1)=\max\left\{0,(1-\alpha)\,y+\dfrac{\alpha}{2}\left[y+Nx\left(1-cNx\right)\right]\right\}=\max\left\{0,f_{y}\right\}\end{cases}\tag{5.33}$$

where the first component is a master equation, i.e. a one-dimensional difference equation uncoupled from the second one, whereas the second component is a slave equation, because it depends also on the first variable[8]. The properties of the one-dimensional map f_x, which is a (piecewise-)linear map, strongly influence the dynamics of the whole system. The Nash equilibrium $E^{*}=\left(\frac{N-1}{cN^{2}},\frac{N-1}{cN^{2}}\right)$ is a fixed point of (5.33) and the asymptotic dynamics depend on the initial conditions of the system (5.33). Specifically, let us consider the following subset of $\mathbb{R}_{+}^{2}$, which represents the points of

[8]Map 5.33, as well as map 5.35 below, are two triangular maps. For more details on these maps see e.g. [41], [42] and [84] .

$\mathbb{R}^2_+$ that are mapped by (5.33) into $(0, y)$ in one iteration:

$$\begin{aligned} \mathcal{B}_1 &:= \left\{(x,y) \in \mathbb{R}^2_+ | x\left(1-\lambda c\right) + \tfrac{\lambda(N-1)}{N^2} \leq 0\right\} \\ &= \left\{(x,y) \in \mathbb{R}^2_+ | x \geq \tfrac{\lambda}{c\lambda - 1}\tfrac{N-1}{N^2}\right\} \end{aligned} \tag{5.34}$$

It is clear that any trajectory starting with initial condition $(x, y) \in \mathcal{B}_1$ does not converge to E^*. Having assumed that E^* is asymptotically stable and being the only attractor in the invariant region $\mathbb{R}^2_+ \setminus \cup_{n=0}^{+\infty} T_2^{-n}(\mathcal{B}_1)$, it follows that $\mathcal{B}(E^*)_{r=1} := \mathbb{R}^2_+ \setminus \cup_{n=0}^{+\infty} T_2^{-n}(\mathcal{B}_1)$.

With $r = 0$, (all LMA-agents), the map (5.21) becomes

$$T_{2,r=0} : \begin{cases} x(t+1) = \max\left\{0, x + \lambda x\left(\frac{(N-1)y}{[x+(N-1)y]^2} - c\right)\right\} = \max\{0, f_x\} \\ \\ y(t+1) = \max\left\{0, (1-\alpha)\, y + \frac{\alpha}{2}\left[y + Ny\left(1 - cNy\right)\right]\right\} = \max\{0, f_y\} \end{cases} \tag{5.35}$$

where the second component is the master equation (uncoupled from the first one), while the first component depends also on the second variable (slave equation). The properties of the one-dimensional map f_y, which is a quadratic map conjugates to the well known logistic map, strongly influence the dynamics of the system. The fixed point of (5.35) is again the Nash equilibrium $E^* = \left(\frac{N-1}{cN^2}, \frac{N-1}{cN^2}\right)$, and the asymptotic dynamics depends on the initial conditions. Specifically, let us consider the following two subregions of $\mathbb{R}^2_+$:

$$\begin{aligned} \mathcal{B}_2 &:= \left\{(x,y) \in \mathbb{R}^2_+ | f_y \leq 0\right\} \\ &= \left\{(x,y) \in \mathbb{R}^2_+ | y \geq \tfrac{2-\alpha+\alpha N}{\alpha c N^2}\right\} \\ \mathcal{B}_3 &:= \left\{(x,y) \in \mathbb{R}^2_+ | f_x \leq 0\right\} \\ &= \left\{(x,y) \in \mathbb{R}^2_+ | x^2 + (N-1)^2 y^2 + (N-1)\, xy - \tfrac{\lambda(N-1)}{\lambda c - 1} y \leq 0\right\} \end{aligned} \tag{5.36}$$

It is clear that any trajectory starting in $(x, y) \in \mathcal{B}_2 \cup \mathcal{B}_3$ will never converge to E^*, while, assuming E^* asymptotically stable, its basin of attraction is given by $\mathcal{B}(E^*)_{r=0} \subseteq \mathbb{R}^2_+ \setminus \cup_{n=0}^{+\infty} T_2^{-n}(\mathcal{B}_2 \cup \mathcal{B}_3)$.

Considering $r = 0$, it is trivial to prove that the set $\mathcal{B}_3$ is empty for $1 - \lambda c > 0$, while any trajectory starting in $\mathcal{B}_2$ is lead in the subregion (axis) $y = 0$, where the dynamics is undefined and so the oligopoly is infeasible. On the contrary, trajectories starting in

$\mathbb{R}^2_+ \setminus \cup_{n=0}^{+\infty} T_2^{-n}(\mathcal{B}_2)$ converge either to E^* (assuming E^* asymptotically stable) or to some attractor contained in the region. Moreover, considering $r = 1$, it is trivial to prove that $\mathcal{B}_1$ is empty for $1 - \lambda c > 0$. It follows that $\mathcal{B}(E^*)_{r=1} := \mathbb{R}^2_+$. Noting that $\mathbb{R}^2_+ \setminus \cup_{n=0}^{+\infty} T_2^{-n}(\mathcal{B}_2) \subseteq \mathcal{B}(E^*)_{r=1} := \mathbb{R}^2_+$, the first part of the proposition follows.

Considering $r = 0$, it is easy to see that for $\lambda c > 1$ the set $\mathcal{B}_1$ is not empty and preimages in $\mathbb{R}^2_+$ of the $x = 0$ and $y = 0$ axis exist as sketched in Figure 5.4. It follows that $\mathcal{B}(E^*)_{r=0} \subseteq \mathbb{R}^2_+ \setminus \cup_{n=0}^{+\infty} T_2^{-n}(\mathcal{B}_2 \cup \mathcal{B}_3)$. Moreover, considering $r = 1$, if $0 > 1 - \lambda c > -1$ it is straightforward to prove that every trajectory starting in $\mathcal{B}_1$ converges to the $x = 0$ axis where the map is undefined as it is a set of focal points whereas each trajectory starting in $\mathbb{R}^2_+ \setminus \mathcal{B}_1$ converges to the asymptotically stable Nash equilibrium E^*, which is also the unique attractor in the region. This can be proved easily noting that the map f_x is linear in $\mathbb{R}^2_+ \setminus \mathcal{B}_1$, so it follows that $\mathcal{B}(E^*)_{r=1} := \mathbb{R}^2_+ \setminus \mathcal{B}_1$ and $\cup_{n=0}^{+\infty} T_2^{-n}(\mathcal{B}_1) = \mathcal{B}_1$. If condition (5.30) holds, it is easy to see that the area of $\mathcal{B}_1$ is smaller then the area of $\mathcal{B}_2$. Thus the second part of the proposition follows.

Considering $r = 1$, if $1 - \lambda c < -1$, then the Nash equilibrium E^* is unstable and the first recurrence of $T_{2,r=1}$, i.e. $\max\{0, f_x\}$ in (5.33), is a linear function as long as $x(t) > 0$. It follows that each trajectory of f_x starting in $\mathbb{R}^2_+ \setminus E^*$ diverges to $-\infty$ and so every trajectory of T_2 starting in $\mathbb{R}^2_+ \setminus E^*$ converges to the focal point $(0, 0)$. The third point of the proposition follows. ■

Proposition 8 provides important insights about the robustness of the asymptotic stability of the Nash equilibrium, measured by the area of the basin of attraction of the equilibrium itself, when all the firms involved in the oligopoly adopt the same heuristic, i.e. either the G or the LMA rule. In particular, the three cases discussed in Proposition 8 are depicted in Figure 5.4, while in Figure 5.5 regions $\mathcal{B}_2$ and $\mathcal{B}_3$ are depicted for $r = 0$, together with the basin of attraction $\mathcal{B}(E^*)_{r=0}$. The picture shows the presence of lobes, which are typical when there are focal points, as it is the point $(0, 0)$ for map T_2, see e.g. [18], [19] and [17] for details.

The economic intuition behind the results of this analysis is synthesized in the following remark.

Remark 9 *Consider the dynamical system T_2 in* (5.21) *and its non-trivial Nash equilibrium E^* in* (5.22)*. As long as the conditions for the asymptotic stability of the Nash equilibrium are ensured for the oligopoly with all G-firms, i.e. $\lambda c < 2$, and the following inequality holds*

$$\frac{\lambda}{|1 - \lambda c|} \geq \frac{2 - \alpha + \alpha N}{(N - 1)\,\alpha c} \tag{5.37}$$

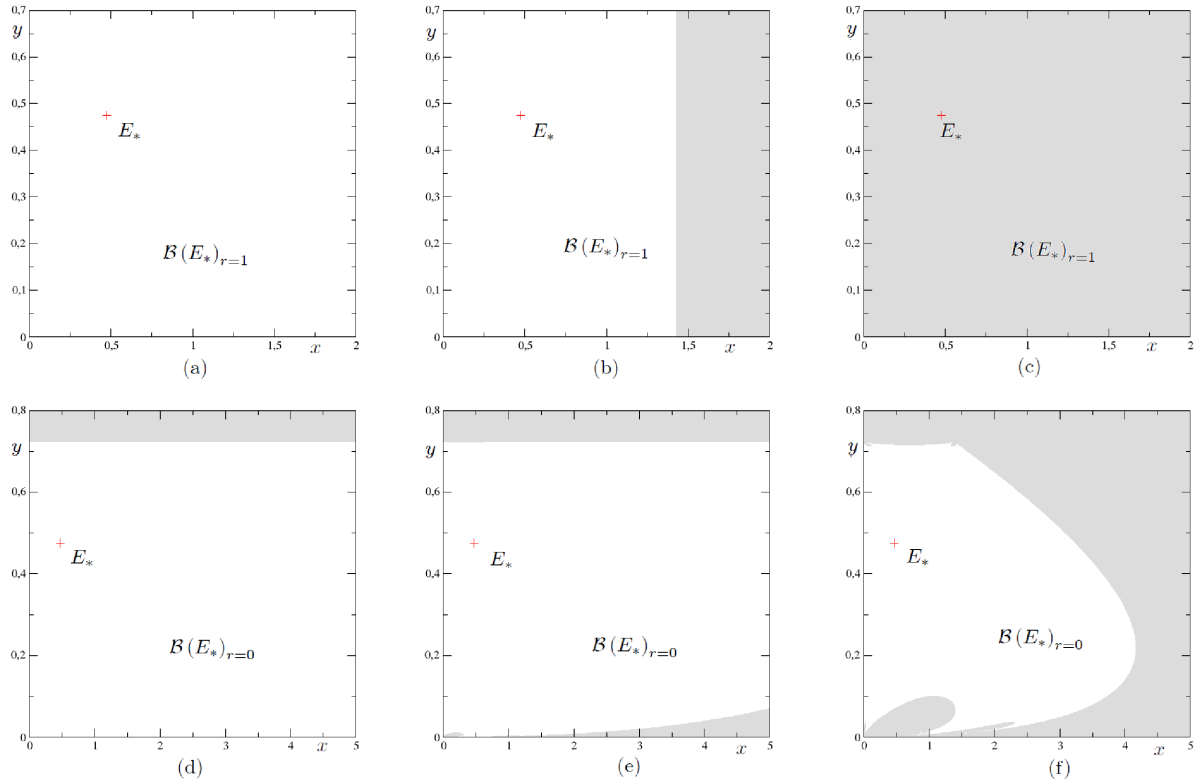

Fig. 5.4 Basins of attraction $\mathcal{B}(E^*)_{r=1}$ (first row) and $\mathcal{B}(E^*)_{r=0}$ (second row) depicted as white regions. Regions of infeasible trajectories are in gray. Cases of Proposition 8 are represented from the left to the right: $\lambda c < 1$ with $\lambda = 1$ and $c = 0.1$ (first column), $1 < \lambda c < 2$ with $\lambda = 15$ and $c = 0.1$ (second column) and $\lambda c > 2$ with $\lambda = 25$ and $c = 0.1$ (third column). Parameters $N = 20$, $\alpha = 0.2$.

then $\mathcal{B}(E^*)$, the basin of attraction of the Nash equilibrium E^*, with all G-firms is at least as large as the corresponding basin in the case of all LMA-firms. On the contrary, when the Nash equilibrium with all G-firms is unstable, i.e. $\lambda c > 2$, the presence of LMA-firms is necessary, but not sufficient, to ensure the feasibility of the oligopoly.

In order to provide some insights about the dimensions of the basins of attraction of the Nash equilibrium E^* also with a mixture of G-firms and LMA-firms, i.e. $r \in (0, 1)$, two cases are shown in Figures 5.6 and 5.7. In Figure 5.6 we have the first case discussed in Proposition 8, i.e. $\lambda c < 1$. In particular, for $r = 1$ and $r = 0$, we have the same cases of Panels (a) and (d) of Figure 5.4, respectively. Note that for $r = 0.5$, i.e. half of the firms adopt the LMA rule and the other half the G-rule, the basin of attraction of E^* increases considerably with respect to the case $r = 0$, and it becomes similar to

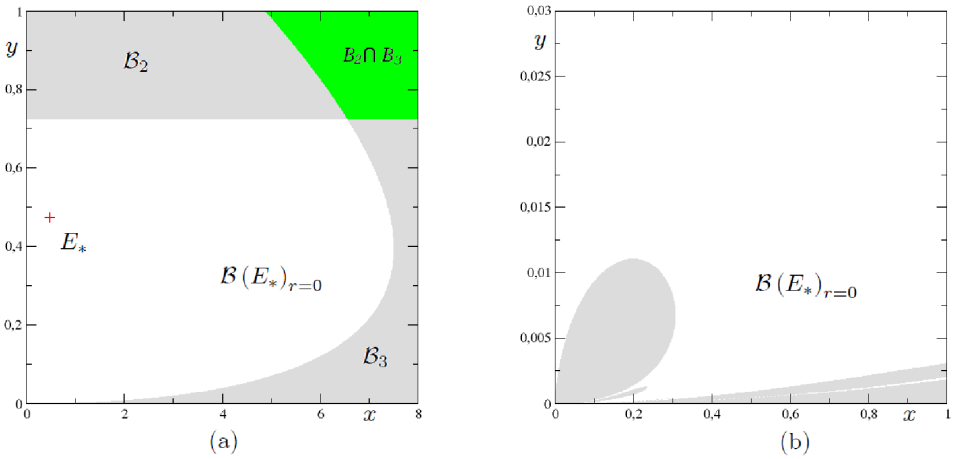

Fig. 5.5 Panel (a) the white region is $\mathcal{B}(E^*)_{r=0} \subseteq \mathbb{R}^2_+ \setminus \cup_{n=0}^{+\infty} T_2^{-n}(\mathcal{B}_2 \cup \mathcal{B}_3)$. Points in $\mathcal{B}_2 \cap \mathcal{B}_3$ (green region) are mapped in one iteration in $(0,0)$. Panel (b) zoom of $\mathcal{B}(E^*)_{r=0}$ near the origin, which is a focal point of the map. The regions of infeasible trajectories, i.e. $\mathcal{B}_2$ and $\mathcal{B}_3$, and their preimages are in gray. Parameters: $N = 20$, $c = 0.1$, $\lambda = 15$, $\alpha = 0.2$.

the basin obtained with $r = 1$. In Figure 5.7, the case $1 < \lambda c < 2$ is considered. In particular, for $r = 0$ and $r = 1$, we have the same cases of Panels (b) and (d) of Figure 5.4, respectively. In this case, the presence of a very small fraction of G-firms in the oligopoly ($0,1\%$ in the example) considerably enlarges $\mathcal{B}(E_*)$, the basin of attraction of the Nash equilibrium, so that the oligopoly acquires stability in the state space.

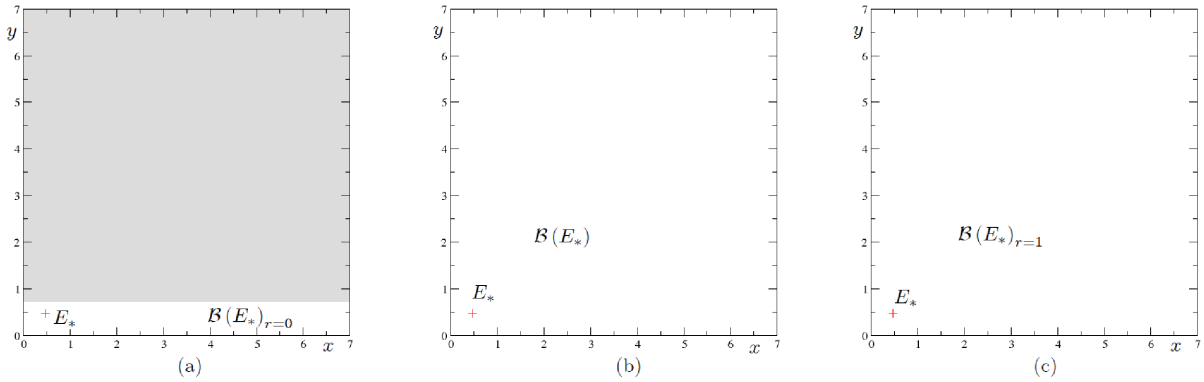

Fig. 5.6 Basins of attraction of E^* (white region), for different values of r: panel (a) $r = 0$, panel (b) $r = 0.5$ and panel (c) $r = 1$. Region of infeasible trajectories in gray. Parameters: $\lambda = 1, N = 20, c = 0.1, \alpha = 0.2$.

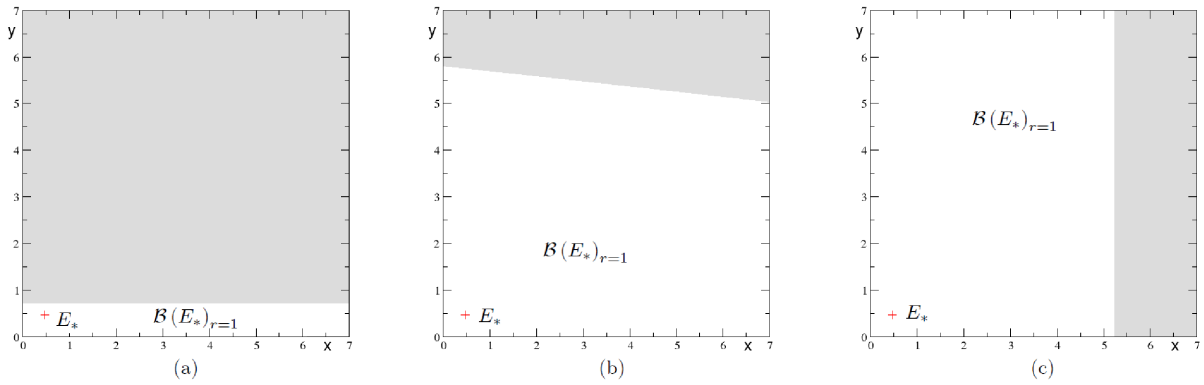

Fig. 5.7 Basins of attraction of the Nash-equilibrium E^* (white region) for different values of r: panel (a) $r = 0$, panel (b) $r = 0.001$ and panel (c) $r = 1$. Region of infeasible trajectories in gray. Parameters: $\lambda = 15, N = 20, c = 0.1, \alpha = 0.2$.

5.3.2 Dynamic analysis of the evolutionary model

Let it begin the analysis of the dynamical system T in (5.18) by studying the existence and local stability of equilibria. This question is quite simple whenever the Nash equilibria of the two-dimensional restrictions to the invariant planes $r = 0$ or $r = 1$ are stable. Proposition 4 and Corollary 5 with the specific map (5.18) can be reformulate in a unique proposition:

Proposition 10 *Consider the dynamical system T in* (5.18).

- *If $K_G = K_L$, then a continuum of equilibrium points E^* exists along the segment $E = \left(\frac{N-1}{cN^2}, \frac{N-1}{cN^2}, r\right)$, with $r \in [0,1]$. These equilibria are stable as long as the stability conditions for the Nash equilibrium stated in Proposition 4 are satisfied. One fixed point in E undergoes a codimension-two bifurcation changing $K_G - K_L$ with an associated eigenvalue equal to 1 and another one equal to -1, with the possible creation of a stable 2-cycle $\left\{\left(\underline{x}, \underline{y}, \underline{r}\right), (\overline{x}, \overline{y}, \overline{r})\right\}$. The point in E that undergoes the codimension-two bifurcation is the one such that $(x^+, y^+, r^+) = \left(\underline{x}, \underline{y}, \underline{r}\right) = (\overline{x}, \overline{y}, \overline{r})$ and $\lambda = \lambda^*(\alpha, r^+)$, where*

$$\lambda^*\left(\alpha, r^+\right) = \frac{2N\left(\alpha\left(1 - 2r^+ - N\left(1 - r^+\right)\right) + 4\right)}{c\left(r^+\left(\alpha + 4\right)\left(N - 2\right) - 2\alpha\left(N - 1\right) + 8\right)} \tag{5.38}$$

- *If $K_G \neq K_L$, then only the two extremum points of the segment E are equilibria, namely*

$$E_0 = \left(\frac{N-1}{cN^2}, \frac{N-1}{cN^2}, 0\right) \quad \text{and} \quad E_1 = \left(\frac{N-1}{cN^2}, \frac{N-1}{cN^2}, 1\right) \tag{5.39}$$

  in which all agents adopt the same strategy, which is LMA or G respectively:

  - *If $K_L < K_G$, then equilibrium E_0 is stable for $2 \leq N < 1 + \frac{4}{\alpha}$ and $\lambda < \frac{N}{c}$, and it loses stability through a period doubling bifurcation at $N = 1 + \frac{4}{\alpha}$ given $\lambda < \frac{N}{c}$. E_1 is always unstable.*
  - *If $K_L > K_G$, then equilibrium E_1 is stable for $\lambda < \frac{2}{c}$ and loses stability for $\lambda > \frac{2}{c}$. At $\lambda = \frac{2}{c}$ no bifurcation occurs. E_0 is always unstable.*

Proof. The proof is a direct application of Proposition 4, Corollary 5 and Proposition 8. ■

Starting from the previous investigation of the dynamics of the model on the invariant subspaces $r = 0$ and $r = 1$, Proposition 10 describes, for the case $K_G \neq K_L$, the local asymptotic stability of the two Nash equilibria E_0 and E_1, which are located on the invariant planes $r = 0$ and $r = 1$ respectively. For the three-dimensional model, the main question related to these equilibria concerns their *local transverse stability*. When an equilibrium on an invariant plane (either $r = 0$ or $r = 1$) is locally asymptotically stable for the bidimensional map (5.21) then it obviously attracts sufficiently nearby trajectories of the plane, i.e. it is stable with respect to perturbations along the plane. Transverse stability occurs when an attractor on the plane is also an attractor for the complete map (5.18), i.e. if it is stable with respect to perturbations that are *transverse* to the plane; in particular, these perturbations have initial conditions $(x(0), y(0), r(0))$ with $r(0) \in (0, 1)$. In this case, the basin of attraction of the attractor on the plane has positive measure, i.e. the basin has positive volume, being a subset of $\mathbb{R}^3$.

For the sake of clarification, it is worth pointing out that the local transverse instability of one of the two equilibria, be it E_0 or E_1, does not exclude that they may also have a basin of attraction of positive Lebesgue measure in $\mathbb{R} \times \mathbb{R} \times [0, 1]$. In other words, the Nash equilibria E_0 and E_1 might be *Milnor* (or weak) attractors, see [101] and [19]. To have this, it is sufficient that a Nash equilibrium that belongs to an invariant plane is: 1) stable along the plane and 2) its basin of attraction on the plane intersects a set of points (with non-zero area) that are transversely stable. These points in the plane, which do not include the Nash equilibrium on the plane as we have assumed that it is transversely unstable, attract some trajectories with

initial conditions $(x(0), y(0), r(0))$ with $r(0) \in (0,1)$. Once these trajectories reach the invariant plane, they converge to the Nash equilibrium, since they are in its basin of attraction.

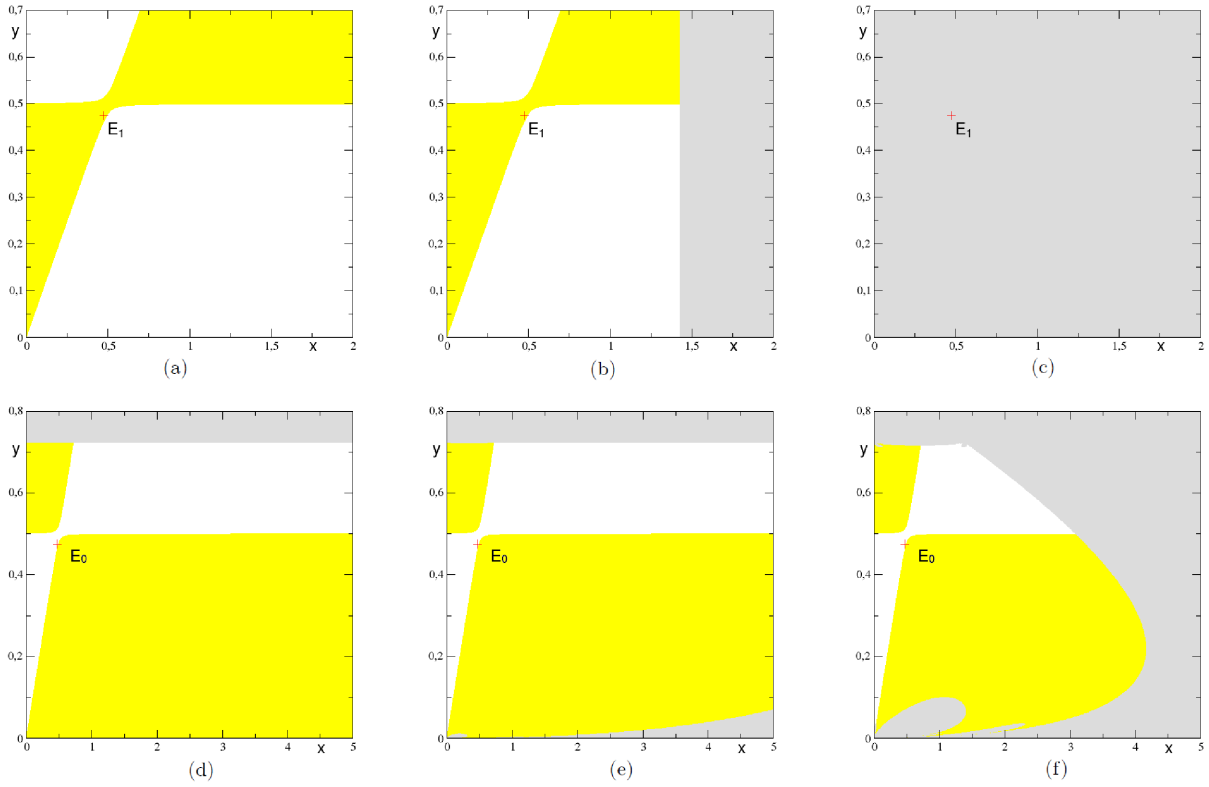

Fig. 5.8 Regions of transversely unstable points (yellow region) and transversely attractive ones (white region) on invariant planes $r = 1$ (first row) and $r = 0$ (second row), when $K_G > K_L$. Regions of infeasible trajectories are in gray. Panels (a)-(d) $\lambda = 1$. Panels (b)-(e) $\lambda = 15$. Panels (c)-(e) $\lambda = 25$. Parameters: $N = 20$, $c = 0.1$, $\beta = 1$, $K_G = 0.0001$, $K_L = 0$, $\alpha = 0.3$.

We illustrate this occurrence by numerical findings. Let us start considering the case $K_G > K_L$, i.e. agents have a propensity to adopt the LMA rule even in case the profits generated by the two heuristics are the same. In this case, as stated in Proposition 10, the Nash equilibrium E_0 is asymptotically stable while the Nash equilibrium E_1 is unstable. Nevertheless, in the basin of attraction of the Nash equilibrium E_1 are included points characterized by transverse attractivity (this set of points is represented by the white region in Figure 5.8) which attract trajectories coming from outside the invariant subspace. That is, the Nash equilibrium E_1 is a Milnor attractor. In Figure 5.8, the situation is depicted both for the cases such that E_1 is stable, see panels (a) and (b), and unstable, see panel (c), on the invariant plane $r = 1$. It is worth noticing

that the dynamics of T on the restrictions $r = 0$ and $r = 1$, is the same as the one depicted in Figure 5.4 and described in Proposition 8.

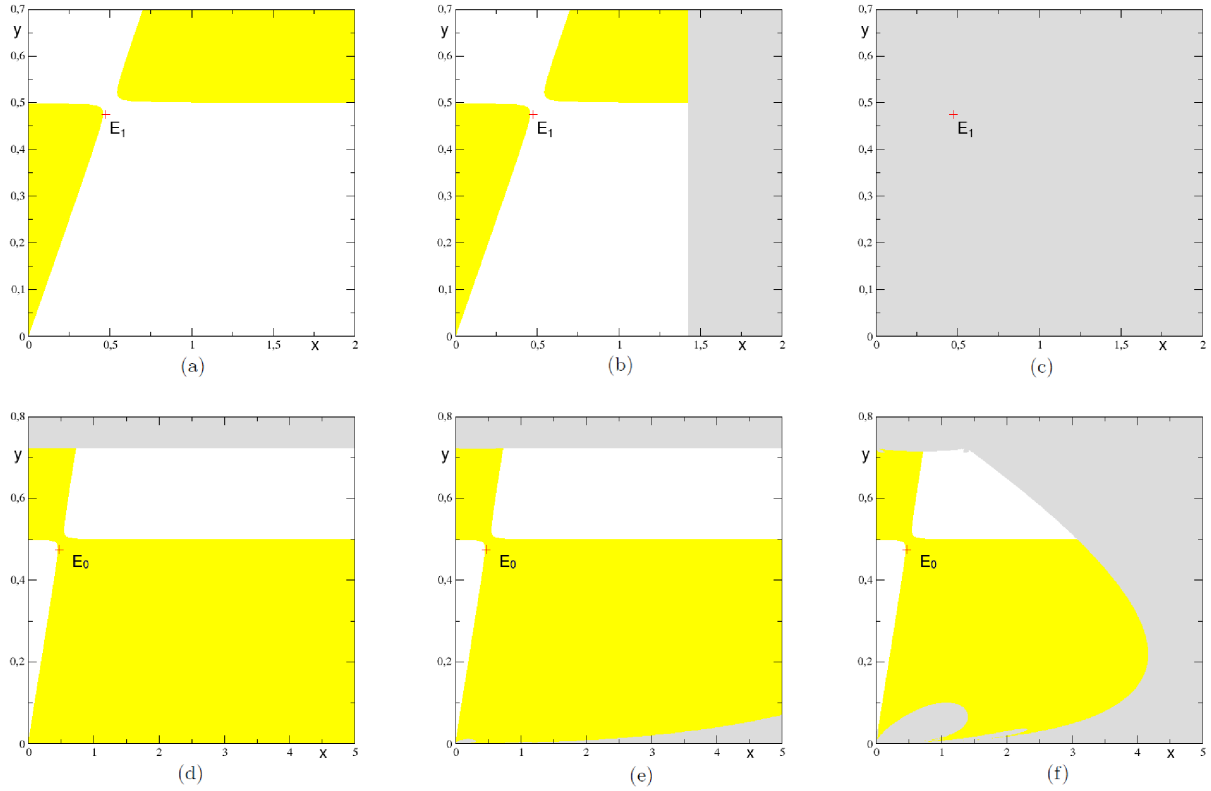

Fig. 5.9 Regions of transversely unstable points (yellow region) and transversely attractive ones (white region) on invariant planes $r = 1$ (first row) and $r = 0$ (second row), when $K_G < K_L$. Regions of infeasible trajectories are in gray. Panels (a)-(d) $\lambda = 1$. Panels (b)-(e) $\lambda = 15$. Panels (c)-(e) $\lambda = 25$. Parameters: $N = 20$, $c = 0.1$, $\beta = 1$, $K_G = 0$, $K_L = 0.0001$, $\alpha = 0.3$.

A similar situation occurs for cases with $K_G < K_L$, i.e. when agents have a propensity to adopt the G-rule even when profits generated by the two heuristics are equal. In this case, as stated in Proposition 10, the Nash equilibrium E_1 is asymptotically stable while the Nash equilibrium E_0 is unstable. Nevertheless, the basin of attraction of the Nash equilibrium E_0 includes a set of points characterized by transverse attractivity (this set of points is represented by the white region in Figure 5.9). That is, the Nash equilibrium E_0 is a Milnor attractor. It is worth remembering that the structure of the basins of attraction of the two Nash equilibria E_0 and E_1 on $r = 0$ and $r = 1$ respectively is the same in Figures 5.8 and 5.9 as the only difference in the two cases regards the values of K_G and K_L, which are two parameters that

influence only the transverse stability. In particular, the particular shape of the basins of attraction, with the presence of lobes, is illustrated in details in the previous sections (see in particular Proposition 8), so it is not discussed here.

The analysis of transverse stability underlines another interesting dynamic property of the model. This occurs when, for $K_G > K_L$, the Nash equilibrium E_0 is unstable and the attractor on the invariant subspace $r = 0$, generated by a sequence of period-doubling bifurcations, becomes transversely unstable. This situation is depicted in Figure 5.10.[9] From panel (a) of this figure we note that the attractor indicated by black dots has portions in both the white region and the yellow region. This indicates that along the attractor there are points that are transversely unstable (yellow region) and points that are transversely stable (white region). To provide a measure of the transverse attractivity of trajectory along the attractor, we compute the transverse Lyapunov exponents:

$$\Lambda_{\perp}\left(T^{\infty}\left(x\left(0\right),y\left(0\right),r\left(0\right)\right)\right)=\lim_{T\to\infty}\frac{1}{T}\sum_{i=0}^{T}\ln\left|v_{3}\left(x\left(i\right),y\left(i\right),r\left(i\right)\right)\right| \tag{5.40}$$

where $T^{\infty}\left(x\left(0\right),y\left(0\right),r\left(0\right)\right):=\left\{\left(x\left(i\right),y\left(i\right),r\left(i\right)\right)=T^{i}\left(x\left(0\right),y\left(0\right),r\left(0\right)\right),i\geq 0\right\}$ is a generic trajectory along the attractor itself and

$$v_{3}=\left.\frac{\partial r^{'}}{\partial r}\right|_{r=0}=e^{\beta\Delta\pi(x(i),y(i),0)} \tag{5.41}$$

is the eigenvalue of the map T corresponding to the transversal direction. If $\Lambda_{\perp}\left(T^{\infty}\left(x\left(0\right),y\left(0\right),r\left(0\right)\right)\right)$ 0 holds, then average transversely stability of $T^{\infty}\left(x\left(0\right),y\left(0\right),r\left(0\right)\right)$ is proved. In Figure 5.10 panel (b), we note that the transverse stability of the attractor is lost as α increases. When the attractor is transversely unstable, a situation of high uncertainty occurs for the evolutionary oligopoly game. Indeed, firms may fail to select a unique and common heuristic.

The analysis of the transverse stability of the attractors on the two invariant planes $r = 0$ and $r = 1$ underlines that the evolutionary selection of the heuristics by firms is a quite complicated nonlinear phenomenon and that a simple propensity of one rule to the other one does not necessary leads firms to adopt homogeneous behaviors.

This aspect is further confirmed by the possibility that an attractor not belonging to an invariant plane ($r = 0$ or $r = 1$) exists. As indicated in Proposition 10, this attractor originates by a codimension-two bifurcation at $K_G = K_L$ from which a stable

[9]Note that in this case E_0 is transversely stable as long as it is stable for the restriction of the map on the invariant plane $r = 0$.

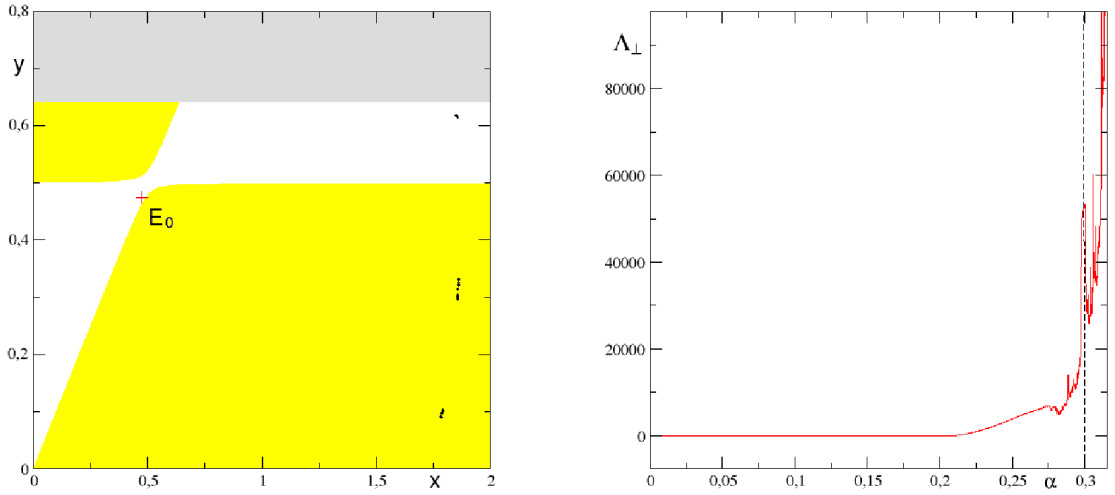

Fig. 5.10 Panel (a) attractor on the invariant plane $r = 0$. Its basin of attraction is in red. In yellow the set of points that are transversely unstable. Panel (b) Lyapunov exponent along the attractor of panel (a) as α varies in the range $[0, 0.3]$. Parameters: $K_G = 0.0001$, $K_L = 0$, $N = 20$, $\alpha = 0.3$, $\lambda = 1$, $N = 20$.

2-cycle may appear. Moreover, this cycle may not be the unique stable attractor in $\mathbb{R} \times \mathbb{R} \times (0, 1)$, as numerical evidence shows that other stable attractors could exist, see in particular the bifurcation diagram of Figure 5.11.

The evolutionary oligopoly under analysis can exhibit further nonlinear phenomena originated by additional bifurcations that lead to complicated dynamics. For instance, the 2-cycle that is generated through the described codimension-two bifurcation (see e.g. Figure 5.12) represents two fixed points of the map T^2. Each of these two fixed points of T^2 can undergo a Neimark-Sacker bifurcation as the intensity of choice β is increased. As a result, we detect the presence of an asymptotically stable attractor with $r \in (0, 1)$ for T, see e.g. Figure 5.13. If the intensity of choice β is further increased, the attractor takes a particular shape, see Figure 5.14 panel (d). The dynamics along this attractor is of particular interest from an economic point of view. Figure 5.14 presents a time series for the level of production. The dynamics of the quantity of production for LMA-firms and for G-firms follow a very strange pattern, which is characterized by long periods of almost constant production levels - very close to the Nash quantity - that are interrupted by shorter periods of high production fluctuations. These dynamic scenarios shed some light on the high unpredictability of agents' behavior in the evolutionary oligopoly. Indeed, a long time period on which

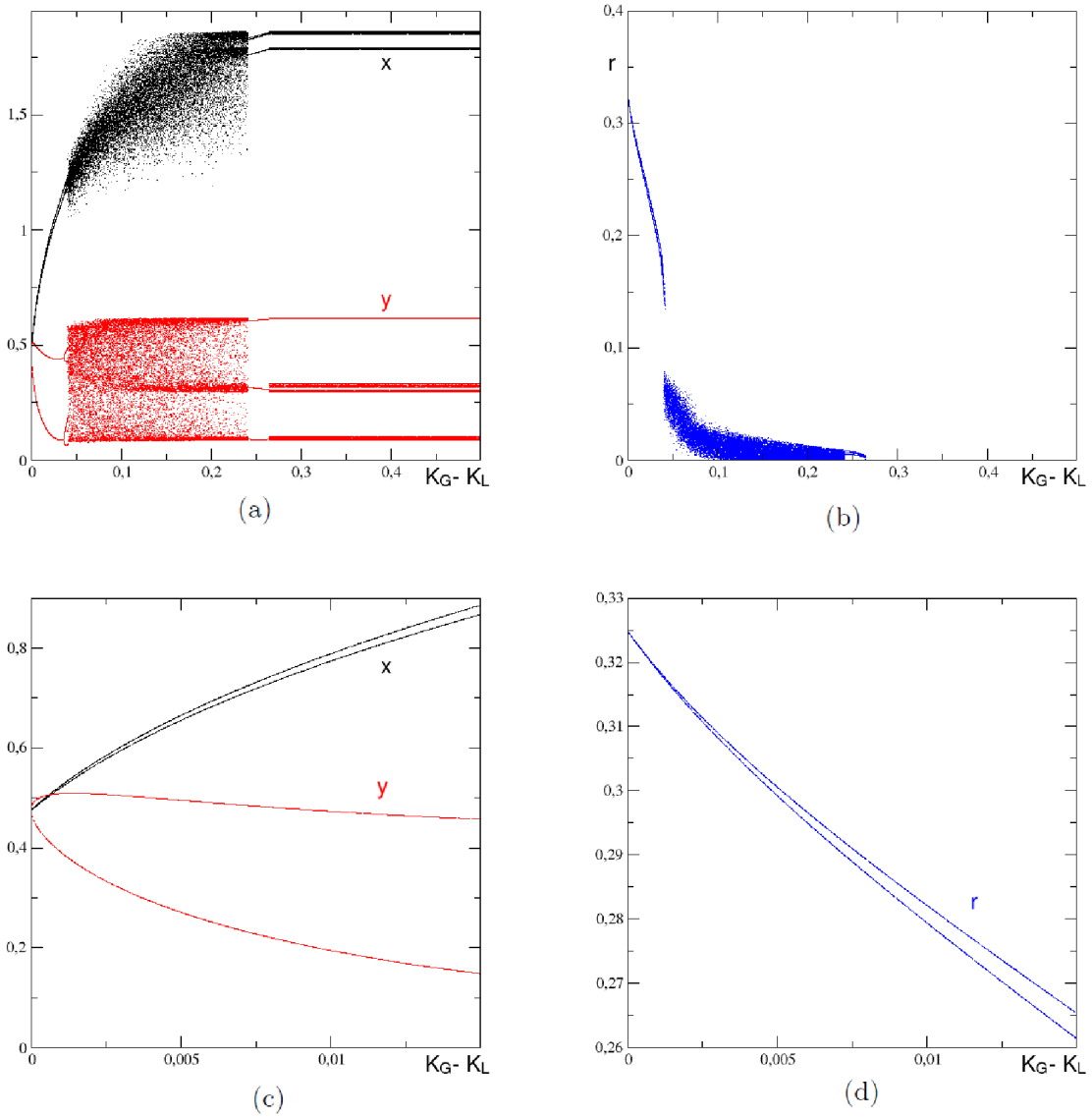

Fig. 5.11 1D-bifurcation diagram as $K_G - K_L$ varies on the range $[0, 0.5]$. Panel (a), productions x of a G-firm (black) and y of a LMA-firm (red) as $K_G - K_L$ varies. Panel (b), dynamic of r as $K_G - K_L$ varies. Panels (c) and (d) a zoom of the bifurcations diagrams on the upper line for $K_G - K_L$ close to zero. Parameters: $N = 20$, $\beta = 1$, $\alpha = 0.3$, $\lambda = 1$ and $c = 0.1$.

firms deliver almost constant productions, very close to the Nash equilibrium level, could lead an observer to think that the oligopoly is reaching a stationary equilibrium. Nevertheless, large bursts appear for short periods of times and at regular intervals to break the time series of constant productions.

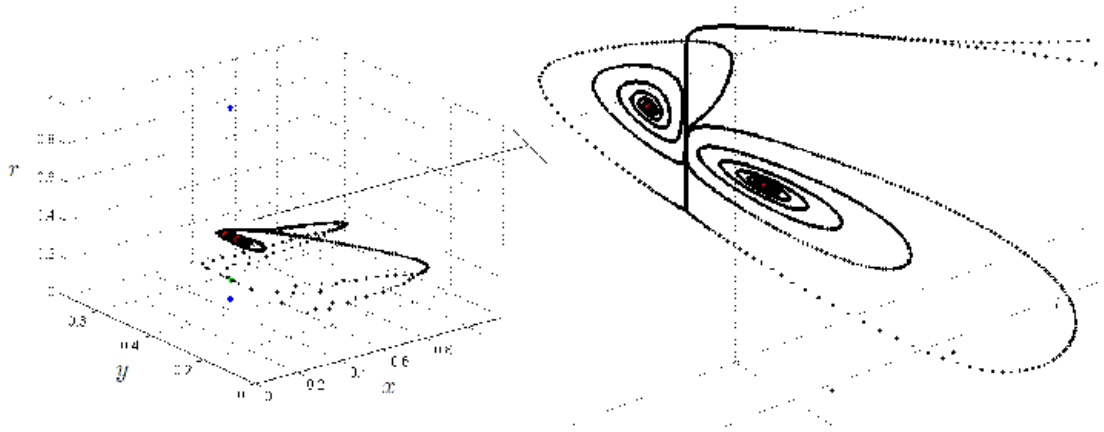

Fig. 5.12 Trajectory for i.c. $(q^* - 0.002, q^* + 0.002, 0.1)$. Parameters: $\lambda = 1$, $N = 20$, $c = 0.1$, $\alpha = 0.3$, $\beta = 1$, $K_y = 0$, $K_x = 0.0001$. The Nash equilibria E_1 and E_0 are depicted in blue. The i.c. in green. The ω-limit set is in red.

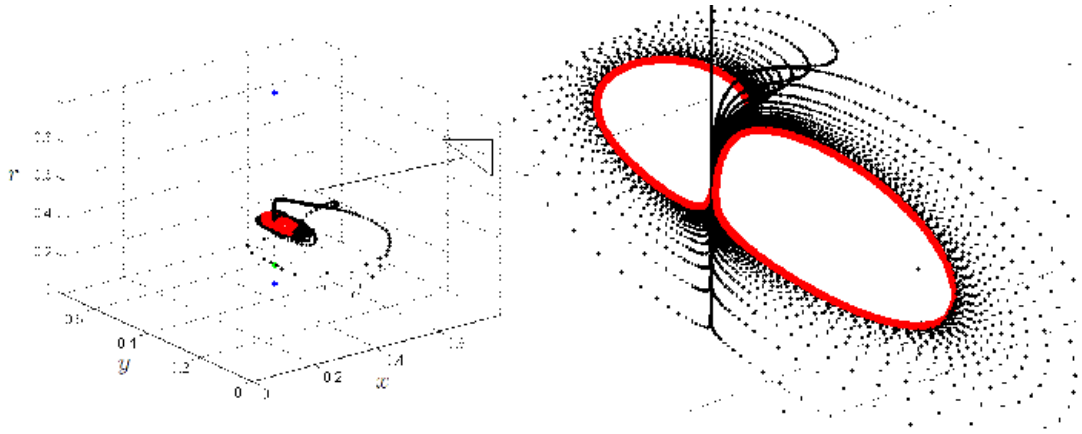

Fig. 5.13 Trajectory for i.c. $(q^* - 0.002, q^* + 0.002, 0.1)$. Parameters: $\lambda = 1$, $N = 20$, $c = 0.1$, $\alpha = 0.3$, $\beta = 6$, $K_y = 0$, $K_x = 0.0001$. The Nash equilibria E_1 and E_0 are depicted in blue. The i.c. in green. The ω-limit set is in red.

Another aspect is worth of being mentioned. The periodic and aperiodic attractors depicted in Figures 5.12, 5.13 and 5.14 provide indication that it may be more profitable for firms to behave differently than similarly. Indeed, along these inner attractors the average level of production is lower than in the Nash equilibrium and this implies, given the profit function of the industry here assumed, that the average profit of the industry is higher than the profit with all firms at the Nash equilibrium. Specifically, we observe that the level of production of G-firms is always lower than the Nash equilibrium quantity and their profits are always higher than the one obtainable at

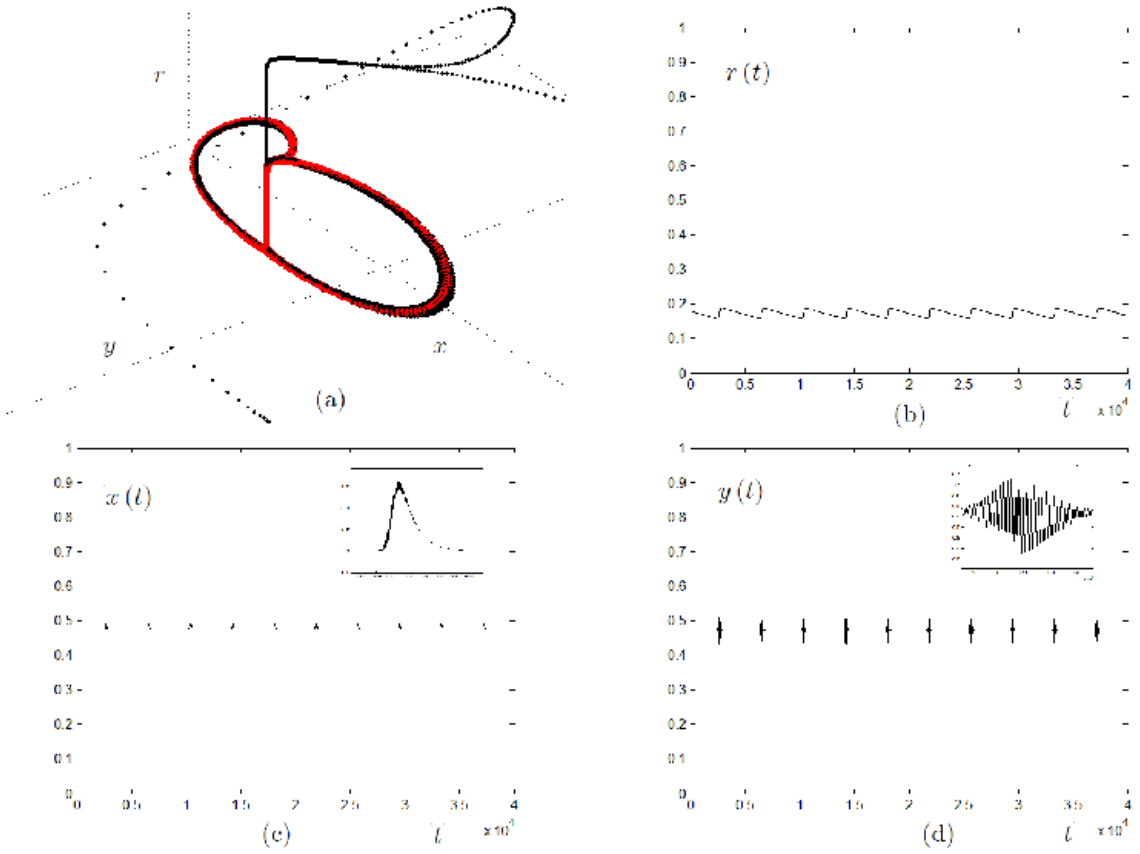

Fig. 5.14 Panel (a) trajectory for i.c. $(q^* - 0.002, q^* + 0.002, 0.1)$. The ω-limit set is in red. Panels (b)-(d) time series of r, x and y. Parameters: $\lambda = 1$, $N = 20$, $c = 0.1$, $\alpha = 0.25$, $\beta = 6$, $K_y = 0$, $K_x = 0.00001$.

the Nash equilibrium, see Figure 5.15 where we depicted the profit dynamics along the attractors of the previous examples. On the contrary, the levels of production of LMA-firms can oscillate around the Nash quantity and the profits can oscillate above and below the ones obtainable at the Nash equilibrium. However, relative to the dynamic scenario depicted in Figure 5.14, this occurs only for short intervals of time, while for most of the time both G-firms and LMA-firms experience higher profits along the inner attractor than at the Nash equilibrium. The economic explanation of this phenomenon is clear and based on the fact that for firms it is sufficient to produce less than the Nash quantity to increase their profits. This requires capability of coordination between firms, for example as if they would be able to constitute a cartel, which is not achievable within the simple evolutionary model proposed. However, a sufficient level of evolutionary competition (remember that inner attractors appear as the value of β increases, parameter that measures the evolutionary pressure) between

two boundedly-rational behavioral rules can sustain unexpected forms of coordinations that lead the industry as a whole and both groups of players as well to experience average levels of profits, which are higher than those obtainable at the Nash equilibrium. This observation leads to the conclusion that in some cases firms might prefer to be in a polymorphic rather than monomorphic state. Recapping, the heterogeneity in the firms' choice of the behavioral rules may lead to increments in the producer surplus (total profit of the industry), even though at the expenses of reducing the consumer surplus.

Besides the described phenomena, other form of complexity can arise as well. An example is depicted in Figure 5.16 where in panel (d) we observe a quite irregular dynamics of the fraction of G-firms that populates the evolutionary game as time evolves. In this case, a chaotic inner attractor exists.

To conclude the investigation on the dynamics of the evolutionary model, we can sum up by saying that asymptotic dynamics can exhibit *evolutionary stable heterogeneity*: the dynamics along the asymptotically stable attractors on $\mathbb{R} \times \mathbb{R} \times (0, 1)$ indicate that heterogeneous behavior can be more profitable, in an evolutionary sense, than following a homogeneous strategy over time. Indeed, this heterogeneous behavior is the result of the evolutionary selection based on profits. The proposed analysis underlines also that a bias for playing one strategy does not necessarily imply that in the long run all the firms decide to adopt that strategy. More precisely, the propensity for playing one strategy does not exclude that firms select in the evolutionary process the other strategy in the long run. This crucially depends on several elements, but principally on the initial condition of the system. As a final note, we emphasize the possibility of complicated dynamics of the state variables generated by the evolutionary stable heterogeneities, which are particular interesting both from an economic and mathematical point of view.

To conclude it can be noted that several extensions of this model are worth being considered further. First of all, an interesting addition is to include memory in the fitness measures of the two strategies, following [75]. With respect to the economic structure, another interesting question, often overlooked by the existing literature, is to study how the elasticity of demand influences the overall properties of the system.

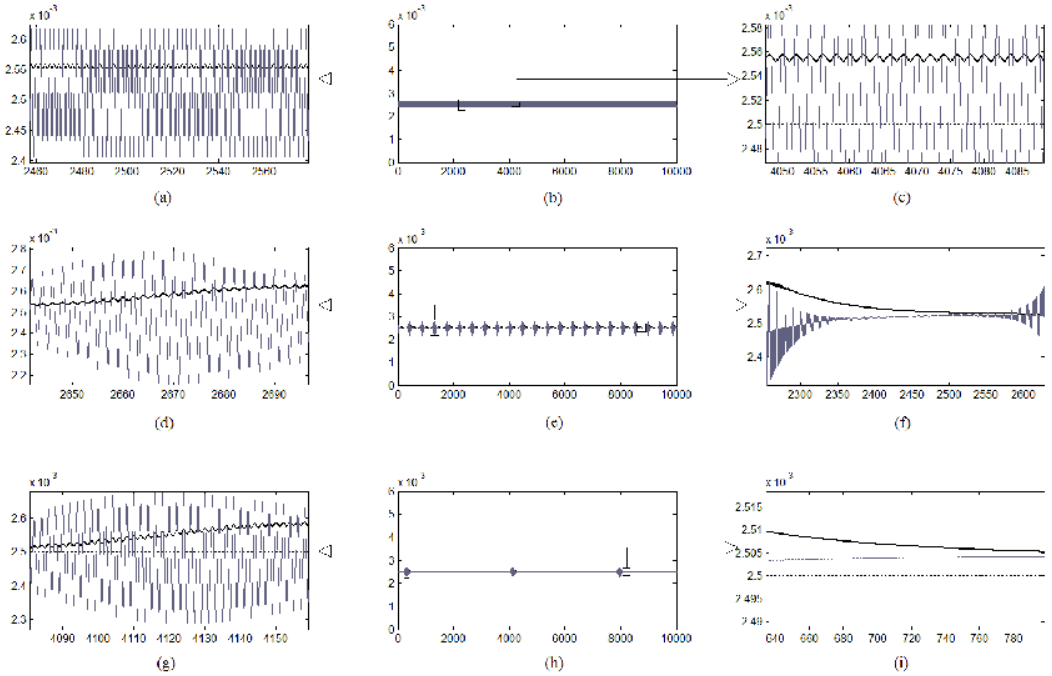

Fig. 5.15 Dynamics of profits: Dotted line represents profits that firms would obtain at the Nash equilibrium, black solid line represents profits made by G-firms and gray solid line represents profits made by LMA-firms. First row, profit dynamics along the attractor depicted in Figure 5.12. Second row, profit dynamics along the attractor depicted in Figure 5.13. Third row, profit dynamics along the attractor depicted in Figure 5.14. Central column contains panels representing the profit dynamics along an attractor. Left and Right columns contains panels representing enlargements of some interesting parts of the profit dynamics.

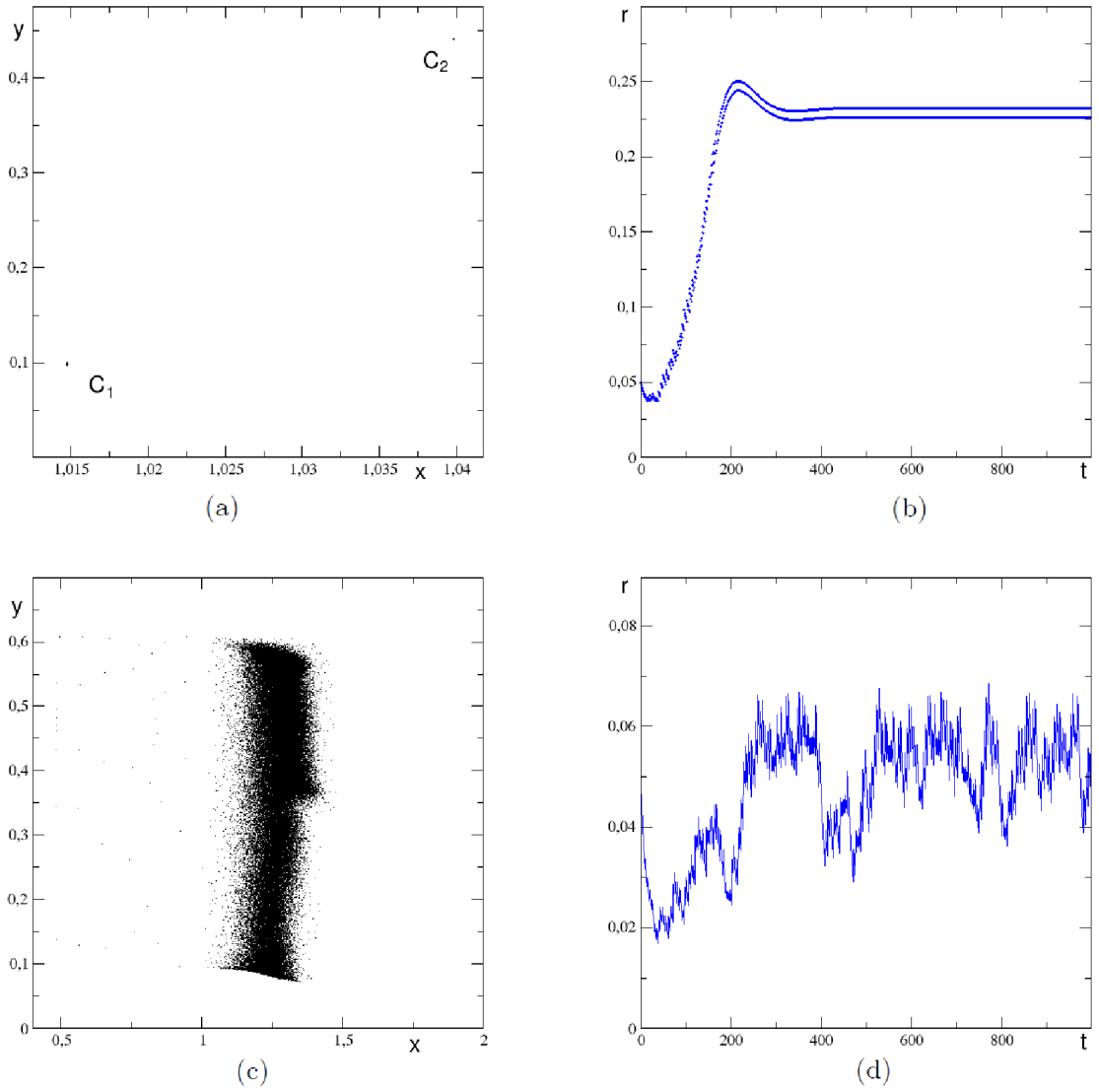

Fig. 5.16 On the left column two projections on the $x-y$ plane of the trajectory (x, y, r) of the evolutionary oligopoly model. On the right column the dynamics of variable r. Upper line $K_G = 0.025$ and $K_L = 0$. Bottom line $K_G = 0.05$ and $K_L = 0$. Parameters: $N = 20$, $\beta = 1$, $K_G = 0.05$, $K_L = 0$, $\alpha = 0.3$, $\lambda = 1$ and $c = 0.1$.

Chapter 6

Reinforcement Learning (RL) Based Control with Applications

6.1 Aim and scope

The Virgo/LIGO gravitational wave (GW) detectors are Michelson interferometers trying to observe gravitation signals typically emitted by binary systems of neutron stars and/or black holes.

Interferometers' mirrors vary their relative distances due to the gravitational perturbation produced by the GW passage. In principle mirrors' relative motion can be used to reconstruct the GW form. However mirrors' motion is caused also by other terrestrial perturbations such as Newtonian noise, that are perturbations of the gravitational field of the earth, and seismic noise which perturbs directly the mirrors' position through their connection to the earth's surface. In order to suppress the perturbations of the terrestrial noise on the relative distance among mirrors, control forces on mirrors' suspensions are needed. Such forces are typically the outcome of linear controllers, such as PID of LQG, whose design is based on a model of the physical plant. It is worth noting that a disadvantage, which may arise using linear controllers, comes from unavoidable errors in plant modeling that could invalidate, or weaken, the utility of the classical optimal feedback design.

The objective of the control problem here considered is to make a first attempt towards the realization of an adaptive feedback controller based on reinforcement learning, which will be called the "*RL Agent*" in the following, in order to improve the linear controller effectiveness. What is of interest here is that the *RL Agent* learns from real data and it does not need any prior knowledge of the plant. Indeed the *RL Agent* consists in a controller that adapts its feedback action based on experience, that

is on the observations of the effects that past feedback actions have produced on the plant, improving its effectiveness as long as new information shall be obtained from data.

In order to realize such a controller, the *RL Agent* must be capable of forecasting which effects a certain action will produce on the plant, learning the causal relations which determine the transitions between successive states. In order to do this the *RL Agent* will improve its evaluations of the transition probabilities of the physical environment through the balancing between the exploration activity, by performing random actions, and the exploitation of the acquired knowledge, by selecting actions based on expectations of future rewards from it.

Stability and performance of the *RL Agent* are determined by a number of factors, one of the most important of which is that the learning process must proceed as efficient as possible. This is mainly favored by the Markovianity of the environment[1] and by an appropriate balance between the exploration of the environment and the exploitation of the acquired knowledge about it. Furthermore, another advantage from using a reinforcement learning controller is that, if feedback forces are conveniently chosen in a bounded set, then problems about reliability of the controller are avoided. This aspects, as well as other important ones, will be discussed in details in the following.

The plain of the present Chapter is as follows. In Section 6.2 is described a two-pendulum system perturbed by colored noise while in Section 6.2.1 is described the filtering process needed to estimate the dynamical state of the system based on noisy measures. In Section 6.3 is outlined how the reinforcement learning controller can be used for the dynamical system control and a brief overview of the reinforcement learning topic is presented. In Section 6.4 simulations of the two-pendulum system using both the reinforcement learning controller and a classical linear PID controller are used. Finally, in Section 6.5 are suggested further developments.

6.2 Coupled pendulums

The reinforcement learning based controller is here applied to a simplified model of superattenuators of a gravitational wave detector. Superattenuators are indeed complex mechanical elements characterized by a high number of degrees of freedom (approximately $60 - 70$ each) that are connected to the earth through suspensions, that have the function of supporting the mirrors and are designed to suppress the noise coming from the earth surface. At a very first approximation, superattenuators

[1]This makes possible to isolate the direct effect of feedback actions on the plant's dynamics.

and mirrors are expected to behave like two identical pendulums perturbed, at their suspensions, by white and correlated seismic noises with higher correlation at lower frequencies. The measures on the plant that can be performed are those that return the relative distance between the mirrors. In this simplified model of the plant it is assumed that such measures are affected by a simplified sensor noise, meaning by this that it is white, Gaussian and independent from the seismic noise that perturbs the mirrors' motion. This can be seen as a first step towards the real application of a *RL Agent* controller to gravitational interferometers.

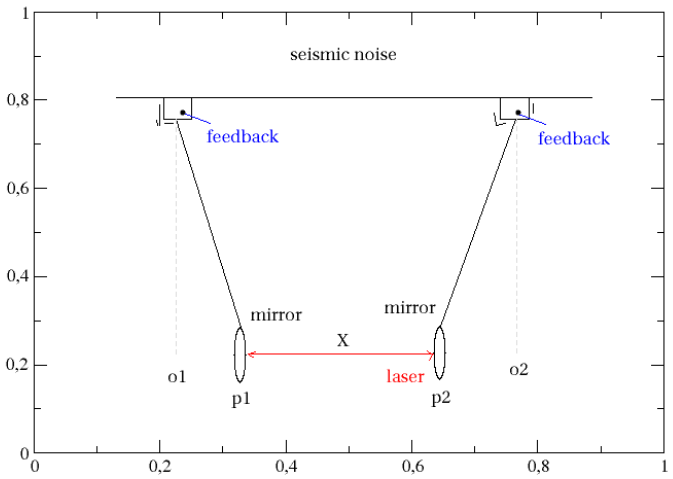

Fig. 6.1 Schematic representation of the plant: the mirrors, located in p_1 and p_2 with respect to a fixed reference frame in the laboratory, and the superattenuators behave like two pendulums; their suspensions at the top, located in o_1 and o_2 in the same frame, are perturbed by seismic noise; feedback actuators are present; a laser measures the relative distance between the mirrors.

Let p_1 and p_2 be the positions of each pendulum in a certain reference frame, and let o_1 and o_2 be the positions of their suspension points in the same frame. Since the force on each pendulum depends only on the displacement $p_i - o_i$, $i = 1, 2$, the equations of motion of the system can be written as:

$$\ddot{p}_1 = -\omega^2(p_1 - o_1) - \nu\dot{p}_1 \tag{6.1a}$$

$$\ddot{p}_2 = -\omega^2(p_2 - o_2) - \nu\dot{p}_2 \tag{6.1b}$$

where the oscillation frequency ω is the same for the two pendulums and the dumping coefficient ν accounts for air friction. In gravitational interferometers the relevant and measurable quantity is the distance between the mirrors. If there was no noise acting

on the pendulums, then their relative distance would be fixed at X_0. However, such distance is $X_t = p_1(t) - p_2(t)$ and evolves according to the evolution equation obtained subtracting the equations (6.1) one from the other:

$$\ddot{X}_t = -\omega^2(X_t - O_t) - \nu\dot{X}_t \tag{6.2}$$

where $O_t = o_1 - o_2$ is the distance between the two suspensions. We want to take into account that the suspensions o_1 and o_2, because of their finite distance on the earth surface, are subjected to seismic perturbations that are correlated at low frequencies. It results that the noise O_t will have higher intensity at high frequencies. A model for the noise of O_t will be obtained from a white and Gaussian noise ξ_t with variance q, that is a noise for which it results that $\xi_t \sim \mathcal{N}(0,1)$ and $\langle \xi_t \xi_s \rangle = q\delta(t-s)$, considering the following stochastic differential equation (SDE):

$$\dot{x}_t = -px_t + \xi_t \tag{6.3}$$

where p is a positive constant. Indeed the power spectral density (PSD) of $\dot{x}_t$ as a function of the frequency f is:

$$PSD(\dot{x}_t) \propto \frac{f^2}{p^2 + f^2} \tag{6.4}$$

The process $\dot{x}_t$ has the qualitative features desired for the effective noise perturbing the distance O_t since it is characterized by a lower energy content at low frequencies rather than at high frequencies.

Equation (6.2) and (6.3) are rewritten in the concise matrix form which highlights that the physical plant is a linear system driven by white and Gaussian noise:

$$\frac{d}{dt}\begin{pmatrix} X_t \\ \dot{X}_t \\ x_t \end{pmatrix} = \begin{pmatrix} 0 & 1 & 0 \\ -\omega^2 & -\nu & -\omega^2 p \\ 0 & 0 & -p \end{pmatrix}\begin{pmatrix} X_t \\ \dot{X}_t \\ x_t \end{pmatrix} + \begin{pmatrix} 0 & 0 & 0 \\ 0 & 0 & \omega^2 \\ 0 & 0 & 1 \end{pmatrix}\begin{pmatrix} 0 \\ 0 \\ \xi_t \end{pmatrix} \tag{6.5}$$

In the following we will write the equation (6.5) in compact form:

$$\dot{\mathbf{X}}_t = \mathbf{A} \cdot \mathbf{X}_t + \mathbf{G} \cdot \boldsymbol{\xi}_t \tag{6.6}$$

where $\mathbf{X}_t$ is the dynamical state of the plant, the matrix $\mathbf{A} \in \mathbb{R}^{i \times i}$ is the reaction matrix while the matrix $\mathbf{G} \in \mathbb{R}^{k \times i}$ accounts for stochastic diffusion.

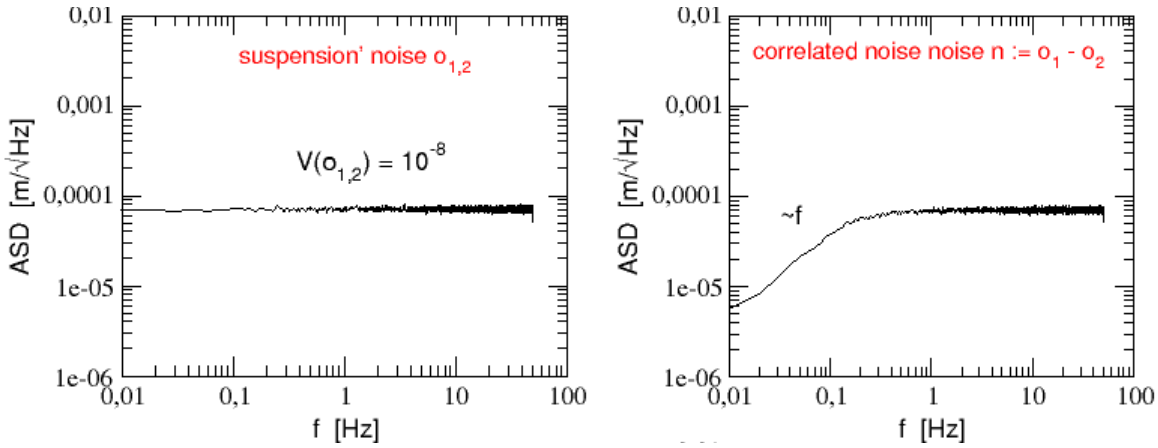

Fig. 6.2 Amplitude spectral densities (ASD) of noises' signals of displacements. Left: the ASD of the positions o_1 and o_2 of the suspensions with respect to the laboratory reference frame which are assumed to be white noises with unitary variance ($q = 1$). Right: the ASD of the process obtained by solving the SDE (6.3), that is a colored noise used to model the difference between the positions of the suspensions of the mirrors in a laboratory reference frame, that is $o_1 - o_2$.

In all the simulations that follow it will be used a 5-th order Runge-Kutta numerical integrator with Cash–Karp coefficients (see [129]) to provide a solution of the equation (6.5) with initial condition $X_0 = 0$.

6.2.1 Filtering

For reasons that will be set out below, the measures of the distance between the mirrors will not be sufficient to obtain effective control policies. The problem of having an estimate of the dynamical state $\widehat{\mathbf{X}}_t := \mathbb{E}[\mathbf{X}_t | Z_{t'}, 0 \leqslant t' \leqslant t]$ given the observation $Z_{t'} = X_{t'} + \eta_{t'}$ up to time t is tackled using a Kalman filter (see [72] or every standard text book on time series analysis).

The discrete time Kalman filer problem is formulated in the following way. Consider a linear discrete model of an unknown plant involving the variable $\mathbf{x}$ and its measures provided by $\mathbf{z}$. Denoting by k the time advancement, the equations of the discrete model are:

$$\textit{(linear system)} \quad \mathbf{x}_{k+1} = \mathbf{a} \cdot \mathbf{x}_k + \mathbf{f}_k + \mathbf{g} \cdot \mathbf{u}_k \qquad (6.7)$$
$$\mathbf{a} \in \mathbb{R}^{i \times i},\ \mathbf{g} \in \mathbb{R}^{i \times j}$$
$$\textit{(linear observation)} \quad \mathbf{z}_k = \mathbf{c} \cdot \mathbf{x}_k + \mathbf{v}_k \qquad (6.8)$$
$$\mathbf{c} \in \mathbb{R}^{l \times i}$$

where $\mathbf{f}$ accounts for known externalities and where the noise $\mathbf{u}$ and the sensor noise $\mathbf{v}$ are assumed to be white and Gaussian, that is $\mathbf{u} \sim \mathcal{N}(0, \mathbf{q})$ and $\mathbf{v} \sim \mathcal{N}(0, \mathbf{r})$ respectively, and also mutually independent and independent from the initial condition $\mathbf{x}_0$.

The estimate $\widehat{\mathbf{x}}_{k+1|k+1} := \mathbb{E}\left[\mathbf{x}_{k+1} \,|\mathbf{z}_{k'}, 0 \leqslant k' \leqslant k+1\right]$ of the state $\mathbf{x}_{k+1}$ given the observations $\mathbf{z}_{k'}$ up to time $k+1$ is provided by the recursive estimations for the Kalman filtering which, at stage $k+1$, reads as follows:

Prediction (6.9a)

$$\widehat{\mathbf{x}}_{k+1|k} = \mathbf{a}\widehat{\mathbf{x}}_{k|k} + \mathbf{f}_k$$
$$\mathbf{P}_{k+1|k} = \mathbf{a}\mathbf{P}_{k|k}\mathbf{a}^T + \mathbf{g}\mathbf{q}\mathbf{g}^T$$

Filtering (6.9b)

$$\tilde{\mathbf{y}}_{k+1} = \mathbf{z}_{k+1} - \mathbf{c}\widehat{\mathbf{x}}_{k+1|k}$$
$$\mathbf{K}_{k+1} = \mathbf{P}_{k+1|k}\mathbf{c}^T\left[\mathbf{c}\mathbf{P}_{k+1|k}\mathbf{c}^T + \mathbf{r}\right]^{-1}$$
$$\widehat{\mathbf{x}}_{k+1|k+1} = \widehat{\mathbf{x}}_{k+1|k} + \mathbf{K}_{k+1}\tilde{\mathbf{y}}_{k+1}$$
$$\mathbf{P}_{k+1|k+1} = \mathbf{P}_{k+1|k} - \mathbf{K}_{k+1}\mathbf{c}\mathbf{P}_{k+1|k}$$

The prediction and filtering updates propagate the initial conditions $\widehat{\mathbf{x}}_{0|0}$ and $\mathbf{P}_{0|0} = \mathbb{E}[(\mathbf{x}_0 - \widehat{\mathbf{x}}_0)^T(\mathbf{x}_0 - \widehat{\mathbf{x}}_0)]$ which are included in the model of the plant providing the expected initial distribution of state of the system. In particular the matrix $\mathbf{P}_k \in \mathbb{R}^{i\times i}$ is the covariance matrix of the innovation process, $\mathbf{P}_k = \mathbb{E}[(\mathbf{x}_k - \widehat{\mathbf{x}}_k)^T(\mathbf{x}_k - \widehat{\mathbf{x}}_k)]$. The Kalman filter is a recursive estimator meaning by this that only the estimated state from the previous time step and the current measurement are needed to compute the estimate for the current state. So the Kalman filter signal is a Markov process.

It is proved that, with the previous assumptions on noises and the linearity of the system, the Kalman filter is the optimal estimator minimizing a quadratic error function. It is straightforward that if the model of the plant does not match exactly the real unknown plant (noises' and initial innovation process' covariances included) the Kalman filtering is not optimal anymore (but, however, it is still the best linear estimator, see [50]). In particular, it is worth noting that when the Kalman filter works optimally, the innovation process $\tilde{\mathbf{y}}_{k+1} = \mathbf{z}_{k+1}\mathbf{c}\widehat{\mathbf{x}}_{k+1|k}$, given by the difference between the predicted state at step $k+1$ and the measured state at the same step, carries no systematic errors and it must be a white noise. The whiteness property of the innovation process is a measure of the filter's performance.

In agreement with what was stated in the previous Section (6.2) the two pendulums system can be described by:

$$\textit{plant's model (linear system):}\quad \dot{\mathbf{X}}_t = \mathbf{A}\mathbf{X}_t + \mathbf{f}_t + \mathbf{G}\boldsymbol{\xi}_t \qquad (6.10)$$
$$\mathbf{A} \in \mathbb{R}^{i\times i},\ \mathbf{G} \in \mathbb{R}^{i\times j}$$
$$\textit{measures:}\quad \mathbf{Z}_t = \mathbf{C}\mathbf{X}_t + \boldsymbol{\eta}_t \qquad (6.11)$$
$$\mathbf{C} \in \mathbb{R}^{l\times i}$$

where $\mathbf{f}$ accounts for external, and known, feedback forces. In particular it is a linear system where the noises ξ and η are assumed to be white, Gaussian and mutually independent, and it is that

$$\mathbb{E}\left[\begin{pmatrix}\boldsymbol{\xi}\\ \boldsymbol{\eta}\end{pmatrix}(\boldsymbol{\xi},\boldsymbol{\eta})\right] = \begin{pmatrix}\mathbf{P}_{\boldsymbol{\xi}} & 0\\ 0 & \mathbf{P}_{\boldsymbol{\eta}}\end{pmatrix}$$

The first order discretization of the equations (6.10) and (6.11) leads to the discrete time equations (6.7) and () with the following correspondences:

$$\mathbf{a} \leftrightarrow \mathbb{I} + \mathbf{A}dt\ ,\quad \mathbf{q} \leftrightarrow dt\mathbf{P}_{\boldsymbol{\xi}}\ ,\quad \mathbf{r} \leftrightarrow \mathbf{P}_{\boldsymbol{\eta}}/dt\ ,\quad \mathbf{c} \leftrightarrow \mathbf{C}\ ,\quad \mathbf{g} \leftrightarrow \mathbf{G} \qquad (6.12)$$

For the sake of completeness it is noted that the covariance matrices $\mathbf{P}_{\boldsymbol{\xi}} \in \mathbb{R}^{j\times j}$ and $\mathbf{P}_{\boldsymbol{\eta}} \in \mathbb{R}^{l\times l}$ have only one element each different from zero which coincides with the variance of the process ξ and η.

In figure 6.3 the comparisons between the time series of the position and the velocity, from solving (6.5) with a high order numerical integrator, with their estimations provided by the application of the Kalman filtering, are shown.

When the discretization time dt is too large, the first order discretization of the equations (6.5) is no longer a good approximation of these and the Kalman filer will be based on a wrong plant model. In figure 6.4 the power spectral densities (PSD) of the innovation processes of Kalman filtering applied to equation (6.5) for different discretization times and the same parameters chosen in the simulation in figure 6.3 are plotted. The qualitative non whiteness of the innovation press reveald that the Kalman filter does not works optimally.

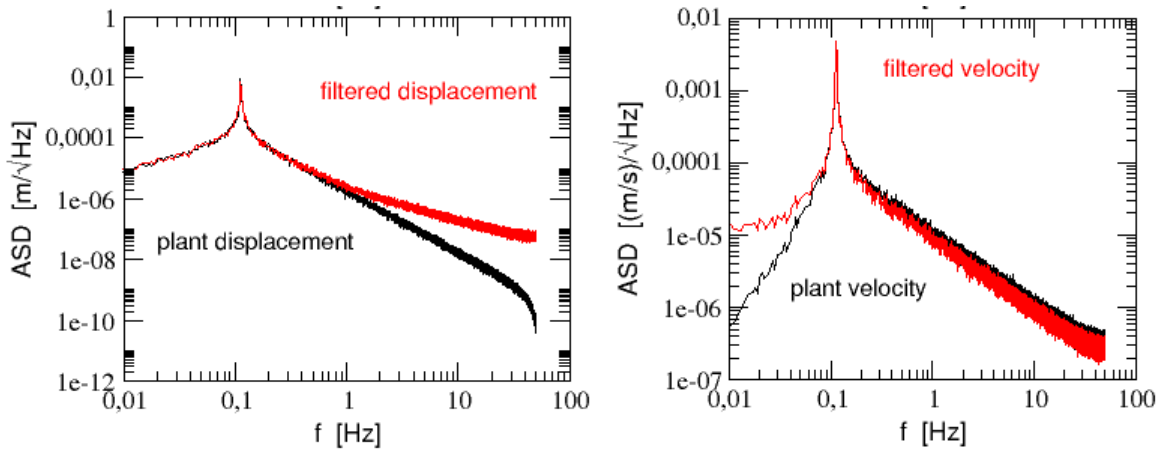

Fig. 6.3 Application of Kalman filtering to equation (6.5) with frequency $\omega = \sqrt{0.5}Hz$, air friction $\nu = 0.005Hz$, seismic noise variance $\sigma_\xi = 10^{-4}$, sensor noise variance $\sigma_\eta = 10^{-5}$, discretization time $dt = 10^{-2}s$. Left: comparison between the ASDs of the position $X_t - X_0$ (black) and of its estimate $\widehat{X}_t - X_0$ (red). Right: comparison between the ASDs of the velocity $\dot{X}_t$ (black) and of its estimate $\widehat{\dot{X}}_t$ (red).

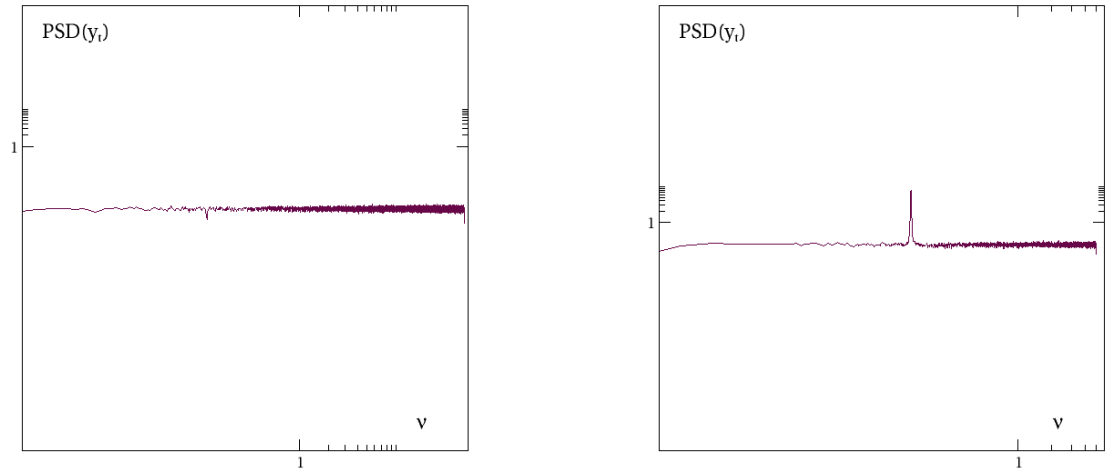

(a) PSD($\tilde{y}_k$) for $dt = 0.01s$

(b) PSD($\tilde{\mathbf{y}}_k$) for $dt = 0.1s$.

Fig. 6.4 A qualitative evaluation of the PSD of the innovation process $\tilde{y}_k$, expressed in $[m^2/Hz]$, using the discrete Kalman Filter (6.9) applied to (6.5), shows the higher performances of the filter with lower discretization time: $dt = 0.01s$ (left) and $dt = 0.1s$ (right). All the parameters are the same as in figure 6.3.

6.3 Application to the two-pendulum system

In many situations that involve the dynamical system control, optimal control design of classical linear feedbacks may be invalidated or weakened since the available model of the plant is wrong. Another disadvantage of linear controllers may arises because of their unboundedness. Indeed feedback actuators are real physical devices and give a linear response with good approximation only in a limited working region and unsuspected nonlinearities may arise depending on whether the plant's dynamical state goes outside this region.

We study how traditional control techniques can be assisted by reinforcement learning based nonlinear adaptive controller, which is the *RL Agent*, to be applied to the two-pendulum system governed by the equation of motion (6.5) where the control task is to keep the relative position fixed between the pendulums as if there were no seismic noise, that is when the reference signal to the plant is provided by the fixed distance given by $X_0 = 0$.

It is worth noting that the *RL Agent* learns a control policy if all the information about the causes that induce transitions among plant's dynamical states are available to it. So since the plant evolves in part due to its initial conditions and in part due to external feedback forces, then the *RL Agent* has to know, at each time step, the information about the dynamical state of the plant together with the other feedback forces acting on it, its own included. However, the noisy measure Z_t of the relative position X_t between the mirrors is, by itself, is not sufficient to determine the subsequent position X_{t+dt} since, at time t, the system is also characterized by a certain velocity $\dot{X}_t$. For this reason it is needed an estimate $\widehat{\mathbf{X}}_t$ of the full dynamic variable $\mathbf{X}_t$ of the system. The same estimates $\widehat{\mathbf{X}}_t$ are also necessary to realize any other classical controllers. Such estimates are provided by Kalman filtering (see Section 6.2.1).

The equation of motion (6.6) with feedbacks can be written as:

$$\dot{\mathbf{X}}_t = \mathbf{A} \cdot \mathbf{X}_t + \mathbf{f}_t(\widehat{\mathbf{X}}_t) + \boldsymbol{\pi}(\widehat{\mathbf{X}}_t, \mathbf{f}_t) + \mathbf{G} \cdot \boldsymbol{\xi}_t \tag{6.13}$$

where $\mathbf{f}_t$ accounts for classical linear feedback control forces and where the term $\pi(\widehat{\mathbf{X}}_t, \mathbf{f}_t)$ accounts for the feedback provided by the *RL Agent* which will be computed based on the estimation $\widehat{\mathbf{X}}_t$ and the feedback $\mathbf{f}_t$.

In what follows the vector $\mathbf{f}_t$ is assumed to be a force of which the sole non-zero component is obtained from a Partial-Integral-Differential (PID) controller given by:

$$f_t = -K_i \int_{-\infty}^{t} \widehat{X}_s ds - K_p \widehat{X}_t - K_d \widehat{\dot{X}}_t \tag{6.14}$$

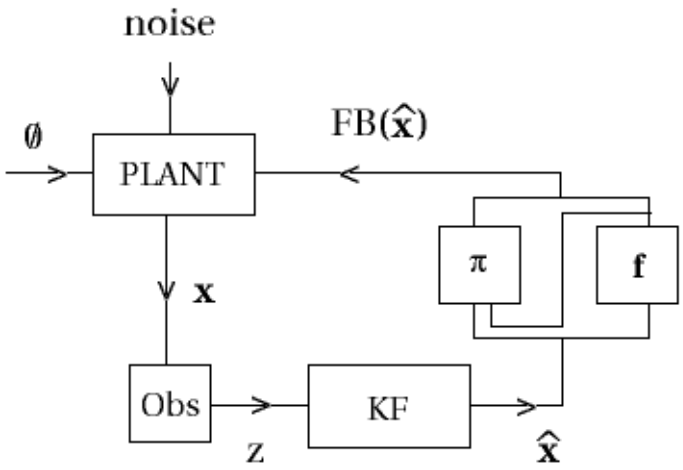

Fig. 6.5 Scheme of the plant. The "plant" box returns as output the dynamical state $\mathbf{X}$ of the plant; the "obs" box gives measures of $\mathbf{X}$; the "KF" box is Kalman filter which gives the estimates $\widehat{\mathbf{X}}$ of $\mathbf{X}$ based on measures Z; the "$\mathbf{f}$" box gives a linear feedback force $\mathbf{f}$ according to (6.14); the "π" box is the *RL Agent* which chooses the additional feedback force based on estimates $\widehat{\mathbf{X}}$ and the feedback $\mathbf{f}$. The plant is to be controlled towards the rest configuration, that is the null reference signal $X_0 = 0$.

where K_i, K_p and K_d are parameters.

A scheme of the plant is sketched in figure 6.5: the measures Z of the dynamical state $\mathbf{X}$ are filtered to obtain the estimate $\widehat{\mathbf{X}}$. Both the control policies of the *RL Agent* and the linear controller use the estimate $\widehat{\mathbf{X}}$ to control the plant towards the null reference signal.

6.3.1 How the *RL Agent* works

To grasp how artificial intelligence can be used to control an unknown dynamical system, a brief overview of reinforcement learning topic is presented in what follows. For a more comprehensive treatment of reinforcement learning concepts and applications see, for example, the classic text by R.S. Sutton and A.G. Barto, [112].

Reinforcement learning is based on the idea that learning can be realized through interaction with the environment, that is a source of experience from which a wealth of information about causes and effects that actions on it will produce is obtained.

Basically, to each state of the environment a reward is corresponded to the *RL Agent*. The reward can be thought as an environmental circumstance and it is used by the *RL Agent* to built its preferences on environmental states: a state will be preferred

instead of another one if the expected sum of future discounted rewards achievable from it is higher. On the basis of such preferences the *RL Agent* will be able to realize a goal-directed behavior.

The agent's goal is to maximize the total amount of reward it will receive over the long run: the sum of discounted rewards achievable from time t onward is given by

$$R_t = r_{t+1} + \gamma r_{t+2} + \gamma^2 r_{t+3} + ... = \sum_{k=0}^{\infty} \gamma^k r_{k+t+1} \tag{6.15}$$

where the discount rate γ is such that $0 \leqslant \gamma \leqslant 1$. The parameter γ tunes how far in time action effects are taken into account: if $\gamma = 0$, the agent is "myopic" in being concerned only with maximizing immediate rewards: its objective in this case is to learn how to choose an action A so as to maximize only r_{t+1}. But in general, acting to maximize immediate reward can reduce access to future rewards so that the return may actually be reduced. As γ approaches 1 the agent becomes more farsighted and looking forward at future rewards.

Let $\mathcal{S}$ be the set of all possible states of environment in which the *RL Agent* acts and let $\mathcal{A}$ be the set of all possible actions the *RL Agent* can execute on it. Therefore, given the agent's policy π defined as the probability to choose an action A in state S, that is $\pi(S, A) := \mathbb{P}\{A_t = A | S_t = S\}$, the *RL Agent* assigns a value to the state-action pairs $(S, A) \in \mathcal{S} \times \mathcal{A}$ that accounts for the amount of expected future rewards achievable in the future, that is along the trajectory of the environment that starts from there and which is driven according to π thereafter:

$$\begin{aligned} Q_\pi(S, A) &= \mathbb{E}_\pi[R_t | S_t = S, A_t = A] \\ &= \mathbb{E}_\pi \left[\sum_{k=0}^{\infty} \gamma^k r_{k+t+1} \, | S_t = S, A_t = A \right] \end{aligned} \tag{6.16}$$

The function $Q_\pi : \mathcal{S} \times \mathcal{A} \to \mathbb{R}$ is exactly the *state-action value function*, the Q-function in the following.

The most widely used method to obtain the Q-function if the policy π is provided is the so called *temporal difference* (TD) recurrence, named TD SARSA, which reads as follow:

$$Q_{k+1}(s_t, a_t) \leftarrow Q_k(s_t, a_t) + \alpha[r_{t+1} + \gamma Q_k(s_{t+1}, a_{t+1}) - Q_k(s_t, a_t)] \tag{6.17}$$

TD methods (6.17) evaluate the Q_π-function on the basis of the acquired experience providing at each time step both the estimation of the expected value (6.16), by

means of $r_{t+1} + \gamma Q_k(s_{t+1}, a_{t+1})$, and the estimation of the true value $Q_\pi(s_t, a_t)$, by means of $Q_k(s_t, a_t)$. In other words the recurrence (6.17) adjusts the current value $Q_k(s_t, a_t)$ according to the TD error, defined by $\delta_t = r_{t+1} + \gamma Q_k(s_{t+1}, a_{t+1}) - Q_k(s_t, a_t)$, indicating that the estimate $Q_k(s_t, a_t)$ should be more like $r_{t+1} + \gamma Q_k(s_{t+1}, a_{t+1})$. By these features, TD methods result appropriate to be implemented on-line and in unknown environments, exactly because at each time step better estimates of expected returns rather than the available current ones are provided.

However, when the environment is unknown and no experience about it is owned, the *RL Agent* does not know which rewards can be achieved from a state or, equivalently, which effect its actions will produce on the environment: it must discover it *exploring* the environment through random actions. As the exploration activity proceeds, more and more knowledge about the environment is acquired and this experience is used to map states to actions in order to maximize the expected rewards it will receive. In fact a single action may determine not only the immediate reward but also the next and, through that, all subsequent rewards. As such learning process goes on the *RL Agent* increases the *exploitation* of the acquired knowledge executing actions that are expected to bring the system towards its goal.

This is realized along the on-line implementation of the TD recurrence scheme (6.17), by balancing the exploration and the exploitation activities to assure that as much state-action pairs as possible are visited avoiding to neglect every relevant information about the environment. For a given policy π there is, at least, one action in every state supposed to bring higher benefit (the so called *greedy action*): exploiting the current knowledge means exactly select the greedy action, while selecting one of the non-greedy actions means exploring the environment. The balancing between the exploration and exploitation activities enables the *RL Agent* to evaluate the non-greedy action's effects and it is realized embedding a stochastic component to the deterministic policy π in the following way:

$$\pi^\epsilon(s) = \begin{cases} \pi(s) & \text{with probability} \quad 1 - \epsilon \\ \text{every } A \in \mathcal{A}(s) & \text{with probability} \quad \epsilon \,/ |\mathcal{A}(s)| \end{cases} \tag{6.18}$$

The stochastic policy π^ϵ is the so called ϵ-greedy policy. Exploration, of course, will be more beneficial in unknown environment. Then the higher the knowledge, the higher the probability of exploitation rather than exploration: in the limit in which state-action pairs are visited a great number of times, the ϵ-greedy policy must converge to the deterministic policy π to make the TD methods convergent.

It is worth noting that a new policy π' can be obtained from a given Q_π-function, based on an original policy π, from selecting, in every state $s \in \mathcal{S}$, the actions which maximize the expected future rewards:

$$\pi'(S) = \arg\max_A Q_\pi(S, A) \tag{6.19}$$

The policy defined in (6.19) is the so called *greedy* policy and it can be proved, using the *policy improvement theorem* (see again [112]), that is strictly better than π meaning by this that π' is capable of driving the environment obtaining higher rewards along its future trajectory rather then with π, except when there is no further room for improvements and in this case it is said to be *optimal*,

At the light of the policy improvement theorem, the *RL Agent* can improve its policy during the implementation of the TD recurrence. Indeed the value function Q_π provides a new greedy policy π', according to the definition (6.19), which results to be as good as, or even better than, the starting policy π. Based on the new improved policy π' a new value function $Q_{\pi'}$ can be computed and, in turn, an even better greedy policy π'' can be obtained from it. As the succession of policy improvements and policy evaluations proceeds, a sequence of monotonically improving value functions and policies is obtained, unless they are already optimal. If the policy improvement and the policy iteration succession - not necessarily each is completed before the other begins - stabilizes, then both the policy and the Q-function must be optimal. It is proved that the TD algorithm (6.17) converges with probability 1 to an optimal policy and optimal Q-function if all state-action pairs are visited an infinite number of times and the stochastic ϵ-greedy policy reduces to the deterministic greedy policy in the limit. A sketch of the succession could be illustrate as follows:

$$\pi_0 \to Q_{\pi_0} \to \pi_1 \to Q_{\pi_1} \to ... \to \pi_n \to Q_n \to ... \to \pi_* \to Q_* \to ... \tag{6.20}$$

The two joint process realizes an adaptive learning process.

6.3.2 A preliminary control task

A first example was developed as a first application of the reinforcement learning concepts. In particular, it is considered the control task in which an ideal point has to be driven towards a target in a 2D discrete space in which barriers, or walls, that limit the movements, are present. This space is divided in a grid of 10×10 dimensions and in each state, having coordinates $\mathbf{X} = (i, j)$, 4 actions are available:

$\mathcal{A} = (\text{left}, \text{right}, \text{up}, \text{down})$. The target is located in $\mathbf{X}_0 = (i_0, j_0)$ and it is represented in the left figure 6.7 by a red dot where, also, the straight black lines stand for the walls. The *RL Agent* receives the reward value $+1$ corresponding to the transition towards the slot containing the red dot from the adjacent slots. This happens when the action "left" in the slot $(i_0 + 1, j_0)$ or the action "down" in the slot $(i_0, j_0 + 1)$ are selected. The *RL Agent* receives a punishment of value -1 if it prescribes movements that would be possible only if walls are absent. The Q-function is stacked in a 3D array of $10 \times 10 \times 4$ dimensions and provide the ϵ-greedy policy, from the definition (6.19), whose deterministic part is given by

$$A(\mathbf{X}) = \arg\max_{A'} Q(\mathbf{X}, A') \tag{6.21}$$

while the stochastic part is provided by a fixed probability ϵ of exploration. The Q-function results from a learning process in which temporal difference errors are used to update the values of every state-action pairs $(\mathbf{X}, A)$. Such procedure is computationally feasible because of the limited number of possible state-action pairs, that are $10 \cdot 10 \cdot 4 = 400$. So the TD recurrence

$$Q'(\mathbf{X}_t, A_t) = Q'(\mathbf{X}_t, A_t) + \alpha \left(r_{t+1} + \gamma Q(\mathbf{X}_{t+1}, A_{t+1}) - Q(\mathbf{X}_t, A_t) \right) \tag{6.22}$$

can be implemented at the end of each episode, that is once the target is reached starting from a random initial condition. Of course the next update of Q will be performed at the end of the subsequent episode which takes place with new initial conditions. The number of steps to the target decreases in few episodes and it is lower for decreasing values of the fixed exploration probability, as showed in the figure 6.6.

In figure 6.7 on the right the Q-function is represented once the learning process has been completed. The colors distinguish among the maximum values $\max_A Q(\mathbf{X}, A)$ of the Q-function in each state $\mathbf{X}$ over the actions and the arrows indicate the deterministic greedy actions induced by the Q-function itself.

6.3.3 *RL Agent* design

In the application of reinforcement learning to the two-pendulum system, the ϵ-greedy action of the *RL Agent* enters in the equation of motion (6.13) by the term $\pi(\widehat{\mathbf{X}}, f)$. Indeed, considering that the transition probabilities between two dynamical states of the plant are determined by the feedback actions $A \in \mathcal{A}$ of the *RL Agent*, by the

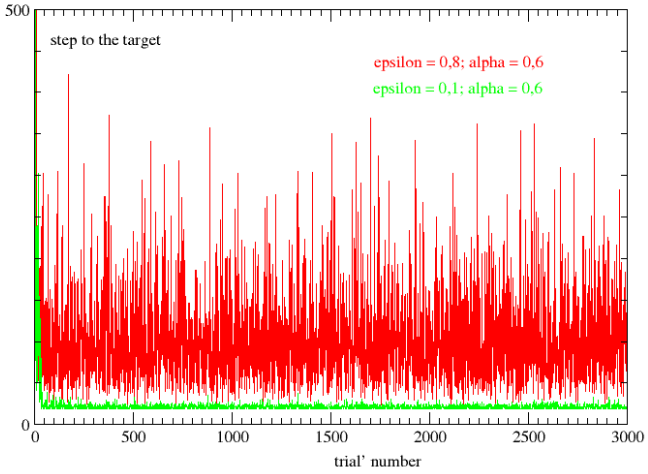

Fig. 6.6 The number of steps to reach the target at different probabilities of exploration: $\epsilon = 0.8$ (red) and $\epsilon = 0.1$ (green) for the speed of adjustment $\alpha = 0.6$.

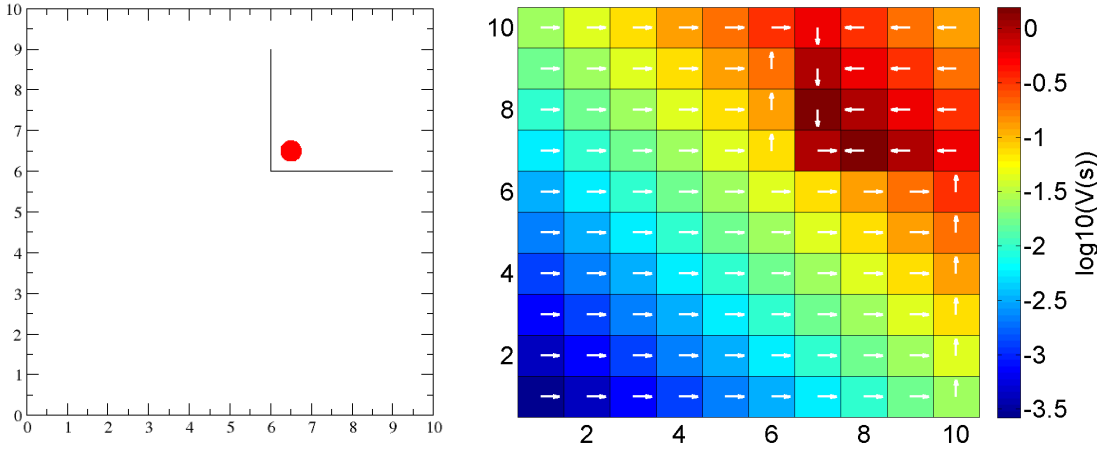

Fig. 6.7 Left: the space with walls and the target (red dot). Right: the maximum values of Q-function, the arrows shows the deterministic greedy policy provided by Q.

external feedback forces f_t and, of course, by the states $\widehat{\mathbf{X}}_t$, and then the Q-function of the *RL Agent* will be a function of the type $Q = Q(\widehat{\mathbf{X}}, f, A)$.

However, simulations show that it is more convenient to obtain an evaluation from the *RL Agent* of the total feedback applied to the plant, that is the sum $\pi + f$, based on the state $\widehat{\mathbf{X}}$ rather than an evaluation of only the action π based on the state $\widehat{\mathbf{X}}$ and the feedback f. Based on this choice, the environment of the *RL Agent* will be identified by the set of estimates of the plant's dynamical states, that is $\mathcal{S} \equiv \left\{\widehat{\mathbf{X}}\right\}$, and then the Q-function will return the values of the feedback $f + A$ when the estimated

dynamical state of the plant is $\widehat{\mathbf{X}}$, that is

$$Q(\widehat{\mathbf{X}}, f, A) = Q(\widehat{\mathbf{X}}, f + A) \tag{6.23}$$

Furthermore, because of the infinite cardinality of the set $\mathcal{S}$, the Q-function have to be represented by a parametrize function approximator instead of stacking them in multidimensional arrays as in the example presented in (6.3.2). A further advantage coming from having a parametrization of the Q-function is that the values of state-action pairs are better matched with the observed returns because of the interpolating nature of the approximator. Indeed, in principle, the value of each state is determined by the discounted sum of returns achievable from it. But, since in real learning experience as well as in simulations the *RL Agent* will visit only a finite subset of possible plant's dynamical states, it could happen that the estimation of the value of a particular state results from a sampling of smaller size than that used for the estimation of the values of its adjacent states. So, because of the continuity property of the function approximator, such a raw estimate will be adjusted to better fit with the values of its neighborhood. This aspect reveals the capability of the *RL Agent*, implemented with a function approximator, of generalizing value functions also to states which haven't been previously experienced. On the other hand, however, the finiteness of parameters' number limits the complexity of the approximation determining some errors in the representation .

A typical choice to tackle reinforcement learning tasks in the case of infinite state space $\mathcal{S}$ consists of using a neural network as a parametrized function approximator (see for example [7] or [8]).

For the sake of completeness it can be recalled that a neural network consists of a sequence of layers of nodes: the input layer of n_i nodes represents the entry variables in input, the nodes of hidden layers transform the linear combinations of values of the nodes in the preceding layer through *activation functions* and, finally, an output layer returns linear combinations of the values of the nodes in the last hidden layer. In figure 6.8 a neural network with one hidden layer and a unique node as the output layer is depicted.

Following this approach, the Q-function will be the neural network output denoted by $Q_{\mathbf{w}}$ where $\mathbf{w}$ is the weights' vector. In order to approximate a target function $\mathcal{T}$, the values of which are available only at the sampling points $\{\mathbf{x}_k\}_{k=1,..,K} \in \mathcal{S} \times \mathcal{A}$, the

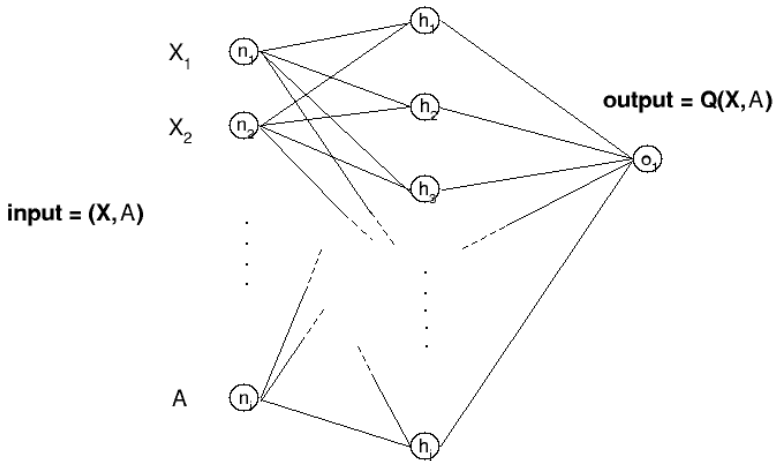

Fig. 6.8 A sketch of a one-hidden layer neural network that parametrizes a Q-function $Q(\mathbf{X}, A)$.

weights $\mathbf{w}$ are chosen to minimize an error function of the form

$$E_{\mathbf{w}} := \sum_{k=1}^{K} E(\|\mathcal{T}(\mathbf{x}_k) - Q_{\mathbf{w}}(\mathbf{x}_k)\|) \tag{6.24}$$

using a backpropagation algorithm based on a gradient descent method. The backpropagation algorithm used to adjust the initial weights $\mathbf{w}_0$ of the neural network is the *scaled conjugate gradient* descent algorithm, SCG in what follows, which is a method that provides a fasten convergence towards the minimum of the error function regarding other gradient descent methods and requires a quadratic error (further details on SCG algorithm can be found in [102]).

In order to realize an on-line learning process taking place along the plant's evolution where the Q-function is provided by a neural network, the implementation of the policy improvement scheme (6.20) realized through the TD SARSA recurrence (6.17) has to be adapted to include parameters' adjustments. More precisely, at the initial time $t_0 = 0$ the plant is unknown to the *RL Agent* and it explores the environment choosing random actions with probability $\epsilon_0 = 1$. The initial weights of the neural network are random in $[-1, 1]$ and are denoted by $\mathbf{w}_0$. Similarly the initial Q-function is denoted by $Q_{\mathbf{w}_0}$. Up to a certain time $t_1 = N_T \times dt$, where N_T is a parameter to be determined experimentally and dt is a suitable discretization time, the temporal difference errors $\delta_{\mathbf{w}_0}$, that have been obtained along the trajectory up to the time t_1, are a record of length N_T which is stored in a memory support. At time $t_1 + dt$ this record is used to

compute the quadratic error function:

$$\begin{aligned} E_{\mathbf{w}_0} &= \sum_{t=0}^{N_T} \|\delta_{\mathbf{w}_0}(t)\|^2 \\ &= \sum_{t=0}^{N_T} \|r_{t+dt} + \gamma Q_{\mathbf{w}_0}(t+dt) - Q_{\mathbf{w}_0}(t)\|^2 \end{aligned} \tag{6.25}$$

where r_{t+dt} is the reward at time $t+dt$ and with the notation $Q_{\mathbf{w}_0}(t)$ the value of the state-action pair along the plant trajectory at time t is meant:

$$Q_{\mathbf{w}_0}(t) := Q_{\mathbf{w}_0}(\widehat{\mathbf{X}}_t, f_t + A_t) \tag{6.26}$$

From minimizing (6.25) through the SCG algorithm a new weights' vector $\mathbf{w}_1$ is obtained and therefore also a new Q-function, namely $Q_{\mathbf{w}_1}$. It is worth noting that, from the starting vector $\mathbf{w}_0$, more intermediate adjustments of the weights through the SCG algorithm are needed to end up with the final vector $\mathbf{w}_1$ in order to get as close as possible to the minimum, or a local minimum, of the error function. Such number of iterations of the SCG algorithm at the first stage of the learning process is denoted by $N_{scg}(1) = N_{scg}^{\text{MAX}}$. After time t_1, the exploration probability is decreased to ϵ_1 and a new record of temporal difference errors is stored replacing the previous one. At time $t_2 = t_1 + N_T \times dt$, a number $N_{scg}(2)$ of SGC iterations are performed to get the new weights $\mathbf{w}_2$ and than the new Q-function $Q_{\mathbf{w}_2}$. At the k-th stage of the on-line learning process the greedy policy π_k provided by the current value function $Q_{\mathbf{w}_k}$ is expected to drive the plant towards a goal-directed behavior better than the starting policy π_0 provided by $Q_{\mathbf{w}_0}$. The weights' vector $\mathbf{w}_k$ is updated by iterating $N_{scg}(k+1)$ times the SGC algorithm to reduce the error $E_{\mathbf{w}_k}$

$$E_{\mathbf{w}_k} = \sum_{t=t_k}^{t_k+N_T} \|r_{t+1} + \gamma Q_{\mathbf{w}_k}(t+1) - Q_{\mathbf{w}_k}(t)\|^2 \tag{6.27}$$

As the learning proceeds the exploration probability ϵ_k can be decreased in favor of the exploitation probability given by $1 - \epsilon_k$. The exploration probability will be updated, at each stage k, according to the following recurrences:

$$\epsilon_{k+1} = \epsilon_k \epsilon_0^{1/N} + \epsilon_0 \frac{1 - \epsilon_0^{1/N}}{1 + \epsilon_0} \longrightarrow \frac{\epsilon_0}{1 + \epsilon_0} \text{ as } k \to \infty \tag{6.28}$$

where the parameter $N = N_T \times N_K$ depends on the length N_T of the stretch of the trajectory while the other parameter N_K, which has to be determined experimentally,

gives an order of magnitude of how many weights' adjustments are needed to complete most of the learning process. Furthermore, the number $N_{scg}(k)$ of SCG iterations are decreased form the initial value $N_{scg}(0) = N_{scg}^{\text{MAX}}$ downwards to a minimum positive value $N_{scg}^{\min}$ becoming less necessary as $Q_{\mathbf{w}_k}$ becomes more self-consistent and the error function becomes flatter near to zero. In the application it is $N_{scg}(k) = \max\left\{N_{scg}^{\min}, \epsilon_k \times N_{scg}^{\text{MAX}}\right\}$. It is now observed that, according to the recurrence (6.28), a residual exploration activity is maintained even for a high state of progress of the learning, since $\epsilon_k > 0$ for any k. This will be helpful in the case the plant is supposed to vary slowly in time: a residual stochastic component of the greedy policy and the strict positivity of the minimum number of SCG iterations, $N_{scg}(\infty) := N_{scg}^{\min}$, ensure that the learning process never ends.

6.4 Numerical simulations

A one-hidden layer neural network-like function approximator will be used to give an approximation of the Q-function of the *RL Agent*, whose output can be generically expressed as

$$Q_{\mathbf{w}}(\mathbf{x}) = \sum_{j=1}^{n_h} h\left(\sum_{i=1}^{n_i} x_i V_{ij}\right) W_j \tag{6.29}$$

where, again, to simplify the notation the state-action vector is denoted by $\mathbf{x}$, that is $\mathbf{x} =\in \mathcal{S} \times \mathcal{A}$, and x_i is its i-th component. $\mathbf{V}$ and $\mathbf{W}$ are the matrices of weights with dimensions respectively given by $n_i \times n_h$ and $n_h \times 1$ where n_i is the number of the entries in input to the neural network and n_h is the number of nodes in its unique hidden layer. The function $h(\cdot) : \mathbb{R} \to \mathbb{R}$ is the activation function. Finally, the vector $\mathbf{w} = \{\mathbf{V}, \mathbf{W}\}$ combines the matrices $\mathbf{V}$ and $\mathbf{W}$ in a unique element and it is introduced to simplify the notation.

The choice of a one-hidden layer neural network is due to the fact that backpropagation algorithms, that are gradient descent methods, may become unstable when more than one hidden layer is present, while the number of hidden nodes are chosen with regard to the desired performance of the *RL Agent* control. The activation function will be given by nonlinear functions as the target Q-function is.

Moreover, backpropagation consists in gradient descent methods and requires the computation of the derivatives of activation functions. Then the SGC algorithm will adjust the weights' vector taking steps size proportional to that derivative and, if the derivative gets huge, the gradient descent results unstable and it will shoot the point vector $\mathbf{w}$ far away from a close local minimum of the error function. To avoid this

scenario, an activation function, having well-behaved derivatives, has to be chosen. Common examples are the hyperbolic tangent or the sigmoid given respectively by:

$$\tanh(x) := \frac{e^x - e^{-x}}{e^x + e^{-x}} \quad , \qquad \sigma(x) := \frac{1}{1 + e^{-x}}$$

In particular the hidden nodes of the neural network used in the present application will be characterized by hyperbolic tangent as activation functions (see figure 6.9).

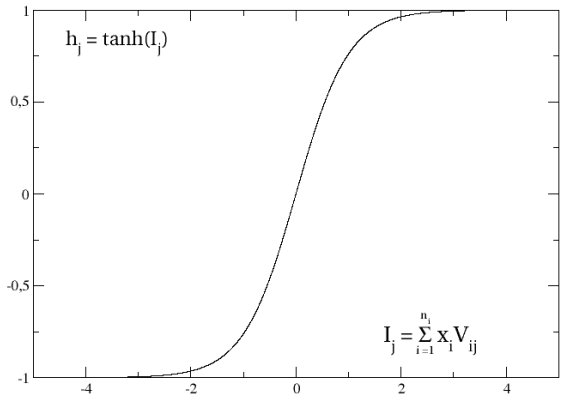

Fig. 6.9 Hyperbolic tangent activation function.

The reinforcement learning controller will be based on a scalar and deterministic reinforcement signal. This reinforcement induces preferences on the state-action pairs which are propagated backwards from the goal to peripheral states during the on-line learning process by means of value functions. In particular the reinforcement signal had to assign to the *RL Agent* higher rewards as closer the plant's dynamical state is to the reference signal. In the present application, as sketched in figure 6.5, the reference signal is zero and this suggests that a suitable reward function has to favor the convergence of the plant towards the rest configuration as if there was no noise or feedback and it will be shaped likewise the ones in figure (6.10). The reward function will contribute to the behaviors reinforcement learning controller, but there is no methodology to choose it, assuring established performances and stability properties (see again [112]). It has to be chosen regarding the effectiveness of the controller when applied. Simulations shows that the reward signal that had determined the best performances in control of the two-pendulum system is the one given in figure 6.10c whose expression is

$$r(\mathbf{X}) = 1.8 \times (e^{-|X|} + 0.3)e^{-|X+\dot{X}/0.7|} \tag{6.30}$$

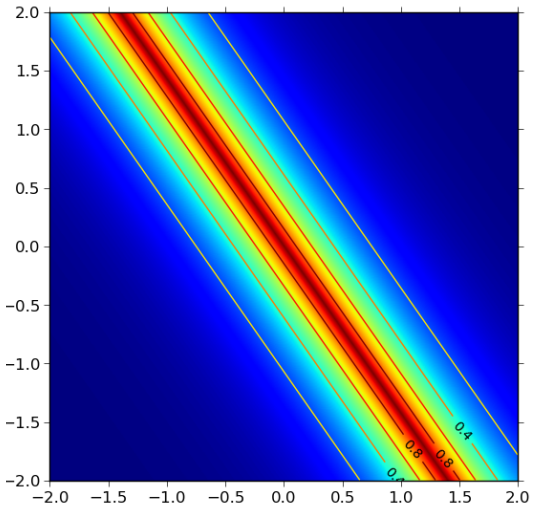

(a) The reward which has the maximum value along the line $\dot{X} = -X/\theta$ and decreases exponentially from that line. Its expression is $\theta = 0.7$ and given by $r(\mathbf{X}) = e^{-|X+\dot{X}/0.7|}$.

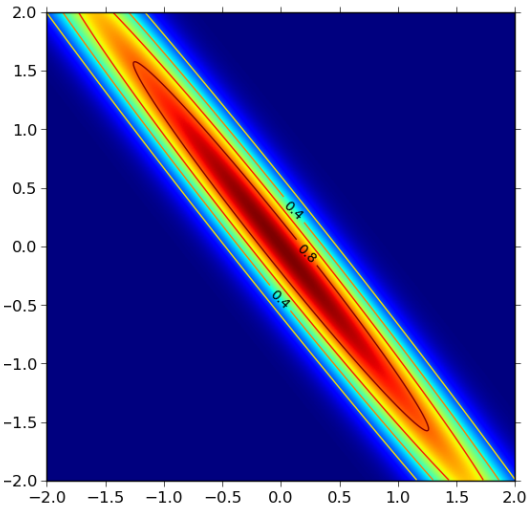

(b) A bivariate Gaussian with center in the origin.

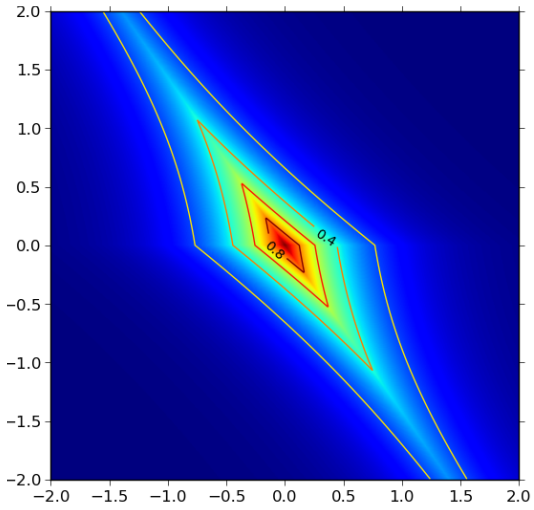

(c) A reward given by $r(\mathbf{X}) = 1.8 \times (e^{-|X|} + 0.3)e^{-|X+\dot{X}/0.7|}$

Fig. 6.10 Possible reward functions in $\mathbb{R}^2$.

Another important aspect to be taken into account is that, despite it is not theoretically needed, in practice the neural network inputs need to be standardized to avoid the saturation of activation functions near their limit values (-1 and 1 in the case of tanh). Indeed if inputs are far from the interval $[-1, 1]$ the tanh activation function will take only values 1 or -1 and does not distinguish among different inputs. Indeed each element $\mathbf{x}$ of the state-action space $\mathcal{S} \times \mathcal{A}$ in input to the neural network at

the $k+1$-th stage of the learning process, let it be denoted as $\mathbf{x}(k+1)$, is standardized according to the following formula:

$$x_i(k+1) \to x_i'(k+1) = \frac{x_i - \mu_{x_i}(k)}{\sigma_{x_i}(k)} \sim [-1, 1] \tag{6.31}$$

where $x_i = x_i(k+1)$ is i-th component of $\mathbf{x}$ and $\mu_{x_i}(k)$ and $\sigma_{x_i}(k)$ are respectively its average value and its standard deviation at the k-th stage of the learning process computed over N_T points along the plant's evolution. In this way the values $\sum_i x_i V_{ik}$ in input to the hidden nodes are roughly within the range of the activation function working region.

It is worth noting that the standardization is adapted to the variance of the inputs along the learning to improve the performance of the *RL Agent* controller. In figure 6.11 a simulations is presented to stress the importance of the varying standardization: it is evident that the performance with the varying standardization, provided by the ASDs, is higher rather than the case of fixed standardization. In this particular simulation the plant is acknowledged and no Kalman filtering is needed. Further the linear PID controller is absent and only the *RL Agent* acts on the plant. The neural network is trained based on the true plant's dynamical states $\mathbf{X}_t$. On the left side of the figure the variation of the distance between the mirrors is depicted, that is $X_t - X_0$, while on the right side the ASDs of the same signal are presented once the learning process is, for the most part, accomplished over 10^6 samples each. In all cases the initial standardization is computed using the first 50000 states of the trajectory of the uncontrolled plant before the beginning of the learning process. In the upper figures the standardization varies according to (6.31) while in the lower figures the initial standardization is kept fixed. Other parameters are: $dt = 0.1s$, $N_K = 100$, $N_T = 1500$, $N_{scg}^{\max} = 120$, $N_{scg}^{\min} = 15$, $\gamma = 0.95$, $\epsilon_0 = 0.001$, $n_h = 7$, $\mathcal{A} = \{-10, -1, -0.1, -0.01, -0.001, -0.0001, 0, 0.0001, 0.001, 0.01, 0.1, 1, 10\}\, m/s^2$, the reward is given by $r(\widehat{\mathbf{X}}) = e^{-|\widehat{X}+\widehat{\dot{X}}/0.7|}$ (figure 6.10a), the frequency of the pendulums is $\omega = 0.5$, the air friction is $\nu = 0.005Hz$. The white and Gaussian noise ξ_t is characterized by a unitary variance, that is ($\mathbb{E}(\xi) = 0$ and $\mathbb{V}(\xi) = 1$).

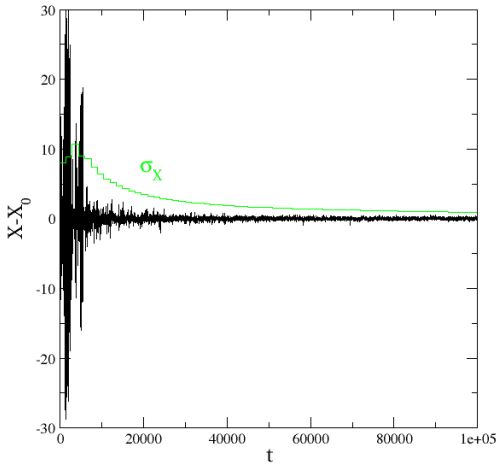

(a) The standardization variance σ_x varies at each stage of the learning process according to (6.31) and it is depicted by the green line.

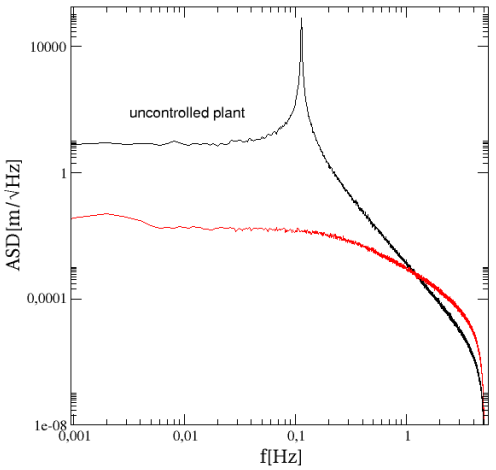

(b) The ASD of the time series of $X_t - X_0$ once the learning process is, for the most part, accomplished (red) compared to the ASD of $X_t - X_0$ relative to the uncontrolled plant (black).

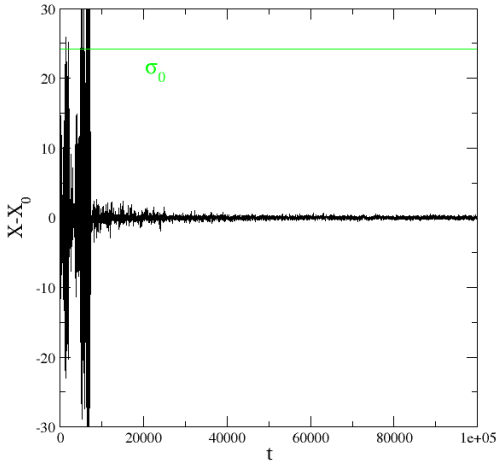

(c) The standardization variance σ_0 is fixed and it is depicted by the green line.

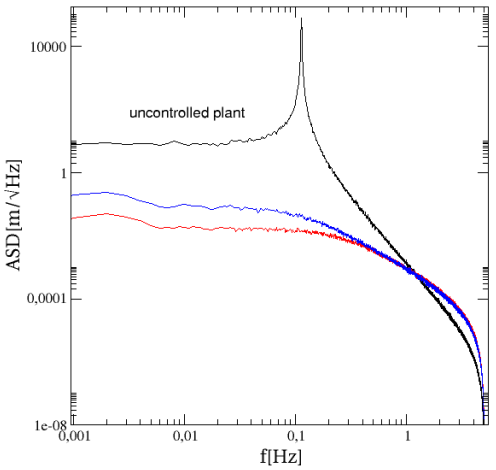

(d) Comparison among the ASDs of the uncontrolled plant (black), of the controlled plant with fixed standardization (blue) and of the controlled plant with varying standardization (red).

Fig. 6.11 Simulations to stress the importance of the varying standardization

However, in order to reproduce a more real control problem, the PID linear controller and the Kalman filter are introduced as a control device. The physical system is governed by the equation of motion (6.13). The parameters of the pendulums are as follows:

$$\begin{aligned} \text{frequency: } & \omega = \sqrt{0.5} Hz \\ \text{air friction: } & \nu = 0.005 Hz \\ \text{seismic noise variance: } & \sigma_\xi = 10^{-4} \\ \text{sensor noise variance: } & \sigma_\eta = 10^{-5} \end{aligned}$$

The parameters that regulate the learning process are as follows:

$$\begin{aligned} \text{learning step length: } & N_T = 1500 \\ \text{- } & N_K = 70 \\ \text{discount factor: } & \gamma = 0.95 \\ \text{max. SCG iterations: } & N_{scg}^{\text{MAX}} = 150 \\ \text{min. SCG iterations: } & N_{scg}^{\text{min}} = 15 \\ \text{hidden neurons nr.: } & n_h = 13 \\ \text{final exploration prob.: } & \epsilon_0 = 0.001 \\ \text{time step : } & dt = 10^{-2} s \end{aligned}$$

The scheme of the plant is represented by the scheme (6.5) where the feedback architecture is recalled in figure 6.12.

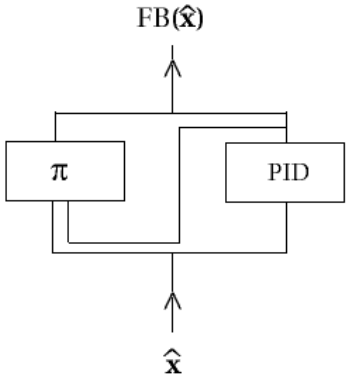

Fig. 6.12 Feedback architectures

The PID parameters, K_i, K_p and K_d, are selected to have the gain margin in the frequency range $1 \div 10\ Hz$ similarly to the case of suspended mirrors in the Virgo gravitational interferometer. In figure 6.13 the open loop transfer function is given, obtained when only the PID controller is present (black line), where the gain margin is exactly in the frequency range $1 \div 10\ Hz$.

$$K_i = 10^{-2}\ , \quad K_p = 10^{-2}\ , \quad K_d = 10^{-1} \tag{6.32}$$

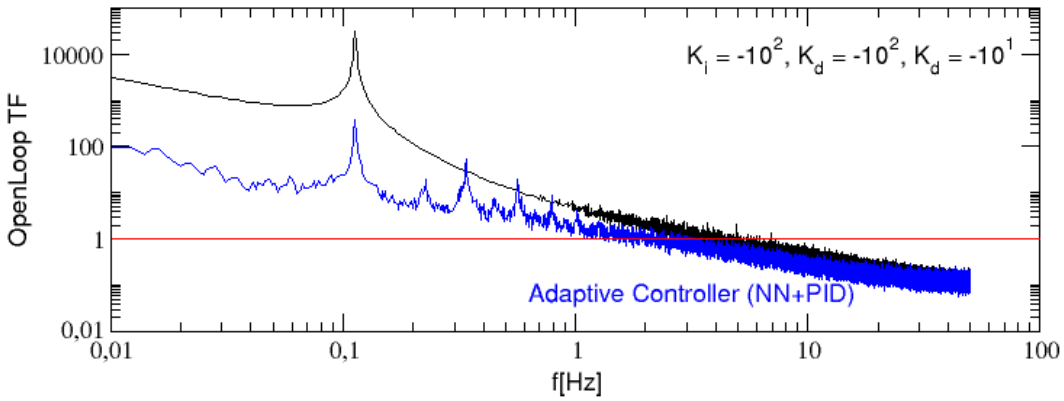

Fig. 6.13 Open loop transfer functions between the input noise and the output feedback from the PID controller (black) and the PID + *RL Agent* controller (blue).

In figure 6.14 the results of the control from the application of both the *RL Agent* and the PID controllers are presented. In the upper image the exploration probability ϵ_k profile is depicted as the learning advances, while in the lower image the variation of the distance between the mirrors can be seen, that is $X - X_0$, showing qualitatively the effectiveness of the reinforcement learning controller. The stability of the controller occurs when there is no continuous growth of noise or, equivalently, whenever the noise stays below a certain level. From a look at the time series of the relative position $X - X_0$ in the figure 6.14 below, the control can be said stable. However for a more informative analysis, stability can be checked through Bode plots (see for example [56]). In figure 6.13 the open loop transfer function of the feedback controllers of the *RL Agent* embedded with the linear PID (blue line) is given. However the bode plot has to be completed including the phase margin. However the plot is presented anyway to show that we are searching in this direction.

In figure 6.15 the mean value $\langle Q \rangle_k$ of the rewards obtained during the plant evolution at each stage k of the learning process is represented. As expected, it results a growing

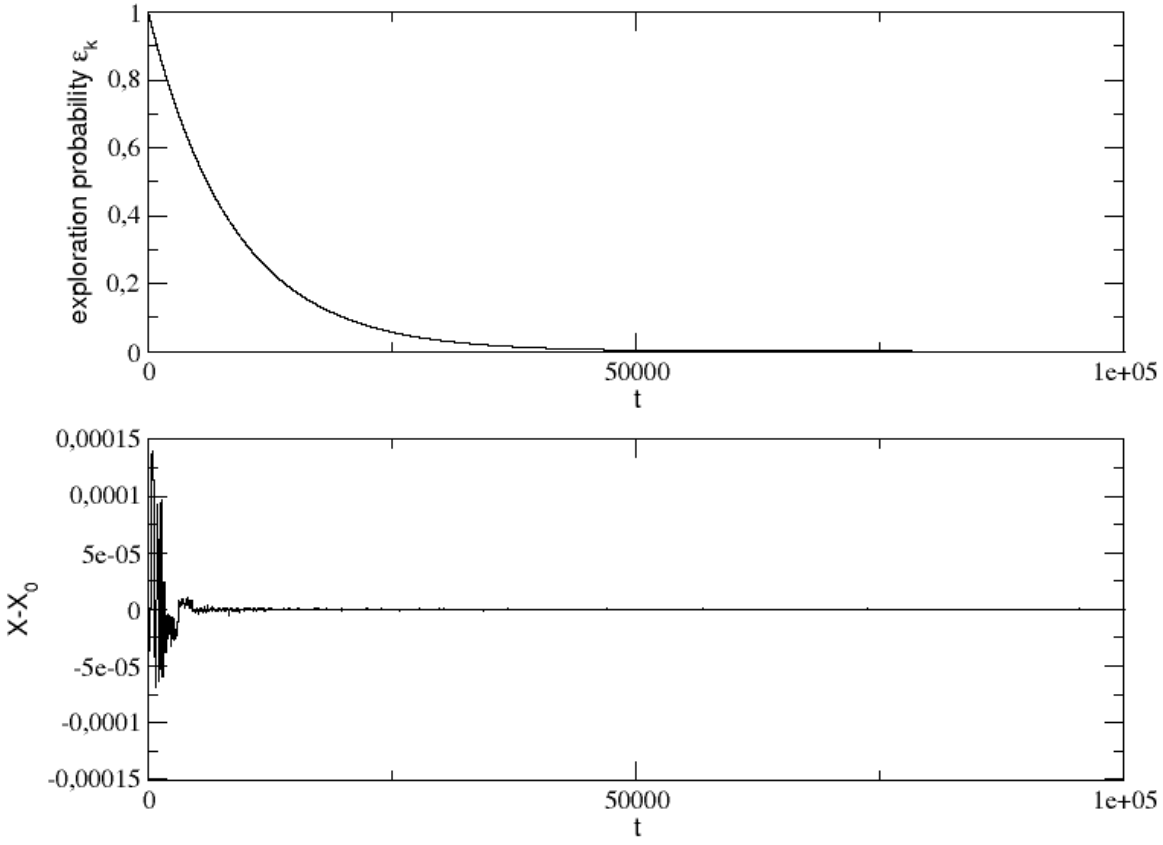

Fig. 6.14 Up: the ϵ probability profile. Down: time series of the variation of the distance between the mirrors, that it $X_t - X_0$. The plant is definite by equation of motion (6.5).

function and this reveals that the *RL Agent* learns how to act on the plant with increasing effectiveness.

In figure 6.16 the noise spectrum obtained with the *RL Agent* and the PID controller (red line) is drawn and compared to the spectrum of the uncontrolled plant (orange) in order to quantify the performance of the controller. Furthermore, also the performance of the same controller, when the Kalman filter is based on a wrong plant model, it is presented, showing that the *RL Agent* will be effective also in that case (magenta line). The other ASDs are obtained for different feedback architectures that have been tried in simulations, that is when only the PID is applied (black line) and when only the *RL Agent* is applied (blue line).

To check the behavior of the neural network, the transfer function between its output and the input velocity is computed as $T^2_{RL} := PSD(\int A(\widehat{\mathbf{X}})dt) \times PSD\left(d\widehat{X}/dt\right)^{-1}$ and showed in figure 6.17. Indeed the use of nonlinear activation functions tanh, which

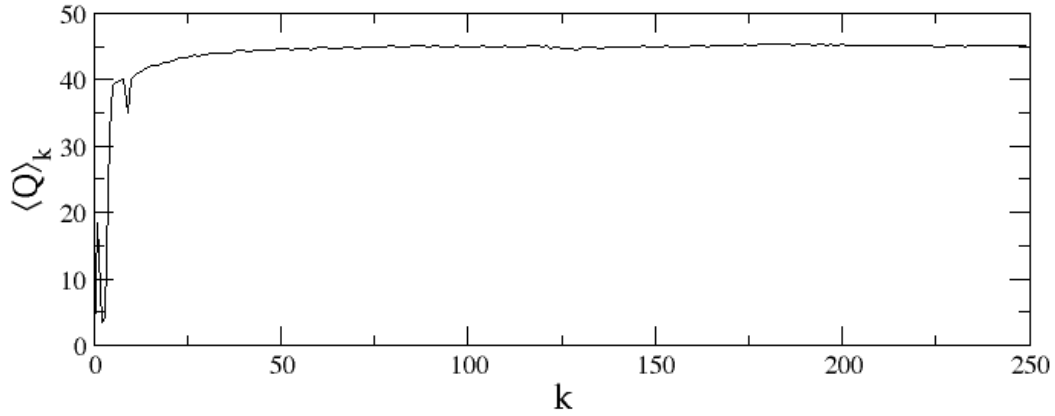

Fig. 6.15 In the ordinate axis the mean values $\langle Q \rangle_k$ of the Q-function computed at each k-th stage of the learning process over $N_T = 1500$ values.

is needed to represent the nonlinearities of the Q-function, may lead the plant towards uncontrollable states resulting that the *RL Agent* is not a stable controller. However it is worth noting that the transfer function depicted in figure 6.17 reveals a well shaped behavior of the *RL Agent* which is mainly linear since it takes high values correspondingly to the linear response with respect to the input velocity and to the harmonic modes of the plant. Less important contributions due to nonlinearities are present where, out of the linear response regions, the transfer function is not exactly zero. Such contributions will be used to improve the performances of the controller, as showed in figure 6.16, and in particular in the control of real physical systems where nonlinearities, even very small, are necessarily present.

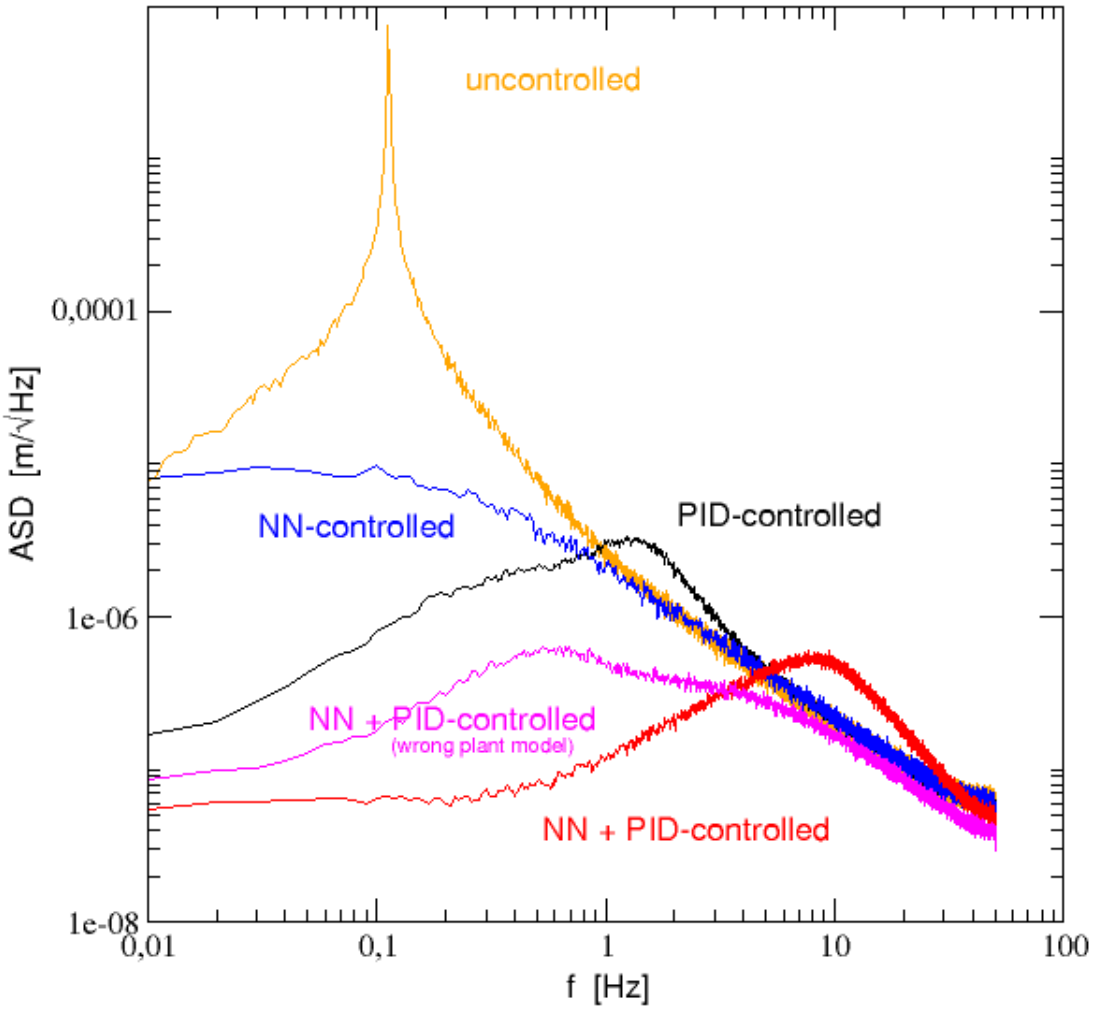

Fig. 6.16 Amplitude spectral densities of the estimated displacement $\widehat{X}$ of a two-pendulum system with frequency $\omega = \sqrt{0.5}Hz$, friction $\nu = 0.005Hz$, seismic noise s.d. $\sigma_{\xi_{1,2}} = 10^{-4}$, sensing white noise s,.d. $\sigma_{\tilde{X}} = 10^{-5}$. Kalman filter used to get the estimates $\tilde{\mathbf{X}}$ is based on an exact plant model. The action set of the *RL Agent* is as follows: $\mathcal{A} = \{-10^{-2}, -10^{-3}, ..., -10^{-8}, 0, 10^{-8}, ..., 10^{-2}\}$. Orange: plant. Black: PID control. Blue: RL control. Red: PID and RL controls. Homogeneous results are obtained for the RL and PID architectures also when the Kalman filter is based on wrong plant model (with $\omega_{_{Kalman}} = \sqrt{0.2}Hz$ and $\nu_{_{Kalman}} = 0.002Hz$) as the Magenta PSD of $\tilde{\mathbf{X}}$, obtained with the PID+RL controller, shows.

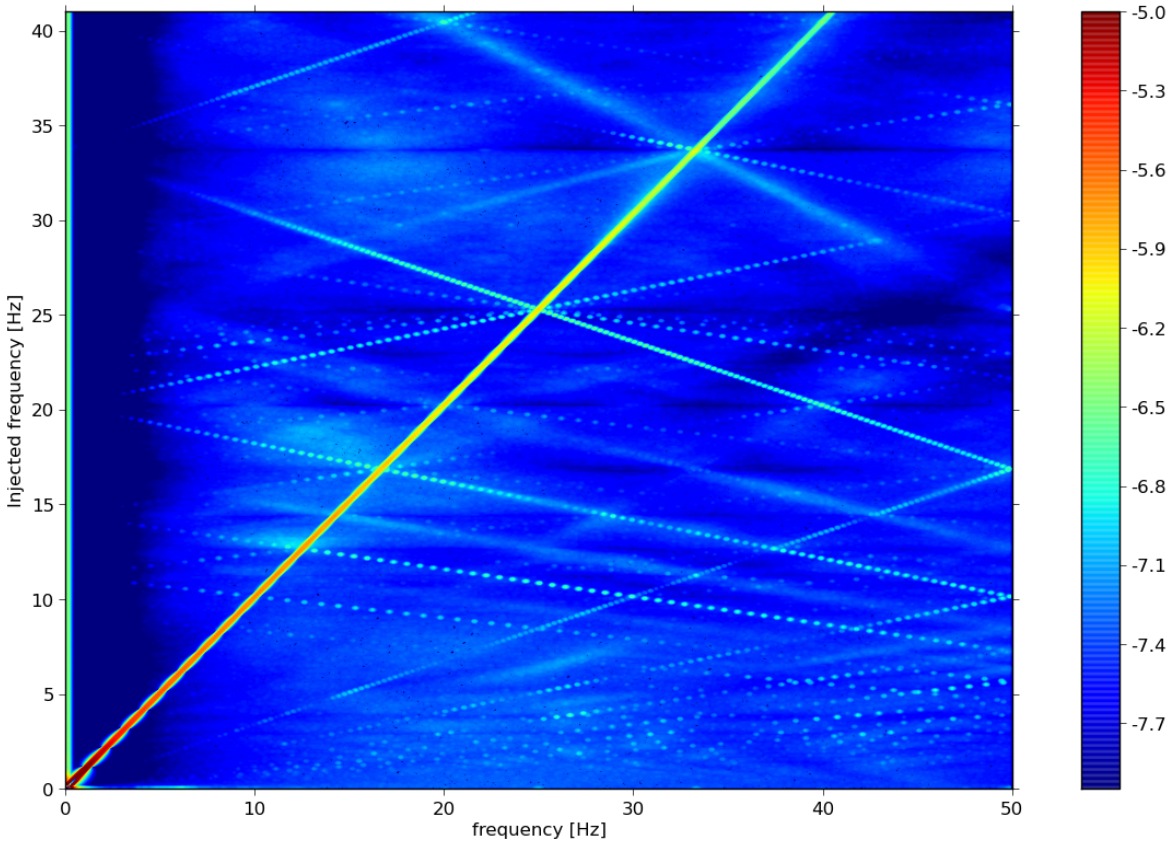

Fig. 6.17 Logarithmic values of the transfer function T_{RL} of the RL controller between the integral of its output and the estimate velocity in input, obtained from $T^2_{RL} := PSD(\int A(\widehat{\mathbf{X}})dt) \times PSD\left(d\widehat{X}/dt\right)^{-1}$, for an input signal (instead of seismic noise) characterized by a single frequency. On the x axis frequencies of the transfer function are placed and on the y axis the frequency f of the input signal $\sin(2\pi f)$.

Reinforcement Learning (RL) Based Control for Seismic Noise Reduction

Lorenzo Cerboni Baiardi, Jan Harms
University of Urbino

Double pendulums system

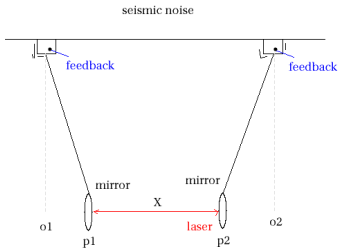

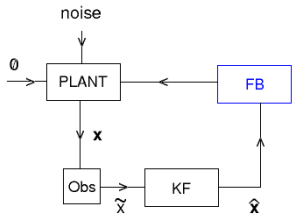

Two pendulums system

- The system is described by the ODE $\ddot{X} = -\omega^2(X - n) - \nu\dot{X}$ where X is differential displacement between the two pendulums varying due to seismic noise
- $n = \xi_1 - \xi_2$ is modeled as a low-frequency correlated process, where $\xi_{1,2}$ are the seismic noises at the two suspension points assumed white noises with s.d. $\sigma_{\xi_{1,2}}$
- only measures $\tilde{X}$ of X are available with a white noise sensing error with s.d. $\sigma_{\tilde{X}} \ll \sigma_{\xi_{1,2}}$
- a Kalman filter is used to get the estimate of the full dynamical state $\widehat{X}$ of the system
- feedback control based on the estimation $\widehat{X}$

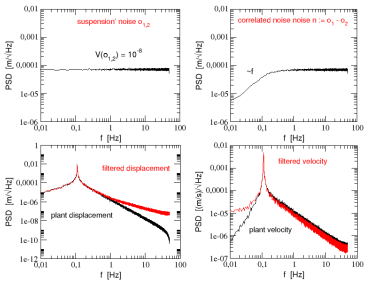

RL control for pendulums

Generalities on RL based control

- Choose a finite bounded set of feedback values: $\mathcal{A} = \{A_i\}_{i=0}^{N}$
- The algorithm observes the Markov process $\boldsymbol{X}$ (as the time series of estimates $\widehat{\boldsymbol{X}}$ from the Kalman filtering is) assigning to it a value $Q = Q(\boldsymbol{X}_t, A_t)$
- Given $\boldsymbol{X}$ the selected feedback is such that

$$A = \max_{A \in \mathcal{A}} Q(\boldsymbol{X}, A)$$

- The function Q is adjusted during the learning process observing how it leads of the system with $\boldsymbol{X}_0$ being the target state in which the system desired to be
- A suitable reward function $r = r(\boldsymbol{X})$, based on the error signal, is used to make correct the Q function during the learning process bbased on its effectivness. Reward function is not unique and it is choosen with care to the structure on the system to control
- A hidden layer Neural Network, *atan* as activation function, is used to represent Q

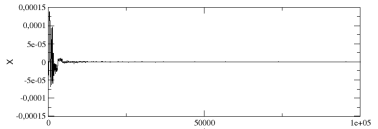

Example of the relative position X time series of a RL-controlled double pendulum system.

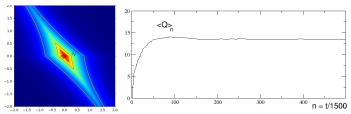

Left: reward function $r(\boldsymbol{X}) = 1.8 \times (e^{-|x|} + 0.3)e^{-|x+v/0.7|}$. Right: the mean value $\langle Q \rangle_n$ of the pair $(\boldsymbol{X}_t, A_t)$ along a trajectory where $n = t/1500$ stands for the samples block over which the mean value of Q is computed. Simulation is performed with the time step $dt = 10^{-2}s$.

RL control design

Main features of the RL control

- Various feedback are used:
  - the traditional linear PID controller
  - the RL control alone
  - the RL embedded with the PID
- input signals of the PID are the estimated states $\widehat{\boldsymbol{X}} = (\int \widehat{X}dt, \widehat{X}, d\widehat{X}/dt)$
- input signals of the RL control are $(\widehat{\boldsymbol{X}}, \boldsymbol{B} \cdot \widehat{\boldsymbol{X}} + A)$, that is the estimated state and the PID feedback added to the RL feedback in order to make the input process Markov
- it results a nonlinear adaptive control based on a machine learning algorithm

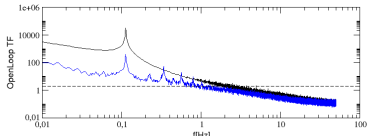

Open loop transfer functions between the input noise and the output feedback: PID (black) and RL agent (blue).

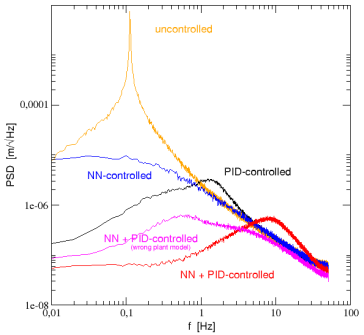

Power spectral densities of the estimated displacement $\widehat{X}$ of a double pendulums system with frequency $\omega = \sqrt{0.5}Hz$, friction $\nu = 0.005Hz$, seismic noise s.d. $\sigma_{\xi_{1,2}} = 10^{-4}$, sensing white noise s.d. $\sigma_{\tilde{X}} = 10^{-5}$. Kalman filter used to get the the estimates $\widehat{\boldsymbol{X}}$ is based on an exact plant model. Orange: plant. Black: PID control. Blue: RL control. Red: PID and RL controls. Homogeneous results are obtained for the RL and PID architectures also when the Kalman filter is based on wrong plant model (with $\omega_{Kalman} = \sqrt{0.2}Hz$ and $\nu_{Kalman} = 0.002Hz$) as the Magenta PSD of $\widehat{\boldsymbol{X}}$, obtained with the PID+RL controller, shows.

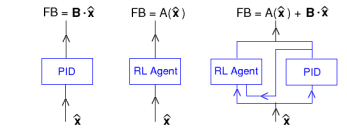

Considered feedback architectures. PID gains are: $K_p = -10^2$, $K_i = -10^2$, $K_d = -10^1$. RL feedback values selected are: $\mathcal{A} = \{-10^{-1}, -10^{-2}, ..., -10^{-8}, 0, 10^{-8}, ..., 10^{-1}\}$.

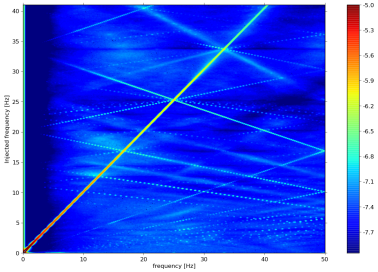

Logarithmic values of the transfer function T_{RL} of the RL controller between the integral of its output and the estimate velocity in input, obtained from $T^2_{RL} := PSD(\int A(\widehat{\boldsymbol{X}})dt) \times PSD\left(d\widehat{X}/dt\right)^{-1}$, for an input signal (instead of seismic noise) characterized by a single frequency. On the x axis are frequencies of the transfer function and on the y axis the frequency f of the input signal $\sin(2\pi f)$.

Conclusions and future developments

- RL adaptive control avoids the problems arising from the use of wrong plant models needed to compute traditional feedback
- Varying set of feedback values $\mathcal{A}$, the shapes of the PSD of $\widehat{X}$ can be shifted to be more effective at a certain frequency range
- Additional RL controllers can be introduced to be trained from filtered signal in order to be effective only in a specific frequency range
- The method is applied to the model of a real superattenuator to test the RL control performance embedding it with the LQG control

The poster shown at the conference on advanced gravitational wave detectors, GWADW 2015, Alaska.

6.5 Further developments

The next step of this work will be to apply the reinforcement learning techniques to control more complex and high dimensional physical systems. This will be a non trivial task since the stability is not only affected by the non Markovianity of the environment, see the figure 6.18, and the architecture of the controller, but also by the reward function, by the complexity of the function approximator and by the learning process in general.

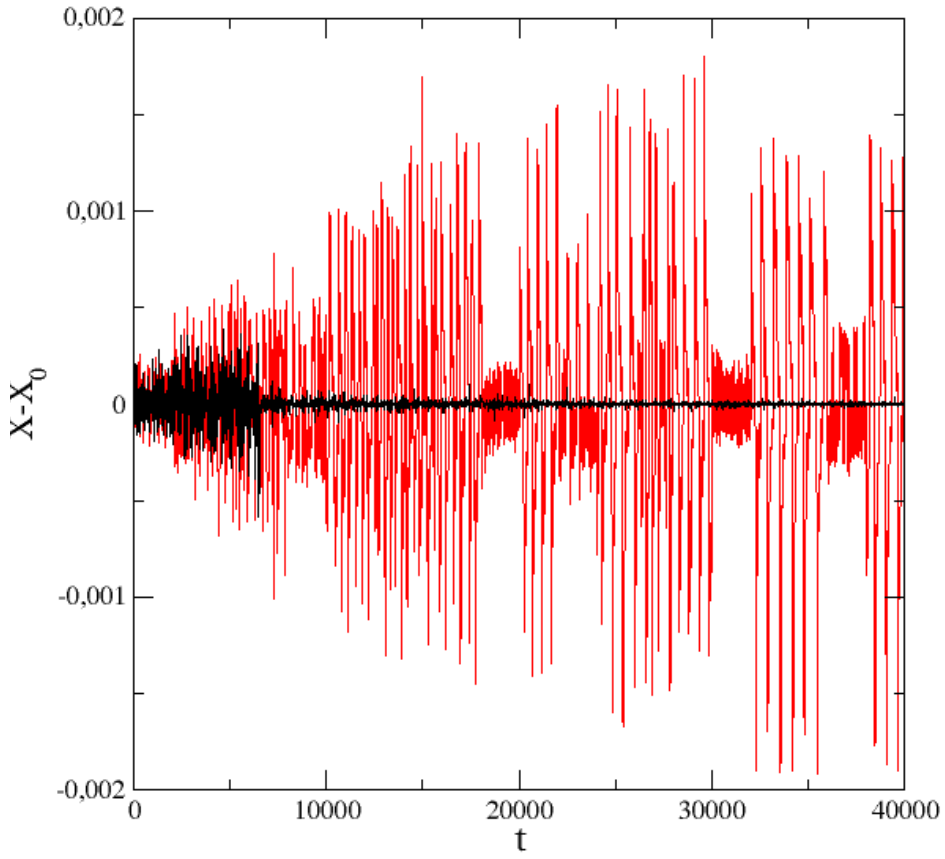

Fig. 6.18 An example of non stable controller provided by the *RL Agent* applied to the two-pendulum system in the case in which it does not receive one of the components of the vector $\widehat{\mathbf{X}}$ in input. The stable data series, the black one, is obtained when $\widehat{\mathbf{X}}$ is in input to the *RL Agent*, while the unstable data series (the red one) is obtained when the estimate of the velocity is removed from $\widehat{\mathbf{X}}$.

Performance can be improved by changing the action set $\mathcal{A}$ of the *RL Agent*, as shown in figure 6.19. Moreover, further neural network can be embedded in the *RL*

Agent each of which receiving a specific frequency band of the inputs signal in order to be more effective where is necessary.

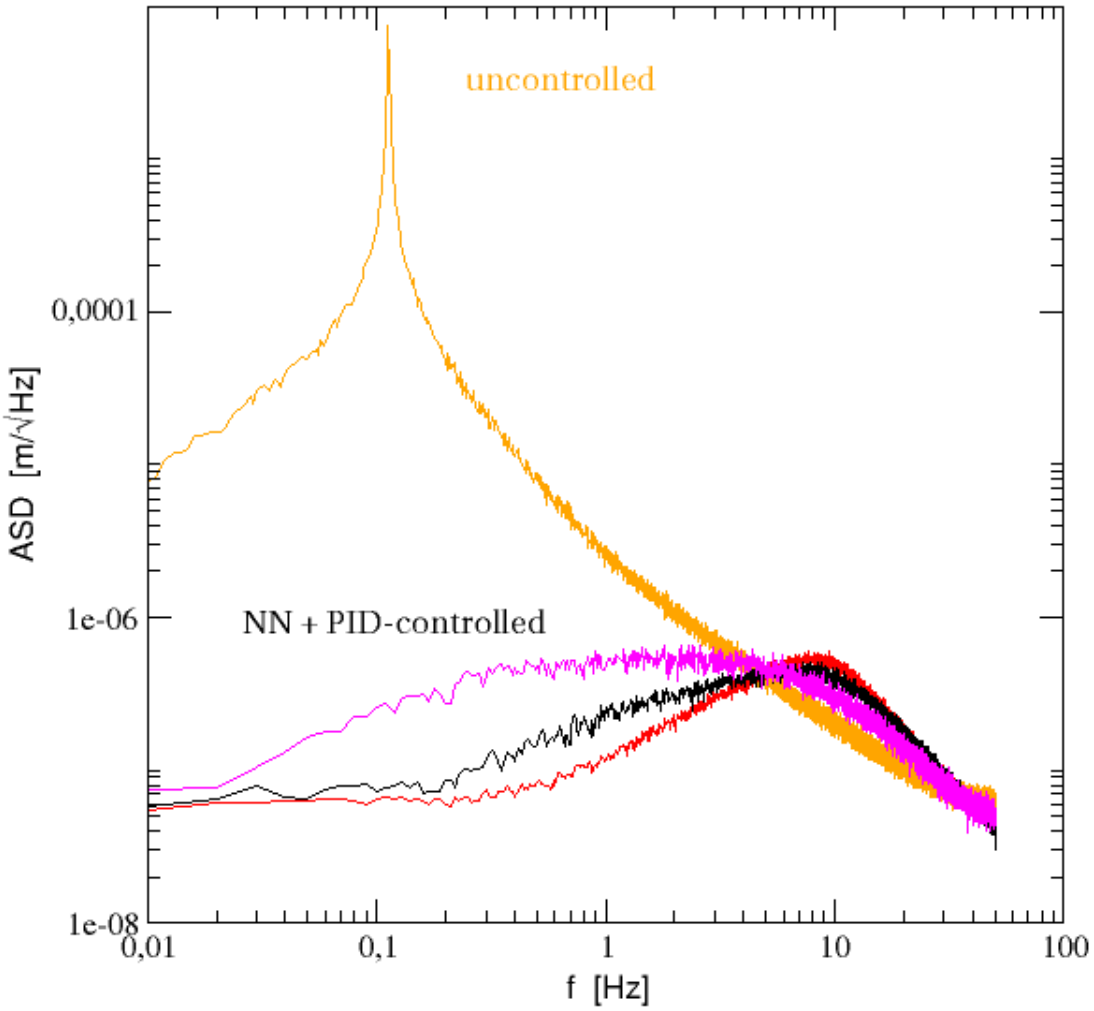

Fig. 6.19 Amplitude spectral densities as in figure 6.16 where only the architecture of *RL Agent* and the PID, showed in figure (6.12), are used. Different from the previous simulation in the present case the *RL Agent* is endowed with different action sets $\mathcal{A}$. Red: $\mathcal{A} = \{-10^{-2}, -10^{-3}, ..., -10^{-8}, 0, 10^{-8}, ..., 10^{-2}\}$. Black: $\mathcal{A} = \{-10^{-2}, -10^{-3}, 10^{-4}, -5 \times 10^{-4}, ..., -10^{-8}, 0, 10^{-8}, ..., 5 \times 10^{-4}, 10^{-3}, 10^{-2}\}$. Magenta: $\mathcal{A} = \{-10^{-2}, -10^{-3}, ..., -5 \times 10^{-5}, ..., -10^{-8}, 0, 10^{-8}, ..., 5 \times 10^{-5}, ..., 10^{-2}\}$

References

[1] A. Agliari, L. Gardini, T. P. (2006). Global bifurcations in duopoly when the cournot point is destabilized via a subcritical neimark bifurcation. *International Game Theory Review*, 8:1–20.

[2] A. Medio, M. L. (2001). *Nonlinear Dynamics*. Cambridge University Press.

[3] Agliari, A. (2006). Homoclinic connections and subcritical neimark bifurcation in a duopoly model with adaptively adjusted productions. *Chaos, Solitons and Fractals*, 29(3):739–55.

[4] Agliari, A. A., Gardini, L., and Puu, T. (2006). Global bifurcations in duopoly when the Cournot point is destabilized via a subcritical Neimark bifurcation. *International Game Theory Review*, 8(1):1–20.

[5] Alexander, J. C., Yorke, J. A., You, Z., and Kan, I. (1992). Riddled basins. *International Journal of Bifurcation and Chaos*, 2(4):795–813.

[6] A.N. Sharkovsky, Yu.L. Maistrenko, E. R. (1993). *Difference Equations and Their Applications*. Kluwer Academic Publishers.

[7] Anderson, C. W., Hittle, D. C., Katz, A. D., and Kretchmar, R. M. (1997). Synthesis of reinforcement learning, neural networks and pi control applied to a simulated heating coil. *Artificial Intelligence in Engineering*, 11(4):421–429.

[8] Anderson, C. W. and Hong, Z. (1994). Reinforcement learning with modular neural networks for control. In *IEEE International Workshop on Neural Networks Application to Control and Image Processing*. Citeseer.

[9] Anufriev, M., Kopanyi, D., and Tuinstra, J. (2013). Learning cycles in bertrand competition with differentiated commodities and competing learning rules. *Journal of Economic Dynamics & Control*, 37(12):2562–2581.

[10] Aoki, M. (1996). *New Approaches to Macroeconomic Modelling*. Cambridge University Press, New York.

[11] Arrow, K. (1988). The economic implications of learning by doing. *The Review of Economic Studies*, 29(3):155–173.

[12] A.S. Pikovsky, P. G. (1991). Symmetry breaking bifurcation for coupled chaotic attractors. *J. Phys. A: Math. Gen.*, 24:4587–4597.

[13] Ashwin, P., Buescu, J., and Stewart, I. (1996). From attractor to chaotic saddle: a tale of transverse instability. *Nonlinearity*, 9(3):703–737.

[14] B. Wansink, R.J. Kent, S. H. (1998). An anchoring and adjustment model of purchase quantity decisions. *Journal of Marketing Research*, 35:71–8.

[15] Binmore, K. (2007). *Playing for Real. A Text on Game Theory*. Oxford University Press.

[16] Bischi, G. I., Chiarella, C., Kopel, M., and Szidarovszky, F. (2010). *Nonlinear Oligopolies: Stability and Bifurcations*. Springer-Verlag.

[17] Bischi, G.-I., Gardini, L., and Mira, C. (2001a). Maps with a vanishing denominator. A survey of some results. *Nonlinear Analysis*, 47:2171–2185.

[18] Bischi, G.-I., Kopel, M., and Naimzada, A. (2001b). On a rent-seeking game described by a non-invertible iterated map with denominator. *Nonlinear Analysis: Theory, Methods & Applications*, 47(8):5309–5324.

[19] Bischi, G.-I. and Lamantia, F. (2005). *Nonlinear Dynamical Systems in Economics - CISM Lecture Notes*, chapter Coexisting attractors and complex basins in discrete-time economic models, pages 187–231. Springer.

[20] Bischi, G. I., Lamantia, F., and Radi, D. (2013a). Multi-species exploitation with evolutionary switching of harvesting strategies. *Natural Resource Modeling*, 26(4):546–571.

[21] Bischi, G. I., Lamantia, F., and Radi, D. (2013b). A prey-predator model with endogenous harvesting strategy switching. *Applied Mathematics and Computation*, 219(20):10123–10142.

[22] Bischi, G. I., Lamantia, F., and Radi, D. (2015). An evolutionary Cournot model with limited market knowledge. *Journal of Economic Behavior & Organization*, 116:219–238.

[23] Bischi, G. I., Lamantia, F., and Sbragia, L. (2009). *Competition and cooperation in natural resources exploitation: an evolutionary game approach*. In: Carraro, C., Fragnelli, V. (Eds.), Game Practice and the Environment, edward elgar publishing edition.

[24] Bischi, G. I., Lamantia, F., and Tramontana, F. (2014). Sliding and oscillations in fisheries with on-off harvesting and different switching times. *Communications in Nonlinear Science and Numerical Simulation*, 19(1):216–229.

[25] Bischi, G. I. and Naimzada, A. (2000). *Advances in Dynamic Games and Applications*, chapter Global Analysis of a Duopoly Game with Bounded Rationality, pages 361–385. Birkhauser.

[26] Bischi, G. I., Naimzada, A. K., and Sbragia, L. (2007). Oligopoly games with local monopolistic approximation. *Journal of Economic Behavior & Organization*, 62(3):371–388.

[27] Bonanno, G. (1988). Oligopoly equilibria when firms have local knowledge of demand. *International Economic Review*, 29:45–55.

[28] Brauer, F. and Castillo-Chavez, C. (2001). *Mathematical Models in Population Biology and Epidemiology*, volume Texts in Applied Mathematics 40. Springer-Verlag, New York.

[29] Brousseau, V. and Kirman, A. (1992). *Game Theory and Economic Applications*, chapter Apparent convergence of learning processes in mis-specified games. Springer.

[30] Buescu, J. (1997a). *Exotic Attractors*. Birkhäuser, Basel.

[31] Buescu, J. (1997b). *Exotic Attractors*. Birkh´auser, Basel.

[32] C. Grebogi, E. Ott, J. Y. (1982). Chaotic attractors in crisis. *Physical Review Letters*, 48:1507–13.

[33] C. Mira, L. Gardini, A. B. J. C. (1996a). *Chaotic Dynamics in Two-Dimensional Noninvertible Maps*. World Scientific, Singapore.

[34] C. Mira, L. Gardini, A. B. J. C. (1996b). *Chaotic Dynamics in Two-Dimensional Noninvertible Maps*. World Scientific, Singapore.

[35] Cabrales, A. and Sobel, J. (1992). On the limit points of discrete selection dynamics. *Journal of Economic Theory*, 57(2):407–419.

[36] Cooper, L. (1988). Competitive maps: The structure underlying asymmetric cross elasticities. *Management Science*, 34:707–23.

[37] Cournot, A. (1838). *Researches into the principles of the theory of wealth*. Irwin Paperback Classics in Economics.

[38] Cushing, J. M. (2004). Some discrete competition models and the competitive exclusion principle. *Journal of Difference Equations and Applications*, 10(13-15):1139–1151.

[39] D. Fudenberg, J. T. (1995). *Game Theory*. The MIT Press.

[40] D.E. Bell, R.L. Keeney, J. L. (1975). A market share theorem. *Journal of Marketing Research*, 120:136–41.

[41] Dieci, R., Bischi, G., and Gardini, L. (2003). Routes to complexity in a business-cycle model described by a noninvertible triangular map. *Cubo A Mathematical Journal*, 5(3):367–396.

[42] Dieci, R., Bischi, G. I., and Gardini, L. (2001). From bi-stability to chaotic oscillations in a macroeconomic model. *Chaos, Solitons & Fractals*, 12(5):805–822.

[43] Droste, E., Hommes, C. H., and Tuinstra, J. (2002). Endogenous fluctuations under evolutionary pressure in Cournot competition. *Games and Economic Behavior*, 40(2):232–269.

[44] E. Ott, J. S. (1994). Blowout bifurcations: the occurrence of riddled basins. *Phys. Lett. A*, 188:39–47.

[45] Elaydi, S. (1995a). *An Introduction to Difference Equations*. Springer, New York.

[46] Elaydi, S. N. (1995b). *An introduction to difference equations*. New York, Springer.

[47] et al., V. M. (2015). Human-level control through deep reinforcement learning. *Nature*, (518):529–533.

[48] Flam, S. (1993). *Nonlinear Dynamics in Economics and Social Sciences. Lecture Notes in Economics and Mathematical Systems. Vol. 399, p.232-237*, chapter Oligopolistic Competition: from Stability to Chaos. Springer-Verlag.

[49] Föllmer, H. (1974). Random economies with many interacting agents. *Journal of Mathematical Economics*, 1:51–62.

[50] Friedland, B. (1986). *Control System Design, an Introduction to State-Space Methods*. McGraw-Hill, Inc., New York.

[51] G. Bonanno, C. Z. (1985). Limited knowledge of demand and oligopoly equilibria. *Journal of Economic Theory*, 35:276–283.

[52] Gandolfo, G. (2010a). *Economic Dynamics*. Springer.

[53] Gandolfo, G. (2010b). *Economic Dynamics*. Springer-Verlag.

[54] Geritz, S. A. and Kisdi, E. (2004). On the mechanistic underpinning of discrete-time population models with complex dynamics. *Journal of Theoretical Biology*, 228(2):261–269.

[55] Getz, W. M. and Haight, R. (1989). *Population Harvesting: Demographic Models of Fish, Forest, and Animal Resources*. Princeton University Press.

[56] G.Franklin, J.D. Powell, A. E.-N. (1994). *Feedback control of dynamical systems*. Addison-Wesley Publishing Company.

[57] G.I. Bischi, A. N. (2000a). Global analysis of a duopoly game with bounded rationality. *Advances in Dynamic Games and Applications*, 5:361–385.

[58] G.I. Bischi, M. Gallegati, A. N. (1999). Symmetry-breaking bifurcations and representative firm in dynamic duopoly games. *Annals of Operations Research*, 89:253–272.

[59] G.I. Bischi, L. Cerboni Baiardi, D. R. (2015a). On a discrete-time model with replicator dynamics in renewable resource exploitation. *Journal of Difference Equations and Applications*.

[60] G.I. Bischi, L. C. B. (2015b). A dynamic marketing model with best reply and inertia. *Chaos, Solitons and Fractals*, 79:145–156.

[61] G.I. Bischi, L. C. B. (2015c). Fallacies of composition in nonlinear marketing models. *Communications in Nonlinear Science and Numerical Simulation*.

[62] G.I. Bischi, L. G. (1998a). Role of invariant and minimal absorbing areas in chaos synchronization. *Physical Review E*, 58:5710–5719.

[63] G.I. Bischi, L. G. (2000b). Global properties of symmetric competition models with riddling and blowout phenomena. *Discrete Dynamics in Nature and Society*, 5:149–160.

[64] G.I. Bischi, L. Stefanini, L. G. (1998b). Synchronization, intermittency and critical curves in duopoly games. *Mathematics and Computers in Simulations*, 44:559–585.

[65] G.I. Bischi, C. Mammana, L. G. L. (2000c). Multistability and cyclic attractors in duopoly games. *Chaos, Solitons and Fractals*, 11:543–64.

[66] G.I. Bischi, M. K. (2001). Equilibrium selection in a nonlinear duopoly game with adaptive expectations. *Journal of Economic Behavior and Organization*, 46:73–100.

[67] G.I. Bischi, M. K. (2003). Multistability and path dependence in a dynamic brand competition model. *Chaos, Solitons and Fractals*, 18:561–576.

[68] G.I. Bischi, L. Gardini, M. K. (2000d). Analysis of global bifurcations in a market share attraction model. *Journal of Economic Dynamics and Control*, 24:855–79.

[69] G.I. Bischi, C. Chiarella, M. K. S. F. (2010). *Nonlinear Oligopolies: Stability and Bifurcations*. Springer-Verlag.

[70] G.S. Carpenter, L.G. Cooper, D. H. D. M. (1988). Modeling asymmetric competition. *Marketing Science*, 7:393–412.

[71] H. Fujisaka, T. Y. (1983). Stability theory of synchronized motion in coupled-oscillator systems. *Progress of Theoretical Physics*, 69:32–47.

[72] Hamilton, J. (1994). *Time Serie s Analysis*. Princeton University Press, Princeton, New Jersey.

[73] Hofbauer, J. and Sigmund, K. (2003). Evolutionary game dynamics. *Bulletin (New Series) of the American Mathematical Society*, 40(4):479–519.

[74] Hofbauer, J. and Weibull, J. W. (1996). Evolutionary selection against dominated strategies. *Journal of Economic Theory*, 71(2):558–573.

[75] Hommes, C., Kiseleva, T., Kuznetsov, Y., and Verbic, M. (2012). Is more memory in evoluionary selection (de)stabilizing? *Macroeconomic Dynamics*, 16:335–357.

[76] Hommes, C. H., Ochea, M. I., and Tuinstra, J. (2011). On the stability of the Cournot equilibrium: An evolutionary approach. Working paper.

[77] I. Gumowski, C. M. (1980). *Dynamique Chaotique*. Cepadues Editions, Toulose.

[78] J. Von Neumann, O. M. (1944). *Theory of games and economic behavior*. Princeton University Press.

[79] Jakobson, M. (1981). Absolutely continuous invariant measures for one-parameter families of one-dimensional maps. *Commun Math Phys*, 81:39–88.

[80] J.C. Alexander, J.A. Yorke, Z. Y. I. K. (1992). Riddled basins. *Int. Jou. of Bif. and Chaos*, 2:795–813.

[81] Kirman, A. (1983). *Individual Forecasting and Collective Outcomes*, chapter Mistaken beliefs and resultant equilibria. Cambridge University Press.

[82] Kirman, A. P. (1992). Whom or what does the representative individual represent? *Jou. of Econ. Perspectives*, 6:117–136.

[83] K.J. Arrow, L. H. (1960). Stability of the gradient process in n-persons games. *Journal of the Society for Industrial and Applied Mathematics*, 8(2):280–294.

[84] Kolyada, S. F. (1992). On dynamics of triangular maps of the square. *Ergodic Theory and Dynamical Systems*, 12(4):749–768.

[85] Kopel, M. (1996). Simple and complex adjustment dynamics in cournot duopoly models. *Chaos, Solitons and Fractals*, 7:2031–48.

[86] Kopel, M., Lamantia, F., and Szidarovszky, F. (2014). Evolutionary competition in a mixed market with socially concerned firms. *Journal of Economic Dynamics & Control*, 48:394–409.

[87] L. Cerboni Baiardi, F. Lamantia, D. R. (2015). Evolutionary competition between boundedly rational behavioral rules in oligopoly games. *Chaos, Solitons and Fractals*, 79:204–225.

[88] Lamantia, F. (2011). A nonlinear duopoly with efficient production-capacity levels. *Computational Economics*, 38(3):295–309.

[89] Lamantia, F. and Radi, D. (2015). Exploitation of renewable resources with differentiated technologies: an evolutionary analysis. *Mathematics and Computers in Simulation*, 108:155–174.

[90] Lambertini, L. (2010). Oligopoly with hyperbolic demand: A differential game approach. *Journal of Optimization Theory and Applications*, 145(1):108–119.

[91] L.G. Cooper, M. N. (1988). *Market-Share Analysis*. Kluwer Academic Publishers.

[92] L.M. Pecora, T. L. C. (1990). Synchronization in chaotic systems. *Phys. Rev. Lett.*, 64:821.

[93] M. Gallegati, A. K. (1999). *Beyond the Representative Agent*. Elgar Pub. Co.

[94] M. Hasler, Y. M. (1997). An introduction to the synchronization of chaotic systems: Coupled skew tent maps. *IEEE Trans. Circuits Syst.*, 44(10):856–866.

[95] M. Kopel, G.I. Bischi, L. G. (2000). *Interaction and market structure. Essays on Heterogeneity in Economics, Lecture Notes in Economics and mathematical Systems*, chapter On New Phenomena in Dynamic Promotional Competition Models with Homogeneous and Quasi-homogeneous Firms. Springer-Verlag.

[96] Maistrenko, Y. L., Maistrenko, V. L., Popovich, A., and Mosekilde, E. (1998). Transverse instability and riddled basins in a system of two coupled logistic maps. *Physical Review E*, 57(3):2713–2724.

[97] May, R. (1974). *Stability and Complexity in Model Ecosystems*. Princeton University Press, 2nd edition edition.

[98] May, R. M. (1975). Biological populations obeying difference equations: stable points, stable cycles, and chaos. *Journal of Theoretical Biology*, 51(2):511–524.

[99] Medio, A. and Lines, M. (2001). *Nonlinear dynamics*. Cambridge University Press.

[100] Milnor, J. (1985a). On the concept of attractor. *Commun. Math Phys*, 99:177–195.

[101] Milnor, J. (1985b). On the concept of attractor: Correction and remarks. *Communications in Mathematical Physics*, 102(3):517–519.

[102] Moller, M. (1993). A scaled conjugate gradient algorithm for fast supervised learning. *Neural networks*, 6:525–533.

[103] Nagai, Y. and Lai, Y.-C. (1997). Periodic-orbit theory of the blowout bifurcation. *Physical Review E*, 56(4):4031–4041.

[104] P. Ashwin, J. Buescu, I. S. (1996). From attractor to chaotic saddle: a tale of transverse instability. *Nonlinearity*, 9:703–737.

[105] P. Farris, P.E. Pfeifer, E. N. D. R. (2005). When five is a crowd in the market share attraction model: the dynamic stability of competition. *Journal of Research and Management*, 1:29–45.

[106] Plank, M. (1997). Some qualitative differences between the replicator dynamics of two player and n player games. *Nonlinear Analysis: Theory, Methods & Applications*, 30(3):1411–1417.

[107] Puu, T. (1991a). Chaos in duopoly pricing. *Chaos, Solitons and Fractals*, 1:573–81.

[108] Puu, T. (1991b). Chaos in duopoly pricing. *Chaos, Solitons & Fractals*, 1(6):573–581.

[109] Puu, T. (2003). *Attractors, Bifurcations and Chaos*. Springer.

[110] R.I. Schult, D.B. Cramer, F. H. J. W. (1987). Symmetric and nonsymmetric coupled logistic maps. *Phys. Rev A*, 35:3115–3118.

[111] Rosen, J. B. (1965). Existence and uniqueness of equilibrium points for concave N-person games. *Econometrica: Journal of the Econometric Society*, 33(3):520–534.

[112] R.S. Sutton, A. B. (1998). *Reinforcement learning: An introduction*, volume 28. The MIT Press.

[113] Sacco, P. (1991). Adaptive response and cournotian behavior. *Economic Notes*, 20:474–496.

[114] S.C. Venkataramani, B.R. Hunt, E. O. (1996). Bubbling transition. *Phys. Rev. E*, 54:1346–1360.

[115] Smirnov, V. (1964). *A Course of Higher Mathematics, I, Equations of the third degree, p. 491-97*. Pergamon Press.

[116] Sterman, J. (1989). Modeling managerial behavior: misperceptions of feedback in a dynamic decision making experiment. *Management Science*, 35:321–39.

[117] Stoker, T. (1993). Empirical approaches to the problem of aggregation over individuals. *Journal of Economic Literature*, XXXI:1827–1874.

[118] Taylor, P. and Jonker, L. (1978). Evolutionarily stable strategies and game dynamics. *Mathematical Biosciences*, 40(1):145–156.

[119] Teocharis (1960). On the stability of the cournot solution of the oligopoly problem˙ *Review of Economic Studies*, 27:133–134.

[120] Theocharis, R. D. (1960). On the stability of the Cournot solution on the oligopoly problem. *Review of Economic Studies*, 27(2):133–134.

[Thunberg] Thunberg, H. Periodicity versus chaos in one-dimensional dynamics. *SIAM Rev*, 43(1).

[122] Tramontana, F., Gardini, L., and Puu, T. (2010). Global bifurcations in a piecewise-smooth Cournot duopoly game. *Chaos, Solitons & Fractals*, 43(1-12):15–24.

[123] Tuinstra, J. (2004). A price adjustment process in a model of monopolistic competition. *International Game Theory Review*, 6(3):417–442.

[124] Turnovsky, S. (1995). *Methods of Macroeconomic Dynamics*. The MIT Press.

[125] Varian, H. (1992). *Microeconomic Analysis*. W.W. Norton and Company, 3rd edition edition.

[126] Vriend, N. J. (2000). An illustration of the essential di!erence between individual and social learning, and its consequences for computational analyses. *Journal of economic dynamics & control*, 24(1):1–19.

[127] W. Bialek, I. Nemenman, N. T. (2001). Predictability, complexity, and learning. *Neural Computation*, (13):2409–2463.

[128] Webb, G. (2007). *Game Theory. Decisions, interaction and evolution*. Springer-Verlag, London.

[129] W.H. Press, A. Teukolsky, W. V. B. F. (2007). *Numerical Recipes in C, The Art of Scientific Computing*. Cambridge University Press.

[130] W.J. Baumol, R. Q. (1964). Rules of thumb and optimally imperfect decisions. *The American Economic Review*, 54:23–46.

[131] Y. Nagai, Y. L. (1997). Periodic-orbit theory of the blowout bifurcation. *Physical Review E*, 56(4):4031–4041.

[132] Y.C. Lai, C. Grebogi, J. Y. (1996). Riddling bifurcation in chaotic dynamical systems. *Phys. Rev. Lett*, 77:55–58.

[133] Yu. Maistrenko, V.L. Maistrenko, A. P. E. M. (1998a). Role of the absorbing area in chaotic synchronization. *Physical Review Letters*, 88(8):1638–1641.

[134] Yu. Maistrenko, V.L. Maistrenko, A. P. E. M. (1998b). Transverse instability and riddled basins in a system of two coupled logistic maps. *Physical Review E*, 57(3):2713–2724.

Appendix A

Puu's Oligopoly

In this Section we recall the map of the Cournot duopoly model proposed in [107] and its main properties.

The map assumes the form

$$\begin{aligned} q_1' &= (1-\lambda_1)\, q_1 + \lambda_1 \left[\sqrt{\frac{q_2}{c_1}} - q_2\right] \\ y' &= (1-\lambda_2)\, q_2 + \lambda_2 \left[\sqrt{\frac{q_1}{c_2}} - q_1\right] \end{aligned} \tag{A.1}$$

where also in this case the parameters $\lambda_i \in [0,1]$ represent the attitude of firm i to adopt the best reply, hence $(1-\lambda_i)$ represents the inertia of firm i, $i = 1,2$, and $c_i > 0$, $i = 1,2$, represent unitary costs. The fixed points, nonnegative solutions of the algebraic system

$$\begin{aligned} q_1 &= \sqrt{\tfrac{q_2}{c_1}} - q_2 \\ q_2 &= \sqrt{\tfrac{q_1}{c_2}} - q_1 \end{aligned}$$

are the trivial one $E_0 = (0,0)$ and the unique positive solution $E_1 = \left(\frac{c_2}{(c_1+c_2)^2}, \frac{c_1}{(c_1+c_2)^2}\right)$. The Jacobian matrix, computed at the fixed point E_1, becomes

$$\boldsymbol{J}(E_1) = \begin{pmatrix} 1-\lambda_1 & \lambda_1\left(\dfrac{c_1+c_2}{2c_1} - 1\right) \\ \lambda_2\left(\dfrac{c_1+c_2}{2c_2} - 1\right) & 1-\lambda_2 \end{pmatrix}$$

The coefficients of the characteristic equation

$$P(z) = z^2 - Tr \cdot z + Det = 0\ ,$$

are $Tr = 2 - \lambda_1 - \lambda_2$ and $Det = (1-\lambda_1)(1-\lambda_2) - \lambda_1\lambda_2\left(\frac{a_1+a_2}{2a_1} - 1\right)\frac{a_1+a_2}{2a_2} - 1$, hence the Schur conditions for stability become

$$P(1) = \frac{\lambda_1\lambda_2(c_1+c_2)^2}{4c_1c_2} > 0 \text{ for each } c_i > 0,\ \lambda_i \in (0,1]$$
$$P(-1) = 8c_1c_2(2-\lambda_1-\lambda_2) + \lambda_1\lambda_2(c_1+c_2)^2 > 0 \text{ for each } c_i > 0,\ \lambda_i \in (0,1]$$
$$1 - Det > 0 \text{ if } \frac{(c_1+c_2)^2}{4c_1c_2} < \frac{\lambda_1+\lambda_2}{\lambda_1\lambda_2}$$

The third condition is always satisfied for $c_1 = c_2 = c$, whereas the equilibrium may become unstable through a Neimark-Sacker bifurcation when $\frac{c_1}{c_2} \neq 1$. In particular, without any inertia, i.e. $\lambda_1 = \lambda_2 = 1$, the unique positive equilibrium is stable if and only if $c_1/c_2 \in (3-2\sqrt{2}, 3+2\sqrt{2})$.

It is worth to notice that the map (A.1) is a particular case of (2.6) because after the change of coordinates

$$x = c_2q_1\ ;\ y = c_1q_2 \tag{A.3}$$

the following map is obtained

$$x' = (1-\lambda_1)x + a\lambda_1\left(\sqrt{y} - y\right)$$
$$y' = (1-\lambda_2)y + \tfrac{1}{a}\lambda_2\left(\sqrt{x} - x\right)$$

where $a = c_2/c_1$. This is a particular case of (2.6) with $a_1 = a$ and $a_2 = \frac{1}{a}$, and this explains why the creation of further fixed points is not possible, as explained in the remark after Proposition 2, Indeed, the unique equilibrium $E = \left(\frac{1}{(a_1+1)^2}, \frac{1}{(a_2+1)^2}\right)$ existing in the particular case $a_1a_2 = 1$ corresponds to $E_1 = \left(\frac{c_2}{(c_1+c_2)^2}, \frac{c_1}{(c_1+c_2)^2}\right)$ by considering $a_1 = c_2/c_1$, $a_2 = c_1/c_2$, together with (A.3). We refer to [3] and [1] for a deeper analysis of the same model.

Appendix B

Noninvertible maps and critical sets

In this appendix are given some definitions, properties and simple examples about discrete dynamical systems represented by the iteration of noninvertible maps.

B.1 Definitions and simple examples

A map $T : S \to S$, $S \subseteq \mathbb{R}^n$, defined by $\mathbf{x}' = T(\mathbf{x})$, transforms a point $\mathbf{x} \in S$ into a unique point $\mathbf{x}' \in S$. The point $\mathbf{x}'$ is called the *rank-1 image* of $\mathbf{x}$, and a point $\mathbf{x}$ such that $T(\mathbf{x}) = \mathbf{x}'$ is a *rank-1 preimage* of $\mathbf{x}'$.

If $\mathbf{x} \neq \mathbf{y}$ implies $T(\mathbf{x}) \neq T(\mathbf{y})$ for each $\mathbf{x}$, $\mathbf{y}$ in S, then T is an *invertible map* in S, because the inverse mapping $\mathbf{x} = T^{-1}(\mathbf{x}')$ is uniquely defined; otherwise T is a said to be a *noninvertible map*, because points $\mathbf{x}$ exist that have several rank-1 preimages, i.e. the inverse relation $\mathbf{x} = T^{-1}(\mathbf{x}')$ is multivalued. So, noninvertible means "many-to-one", that is, distinct points $\mathbf{x} \neq \mathbf{y}$ may have the same image, $T(\mathbf{x}) = T(\mathbf{y}) = \mathbf{x}'$.

Geometrically, the action of a noninvertible map can be expressed by saying that it "folds and pleats" the space S, so that distinct points are mapped into the same point. This is equivalently stated by saying that several inverses are defined in some points of S, and these inverses "unfold" S.

For a noninvertible map, S can be subdivided into regions Z_k, $k \geq 0$, whose points have k distinct rank-1 preimages. Generally, for a continuous map, as the point $\mathbf{x}'$ varies in $\mathbb{R}^n$, pairs of preimages appear or disappear as it crosses the boundaries separating different regions. Hence, such boundaries are characterized by the presence of at least two coincident (merging) preimages. This leads us to the definition of the *critical sets*,

one of the distinguishing features of noninvertible maps (see Gumowski and Mira, 1980, Mira et al., 1996):

Definition. The *critical set* CS of a continuous map T is defined as the locus of points having at least two coincident $rank-1$ preimages, located on a set CS_{-1}, called *set of merging preimages*.

The critical set CS is generally formed by $(n-1)$-dimensional hypersurfaces of $\mathbb{R}^n$, and portions of CS separate regions Z_k of the phase space characterized by a different number of $rank-1$ preimages, for example Z_k and Z_{k+2} (this is the standard occurrence for continuous maps). The critical set CS is the n-dimensional generalization of the notion of local minimum or local maximum value of a one-dimensional map, and of the notion of *critical curve* LC of a noninvertible two-dimensional map[1]. The set CS_{-1} is the generalization of local extremum point of a one-dimensional map, and of the *fold curve* LC_{-1} of a two-dimensional noninvertible map.

As an illustration, we consider the one-dimensional quadratic map (logistic map)

$$x' = f(x) = \mu x(1-x). \tag{B.1}$$

This map has a unique critical point $c = \mu/4$, which separates the real line into the two subsets: $Z_0 = (c, +\infty)$, where no inverses are defined, and $Z_2 = (-\infty, c)$, whose points have two rank-1 preimages (figure B.1a). These preimages can be computed by the two inverses

$$x_1 = f_1^{-1}(x') = \frac{1}{2} - \frac{\sqrt{\mu\,(\mu - 4x')}}{2\mu}; \quad x_2 = f_2^{-1}(x') = \frac{1}{2} + \frac{\sqrt{\mu\,(\mu - 4x')}}{2\mu}. \tag{B.2}$$

If $x' \in Z_2$, its two rank-1 preimages, computed according to (B.2), are located symmetrically with respect to the point $c_{-1} = 1/2 = f_1^{-1}(\mu/4) = f_2^{-1}(\mu/4)$. Hence, c_{-1} is the point where the two merging preimages of c are located. As the map (B.1) is differentiable, at c_{-1} the first derivative vanishes.

We remark that in general the condition of vanishing derivative is not sufficient to define the critical points of rank-0 since such condition may be also satisfied by points which are not local extrema (e.g. the inflection points with horizontal tangent). Moreover, for continuous and piecewise differentiable maps the condition of vanishing derivative is not necessary as well, because such maps may have the property that the images of points where the map is not differentiable are critical points, according to the

[1]This terminology, and notation, originates from the notion of critical point as it is used in the classical works of Julia and Fatou.

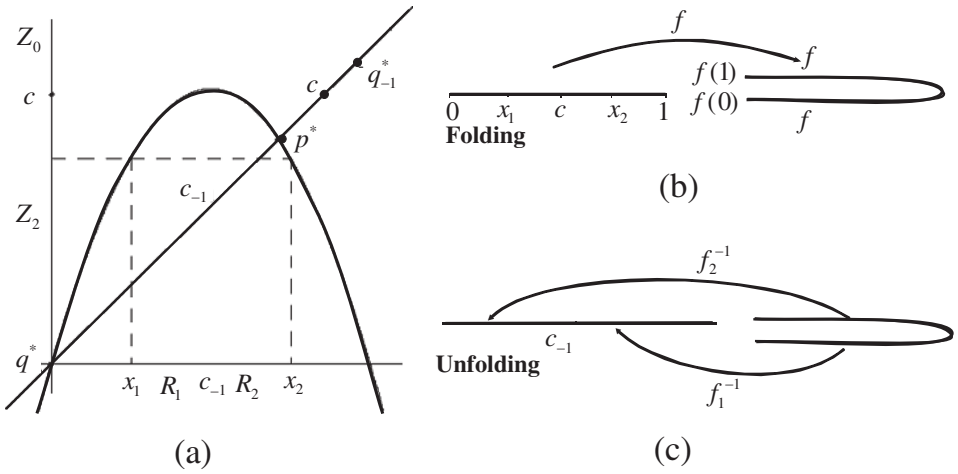

Fig. B.1 (a) The preimmages pf the logistic map. (b) The folding action of the logistic map. (c) The unfolding action of the inverses.

definition given above. This occurs whenever such points are local maxima or minima, like in the cases shown in figures B.2a,b. In figure B.2a, a typical $Z_0 - Z_2$ tent map is shown, where the kink point behaves like the critical point of the logistic map even if it is not obtained as image of a point of vanishing derivative. The same reasoning applies to the "bimodal" $Z_1 - Z_3 - Z_1$ piecewise linear function shown in figure B.2b.

Up to now we have considered continuous maps, but the properties of critical points can easily be extended also to piecewise continuous maps T. In this case a point of discontinuity may behave as a critical point of T, even if the definition in terms of merging preimages cannot be applied. This happens when the ranges of the map on the two sides of the discontinuity have an overlapping zone, so that at least one of the two limiting values of the function at the discontinuity separates regions having a different number of rank-1 preimages (see e.g. the map shown in figure B.2c). The difference with respect to the case of a continuous map is that now the number of distinct rank-1 preimages through a critical point differs generally by one (instead of two), that is, a critical value c (in general the critical set CS) separates regions Z_k and Z_{k+1}. A one-dimensional example is shown in figure B.2c, where the point of discontinuity is a critical point c_{-1}, and both the two limiting values of the function in c_{-1} are critical points, say c^1 and c^2, associated with c_{-1}, as both c^1 and c^2 separate regions Z_1 and Z_2. Notice that now the critical points have no merging rank-1 preimages. More on the properties and bifurcations of discontinuous maps of the plane can be found in Mira et al., 1996.

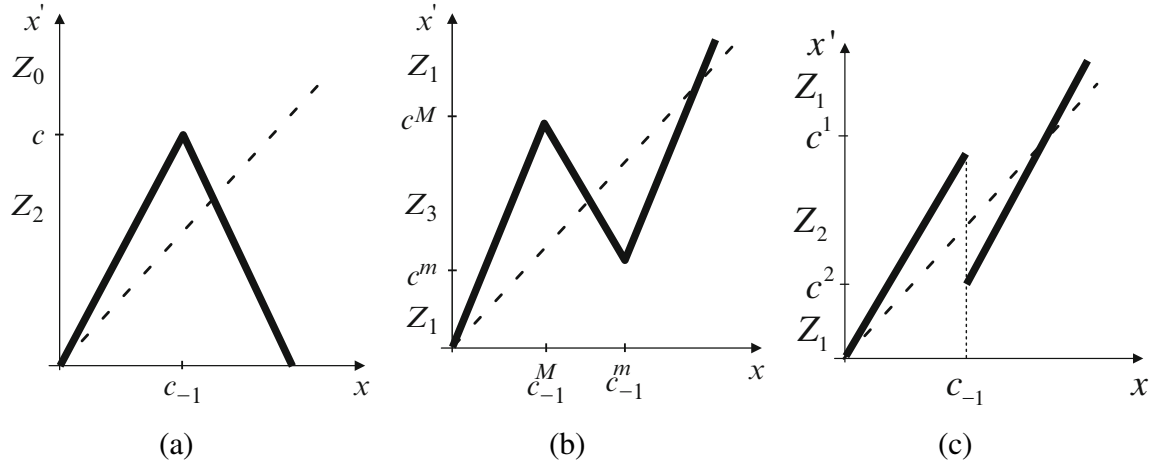

Fig. B.2 The preimage regions of certain maps. (a) The tent-map. (b) A bimodal piecewise linear map. (c) A discontinuous map. Notice that in (a) and (b) the number of preimages in adjacent regions differ by 2, whereas in (c) they differ by 1

In order to explain the geometric action of a critical point in a continuous map, let us consider, again, the logistic map, and let us notice that as x moves from 0 to 1 the corresponding image $f(x)$ spans the interval $[0, c]$ twice, the critical point c being the turning point. In other words, if we consider how the segment $\gamma = [0, 1]$ is transformed by the map f, we can say that it is *folded and pleated* to obtain the image $\gamma' = [0, c]$. Such folding gives a geometric reason why two distinct points of γ, say x_1 and x_2, located symmetrically with respect to the point $c_{-1} = 1/2$, are mapped into the same point $x' \in \gamma'$ due to the folding action of f (see figure B.1b). The same arguments can be explained by looking at the two inverse mappings f_1^{-1} and f_2^{-1} defined in $(-\infty, a/4]$ according to (B.2). We can consider the range of the map f formed by the superposition of two half-lines $(-\infty, a/4]$, joined at the critical point $c = a/4$ (fig. 1c), and on each of these half-lines a different inverse is defined. In other words, instead of saying that two distinct maps are defined on the same half-line we say that the range is formed by two distinct half lines on each of which a unique inverse map is defined. This point of view gives a geometric visualization of the critical point c as the point in which two distinct inverses merge. The action of the inverses, say $f^{-1} = f_1^{-1} \cup f_2^{-1}$, causes an unfolding of the range by mapping c into c_{-1} and by opening the two half-lines one on the right and one on the left of c_{-1}, so that the whole real line $\mathbb{R}$ is covered. So, the map f folds the real line, the two inverses unfold it.

Another interpretation of the folding action of a critical point is the following. Since $f(x)$ is increasing for $x \in [0, 1/2)$ and decreasing for $x \in (1/2, 1]$, its application to a

segment $\gamma_1 \subset [0, 1/2)$ is orientation preserving, whereas its application to a segment $\gamma_2 \subset (1/2, 1]$ is orientation reversing. This suggests that an application of f to a segment $\gamma_3 = [a, b]$ including the point $c_{-1} = 1/2$ preserves the orientation of the portion $[a, c_{-1}]$, i.e. $f([a, c_{-1}]) = [f(a), c]$, whereas it reverses the portion $[c_{-1}, b]$, i.e. $f([c_{-1}, b]) = [f(b), c]$, so that $\gamma_3^{'} = f(\gamma_3)$ is folded, the folding point being the critical point c.

Let us now consider the case of a continuous two-dimensional map $T : S \to S$, $S \subseteq \mathbb{R}^2$, defined by

$$T : \begin{cases} x_1' = T_1(x_1, x_2) \\ x_2' = T_2(x_1, x_2) \end{cases}, \tag{B.3}$$

If we solve the system of the two equations (B.3) with respect to the unknowns x_1 and x_2, then, for a given (x_1', x_2'), we may have several solutions, representing rank-1 preimages (or backward iterates) of (x_1', x_2'), say $(x_1, x_2) = T^{-1}(x_1', x_2')$, where T^{-1} is in general a multivalued relation. In this case we say that T is noninvertible, and the critical set (formed by critical curves, denoted by LC from the French "Ligne Critique") constitutes the set of boundaries that separate regions of the plane characterized by a different number of rank-1 preimages. According to the definition, along LC at least two inverses give merging preimages, located on LC_{-1} (Following the notations of Gumowski and Mira, 1980, Mira et al., 1996).

For a continuous and (at least piecewise) differentiable noninvertible map of the plane, the set LC_{-1} is included in the set where $\det DT(x_1, x_2)$ changes sign, since T is locally an orientation preserving map near points (x_1, x_2) such that $\det DT(x_1, x_2) > 0$ and orientation reversing if $\det DT(x_1, x_2) < 0$. In order to explain this point, let us recall that when an affine transformation $\mathbf{x}' = A\mathbf{x} + \mathbf{b}$, where $A = \{a_{ij}\}$ is a 2×2 matrix and $\mathbf{b} \in \mathbb{R}^2$, is applied to a plane figure, then the area of the transformed figure grows, or shrinks, by a factor $\rho = |\det A|$, and if $\det A > 0$ then the orientation of the figure is preserved, whereas if $\det A < 0$ then the orientation is reversed. This property also holds for the linear approximation of (B.3) in a neighborhood of a point $\mathbf{p} = (x_1, x_2)$, given by an affine map with $A = DT$, DT being the Jacobian matrix evaluated at the point $\mathbf{p}$

$$\mathbf{DT}(\mathbf{p}) = \begin{bmatrix} \partial T_1/\partial x_1 & \partial T_1/\partial x_2 \\ \partial T_2/\partial x_1 & \partial T_2/\partial x_2 \end{bmatrix} \tag{B.4}$$

A qualitative visualization is given in fig. 3. Of course, if the map is continuously differentiable then the change of the sign of DT occurs along points where DT vanishes,

thus giving the characterization of the fold line LC_{-1} as the locus where the jacobian vanishes.

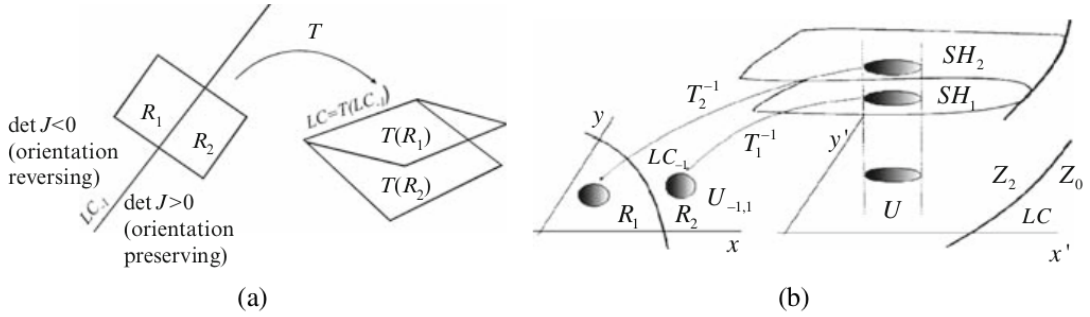

Fig. B.3 (a) A qualitative visualization of a map of the plane, and how the folding relates to the sign of the Jacobian matrix. (b) Visualizing a Riemann foliation of the plane, in the case of a $Z_0 - Z_2$ noninvertible map.

In order to give a geometrical interpretation of the action of a multi-valued inverse relation T^{-1}, it is useful to consider a region Z_k as the superposition of k sheets, each associated with a different inverse. Such a representation is known as *Riemann foliation* of the plane (see e.g. Mira et al., 1996). Different sheets are connected by folds joining two sheets, and the projections of such folds on the phase plane are arcs of LC. This is shown in the qualitative sketch of fig. 3b, where the case of a $Z_0 - Z_2$ noninvertible map is considered. This graphical representation of the unfolding action of the inverses also gives an intuitive idea of the mechanism which causes the creation of non-connected basins for noninvertible maps of the plane.

To give an example, let us again consider a quadratic map $T : (x, y) \to (x', y')$, extensively studied in Mira et al., 1996, and Abraham et al., 1997, defined by

$$T : \begin{cases} x' = ax + y \\ y' = b + x^2 \end{cases} \tag{B.5}$$

Given x' and y', if we try to solve the algebraic system with respect to the unknowns x and y we get two solutions, given by

$$T_1^{-1} : \begin{cases} x = -\sqrt{y' - b} \\ y = x' + a\sqrt{y' - b} \end{cases} \quad ; \qquad T_2^{-1} : \begin{cases} x = \sqrt{y' - b} \\ y = x' - a\sqrt{y' - b} \end{cases} \tag{B.6}$$

if $y' \geq b$, and no solutions if $y' < b$. So, (B.5) is a $Z_0 - Z_2$ noninvertible map, where Z_0 (region whose points have no preimages) is the half plane $Z_0 = \{(x, y) \,|\, y < b\}$ and Z_2 (region whose points have two distinct rank-1 preimages) is the half plane

$Z_2 = \{(x, y) \,|\, y > b\}$. The line $y = b$, which separates these two regions, is LC, i.e. the locus of points having two merging rank-1 preimages, located on the line $x = 0$, that represents LC_{-1}. Being (B.5) a continuously differentiable map, the points of LC_{-1} necessarily belong to the set of points at which the Jacobian determinant vanishes, i.e. $LC_{-1} \subseteq J_0$, where $J_0 = \{(x, y) \,|\, \det DT(x, y) = -2x = 0\}$. In this case LC_{-1} coincides with J_0 (the vertical axis $x = 0$) and the critical curve LC is the image by T of LC_{-1}, i.e. $LC = T(LC_{-1}) = T(\{x = 0\}) = \{(x, y) \,|\, y = b\}$.

In order to show the folding action related to the presence of the critical lines fact, we consider a plane figure (a circle) U separated by LC_{-1} into two portions, say $U_1 \in R_1$ and $U_2 \in R_2$ (fig. 4a) and we apply the map (B.5) to the points of U. The image $T(U_1) \cap T(U_2)$ is a nonempty set included in the region Z_{k+2}, which is the region whose points p' have rank-1 preimages $p_1 = T_1^{-1}(p') \in U_1$ and $p_2 = T_2^{-1}(p') \in U_2$. This means that two points $p_1 \in U_1$ and $p_2 \in U_2$, located at opposite sides with respect to LC_{-1}, are mapped in the same side with respect to LC, in the region Z_{k+2}. This is also expressed by saying that the ball U is "folded" by T along LC on the side with more preimages (see Fig. 4). The same concept can be equivalently expressed by stressing the "unfolding" action of T^{-1}, obtained by the application of the two distinct inverses in Z_{k+2} which merge along LC. Indeed, if we consider a ball $V \subset Z_{k+2}$, then the set of its $rank - 1$ preimages $T_1^{-1}(V)$ and $T_2^{-1}(V)$ is made up of two balls $T_1^{-1}(V) \in R_1$ and $T_2^{-1}(V) \in R_2$. These balls are disjoint if $V \cap LC = \emptyset$ (see figure B.4b)

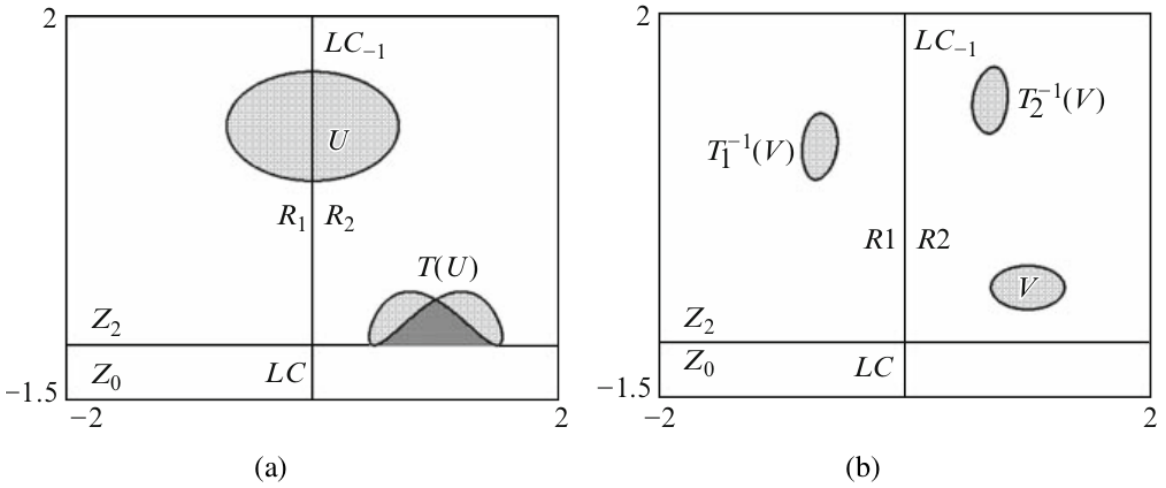

Fig. B.4 A quadratic map example. Here $a = 0.3$ and $b = 1$. (a) The folding of the ball U by the map along the critical line LC. (b) The unfolding action of the inverses of the map.

Many of the considerations made above, for 1-dimensional and 2-dimensional noninvertible maps, can be generalized to n-dimensional ones, even if their visualization becomes more difficult. First of all, from the definition of critical set it is clear that the relation $CS = T(CS_{-1})$ holds in any case. Moreover, the points of CS_{-1} where the map is continuously differentiable are necessarily points where the Jacobian determinant vanishes:

$$CS_{-1} \subseteq J_0 = \{p \in \mathbb{R}^n | \det DT(p) = 0\} \tag{B.7}$$

In fact, in any neighborhood of a point of CS_{-1} there are at least two distinct points which are mapped by T in the same point. Accordingly, the map is not locally invertible in points of CS_{-1}, and (B.7) follows from the implicit function theorem. This property provides an easy method to compute the critical set for continuously differentiable maps: from the expression of the jacobian determinant one computes the locus of points at which it vanishes, then the set obtained after an application of the map to these points is the critical set CS.

Also the geometric properties illustrated above for the two-dimensional noninvertible map (B.5) can be easily generalized to the case of the critical set of an n-dimensional noninvertible map. It is worth to notice that, in general, for piecewise differentiable maps the set of points where the map is not differentiable may belong to CS_{-1}, i.e. the images by T of such points may separate regions characterized by a different number of rank-1 preimages (see e.g. Mira, 1987). Moreover, piecewise continuous maps may have points of CS_{-1} at the discontinuities and, differently from the case of continuous maps, the corresponding portions of CS may separate regions that differ by an odd number of preimages (see e.g. Mira, 1987). In any case, the importance of the set CS lies in the fact that its points separate regions Z_k characterized by different number of preimages[2]

B.2 Discrete dynamical system as iterated maps

A *discrete-time dynamical system*, defined by the difference equation

$$\mathbf{x}(t+1) = T(\mathbf{x}(t)) \tag{B.8}$$

can be seen as the result of the repeated application (or *iteration*) of a map T. Indeed, the point $\mathbf{x}$ represents the state of a system, and T represents the "unit time

[2]This property may also be shared by points where some inverses are not defined due to a vanishing denominator, as shown in Bischi et al. 1999, 2003.

advancement operator" $T : \mathbf{x}(t) \to \mathbf{x}(t+1)$. Starting from an *initial condition* $\mathbf{x}_0 \in S$, the iteration of T inductively defines a unique *trajectory*

$$\tau(\mathbf{x}_0) = \left\{\mathbf{x}(t) = T^t(\mathbf{x}_0), t = 0, 1, 2, ...\right\}, \tag{B.9}$$

where T^0 is the identity map and $T^t = T(T^{t-1})$. As $t \to +\infty$, a trajectory may diverge, or it may converge to a fixed point of the map T, i.e. a point $\overline{\mathbf{x}}$ such that $T(\overline{\mathbf{x}}) = \overline{\mathbf{x}}$, or it may asymptotically approach another kind of invariant set, such as a periodic cycle, or a closed invariant curve or a more complex attractor, for example a so called chaotic attractor (see e.g. Devaney, 1987, Guckenheimer and Holmes, 1983, Medio and Lines, 2001). We recall that a set $A \subset \mathbb{R}^n$ is *invariant* for the map T if it is mapped onto itself, $T(A) = A$. This means that if $x \in A$ then $T(x) \in A$, i.e. A is *trapping,* and every point of A is image of some point of A. A closed invariant set A is an *attractor* if (i) it is *Lyapunov stable,* i.e. for every neighborhood W of A there exists a neighborhood V of A such that $T^t(V) \subset W \ \forall t \geq 0$; (ii) a neighborhood U of A exists such that $T^t(\mathbf{x}) \to A$ as $t \to +\infty$ for each $\mathbf{x} \in U$.

The *basin* of an attractor A is the set of all points that generate trajectories converging to A

$$\mathcal{B}(A) = \left\{\mathbf{x} | T^t(\mathbf{x}) \to A \quad \text{as } t \to +\infty \right\} \tag{B.10}$$

Let $U(A)$ be a neighborhood of an attractor A whose points converge to A. Of course $U(A) \subseteq \mathcal{B}(A)$, and also the points that are mapped into U after a finite number of iterations belong to $\mathcal{B}(A)$. Hence, the basin of A is given by

$$\mathcal{B}(A) = \bigcup_{n=0}^{\infty} T^{-n}(U(A)) \tag{B.11}$$

where $T^{-1}(\mathbf{x})$ represents the set of the rank-1 preimages of $\mathbf{x}$ (i.e. the points mapped into x by T), and $T^{-n}(x)$ represents the set of the rank-n preimages of x (i.e. the points mapped into x after n applications of T).

Let $\mathcal{B}$ be a basin of attraction and $\partial\mathcal{B}$ its boundary. From the definition it follows that $\mathcal{B}$ is trapping with respect to the forward iteration of the map T and invariant with respect to the backward iteration of all the inverses T^{-1}. Points belonging to $\partial\mathcal{B}$ are mapped into $\partial\mathcal{B}$ both under forward and backward iteration of T. This implies that if an unstable fixed point or cycle belongs to $\partial\mathcal{B}$ then $\partial\mathcal{B}$ must also contain all of its preimages of any rank. Moreover, if a saddle-point, or a saddle-cycle, belongs to $\partial\mathcal{B}$, then $\partial\mathcal{B}$ must also contain the whole stable set (see Gumowski and Mira 1980, Mira et al. 1996).

A problem that often arises in the study of nonlinear dynamical systems concerns the existence of several attracting sets, each with its own basin of attraction. In this case the dynamic process becomes path-dependent, i.e. which kind of long run dynamics characterizes the system depends on the starting condition. Another important problems in the study of applied dynamical systems is the delimitation of a bounded region of the state space where the system dynamics are ultimately trapped, despite of the complexity of the long-run time patterns. This is an useful information, even more useful than a detailed description of step by step time evolution.

Both these questions require an analysis of the global dynamical properties of the dynamical system, that is, an analysis which is not based on the linear approximation of the map. When the map T is noninvertible, its global dynamical properties can be usefully characterized by using the formalism of critical sets, by which the folding action associated with the application of the map, as well as the "unfolding" associated with the action of the inverses, can be described. Loosely speaking, the repeated application of a noninvertible map repeatedly folds the state space along the critical sets and their images, and often this allows one to define a bounded region where asymptotic dynamics are trapped. As some parameter is varied, global bifurcations that cause sudden qualitative changes in the properties of the attracting sets can be detected by observing contacts of critical curves with invariant sets. Instead, the repeated application of the inverses "repeatedly unfold" the state space, so that a neighborhood of an attractor may have preimages far from it, thus giving rise to complicated topological structures of the basins, that may be formed by the union of several (even infinitely many) non connected portions. In fact, from (B.11) it follows that in order to study the extension of a basin and the structure of its boundaries one has to consider the properties of the inverse relation T^{-1}.The route to more and more complex basin boundaries, as some parameter is varied, is characterized by global bifurcations, also called contact bifurcations, due to contacts between the critical set and the invariant sets that form the basins' boundaries.

B.3 Critical sets and the delimitation of trapping regions.

Portions of the critical set CS and its images $CS_k = T^k(CS)$ can be used to obtain the boundaries of trapping regions where the asymptotic dynamics of the iterated points of a noninvertible map are confined. This can be easily explained for a one-dimensional noninvertible map, for example the quadratic map (B.1). In fact, it is quite evident

that if we iterate the logistic map for $3 < \mu < 4$ starting from an initial condition inside the interval $[c_1, c]$, with $c_1 = f(c)$, no images can be obtained out of this interval (see Fig.5), i.e. the interval formed by the critical point c and its rank-1 image c_1 is trapping. Moreover, any trajectory generated from an initial condition in $(0, 1)$, enters $[c_1, c]$ after a finite number of iterations. Following the terminology introduced in Mira et al., 1996, the interval $[c_1, c]$ is called *absorbing*.

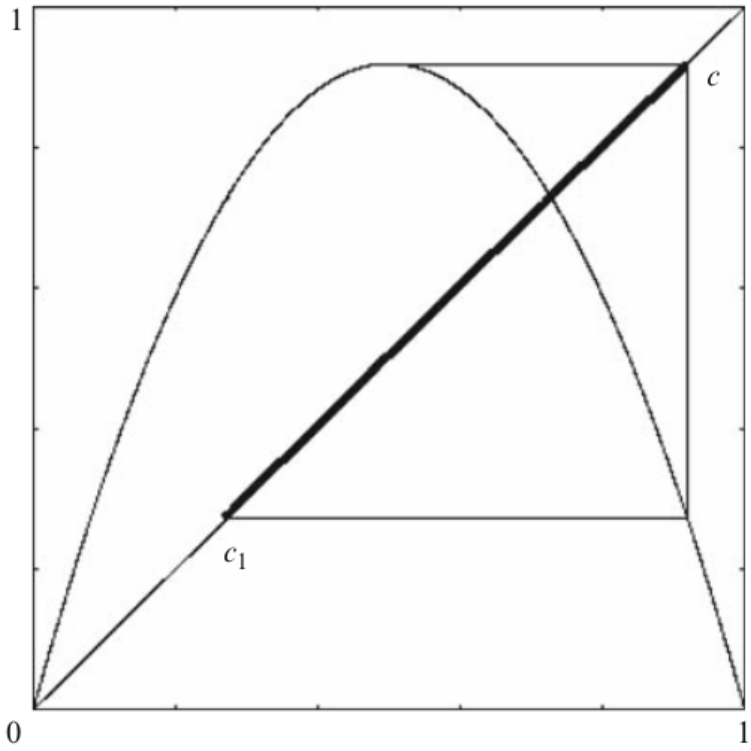

Fig. B.5 The trapping region of the quadratic map. Trajectories starting from any point in $(0, 1)$ will enter the trapping region after a finite number of iterations.

In general, for an n-dimensional map, an *absorbing region* $\mathcal{A}$ *(intervals in R, areas in* R^2*, volumes in* $R^3, ...$*)* is defined as a bounded set whose boundary is given by portions of the critical set CS and its images of increasing order $CS_k = T^k(CS)$, such that a neighborhood $U \supset \mathcal{A}$ exists whose point enter $\mathcal{A}$ after a finite number of iterations and then never escape it, since $T(\mathcal{A}) \subseteq \mathcal{A}$, i.e. $\mathcal{A}$ is trapping (see e.g. Mira et al., 1996 for more details).

Loosely speaking, we can say that the iterated application of a noninvertible map, folding and folding again the space, defines trapping regions bounded by critical sets of increasing order.

Sometimes, smaller absorbing regions are nested inside a bigger one. This can be illustrated, again, for the logistic map (B.1), as shown in Fig.6a, where inside the absorbing interval $[c_1, c]$ a trapping subset is obtained by higher rank images of the critical point, given by $\mathcal{A} = [c_1, c_3] \cup [c_2, c]$. In Fig.6b it is shown that, for the same parameter value $\mu = 3.61$ as in Fig.6a, the numerical iteration of the logistic map gives points which are trapped inside the two-cyclic interval $\mathcal{A}$.

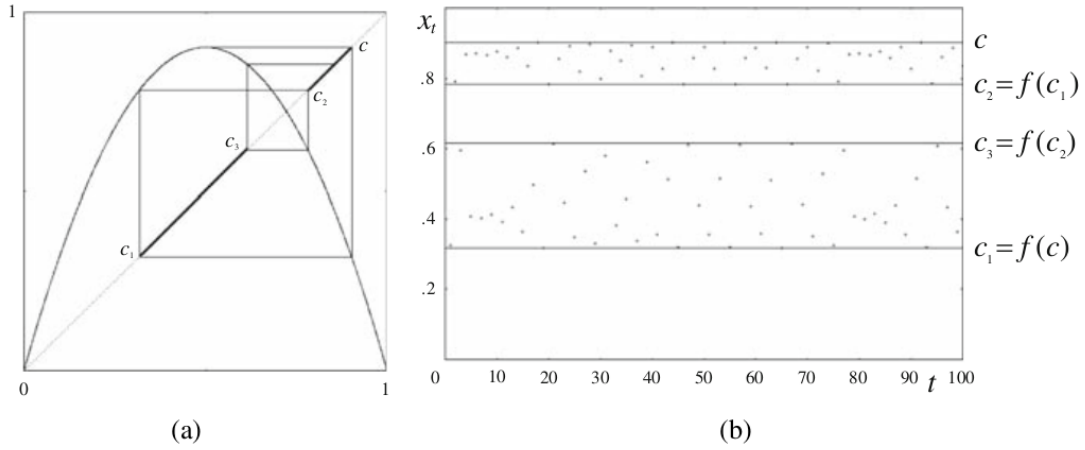

Fig. B.6 Illustrating a trapping subset inside the absorbing set of figure B.5 for the quadratic map with $\mu = 3.61$. (a) The delineation of the trapping subset $[c_1, c_3] \cup [c_2, c]$. (b) The iterates of the map remain trapped inside the two cyclic interval.

Inside an absorbing region one or more attractors may exist. However, if a chaotic attractor exists which fills up a whole absorbing region then boundary of the chaotic attractor is formed by portions of critical sets.

This is the situation shown in Fig.6, where the absorbing interval $\mathcal{A} = [c_1, c_3] \cup [c_2, c]$ is invariant and filled up by a chaotic trajectory, as shown in Fig.6b. To better illustrate this point, we also give a two-dimensional example, obtained by using the map (B.5). In Fig.7a chaotic trajectory is shown, and in Fig.7b its outer boundary is obtained by the union of a segment of LC and three iterates $LC_i = T^i(LC)$, $i = 1, 2, 3$.

Indeed, following Mira et al., 1996 (see also Bischi and Gardini, 1998) a practical procedure can be outlined in order to obtain the boundary of an absorbing area (although it is difficult to give a general method). Starting from a portion of LC_{-1}, approximately taken in the region occupied by the area of interest, its images by T of increasing rank are computed until a closed region is obtained. When such a region is mapped into itself, then it is an absorbing area $\mathcal{A}$. The length of the initial segment is to be taken, in general, by a trial and error method, although several suggestions are

given in the books referenced above. Once an absorbing area $\mathcal{A}$ is found, in order to see if it is invariant or not the same procedure must be repeated by taking only the portion

$$\gamma = \mathcal{A} \cap LC_{-1} \tag{B.12}$$

as the starting segment. Then one of the following two cases occurs:

(**case I**) the union of m iterates of γ (for a suitable m) covers the whole boundary of $\mathcal{A}$; in which case $\mathcal{A}$ is an invariant absorbing area, and

$$\partial\mathcal{A} \subset \bigcup_{k=1}^{m} T^k(\gamma) \tag{B.13}$$

(**case II**) no natural m exists such that $\bigcup_{i=1}^{m} T^i(\gamma)$ covers the whole boundary of $\mathcal{A}$; in which case $\mathcal{A}$ is not invariant but strictly mapped into itself. An invariant absorbing area is obtained by $\cap_{n>0} T^n(\mathcal{A})$ (and may be obtained by a finite number of images of $\mathcal{A}$).

The application of this procedure to the problem of the delimitation of the chaotic area of Fig.7a by portions of critical curves suggests us, on the basis of Fig.7b, to take a smaller segment γ and to take an higher number of iterates in order to obtain also the inner boundary. The result is shown in Fig.8a, where by four iterates we get the outer boundary. By a few more iterates also the inner boundary of the chaotic area is get, as shown in Fig.8b. As it can be clearly seen, and as clearly expressed by the strict inclusion in (B.13), the union of the images also include several arcs internal to the invariant area $\mathcal{A}$. Indeed, the images of the critical arcs which are mapped inside the area play a particular role, because these curves represent the "foldings" of the plane under forward iterations of the map, and this is the reason why these inner curves often denote the portions of the region which are more frequently visited by a generic trajectory inside it (compare Fig.7a and Fig.8b). Many examples are given in the literature on noninvertible maps, see e.g. Mira et al., 1996. This is due to the fact that points close to a critical arc LC_i, $i \geq 0$, are more frequently visited, because there are several distinct parts of the invariant area which are mapped in the same region (close to LC_i) in $i + 1$ iterations.

Examples of applications is dynamic economic modelling are given in Bischi and Naimzada (1999) Bischi, Gardini and Kopel (2000) Puu, 2000, Agliari et al. (2000, 2002, 2004), Chiarella et al., (2001, 2002), Sushko et al. (2003).

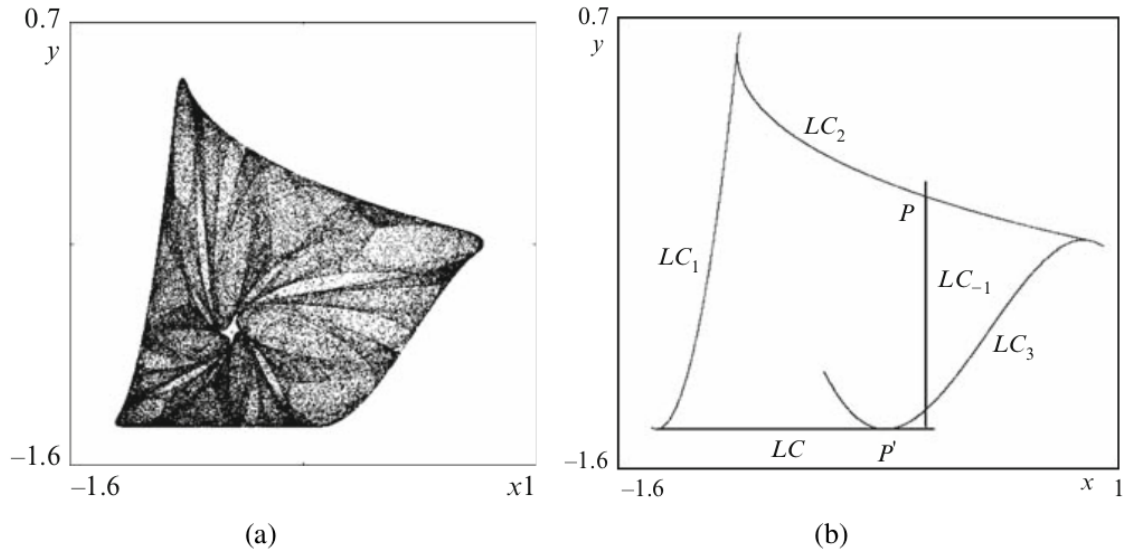

Fig. B.7 Delineating the absorbing area of the two-dimensional map given in (B.5). Here $a = -0.3$ and $b = -1.4$. (a) A chaotic trajectory of the map. (b) The boundary of the absorbing area formed by the critical line and three of its iterates. The location of the starting line LC_{-1} is discussed in the text.

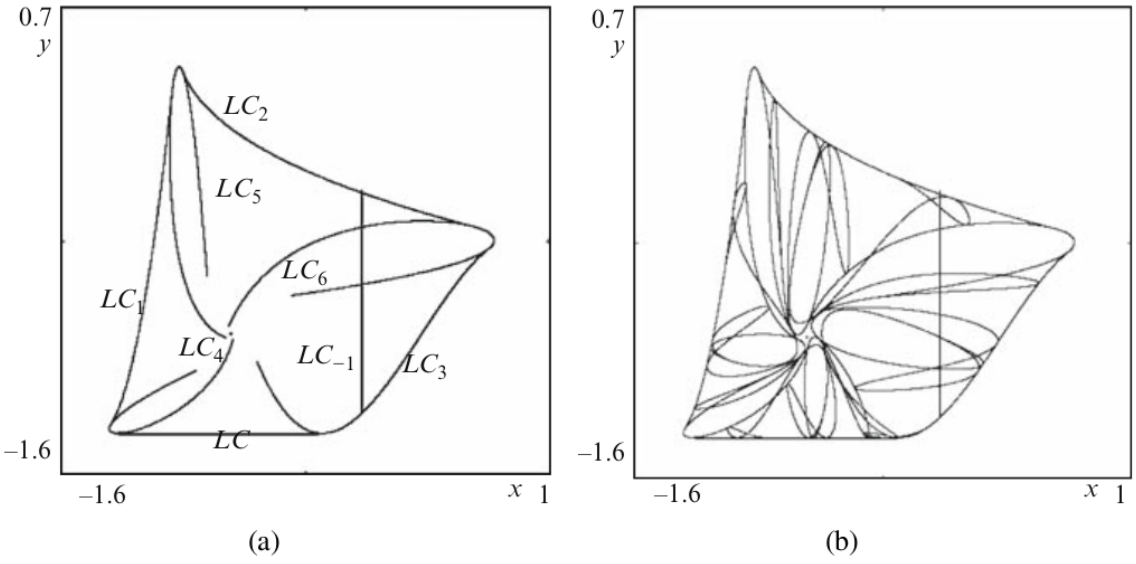

Fig. B.8 Delineating more precisely the structure of the absorbing area of the quadratic map given by (B.5). (a) Higher order iterates of the boundary curves. (b) After a sufficient number of further iterates the inner boundaries of the chaotic area emerge. These should be compared with the frequently visited areas of the chaotic trajectory in figure B.7a.

B.4 Critical sets and the creation of non connected basins

From (B.11) it is clear that the properties of the inverses are important in order to understand the structure of the basins and the main bifurcations which change their qualitative properties. In the case of noninvertible maps, the multiplicity of preimages may lead to basins with complex structures, such as multiply connected or non connected sets, sometimes formed by infinitely many non connected portions (see Mira et al., 1994, Mira and Rauzy, 1995, Mira et al., 1996, ch.5, Abraham et al., 1997,ch.5). In the context of noninvertible maps it is useful to define the *immediate basin* $\mathcal{B}_0(A)$, of an attracting set A, as the widest connected component of the basin which contains A. Then the total basin can be expressed as

$$\mathcal{B}(A) = \bigcup_{n=0}^{\infty} T^{-n}(\mathcal{B}_0(A))$$

where $T^{-n}(x)$ represents the set of all the rank-n preimages of x, i.e. the set of points which are mapped in x after n iterations of the map T. The backward iteration of a noninvertible map *repeatedly unfolds* the phase space, and this implies that the basins may be non-connected, i.e. formed by several disjoint portions.

Also in this case, we first illustrate this property by using a one-dimensional map[3] In Fig.9 the graph of a $Z_1 - Z_3 - Z_1$ noninvertible map is shown, where Z_3 is the portion of the codomain bounded by the relative minimum value $c_{\min}$ and relative maximum value $c_{\max}$. In the situation shown in fig. 9a we have three attractors: the fixed point z^*, with $\mathcal{B}(z^*) = (-\infty, q^*)$, the attractor A around x^*, with basin $\mathcal{B}(A) = (q^*, r^*)$ bounded by two unstable fixed points, and $+\infty$ (i.e. positively diverging trajectories) with basin $\mathcal{B}(+\infty) = (r^*, +\infty)$. In this case all the basins are immediate basins, each being given by an open interval. In the situation shown in fig. 9a, both basin boundaries q^* and r^* are in Z_1, so they have only themselves as unique preimages (like for an invertible map). However, the situation drastically changes if, for example, some parameter changes causes the minimum value $c_{\min}$ to move downwards, until it goes below q^* (as in fig. 9b). After the global bifurcation, when $c_{\min} = q^*$, the portion $(c_{\min}, q^*)$ enters Z_3, so new preimages $f^{-k}(c_{\min}, q^*)$ appear with $k \geq 1$. These preimages constitute an infinite (countable) set of non-connected portions of $\mathcal{B}(z^*)$ nested inside $\mathcal{B}(A)$, represented by the thick portions of the diagonal in fig. 9b, bounded by the infinitely many preimages of any rank, say q^*_{-k}, $k \in \mathbb{N}$, of q^*, that accumulate in a left neighborhood of the fixed

[3]The example is taken from an evolutionary game proposed in Bischi, Dawid and Kopel, 2000.

point r^*. In fact, as r^* is a repelling fixed point for the forward iteration of f, it is an attracting fixed point for the backward iteration of the same map.. So, the contact between the critical point $c_{\min}$ and the basin boundary q^* marks the transition from simple connected to non connected basins. Similar global bifurcations, due to contacts between critical sets and basin boundaries, also occur in higher dimensional maps.

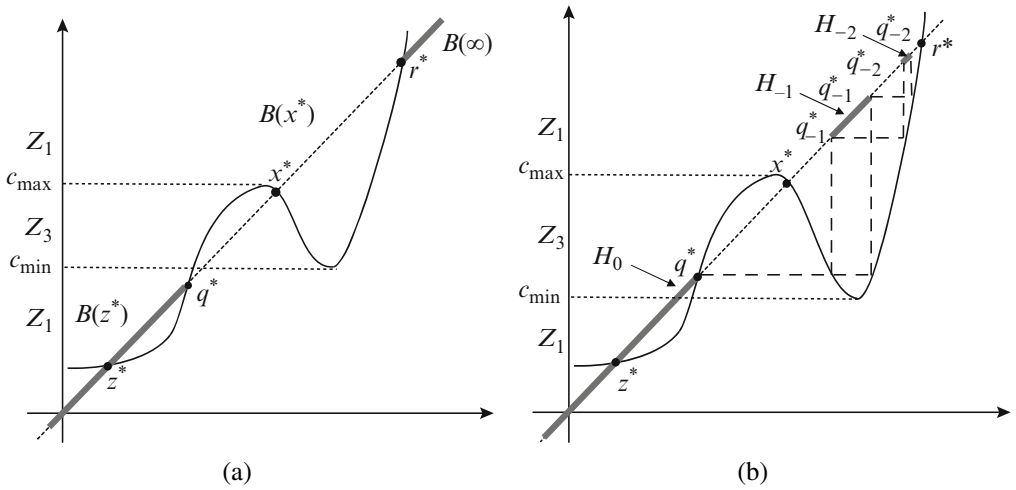

Fig. B.9 The global bifurcation of a one-dimensional noninvertible $Z_1 - Z_3 - Z_1$ map. (a) The attractors of the map are z^*, x^* and $+\infty$ and their basins are $(-\infty, q^*)$, (q^*, r^*) and $(r^*, +\infty)$ respectively. Note that c_{min} is above q^*. (b) After a parametric change c_min moves below q^* and a global bifurcation has occurred. Now the basin of z^* includes the (countably infinite number of) disconnected portions, H_{-1}, H_{-2} etc. on (x^*, r^*). These are the preimages of the portion (c_{min}, q^*).

Also in higher dimensional cases, the global bifurcations which give rise to complex topological structures of the basins, like those formed by non connected sets, can be explained in terms of contacts of basins boundaries and critical sets. In fact, if a parameter variation causes a crossing between a basin boundary and a critical set which separates different regions Z_k so that a portion of a basin enters a region where an higher number of inverses is defined, then new components of the basin may suddenly appear at the contact. However, for maps of dimension greater than 1, such kinds of bifurcations can be very rarely studied by analytical methods, since the analytical equations of such singularities are not known in general. Hence such studies are mainly performed by geometric and numerical methods.

Several examples of two-dimensional noninvertible maps that have non connected basins can be found in this book. See also Puu (2000) Bischi and Naimzada (1999), Bischi, Gardini and Kopel (2000), Bischi and Kopel (2001), Bischi, Dawid and Kopel

(2003), Bischi and Kopel (2003)Agliari et al. (2000, 2002, 2004). Examples in thre dimensions are given in Bischi, Mroz and Hauser (2001), Agliari, Gardini and Puu (2000)

Appendix C

Study of the stability of the steady states of the three models of Section 3.2 of Chapter 3 with two firms

For simpler notations we set:

$$x_i' := x_i(t+1);\ x_i := x_i(t)$$

C.1 Model (3.7) with $n = 2$

Let us consider the model (3.7) with $n = 2$, given by

$$T : \begin{cases} x_1' &= (1-\lambda_1)x_1 + \lambda_1 \left(\sqrt{B\frac{a_2 x_2}{a_1}} - a_2 x_2 \right) \\ x_2' &= (1-\lambda_2)x_2 + \lambda_2 \left(\sqrt{B\frac{a_1 x_1}{a_2}} - a_1 x_1 \right) \end{cases}$$

The fixed points are the solutions of the algebraic system

$$T : \begin{cases} x_1 &= \sqrt{B\frac{a_2 x_2}{a_1}} - a_2 x_2 \\ x_2 &= \sqrt{B\frac{a_1 x_1}{a_2}} - a_1 x_1 \end{cases}$$

This system can be analytically solved in the symmetric case $a_1 = a_2 = a$, and the following fixed points are obtained: $O = (0,0)$; $E^* = \dfrac{B}{(1+a)^2}(1,1)$, both located along the invariant diagonal Δ, and, for $a \geq 3$, two further fixed points in symmetric positions with respect to Δ

$$E_1^* = \frac{B}{(a-1)^2(a+1)}\left(a-1+\sqrt{(a+1)(a-3)},\ a-1-\sqrt{(a+1)(a-3)}\right)$$
$$E_2^* = \frac{B}{(a-1)^2(a+1)}\left(a-1-\sqrt{(a+1)(a-3)},\ a-1+\sqrt{(a+1)(a-3)}\right)$$

The conditions for the stability of the central positive equilibrium E^* are obtained from the Jacobian matrix

$$\boldsymbol{J}(x_1,x_2) = \begin{pmatrix} 1-\lambda_1 & \lambda_1\left(\dfrac{1}{2}\sqrt{\dfrac{B}{x_2}}-a\right) \\ \lambda_2\left(\dfrac{1}{2}\sqrt{\dfrac{B}{x_1}}-a\right) & 1-\lambda_2 \end{pmatrix} \tag{C.2}$$

computed at the fixed point

$$\boldsymbol{J}(E^*) = \begin{pmatrix} 1-\lambda_1 & \lambda_1\dfrac{1-a}{2} \\ \lambda_2\dfrac{1-a}{2} & 1-\lambda_2 \end{pmatrix}$$

In fact, from the characteristic equation

$$P(z) = z^2 - Tr\cdot z + Det = 0\ ,$$

where $Tr = 2-\lambda_1-\lambda_2$ and $Det = (1-\lambda_1)(1-\lambda_2) - \lambda_1\lambda_2(1-a)^2/4$ are the trace and the determinant of $\boldsymbol{J}(E^*)$ respectively, a sufficient condition for the stability is expressed by the following system of inequalities

$$\begin{aligned} P(1) = 1 - Tr + Det &> 0 \\ P(-1) = 1 + Tr + Det &> 0 \\ 1 - Det &> 0 \end{aligned}$$

that give necessary and sufficient conditions for the two eigenvalues be inside the unit circle of the complex plane. In our case

$$P(1) = \lambda_1\lambda_2\left(1 - \frac{(1-a)^2}{4}\right) > 0 \implies a < 3$$
$$P(-1) > 0 \implies a < a_f$$
$$1 - Det = \lambda_1 + \lambda_2 - \lambda_1\lambda_2 + \lambda_1\lambda_2\frac{(1-a)^2}{4} > 0 \implies \forall a,\ \lambda_i \in [0,1]$$

where

$$a_f := 1 + 2\sqrt{1 + 2\frac{2 - \lambda_1 - \lambda_2}{\lambda_1\lambda_2}}\,.$$

Hence, the equilibrium is stable for $a < 3$. At the bifurcation value $a = 3$ a pitchfork bifurcation occurs at which E^* becomes a saddle point and the two equilibriums E_1^* and E_2^* are created. Moreover, at $a = a_f \geq 3$ a flip bifurcation of E^* occurs at which E^* is transformed into an unstable node and a saddle cycle of period 2 is created. Notice that for $\lambda_1 = \lambda_2 = 1$ (the case of best reply without inertia) $a_f = 3$, so the pitchfork and flip bifurcations occur simultaneously.

C.2 Model (3.9) with $n = 2$

Let us consider the model (3.9) for $n = 2$, given by

$$T : \begin{cases} x_1' = x_1 + \lambda_1 x_1\left(B\dfrac{a_1 x_1^{\beta_1}}{a_1 x_1^{\beta_1} + a_2 x_2^{\beta_2}} - x_1\right) \\ \\ x_2' = x_2 + \lambda_2 x_2\left(B\dfrac{a_2 x_2^{\beta_2}}{a_1 x_1^{\beta_1} + a_2 x_2^{\beta_2}} - x_2\right) \end{cases} \tag{C.4}$$

Its fixed points are the solutions of the system

$$\begin{cases} x_1\left(B\dfrac{a_1 x_1^{\beta_1}}{a_1 x_1^{\beta_1} + a_2 x_2^{\beta_2}} - x_1\right) = 0 \\ x_2\left(B\dfrac{a_2 x_2^{\beta_2}}{a_1 x_1^{\beta_1} + a_2 x_2^{\beta_2}} - x_2\right) = 0 \end{cases} \tag{C.5}$$

There are three evident "boundary solutions":

$$O = (0,0)\,;\ E_1 = (B,0)\,;\ E_2 = (0,B) \tag{C.6a}$$

but O is not a fixed point because the map is not defined in it. There is also a positive fixed point, given by the solution of the system

$$\begin{cases} B\dfrac{a_1 x_1^{\beta_1}}{a_1 x_1^{\beta_1} + a_2 x_2^{\beta_2}} - x_1 = 0 \\ B\dfrac{a_2 x_2^{\beta_2}}{a_1 x_1^{\beta_1} + a_2 x_2^{\beta_2}} - x_2 = 0 \end{cases} \tag{C.7}$$

It is possible to see that one and only one solution exists given by

$$E^* = (x^*, B - x^*) \tag{C.8}$$

with $x^* \in (0, B)$ unique solution of the equation

$$F(x) = \left(\frac{a_2}{a_1}\right)^{1/(1-\beta_2)} x^{(1-\beta_1)/(1-\beta_2)} + x - B = 0$$

obtained from (C.7) after some algebraic manipulations. In fact, F is a continuous function with $F(0) < 0$, $F(B) > 0$ and $F'(x) > 0$ for each $x > 0$. An analytic expression of the solution is obtained in the case $\beta_1 = \beta_2 = \beta$, given by

$$x^* = \frac{B}{1 + \left(\dfrac{a_2}{a_1}\right)^{\frac{1}{(1-\beta)}}}$$

Moreover, under the further assumption $a_2/a_1 = 1$, i.e. in the case of identical firms, we get

$$E^* = \left(\frac{B}{2}, \frac{B}{2}\right) \tag{C.10}$$

With a given set of parameters B, β_1 and β_2 the positive fixed point E^* is locally asymptotically stable for sufficiently small values of the adjustment speeds λ_1 and λ_2 and, as usual in dynamic models with adaptive adjustment, the fixed point E^* loses stability as one or both of the adjustment speeds are increased, after which more complex attractors are created around the unstable fixed point (see [68], where these results are obtained through a standard study of the local stability of the positive fixed point, obtained by a numerical solution of the characteristic equation for the localization, in the complex plane, of the eigenvalues of the Jacobian matrix). In this Chapter we are mainly interested in the symmetric case of identical firms, for which

the Jacobian matrix (3.17) computed at E^* becomes

$$\boldsymbol{J}(E^*) = \begin{pmatrix} 1 - \dfrac{\lambda B}{2}(1-\beta/2) & -\dfrac{\lambda B \beta}{4} \\ -\dfrac{\lambda B \beta}{4} & 1 - \dfrac{\lambda B}{2}(1-\beta/2) \end{pmatrix} \tag{C.11}$$

hence the eigenvalues at the positive fixed point are $\lambda_{||} = 1 - \dfrac{1}{2}\lambda B$, with eigendirection along Δ and $\lambda_{\perp} = 1 - \dfrac{1}{2}\lambda B(1-\beta)$ with eigendirection orthogonal to Δ. It is easy to see that the steady state E^* is locally asymptotically stable for $\lambda B < 4$ and $0 < \lambda B\,(1-\beta) < 4$, however only the first condition is important as only values of $\beta_i \in (0, 1]$ are meaningful in applications, see [91].

C.3 Model (3.12) with $n = 2$

For the model (3.12) with $n = 2$, given by

$$T : \begin{cases} x_1' &= x_1 + \lambda_1 x_1 \left(B \dfrac{a_1 a_2 \beta_1 x_1^{\beta_1} x_2^{\beta_2}}{x_1 \left(a_1 x_1^{\beta_1} + a_2 x_2^{\beta_2}\right)^2} - 1 \right) \\ x_2' &= x_2 + \lambda_2 x_2 \left(B \dfrac{a_1 a_2 \beta_2 x_1^{\beta_1} x_2^{\beta_2}}{x_2 \left(a_1 x_1^{\beta_1} + a_2 x_2^{\beta_2}\right)^2} - 1 \right) \end{cases} \tag{C.12}$$

The fixed points are the solutions of the system

$$\begin{cases} a_1 a_2 B \beta_1 x_1^{\beta_1} x_2^{\beta_2} - x_1 \left(a_1 x_1^{\beta_1} + a_2 x_2^{\beta_2}\right)^2 = 0 \\ a_1 a_2 B \beta_2 x_1^{\beta_1} x_2^{\beta_2} - x_2 \left(a_1 x_1^{\beta_1} + a_2 x_2^{\beta_2}\right)^2 = 0 \end{cases} \tag{C.13}$$

The solutions must belong to the line

$$x_2 = \frac{\beta_2}{\beta_1} x_1 \tag{C.14}$$

and plugging this equation into the first equilibrium condition we obtain $x_1^{\beta_1+\beta_2} F(x_1) = 0$, where

$$F(x) = \frac{a_2}{a_1} \left(\frac{\beta_2}{\beta_1}\right)^{\beta_2} (B\beta_1 - 2x) - x^{\beta_1 - \beta_2 + 1} - \left(\frac{a_2}{a_2}\right)^2 \left(\frac{\beta_2}{\beta_1}\right)^{2\beta_2} x^{\beta_2 - \beta_1 + 1}$$

If $x^* > 0$ is a zero of the function F, then the point $E^* = (x_1^*, x_2^*)$, where x_2^* is computed according to (C.14), is a fixed point of (C.12). As $F(x)$ is continuous with

$$F(0) = \frac{a_2}{a_1}\left(\frac{\beta_2}{\beta_1}\right)^{\beta_2} B\beta_1 > 0$$
$$F\left(\frac{B\beta_1}{2}\right) = -\left[x^{\beta_1-\beta_2+1} + \left(\frac{a_2}{a_1}\right)^2\left(\frac{\beta_2}{\beta_1}\right)^{2\beta_2} x^{\beta_2-\beta_1+1}\right] < 0$$

then a solution $x^* \in \left(0, \frac{B\beta_1}{2}\right)$ exists. Moreover, as

$$F'(x) = -2\frac{a_2}{a_1}\left(\frac{\beta_2}{\beta_1}\right)^{\beta_2} + (\beta_1 - \beta_2 + 1)\, x^{\beta_1-\beta_2} + \left(\frac{a_2}{a_1}\right)^2\left(\frac{\beta_2}{\beta_1}\right)^{2\beta_2}(\beta_2 - \beta_1 + 1)\, x^{\beta_2-\beta_1}$$

uniqueness of such solution is ensured for $x > 0$ provided that $\beta_1 - \beta_2 + 1 \geq 0$ and $\beta_2 - \beta_1 + 1 \geq 0$, a condition usually satisfied in applications, due to the conditions $\beta_i \in (0, 1]$ (see [91]). Moreover it is always trivially satisfied in the case of equal elasticities $\beta_1 = \beta_2$. Indeed, in the case of identical firms $\beta_1 = \beta_2 = \beta$; $a_1 = a_2$, the function $F(x)$ becomes $F(x) = B\beta - 4x$, hence the unique equilibrium is

$$E^* = (x^*, x^*) \quad \text{with} \quad x^* = \frac{B\beta}{4}$$

The Jacobian matrix $\boldsymbol{J}$ has entries

$$J_{11} = 1 - \lambda_1 - \lambda_1 B a_1 a_2 \beta_1^2 x_1^{\beta_1-1} x_2^{\beta_2} \frac{a_1 x_1^{\beta_1} - a_2 x_2^{\beta_2}}{\left(a_1 x_1^{\beta_1} + a_2 x_2^{\beta_2}\right)^3}$$
$$J_{12} = \lambda_1 \beta_1 \beta_2 B a_1 a_2 x_1^{\beta_1} x_2^{\beta_2-1} \frac{a_1 x_1^{\beta_1} - a_2 x_2^{\beta_2}}{\left(a_1 x_1^{\beta_1} + a_2 x_2^{\beta_2}\right)^3}$$
$$J_{21} = \lambda_2 \beta_1 \beta_2 B a_1 a_2 x_1^{\beta_1-1} x_2^{\beta_2} \frac{a_2 x_2^{\beta_2} - a_1 x_1^{\beta_1}}{\left(a_1 x_1^{\beta_1} + a_2 x_2^{\beta_2}\right)^3}$$
$$J_{22} = 1 - \lambda_2 - \lambda_2 B a_1 a_2 \beta_2^2 x_1^{\beta_1} x_2^{\beta_2-1} \frac{a_2 x_2^{\beta_2} - a_1 x_1^{\beta_1}}{\left(a_1 x_1^{\beta_1} + a_2 x_2^{\beta_2}\right)^3}$$

that computed at a point of the diagonal Δ (and, in particular, at the equilibrium E^*) becomes a multiple of the identity matrix

$$\boldsymbol{J}(x, x) = (1 - \lambda)\mathbf{I}$$

so that the equilibrium is an attracting star node or a repelling star node according to $\lambda < 2$ or $\lambda > 2$ respectively. At $\lambda = 2$ a degenerate flip bifurcation occurs.

Appendix D

Chaos synchronization, transverse stability, Milnor attractors and related bifurcations in two-dimensional models.

Let consider a dynamic model represented by a map of the plane into itself $T : (x_1, x_2) \to (x_1^{'}, x_2^{'})$. Let us assume, like in the case of identical competitors, that the map remains the same if the variables x_1 and x_2 are swapped, i.e. $T \circ S = S \circ T$, where $S : (x_1, x_2) \to (x_2, x_1)$ is the reflection through the diagonal

$$\Delta = \left\{(x_1, x_2) \in \mathbb{R}^2 | x_1 = x_2\right\} \ . \tag{D.1}$$

This symmetry property implies that the diagonal is mapped into itself, i.e., $T(\Delta) \subseteq \Delta$, which corresponds with the obvious statement that, in a deterministic framework, identical competitors, starting from identical initial conditions, behave identically for each time. The trajectories embedded into Δ, i.e. characterized by $x_1(t) = x_2(t)$ for every t, are called *synchronized trajectories*, and they are governed by the one-dimensional map given by the restriction of T to the invariant submanifold Δ

$$x(t+1) = f(x(t)) = T_\Delta(x(t)) \quad \text{with} \quad T_{_\Delta} = T|_\Delta : \Delta \to \Delta. \tag{D.2}$$

A trajectory starting out of Δ, i.e. with $x_1(0) \neq x_2(0)$, is said to synchronize if $\|x_1(t) - x_2(t)\| \to 0$ as $t \to +\infty$. A question which naturally arises is whether identical competitors starting from different initial conditions will synchronize in the long run,

so that the asymptotic behavior is governed by the simpler one-dimensional model (D.2). This question can be reformulated as follows. Let A_s be an attractor of the one-dimensional map (D.2). Is it also an attractor for the two-dimensional map T?

To answer this question let us consider the Jacobian matrix of T computed at any point of Δ, say $\boldsymbol{J} = \{J_{ij}(x)\}$ with the double symmetry property $J_{11} = J_{22}$ and $J_{12} = J_{21}$. The two orthogonal eigenvectors of such a symmetric matrix are one parallel to Δ, say $\mathbf{v}_{\|} = (1,1)$, and one perpendicular to it, say $\mathbf{v}_{\perp} = (1,-1)$, with related eigenvalues given by

$$\lambda_{\|}(x) = J_{11}(x) + J_{12}(x) \quad \text{and} \quad \lambda_{\perp}(x) = J_{11}(x) - J_{12}(x)$$

Of course, $\lambda_{\|}(x) = f'(x)$. Since the product of matrices with the structure of J has the same structure as well, a k-cycle $\{s_1, ..., s_k\}$ embedded into Δ has eigenvalues $\lambda_{\|}^k = \prod_{i=1}^k \lambda_{\|}(s_i)$ and $\lambda_{\perp}^k = \prod_{i=1}^k \lambda_{\perp}(s_i)$, with eigenvectors $\mathbf{v}_{\|}$ and $\mathbf{v}_{\perp}$ respectively. So, an answer to the question stated above requires a study of the transverse stability, i.e. stability in the direction orthogonal to Δ. If A_s is a cycle, then the study of the transverse stability is the usual one, based on the modulus of the eigenvalues of the cycle in the direction transverse to Δ. The problem becomes more interesting when A_s is a chaotic attractor. Indeed, dynamical systems with chaotic trajectories embedded into an invariant submanifold of lower dimensionality than the total phase space have raised an increasing interest in the scientific community because the phenomenon of *chaos synchronization* may occur (see e.g. [71], [92], [94], [132]) i.e., the time evolution of the two competitors synchronize in the long run even if each of them behaves chaotically. The key property for the study of the transverse stability of a chaotic attractor $A_s \subset \Delta$ is that it includes infinitely many periodic orbits which are unstable in the direction along Δ. In this case, *Milnor attractors* (see [100]) which are not stable in Lyapunov sense appear quite naturally in this context. To better understand the meaning of this point, we recall some definitions.

Let $\mathcal{A}$ be a closed invariant set such that $T(\mathcal{A}) \equiv \mathcal{A}$, and let $\mathcal{B}(\mathcal{A})$ denote its basin of attraction, i.e. is the set of points whose ω-limit set belongs to $\mathcal{A}$.

Definition. *$\mathcal{A}$ is an asymptotically stable attractor (or topological attractor) if it is Lyapunov stable, i.e. for every neighborhood U of $\mathcal{A}$ there exists a neighborhood V of $\mathcal{A}$ such that $T^t(V) \subset U$ $\forall t \geq 0$, and $B(\mathcal{A})$ contains a neighborhood of $\mathcal{A}$.*

In other words, if $\mathcal{A}$ is a topological attractor then a neighborhood $W \supset \mathcal{A}$ exists such that $T^t(\mathbf{x}) \to \mathcal{A}$ as $t \to +\infty$ for any $\mathbf{x} \in W$. In this case the basin $\mathcal{B}(\mathcal{A})$ is an open set given by $\mathcal{B}(\mathcal{A}) = \bigcup_{t \geq 0} T^{-t}(W)$.

Definition. *A closed invariant set $\mathcal{A}$ is said to be a weak attractor in Milnor sense (or simply Milnor attractor) if its basin of attraction $B(\mathcal{A})$ has positive Lebesgue measure.*

Note that a topological attractor is also a Milnor attractor, whereas the converse is not true. The more general notion of Milnor attractor has been introduced to evidence the existence of invariant sets which "attract" many points even if they are not attractors in the usual topological sense. In this case, [100] denotes $\mathcal{B}(\mathcal{A})$ as "Realm of attraction", reserving the term "basin" when $\mathcal{B}(\mathcal{A})$ is an open set. However, since the term basin is more standard in the literature, we shall use such term even when $\mathcal{A}$ is a Milnor (but not topological) attractor, for which $\mathcal{B}(\mathcal{A})$ is not, in general, an open set.

We now recall some definitions and results related to the problem of chaos synchronization, see e.g. [30], [104]. Let A_s be a chaotic attractor (with absolutely continuous invariant measure on it) of the restriction (D.2) of T to Δ. Its attractivity in the two-dimensional phase space is given in terms of the *transverse Lyapunov exponents*

$$\Lambda_\perp = \lim_{N\to\infty} \frac{1}{N} \sum_{i=0}^{N} \ln |\lambda_\perp (s_i)| \tag{D.3}$$

where $\{s_i = f^i(s_0), i \geq 0\}$ is a trajectory embedded in A_s. For a chaotic set $A_s \subset \Delta$, infinitely many transverse Lyapunov exponents can be defined: If $x(0)$ belongs to a k-cycle then $\Lambda_\perp = \ln \left|\lambda_\perp^k\right|$, so that the cycle is transversely stable if $\Lambda_\perp < 0$, whereas if $x(0)$ belongs to a generic aperiodic trajectory embedded inside the chaotic set A_s then $\Lambda_\perp$ is the *natural transverse Lyapunov exponent* $\Lambda_\perp^{nat}$, where the term "natural" means that the Lyapunov exponent associated to the natural, or SBR (Sinai-Bowen-Ruelle), measure, i.e., computed for a typical trajectory taken in the chaotic attractor A_s. $\Lambda_\perp^{nat}$ gives the "average" local behavior of the trajectories in a neighborhood of the invariant set A_s and allows one to detect new kinds of bifurcations such as the *riddling bifurcation* or the *blowout bifurcation*. Since infinitely many cycles, all unstable along Δ, are embedded inside a chaotic attractor A_s, a spectrum of transverse Lyapunov exponents can be defined, see e.g. [30]

$$\Lambda_\perp^{\min} \leq ... \leq \Lambda_\perp^{nat} \leq ... \leq \Lambda_\perp^{\max} \tag{D.4}$$

The meaning of the inequalities in (D.4) can be intuitively understood on the basis of the property that $\Lambda_\perp^{nat}$ expresses a sort of "weighted balance" between the transversely repelling and transversely attracting cycles (see e.g. [131]). If $\Lambda_\perp^{\max} < 0$, i.e. all the cycles embedded in A_s are transversely stable, then A_s is asymptotically stable, in

the usual Lyapunov sense, for the two-dimensional map T. However, it may occur that some cycles embedded in the chaotic set A_s become transversely unstable, i.e. $\Lambda_\perp^{\max} > 0$, while $\Lambda_\perp^{nat} < 0$. In this case, A_s is no longer Lyapunov stable, but it continues to be a *Milnor attractor,* i.e. it attracts a positive (Lebesgue) measure set of points of the two-dimensional phase space. So, if $\mathcal{A} \subset \Delta$ is a chaotic attractor of $T|_\Delta$ with absolutely continuous invariant measure, then a sufficient condition for a $\mathcal{A}$ to be a Milnor, but not topological, attractor for the two-dimensional map T, is that: (i) at least one k-cycle embedded in $\mathcal{A}$ is transversely repelling, i.e. $\Lambda_\perp^{\max} > 0$, and (ii) the Lyapunov exponent $\Lambda_\perp^{nat}$ is negative. This means that the majority of the trajectories on $\mathcal{A}$ are transversely attracting, but some (even infinitely many) trajectories inside $\mathcal{A}$ can exist whose transverse Lyapunov exponent is positive. In other words, transversely repelling trajectories can be embedded into a chaotic set which is attracting only "on average".

The transition from asymptotic stability to attractivity only in Milnor sense, marked by a change of sign of $\Lambda_\perp^{\max}$ from negative to positive, is denoted as the *riddling bifurcation* (or *bubbling bifurcation*). Even if the occurrence of such bifurcations is detected through the study of the transverse Lyapunov exponents, their effects depend on the action of the nonlinearities far from Δ, that is, on the global properties of the dynamical system. In fact, after the riddling bifurcation two possible scenarios can be observed according to the fate of the trajectories that are locally repelled along (or near) the local unstable manifolds of the transversely repelling cycles (see e.g. [44], [80], [133], [62]):

(**L**) they can be reinjected towards Δ, so that the dynamics of such trajectories are characterized by some bursts far from Δ before synchronizing on it (a very long sequence of such bursts, which can be observed when $\Lambda_\perp$ is close to zero, has been called *on-off intermittency*, see e.g. [114], [104]);

(**G**) they may belong to the basin of another attractor, in which case the phenomenon of *riddled basins* is obtained, see [80], [44].

Some authors call *local riddling* the situation (L) and, by contrast, *global riddling* the situation (G) (see [104], [134]). As shown in [62], see also [63], the reinjection of the locally repelled trajectories can be usefully described by the method of *critical curves* and their folding action (see Appendix B, or [34], for more details on critical curves). When also $\Lambda_\perp^{nat}$ becomes positive, due to the fact that the transversely unstable periodic orbits embedded into A_s have a greater weight as compared with the stable ones, a *blowout bifurcation* occurs, after which A_s is no longer a Milnor attractor, because it attracts a set of points of zero measure, and becomes a *chaotic saddle*, see [30]. Also

the macroscopic effect of a blowout bifurcation is strongly influenced by the behavior of the dynamical system far from the invariant submanifold Δ: The trajectories starting close to the chaotic saddle may be attracted by some attracting set far from Δ or remain inside a two-dimensional compact set located around the chaotic saddle A_s, inside which on-off intermittency occurs.

As noticed by many authors, (see e.g. [104], [30], [94], [133], [64], [62]), even if the occurrence of riddling and blowout bifurcations is detected through the transverse Lyapunov exponents, i.e. from a local analysis of the linear approximation of the map along Δ, their effects are determined by the global properties of the map.

Appendix E

Proof of Proposition 2 of Chapter 4

Let us rewrite the map T as follows:

$$T : \begin{cases} x' &= Ax - Bx^2 + Cxr \\ \\ r' &= \frac{r}{r+(1-r)e^{Dx-\beta\xi}} \end{cases} \tag{E.1}$$

where

$$A = 1 + \alpha - \frac{Na_0q_0}{2\gamma};\ B = \frac{\alpha}{k};\ C = \frac{N}{2\gamma}\left(a_0q_0 - a_1q_1\right);\ D = \beta\frac{a_0^2q_0 - a_1^2q_1}{4\gamma} \tag{E.2}$$

and let us consider the second iterate of the map T, i.e.

$$T^2 : \begin{cases} x' &= \left(Ax - Bx^2 + Cxr\right)\left(A + C\frac{r}{r+(1-r)e^{Dx-\beta\xi}}\right) - B\left(Ax - Bx^2 + Cxr\right)^2 \\ \\ r' &= \frac{\frac{r}{r+(1-r)e^{Dx-\beta\xi}}}{\frac{r}{r+(1-r)e^{Dx-\beta\xi}} + \left(1 - \frac{r}{r+(1-r)e^{Dx-\beta\xi}}\right)e^{D\left(Ax-Bx^2+Cxr\right)-\beta\xi}} \end{cases} \tag{E.3}$$

Its restriction to the invariant line $r = 1$ is

$$T^2|_{r=1} : \begin{cases} x' &= F\left(Fx - Bx^2\right) - B\left(Fx - Bx^2\right)^2 \\ \\ r' &= 1 \end{cases} \tag{E.4}$$

where

$$F = A + C = 1 + \alpha - \frac{Na_1q_1}{2\gamma}. \tag{E.5}$$

The map T^2 can have at most four fixed points, given by the solutions of the equation

$$x\left(B^3x^3 - 2FB^2x^2 + FB\left(1+F\right)x + 1 - F^2\right) = 0 \tag{E.6}$$

from which we obtain

$$E_1^0 = (0,1), E_1^* = (x_1^*, 1), E_1^{*1} = (x_1^{*1}, 1) \text{ and } E_1^{*2} = (x_1^{*2}, 1) \tag{E.7}$$

where x_1^* is given by (4.13) and $x_1^{*1} = \frac{1+F+\sqrt{F^2-3-2F}}{2B}$, $x_1^{*2} = \frac{1+F-\sqrt{F^2-3-2F}}{2B}$.

Assuming the existence of period-2 cycle $\{(x_1^{*1}, 1), (x_1^{*2}, 1)\}$ of T is equivalent to the existence of E_1^{*1} and E_1^{*2} for T^2 which, requiring also $x_1^{*1} > 0$, $x_1^{*2} > 0$, implies $F > 3$, i.e. $\alpha - 2 > \frac{Na_1q_1}{2\gamma}$. The Jacobian matrix associated to T^2 along the restriction $r = 1$ is

$$J^2(x,1) = \begin{bmatrix} (F-2Bx)\left(F - 2BFx + 2B^2x^2\right) & J_{12}^2(x,1) \\ 0 & J_{22}^2(x,1) \end{bmatrix} \tag{E.8}$$

where $J_{22}^2(x,1) = e^{D\left(Fx - Bx^2 + x\right) - 2\beta\xi}$, from which we have the condition for transverse stability of E_1^{*1} and E_1^{*2}, given by $J_{22}^2(x_1^{*1}, 1) = J_{22}^2(x_1^{*2}, 1) < 1$. By trivial algebra we obtain the condition

$$D\left(\frac{F+1}{B}\right) - 2\beta\xi < 0 \tag{E.9}$$

Substituting for D, F and B, we obtain

$$\frac{k\left(a_0^2q_0 - a_1^2q_1\right)\left(4\gamma + 2\gamma\alpha - Na_1q_1\right)}{8\alpha\gamma^2} - 2\xi < 0 \tag{E.10}$$

By similar calculation, the condition to have stable the transverse manifold of the fixed point E_1^* of T^2 is given by

$$\frac{k\left(a_0^2q_0 - a_1^2q_1\right)\left(2\gamma\alpha - Na_1q_1\right)}{8\alpha\gamma^2} - \xi < 0 \tag{E.11}$$

From conditions (E.10) and (E.11) it follows that the transverse invariant manifold of E_1^* is stable and the transverse invariant manifolds of E_1^{*1} and E_1^{*2} are unstable if and only if

$$\frac{k\left(a_0^2q_0 - a_1^2q_1\right)\left(4\gamma + 2\gamma\alpha - Na_1q_1\right)}{8\alpha\gamma^2} - 2\xi > 0 > \frac{k\left(a_0^2q_0 - a_1^2q_1\right)\left(2\gamma\alpha - Na_1q_1\right)}{8\alpha\gamma^2} - \xi \tag{E.12}$$

which can be rewritten as follows:

$$\xi - \frac{k\left(a_0^2 q_0 - a_1^2 q_1\right)}{2\alpha\gamma} < \frac{k\left(a_0^2 q_0 - a_1^2 q_1\right)\left(2\gamma\alpha - N a_1 q_1\right)}{8\alpha\gamma^2} - \xi < 0 \tag{E.13}$$

By simple considerations it is easy to note that conditions (E.13) and condition $\alpha - \frac{N a_1 q_1}{2\gamma} > 2$ required for the existence of E_1^{*1} and E_1^{*2} identify a nonempty set of the parameter space.

Moreover, from stability condition (E.10) and (E.11) it is easy to note that in order to have the instability of the transverse invariant manifold of E_1^* and the stability of the transverse invariant manifolds of E_1^{*1} and E_1^{*2} is required

$$\frac{k\left(a_0^2 q_0 - a_1^2 q_1\right)\left(4\gamma + 2\gamma\alpha - N a_1 q_1\right)}{8\alpha\gamma^2} - 2\xi < 0 < \frac{k\left(a_0^2 q_0 - a_1^2 q_1\right)\left(2\gamma\alpha - N a_1 q_1\right)}{8\alpha\gamma^2} - \xi \tag{E.14}$$

which can be rewritten as

$$\frac{k\left(a_0^2 q_0 - a_1^2 q_1\right)}{2\alpha\gamma} - \xi < \xi - \frac{k\left(a_0^2 q_0 - a_1^2 q_1\right)\left(2\gamma\alpha - N a_1 q_1\right)}{8\alpha\gamma^2} < 0 \tag{E.15}$$

Since throughout Chaper 4 we always assume $a_0^2 q_0 - a_1^2 q_1 < 0$ and $\alpha - \frac{N a_1 q_1}{2\gamma} > 2$ is required for the existence of E_1^{*1} and E_1^{*2}, condition (E.15) implies that ($|\cdot|$ is the absolute value of $\cdot$)

$$|\xi| > \left|\frac{k\left(a_0^2 q_0 - a_1^2 q_1\right)\left(2\gamma\alpha - N a_1 q_1\right)}{8\alpha\gamma^2}\right| > \left|\frac{k\left(a_0^2 q_0 - a_1^2 q_1\right)}{2\alpha\gamma}\right| > |\xi| \tag{E.16}$$

which is a contradiction. It follows that condition (E.15) cannot be satisfied.

Since the condition to have stable (or unstable) transversally manifold of the period 2-cycle $\{(x_1^{*1}, 0), (x_1^{*2}, 0)\}$ of the map T is equivalent to condition to have stable transverse invariant manifold of each of the two fixed points E_1^{*1} and E_1^{*2} of T^2 and the condition to have stable (or unstable) transverse invariant manifold of the fixed point E_1^* are the same for T and T^2, the claim of the proposition follows.

Appendix F

Proof of Proposition 3 of Chapter 4

Let us consider the restriction of T^2, defined in appendix E (see (E.1)), on the invariant line $r = 0$

$$T^2|_{r=0} : \begin{cases} x' &= A\left(Ax - Bx^2\right) - B\left(Ax - Bx^2\right)^2 \\ \\ r' &= 0 \end{cases} \tag{F.1}$$

It has at most four fixed points given by the solutions of the equation

$$x\left(B^3x^3 - 2B^2Ax^2 + AB\left(1 + A\right)x + 1 - A^2\right) = 0 \tag{F.2}$$

from which we obtain:

$$E_0^0 = (0,0)\,, E_0^* = (x_0^*, 0)\,, E_0^{*1} = (x_0^{*1}, 0) \text{ and } E_0^{*2} = (x_0^{*2}, 0) \tag{F.3}$$

where x_0^* is given in (4.10), and $x_0^{*1} = \frac{1+A+\sqrt{A^2-3-2A}}{2B}$, $x_0^{*2} = \frac{1+A-\sqrt{A^2-3-2A}}{2B}$. Assuming the existence of period-2 cycle $\{(x_0^{*1}, 0)\,, (x_0^{*2}, 0)\}$ of T is equivalent to the existence of E_0^{*1} and E_0^{*2} for T^2 which, requiring also $x_0^{*1} > 0$ and $x_0^{*2} > 0$, implies $A > 3$, i.e. $\alpha - 2 > \frac{Na_0q_0}{2\gamma}$. The Jacobian matrix of T^2 along $r = 0$ is

$$J^2\left(x, 0\right) = \begin{bmatrix} \left(A - 2Bx\right)\left(A - 2BAx + 2B^2x^2\right) & J_{12}^2\left(x, 0\right) \\ 0 & J_{22}^2\left(x, 0\right) \end{bmatrix} \tag{F.4}$$

where $J_{22}^2\left(x, 0\right) = e^{-D\left(Ax - Bx^2 + x\right) + 2\beta\xi}$, from which the condition for transverse stability of E_0^{*1} and E_0^{*2} is $J_{22}^2\left(x_0^{*1}, 0\right) = J_{22}^2\left(x_0^{*2}, 0\right) < 1$. By trivial algebra we obtain the condition

$$D\left(\frac{1 + A}{B}\right) - 2\beta\xi > 0 \tag{F.5}$$

Substituting for D, A and B, we obtain

$$\frac{k\left(a_0^2q_0 - a_1^2q_1\right)\left(4\gamma + 2\gamma\alpha - Na_0q_0\right)}{8\alpha\gamma^2} - 2\xi > 0 \tag{F.6}$$

By similar calculation, the condition for transverse stability of the fixed point E_0^* of T^2 is given by

$$\frac{k\left(a_0^2q_0 - a_1^2q_1\right)\left(2\gamma\alpha - Na_0q_0\right)}{8\alpha\gamma^2} - \xi > 0 \tag{F.7}$$

From the conditions (F.6) and (F.7) it follows that transverse invariant manifold of E_0^* is unstable and transverse invariant manifolds of E_0^{*1} and E_0^{*2} are stable if and only if

$$\frac{k\left(a_0^2q_0 - a_1^2q_1\right)\left(2\gamma\alpha - Na_0q_0\right)}{8\alpha\gamma^2} - \xi < 0 < \frac{k\left(a_0^2q_0 - a_1^2q_1\right)\left(4\gamma + 2\gamma\alpha - Na_0q_0\right)}{8\alpha\gamma^2} - 2\xi \tag{F.8}$$

which can be rewritten as follows

$$\xi - \frac{k\left(a_0^2q_0 - a_1^2q_1\right)}{2\alpha\gamma} < \frac{k\left(a_0^2q_0 - a_1^2q_1\right)\left(2\gamma\alpha - Na_0q_0\right)}{8\alpha\gamma^2} - \xi < 0 \tag{F.9}$$

By simple considerations it is easy to note that conditions (F.9) and condition $\alpha - \frac{Na_0q_0}{2\gamma} > 2$ required for the existence of E_0^{*1} and E_0^{*2} identify a nonempty set of the parameter space.

Moreover, from stability condition (F.6) and (F.7) it is easy to note that in order to have the stability of the transverse invariant manifold of E_0^* and the instability of the transverse invariant manifolds of E_0^{*1} and E_0^{*2} is required

$$\frac{k\left(a_0^2q_0 - a_1^2q_1\right)\left(2\gamma\alpha - Na_0q_0\right)}{8\alpha\gamma^2} - \xi > 0 > \frac{k\left(a_0^2q_0 - a_1^2q_1\right)\left(4\gamma + 2\gamma\alpha - Na_0q_0\right)}{8\alpha\gamma^2} - 2\xi \tag{F.10}$$

which can be rewritten as follows

$$0 > -\frac{k\left(a_0^2q_0 - a_1^2q_1\right)\left(2\gamma\alpha - Na_0q_0\right)}{8\alpha\gamma^2} + \xi > \frac{k\left(a_0^2q_0 - a_1^2q_1\right)}{2\alpha\gamma} - \xi \tag{F.11}$$

Since throughout Chapter 4 we always assume $a_0^2q_0 - a_1^2q_1 < 0$ and $\alpha - \frac{Na_0q_0}{2\gamma} > 2$ is required for the existence of E_0^{*1} and E_0^{*2}, condition (F.11) implies that

$$|\xi| > \left|\frac{k\left(a_0^2q_0 - a_1^2q_1\right)\left(2\gamma\alpha - Na_0q_0\right)}{8\alpha\gamma^2}\right| > \left|\frac{k\left(a_0^2q_0 - a_1^2q_1\right)}{2\alpha\gamma}\right| > |\xi| \tag{F.12}$$

which is a contradiction. It follows that condition (F.11) cannot be satisfied.

Since the condition to have stable (or unstable) the transverse invariant manifold of the two period cycle $\{(x_0^{*1}, 0), (x_0^{*2}, 0)\}$ of the map T is equivalent to condition to have stable (or unstable) the transverse invariant manifold of each of the two fixed points E_0^{*1} and E_0^{*2} of T^2 and the condition to have stable (or unstable) the transverse invariant manifold of the fixed point E_0^* are the same for T and T^2, the claim of the proposition follows.